Experimental and simulation studies on plasma gasification of waste feedstocks for clean energy production

A thesis

Submitted in partial fulfillment of the requirements for the Degree of

DOCTOR OF PHILOSOPHY

by

Roni Mallick

Department of Chemical Engineering

Indian Institute of Technology Guwahati

Guwahati, Assam (India) - 781039

January 2024

Department of Chemical Engineering

Indian Institute of Technology Guwahati

Guwahati, Assam - 781039

STATEMENT

I hereby declare that the matter embodied in this thesis, entitled "**Experimental and simulation studies on plasma gasification of waste feedstocks for clean energy production**" is the result of investigation carried out by me in the Department of Chemical Engineering, Indian Institute of Technology Guwahati, Assam, India under the supervision of **Prof. Prabu Vairakannu**.

In keeping with the general practice of reporting scientific observations, due acknowledgement has been made wherever the work described is based on the findings of other investigations.

Guwahati — **Roni Mallick**

January, 2024 — 186107013

Department of Chemical Engineering

Indian Institute of Technology Guwahati

Guwahati, Assam - 781039

CERTIFICATE

It is certified that the work described on this thesis, entitled "**Experimental and simulation studies on plasma gasification of waste feedstocks for clean energy production**", done by **Mr. Roni Mallick** for the award of degree of philosophy is an authentic record of the results obtained from the research work carried out under my supervision in the Department of Chemical Engineering, Indian Institute of Technology Guwahati, Assam, India and this work has not been submitted elsewhere for the award of any other degree or diploma.

This thesis in my opinion, has reached the standard fulfilling the requirements for the award of the degree of Doctor of Philosophy in accordance with the regulations of the institute.

Guwahati

January, 2024

Dr. Prabu Vairakannu

Professor

Department of Chemical Engineering

Indian Institute of Technology Guwahati

Guwahati – 781039, Assam, India

DEDICATION

This Thesis is dedicated to my mother – Mrs. Pratima Mallick for inspiring and guiding me in every step to success with profound wisdom

Acknowledgements

It gives me immense pleasure to extend my sincere gratitude to acknowledge each individual who led me to the completion of the dissertation. I am highly obliged to all the people who have encouraged me during all these years.

First and foremost, I would like to express my sincere thanks to my thesis supervisor, **Prof. Prabu Vairakannu**, for providing relentless support and valuable guidance in various stages of my research journey. His positive attitude and encouragement boosted my inner confidence and helped me to excel even after multiple failures. I am fortunate that he took me under his wings and considered me working under his esteemed guidance. I am greatly indebted for sharing his profound knowledge with me. I have thoroughly enjoyed working with him and I strongly believe that he brought out the best in me in every aspect.

I am also grateful to my doctoral committee members **Prof. Subrata K. Majumder**, **Prof. Pankaj Tiwari** and **Prof. Soumen Kumar Maiti** for reviewing my work and providing their valuable suggestions, which definitely had helped me in improvising my work.

I would like to convey my sincere thanks and gratitude to all the faculty members and staffs of Department of Chemical Engineering, IIT Guwahati for providing me with all the required facilities. I am also thankful to all the centres associated with the instrument facilities for the characterization purposes such as the Analytical Lab Facility (Department of Chemical Engineering), Central Instrument Facility (IIT Guwahati), Guwahati Biotech Park and Sophisticated Analytical Instrument Facility (IIT Bombay).

I would like to thank my lab mates and friends Dr. Barnali Bhui, Dr. Pradeep Sahu, Mr. Shekhar Jyoti Pathak, Mr. Koushik Jena, Mr. Rushabh Kale, Dr. Kakali Priyam Goswami, Mr. Partha Pratim Baruah, Mr. Uttkarsh Goyal and Mr. Gaurav Sharma for their constant help and support in smooth completion of my degree. I thank each one of them for their continuous and timely assistance.

Last but not the least, I will always remain indebted to my mother – Mrs. Pratima Mallick for being the pillar of my life and standing by me throughout this journey. I will always remain reverent and bow down to the Almighty for bestowing blessings on me. It is their blessings that kept me motivated to stay stronger and work harder.

Roni Mallick

Table of contents

ABSTRACT

Poor degradability of plastics and e-waste present in municipal solid waste (MSW) causes severe soil and water contamination. In the cycle of waste generation and management, the recovery of energy from solid wastes through highly efficient and low pollutant technology is a promising way. Hence, the current study focuses on clean syngas production via plasma gasification of mixtures of solid waste termed as refused derived fuel (RDF), computer keyboard plastic waste (CKPW) and electrical switch waste (ESW). A large proportion of plastic waste (35 wt.%) is present in RDF, besides yard (40 wt.%), paper (10 wt.%) and food waste (15 wt.%). High-density polyethylene (HDPE), low-density polyethylene (LDPE), polyethylene (PE), etc., are the major contents of plastic waste in RDF. Similarly, in CKPW plastics, acrylonitrile butadiene styrene (ABS) is found to have the largest share of 30%, followed by polycarbonate (PC). The recycling rate of ABS from the solid waste stream is only 25%. Among the thermosets, phenolic resin, with the trade name of bakelite (BAK), is the most widely used material in the ESW due to flame retardant properties, high hardness and good thermo-oxidative stability. Such complex compounds make the plastic and e-waste difficult to recycle or undergo thermal degradation without pollutant generation. Subsequently, these wastes create human hazards upon accumulation and further release toxic components by conventional degradation methods. Thus, plasma gasification is the best suited technology to process solid waste. Plasma gasification offers great advantages over conventional gasification in terms of higher carbon conversion and low tar content due to high reaction temperature.

The single-stage thermal plasma gasification of RDF, CKPW and ESW is carried out in a carbon dioxide (CO_2) atmosphere using a non-transferred plasma torch. Carbon dioxide is chosen as the gasification agent for the following reasons: (i) to reduce net CO_2 emissions in the environment through consumption, (ii) lower energy required to capture and utilize than

other gasifying agents and (iii) the ability to liberate oxygen-free radicals for producing syngas-rich gaseous products. On a laboratory scale, several experiments are conducted to assess the impact of solid feedstock mass flow rate, feed CO_2 gas flow rate and plasma torch power on the syngas concentration and yield. A 3-E analysis comprising cold gas efficiency (CGE), exergy efficiency and levelized cost of syngas (LCOS) is performed, considering all the feeds. A high-quality syngas with H_2 (32.23 vol.%), CO (51.98 vol.%) content, possessing a lower heating value of 16.46 MJ/m^3 and CGE of 39.04% is obtained for CKPW at the maximum power of plasma torch (2 kW). A medium LHV of 6.16-10.20 MJ/m^3 is found for all ESW feed cases. However, with process parameters of 30 g/10 min, 0.4 lpm and 0.75 kW, a higher CGE of 49.90% and exergy efficiency of 48.30% are achieved using RDF feed. While the lowest LCOS value of 23.40 INR/kWh is estimated for CKPW feed and the highest (62.44 INR/kWh) for ESW feed at their respective optimum condition. This is attributed to the amount of combustible fractions present in the CKPW feed in terms of C and H and the thermal degradation behavior resulted in a higher energy produced per unit cost involved in the plasma gasification.

The obtained by-products in the form of oil and solid residue are characterized for a better understanding of the plasma reactions and potential applications of the products. The proximate and ultimate analysis of oil obtained from CKPW feed showed properties similar to diesel, with high C (90.8 wt.%), H (6.8 wt.%) and LHV (39.13 MJ/kg), and low O (0.46 wt.%) content. A slight lower in viscosity (3.93 cP), density (0.91 g/ml) and increase in pH (6.94) of the CKPW-based oil are beneficial to avoid engine damage. Whereas, the residue of RDF has high ash content of 13.95 wt.%. Ash contains a good amount of Ti, Ba, Ca, Si, Al, etc., which can find applications in healthcare, paints, dye-casting and the cement industry after enrichment. The reaction mechanism of individual feeds to syngas and other products under plasma conditions is also proposed. Finally, an empirical correlation is developed to predict the composition of

each component, calorific value and CGE of the syngas with the experimental results using SPSS software.

Two newly emerging technologies, (a) molten carbonate fuel cell (MCFC) and (b) chemical looping reforming (CLR), are integrated with plasma gasification for hydrogen and electricity production for various system configurations. The simulation of the plants is performed using Aspen plus and consequently, 4-E (energy, exergy, economic and environmental) analyses are executed. Different plant scenarios involving plasma gasification integrated steam turbine (IPGST) with MCFC based on syngas splitting ratio to pressure swing absorption (PSA) and MCFC are considered using RDF feed. The highest energy and exergy efficiencies attained are 54.12% and 52.02% for the system Syngas:CH_4 [PSA: MCFC], respectively. Moreover, considering all the configurations, the cost of electricity (COE) ranges between 77.48 and 107.93 $/MWh, while the levelized cost of hydrogen (LCOH) is between 1.01 and 3.94 $/kg. Likewise, the introduction of MCFC for 0:100 [PSA: MCFC] case reduced the annual CO_2 emissions ~5 times than of 100:0. On the other hand, the feeds such as CKPW and ESW are considered for plasma gasification integrated CLR, working at two pressure levels (1 bar and 15 bar). Based on the simulated results, the net overall energy efficiency is found higher for CKPW (72.35%) than ESW (64.92%) at the base case (i.e., 0% excess OC or air), while the net overall exergy efficiencies are lower by 15% for ESW and 3% for CKPW on average, compared to energy efficiencies. In addition, the COE for all cases remains below 111 $/MWh for ESW and 76 $/MWh for CKPW, while the LCOH lies in the range of 1.7-2.3 $/kg for ESW and 0.8-1.7 $/kg for CKPW. Likewise, the power plants fed with CKPW assured higher sustainability from the ecological point of view as all carbon is captured and stored.

Thus, the experimental study on high-temperature CO_2 plasma gasification using RDF, CKPW and ESW feed and the corresponding 3-E analyses inferred that treating such wastes can be a feasible and economical route for waste-to-energy conversion. Given the high energy

output and low carbon emission, the plasma gasification process is an efficient route to achieve the sustainable development goals (SDGs). Moreover, the wastes seem to be an encouraging feed towards hydrogen and electricity co-generation via plasma gasification technique integrated with MCFC and CLR, except for higher initial investment. Based on the 4-E analyses, a selective fuel with a good heating value is the best option for an energy-intensive plasma gasification process.

Keywords: Plasma gasification, Refused derived fuel, Computer keyboard plastic waste, Electrical switch waste, Molten carbonate fuel cell and Chemical looping reforming.

List of Tables

List of Figures

Chapter 3

Chapter 4

Chapter 5

Nomenclature

T	Temperature, °C or K
$\dot{W}$	Power produced, MW
$\dot{E}$	Energy or Exergy flow rate, MW
T_0	Atmospheric temperature, °C or K
$\ddot{E}$	Emission rate, kg_{CO2} MW h^{-1}
h	Specific enthalpy, J mol^{-1}
s	Specific entropy, J mol^{-1} K^{-1}
e_{ch}	Standard chemical exergy, J mol^{-1}
y	Mole fraction
$\dot{m}$	Mass flow rate, kg s^{-1}
Quot	Quotation
r	Annual interest rate, %
k	Payback period, years
C	Cost, $
P	Equivalent period of utilization, h/year
f	Annuity factor
p	Partial pressure

Subscripts

m	moisture
gp	Plasma gasifier
in	Inlet
out	Outlet
F	Feed
xd	Exergy destruction
elec	Electrical
en	Energy
ex	Exergy
ph	Physical
ch	Chemical
i	Single component

Superscripts

f	Scaling factor
a	Annual
k	Payback period

Greek symbols

β	Correlation factor
Ɛ	Annual emissions
η	Efficiency

Abbreviations

4-E	Energy, exergy, economic and environment
ABS	Acrylonitrile butadiene styrene
AR	Air reactor
ASTM	American society for testing and materials
ASU	Air separation unit
AT	Air separation unit
BAK	Bakelite
CAGR	Compound annual growth rate
CAPEX	Capital expenditure
CC	Combustion chamber
CCLS	Compression, cooling and storage
CCS	Carbon capture and storage
CCU	CO_2 compressor unit
CGE	Cold gas efficiency
CHP	Combined heat and power
CKPW	Computer keyboard plastic waste
CLC	Chemical looping combustion
CLR	Chemical looping reforming
COE	Cost of electricity
DC	Direct current
DCM	Dichloromethane
DHW	Domestic hot water
DTG	Derivative thermogravimetric
EDS	Energy dispersive spectroscopy
ESW	Electrical switch waste

FESEM	Field emission scanning electron microscopy
FID	Flame Ionization detector
FR	Fuel reactor
FTIR	Fourier transform infrared spectroscopy
GC	Gas chromatography
GTU	Gas turbine unit
GWP	Global warming potential
HDPE	High density polyethylene
HPST	High pressure steam turbine
HRSG	Heat recovery steam generator
HTR	High-temperature reactor
IGCC	Integrated gasification combined cycle
INR	Indian rupee
IPGCC	Integrated plasma gasification combined cycle
IPGST	Integrated plasma gasification steam turbine
LCOH	Levelized cost of hydrogen
LCOS	Levelized cost of syngas
LHCs	Lower hydrocarbons
LHV	Lower heating value
LPST	Low pressure steam turbine
LTR	Low-temperature reactor
MCFC	Molten carbonate fuel cell
MEA	Monoethanolamine
MPST	Medium pressure steam turbine
MS	Mass spectrometry
MSW	Municipal solid waste
NPV	Net present value
OC	Oxygen carrier
OPEX	Operating expenditure
PAHs	Polyaromatic hydrocarbons
PC	Polycarbonate
PCCI	Purchasing power parity index
PER	Plasma energy ratio
PG	Plasma gasification
PP	Pollution potential
PPPI	Power capital cost index
PSA	Pressure swing adsorption
SI	Sustainability index
SMR	Steam methane reforming
SOFC	Solid oxide fuel cell
SPECO	Specific exergy cost
SR	Steam reactor
STU	Steam turbine unit
RDF	Refused derived fuel
RF	Radio frequency
TCD	Thermal conductivity detector
TGA	Thermogravimetric analysis
TPD	Tonnes per day
WTE	Waste-to-energy
XRD	X-ray diffraction

Chapter 1

Introduction

CHAPTER 1

INTRODUCTION

The initial section of this chapter presents a brief introduction to the waste generation scenario and its composition worldwide. The detrimental effects of these wastes on the well-being of humans and the environment in terms of climate change are discussed. Based on the waste management hierarchy, an advanced emerging technology known as plasma gasification (PG) is identified as the promising technique to convert complex waste to energy (WTE) with almost zero environmental impact. Further, the global energy demand scenario, emissions released from such sectors and the decarbonization technologies of molten carbonate fuel cell (MCFC) and chemical looping reforming (CLR) for producing hydrogen and electricity are outlined. The motivation behind the research formulation is based on the scope and importance of the plasma gasification process in the thermochemical conversion field. Finally, the basic outline of the doctoral work is summarized.

1.1. Waste generation and its composition

Industrial Revolution 4.0 originated in 2011 led to a rapid increase in the generation of untreated waste, which is due to the growing population, economic growth and globalization. The per capita waste generation in the year 2016 ranges from 0.11-4.54 kg/day and is expected to increase by 19-40% till 2050 worldwide. The world generated around 53.6 Mt of E-waste, with an average of 7.3 kg per capita in 2019. The quantity and composition of waste generated depend on a specific country's income level and geographical zone. Currently, the East Asia and Pacific region generate 23% of the world's waste, while South Asia and the Middle East are the fastest growing regions and are expected to double their waste by 2050, as illustrated in Fig.1.1 (The World Bank, 2022). In India, there has been a marginal change in per capita waste

generation (kg/day) over the last six years and it is estimated to rise 2.5 times by 2031 (Center for Science and Environment, 2021). Continuous solid waste disposal has always been a worldwide issue relating to the safety of the environment and public welfare.

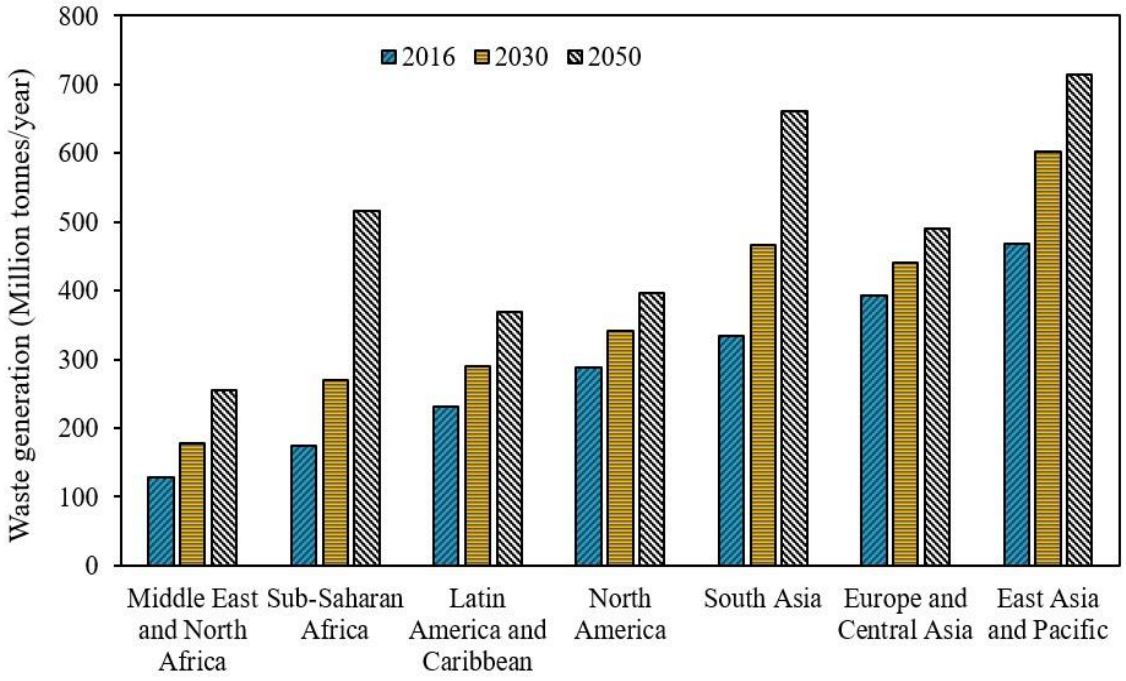

Fig.1.1. Projected waste generation, region-wise (million tonnes per year) (Kaza et al., 2018).

On average, 44% of the global municipal solid waste (MSW) comprises food and green waste, followed by paper and cardboard (17%), plastics (12%), etc. (OECD, 2023; United Nations Environment Programme, 2021). Moreover, the segregation of MSW into combustible and non-combustible components can be a viable solution to utilize the waste efficiently. The fraction of organic waste decreases and dry waste, such as plastic, paper, etc., increases with the economic development of a country. The combustible portion is known as refused derived fuel (RDF) and consists primarily of plastics, paper, cardboard, textiles, wood, food, etc. Although the composition of waste in RDF varies across regions, the content is approximately similar. In general, plastics and paper majorly account for 50-80%. RDF can potentially be another energy source as it has a higher calorific value ranging from 18-23 MJ/kg on a dry

basis (Yang et al., 2021). The usage of RDF was explored in Indian industries like iron and steel, thermal, cement and brick kilns. It possesses negative concerns on the product quality, thermal stability and release of toxic gases (Ministry of Housing and Urban Affairs, 2018). In recent times, Covid-19 has magnified the production of healthcare waste in terms of personal protective equipment (PPE) such as masks, gloves, face shields, etc., and household waste due to lockdown and suspension of reusable items in stores (UNEP, 2020). Plastics have become a basic part of general waste due to their low manufacturing cost and a broad range of applications such as packaging, automotive, electrical and electronics (Lopez et al., 2018). Plastic waste is also a source of greenhouse gas emissions, accounting for 3.4% of the global average (OECD, 2022). Among the plastic produced worldwide, polyolefins account for half of the production and the rest as polyethylene terephthalate (PET), high-density polyethylene (HDPE), polypropylene (PP), polystyrene (PS) and others. The infamous "other" category includes acrylonitrile butadiene styrene (ABS), polycarbonate (PC), bakelite (BAK), polymethyl methacrylate (PMMA), etc. This does not belong to any of the recycling codes or is a mixture of many types of plastics and is indicated as the #7 category (Jung et al., 2018; Tod Hardin, 2021). Compared to 2018, the market demand for plastics (thermoplastics and thermosetting) has grown at a compound annual growth rate (CAGR) of 5.2%. Thermoplastic resins such as polyethylene terephthalate (PET), acrylonitrile butadiene styrene (ABS), nylon, etc., are easier to reshape and degrade on heating than thermosets like phenolic resins or bakelite, polyurethane (PU), etc. (Data Intelo, 2022).

1.2. Effects of greenhouse gas emissions from waste

Nearly 1.6 billion tonnes of waste-associated CO_2 equivalent greenhouse gas were emitted in 2016 alone and it is estimated to rise to 2.38 billion tonnes/year by 2050 if no developments are made. The anaerobic decay of the waste and exposure to solar radiation produce greenhouse gases. Landfill methane (CH_4) is the largest contributor of greenhouse gases released from

post-consumer waste, followed by nitrous oxide (N_2O) and carbon dioxide (CO_2) (Birkmann et al., 2022; Bogner, 2007). Therefore, the management of solid waste has huge implications affecting individual's daily health, contaminating water bodies, blocking drains and causing floods, spreading diseases through breeding vectors and disturbing economic growth via reduced tourism (Kaza et al., 2018; Wilson et al., 2015).

1.3. Waste management methods

Based on the concept of 3R's (Reduce, Reuse and Recycle), the waste management hierarchy is shown in Fig. 1.2. Landfilling in a controlled or uncontrolled manner is the least preferable choice due to the ill effects caused to both land and water body (Wang et al., 2019). More than one-third of the solid waste is disposed of in some type of landfill, 33% is openly dumped, 19% is recycled and the rest is incinerated. While for plastic waste, the incineration process contribution drops to 19% and recycling to 9%, with almost 40% ending in residues. Moreover, higher expenditure, contaminants released during incineration, limited landfill space, unsuitable recycling, etc., are some of the major problems related to disposal (Sanito et al., 2020; Striūgas et al., 2017).

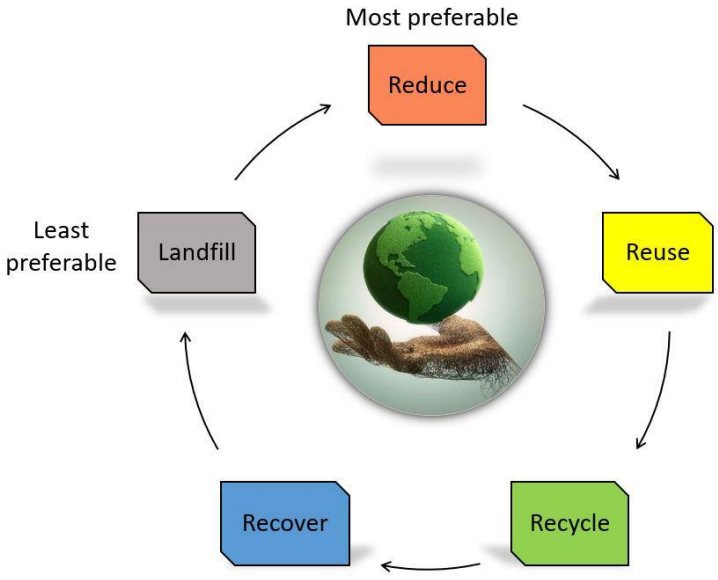

Fig. 1.2. Waste management hierarchy.

Another method of avoiding disposal is to recover the maximum extent from these non-conventional sources via waste-to-energy (WTE) techniques such as incineration, pyrolysis and gasification (UNEP, 2020). There is a growth in the alternative fuel market, especially with the waste that cannot be reused, recycled and recovered (Jagodzińska et al., 2019). A standard waste-to-energy (WTE) plant can generate about 550 kWh/ton at an average revenue of 20-30 $/ton (Environmental Protection Agency, 2023). The different routes of processing waste are shown in Fig. 1.3. Understanding the effective utilization and management of waste allows the local government in both developed and developing countries to formulate policies and strategies for future demand. Most of the studies in scientific literature and the real world are mainly based on the incineration process, whereby the technology offers to recover heat from the combustion of waste in a controlled oxygen-rich environment. However, the incineration process pollutes the atmosphere with the emission of ash, SO_x, NO_x, chlorine and dioxins (Sanito et al., 2020).

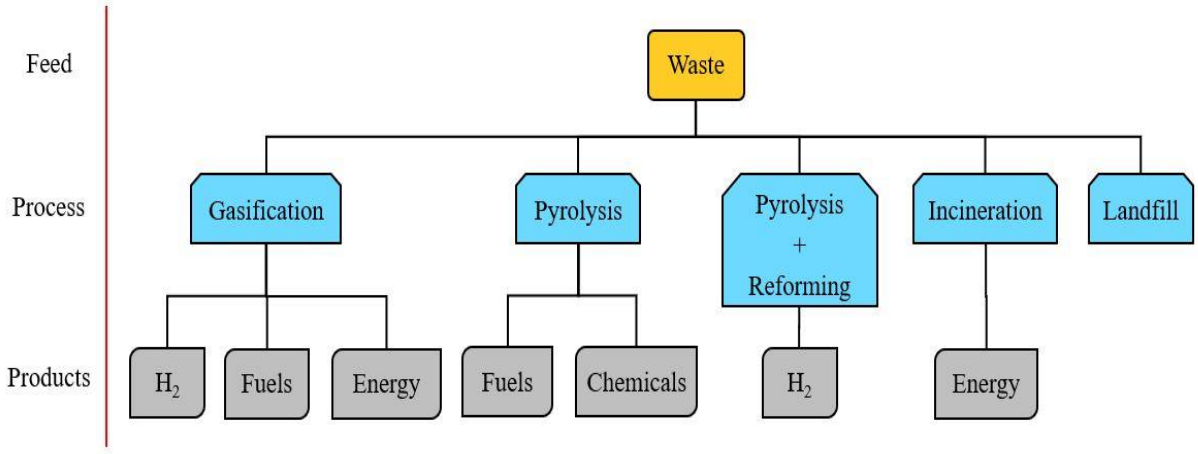

Fig. 1.3. Different routes of processing waste for valuable products.

On that note, gasification proves to be a promising technique for converting the combustible components in the fuel to a high calorific value syngas consisting mainly of H_2, CO, CH_4 and CO_2. However, conventional methods of gasification relatively at a low temperature of 700 °C

produce tar residue consisting of unconverted solid, high-boiling organic compounds and other solid-entrained particles in the product gas (Shen et al., 2019; Zhang and Pang, 2019). The calorific value of synthesis gas (6.1 MJ/Nm^3) obtained from biomass gasification has low to moderate utility and the syngas of high ash Indian coal has a heating value of ~ 3.58-4.81 MJ/m^3 (Gupta and De, 2022; Umeda et al., 2019). The drawback of having a high amount of heavier hydrocarbons (tar) in the syngas and the difficulty possessed in handling a large volume of inorganic substances in MSW limited its application. Moreover, co-gasification of biomass with waste can enhance the quality of the syngas (~ 7 MJ/Nm^3) and coal with biomass can also reduce fossil-derived CO_2 emissions (Barontini et al., 2021; Bhoi et al., 2018; Spiegl et al., 2021). The distribution of syngas production based on feedstock and application in various sectors is shown in Fig. 1.4. The utilization of the waste towards syngas constitutes less than 1% of overall feedstocks available for energy conversion (Khan H, 2018). More studies are still carried out on the gasification process for power generation (Nanda and Berruti, 2021). Therefore, there is a need to research and develop more robust and environmentally friendly technology that utilizes waste effectively.

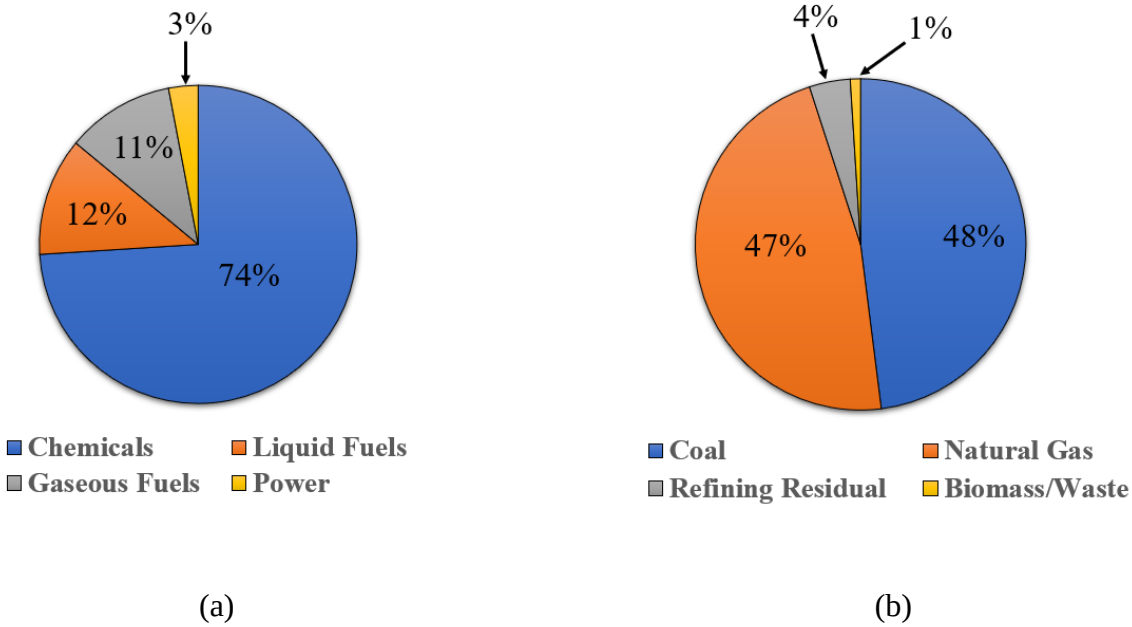

(a) (b)

Fig. 1.4. Global syngas distribution (a) by application and (b) by feedstock.

1.4. Plasma gasification of waste

Plasma gasification in Fig. 1.5 is an exclusive way of converting any type of fuel into clean syngas and vitrified slag at very high temperatures, achieving almost zero pollutant emissions. The heat is supplied externally for creating plasma in a torch. This plasma develops gasification reactions and further enhances the reforming reactions in the gas phase by cracking the undesirable complex hydrocarbons (tars) and dioxins in the syngas into simpler molecules of H_2 and CO (Agon et al., 2016; Jiang et al., 2021; Minutillo et al., 2009). Due to the high energy density and high temperature of plasma, a large waste throughput can be accommodated in the plasma reactor with lower residence time, fast start-up and shutdown (Sikarwar et al., 2020). In plasma gasification, the nitrogen in the feedstock remains unchanged and sulfur gets converted into hydrogen sulfide (H_2S) and carbonyl sulfide (COS), preventing the formation

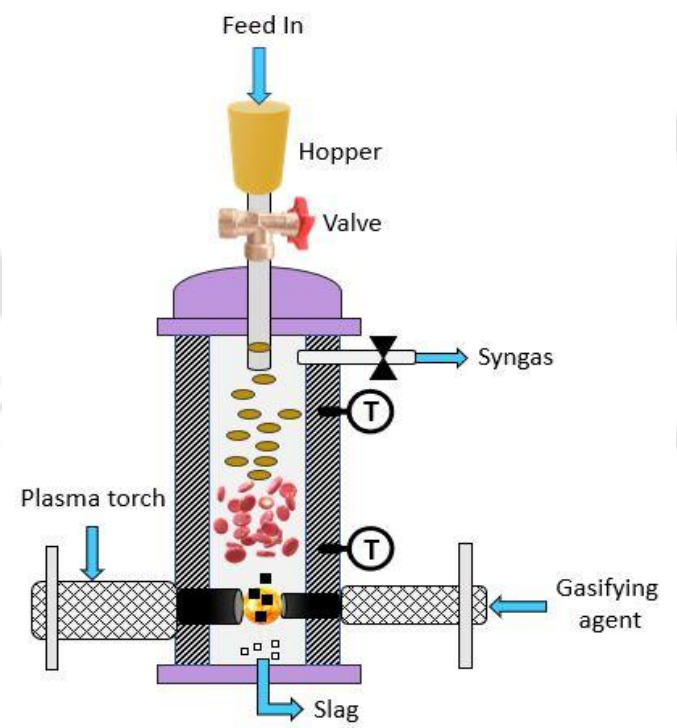

Fig. 1.5. Typical representation of a plasma gasifier.

of nitrogen and sulfur oxides (NO_x and SO_x), respectively (Munir et al., 2019). The only limitation of plasma torches is the high specific energy consumption, which can be as high as approximately 30% of the calorific value of MSW (Kwon and Im, 2022).

The plasma gasification of high calorific RDF and different grades of complex plastic waste, such as ABS and BAK can provide the impetus for the production of affordable and clean energy as part of Goals 3, 7, 11 and 12 of the Sustainable Development Goals (SDGs) of the United Nations (Department of Economic and Social Affairs, 2023). In recent years, this novel approach has undergone comprehensive research for the assessment of organic waste disposal including radioactive waste, bio-medical waste, automobile shredder residue, asbestos fibers and municipal solid waste (MSW) (Kim et al., 2003; Tang et al., 2013; Tzeng et al., 1998). High temperature and energy density, high destruction efficiency and energy recovery, the flexibility of waste, the ability to generate co-products and environment compatibility are the benefits of this plasma technology (Sikarwar et al., 2020).

1.5. Energy (hydrogen and electricity) production statistics in India and worldwide

Globally, the electricity demand will increase at the rate of 2.1% per year, which is twice the primary energy demand by 2040. This is resulting due to the rising household incomes, electrification of transport and the growing nature of digitally connected devices. The electricity demand is led by Asia, with India standing in the second position at 20% share. Although coal and natural gas's yearly growth rates for power production are less than wind and solar PV, they share around 47% of overall electricity production (Energy Agency, 2021; Mondial L, 2013). As per the National Power Portal (NPP), India has an installed capacity of ~404 GW, out of which 58% is produced from thermal sources, 39% from renewables (only 0.43% is from waste-to-energy) and the rest is from nuclear sources (Central Electricity Authority, 2022). Most of the coal-air steam turbine plant configuration of National Thermal

Power Corporation (NTPC), India, under sub-critical conditions, has a net efficiency in the range of ~20-24% with a carbon capture and storage unit (CCS). The cost of electricity (COE) using different carbon-absorbing mediums under post-combustion conditions varies in the range of 90-115 $/MWh (Singh et al., 2017).

In the last few years, hydrogen (H_2) generation has been the subject of interest for many governments and organizations including India (Will Hall, 2020). Based on the process and source of production, it is color-coded into 4 categories as shown in Fig. 1.6. Hydrogen is a clean fuel with several end-use in the industries (steel, chemical and refinery), transport (shipping, aviation, car, etc.), heating and power generation sectors. At present, 95% of the global H_2 production is from coal and natural gas, and 5% from electrolysis as a by-product of chlorine production (Renewable Energy Agency, 2020). The most common method for H_2 production is steam-based methane reforming (SMR), where light hydrocarbons break in the presence of a catalyst to produce H_2 and carbon dioxide (CO_2) (Giuliano et al., 2018). However, the energy penalty and the operating cost increases for hydrogen production owing to the electric power consumption, high cost of working fluid and equipment due to the capture of CO_2 either through amine-based absorption or pressure swing adsorption (PSA) (Cabello et al., 2022). Global CO_2 emissions could be reduced either by improving thermodynamic efficiency, boosting the utilization of renewable energy sources, or implementing carbon capture and storage (CCS) methods (Cormos et al., 2020). As mentioned earlier, CCS methods are expensive, whereas renewable sources of energy are intermittent in nature. Therefore, enhancing overall plant efficiency becomes highly imperative through cogeneration methods by the combined production of heat, power and hydrogen.

Recovering 10-20% of H_2 using a palladium membrane with a cost of 9200 €/m^2 and hydrogen selling price of 3 €/kg from an integrated gasification combined cycle (IGCC) power plant can reduce the mitigation cost of 90% captured CO_2 to below 5 €/ton_{CO2} with COE values

of 50 €/MWh (Giuliano et al. 2018). While, the specific exergy cost (SPECO) of H_2 (208.6 $/GJ) separated from syngas through PSA obtained from plasma gasification of sewage sludge is found higher due to the low concentration of H_2 in the produced gas. This was basically due to the largest exergy destruction in PSA (51.25%) and plasma gasification reactor (28.79%) (Kalinci et al., 2011).

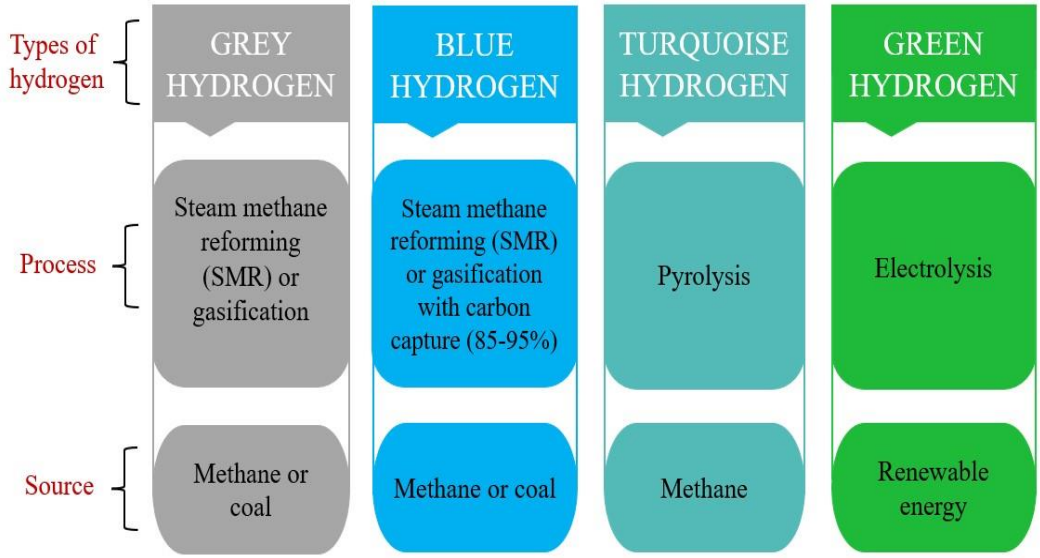

Fig. 1.6. Different shades of hydrogen.

1.6. Status of emissions from the energy sector and mitigation strategies

Greenhouse gases are a natural part of the earth's atmosphere and maintain the planet's energy at an average temperature of around 1.5 °C. However, developmental activities and growing energy demand have consistently increased the carbon dioxide (CO_2) in the air to 149% of the pre-industrial level since the last century (Shaftel et al., 2022; World Meteorological Organization, 2021). The energy sector, including transportation, heat and electricity, fuel combustion, etc., is the biggest contributor of 76% of anthropogenic greenhouse gas emissions worldwide, among which heat and electricity contribute 31% of emissions. Even though the per capita CO_2 emissions are lower for India, still the carbon intensity of the power sector is above the world average. In this regard, the attributes of future

energy systems should reduce the carbon economy, among which renewable sources of energy are the most favorable choice for power generation and the decarbonization process, as suggested by the global climate conventions (UNFCCC, 2021). Shifting to renewable energy, more balanced agricultural practices, curbing forest degradation, electrifying transportation and producing less waste are some of the major steps in reducing emissions (Energy Agency, 2021; Ge et al., 2020). Renewable sources of energy are largely non-dispatchable (intermittent) in nature and thereby unable to cater the constant energy supply. These put additional pressure on the fossil fuels-based energy systems or alternatives (waste-to-energy) that have the potential to replace, at least partially the fossil route (Cormos et al., 2020). While nuclear energy has a very high energy density and emits lower greenhouse gas, on the other hand, it suffers from several drawbacks such as accidents, security threats, enrichment, and waste leaving radioactive particles in the environment, etc. ("The Pros & Cons of Nuclear Energy: Is it safe?," 2018).

Therefore, more robust technologies are required to improve the thermodynamic efficiency, minimize the COE and limit carbon emissions. These can be done either by producing clean energy in the form of hydrogen (H_2) and by using methods that consume carbon dioxide (CO_2) or by combining both. Conventional technologies related to combustion and gasification are practically feasible to handle the waste. However, their commercial relevance has been limited due to high operational investment costs and the formation of pollutants (Belgiorno et al., 2003; Conesa et al., 2020).

Current studies focus on notable technology, such as plasma gasification (PG), which is effective for a wide range of fuels. A high volume (~ 60 vol%) of hydrogen can be recovered from the syngas of the plasma gasification process, followed by pressure swing adsorption (PSA) technique with low energy penalty (Kalinci et al., 2011). H_2 has potential applications in manufacturing industries, transport and power generation sectors (Renewable Energy

Agency, 2020). A drawback of plasma technology is the high electric power consumption of the plasma torch. The integration of plasma gasification with molten carbonate fuel cell (MCFC) and chemical looping reforming (CLR) systems can overcome the high energy penalty associated with plasma generation. The high operating temperature (650-1000 °C) of the MCFC and CLR system improves the efficiency by capturing the waste heat in Heat Recovery Steam Generator (HRSG) for cogeneration (heat and power) (Duan et al., 2015). MCFCs offer a high level of system integration and the use of CO_2 as reaction gas at the cathode. It also allows gaseous feed of low heating value as input to the system and makes sufficient heat and power available at the exhaust (Wee, 2014). Further, integrating with the CLR process helps in the proper utilization of the oxygen carriers (OC) in the system, thereby increasing the overall efficiency of the power plant and reducing specific emissions of carbon. Combining the environmental strength of both processes could bring down the ecological footprint on a large scale.

Although fuel cell and chemical looping reforming mechanization have not yet come to industrial maturity and most experimental activities on these technologies have been ongoing, their performance characteristics are widely studied by varying the operating parameters (utilization factor, temperature, excess OC, etc.). Numerical modeling plays a vital role in the validation of the system performance based on the experimental results or predicting their behavior. The simulations can also be useful in guiding research studies in power plants and the mode of their application (Falcucci et al., 2012).

1.7. Motivation behind the proposed research

Under the circumstances mentioned above, the recovery of energy from waste for electricity and hydrogen cogeneration can bridge the gap of growing energy demand. Moreover, it proposes an alternative solution to the existing issues about waste management. Although the

thermochemical conversion method of plasma gasification is energy intensive but is capable of producing high calorific value syngas even with low-grade (lower LHV) fuels. The product from this route can be directly used in power-generating systems such as steam turbine units (STU) and gas turbine units (GTU) or reformed further in processes like fuel cells and chemical looping with low carbon emissions. The motivation for the stated research is outlined below:

- In municipal solid waste, large quantities of combustible fractions in the form of refused derived fuel (RDF), including large amounts of plastics, can be found. These require specific investigation before processing in order to make the system more flexible in handling feedstock, reduce operational difficulties and increase energy output.
- The fuels of interest in this work are RDF, computer keyboard plastic waste (CKPW) and electrical switch waste (ESW). RDF comprises a mixture of various plastics and biomass such as paper, yard and food waste. While CKPW is a combination of acrylonitrile butadiene styrene (ABS) and polycarbonate (PC), ESW is mainly of bakelite and polyamide.
- The materials are neither open for recycling due to its end-of-life (EOL) use nor safe for open dumping. The presence of butadiene and styrene in thermoplastics and phenol formaldehyde in thermosets generates toxic organic compounds (pollutants) upon conventional thermal degradation.
- The rise of global energy demand (mainly electricity) and international commitments such as the Basel Convention (waste disposal), Stockholm Convention (reduce persistent organic pollutants) and Paris Agreement (limit global warming) provide the impetus for robust mechanisms. Additionally, the global market of clean energy technologies is expected to be around USD 600 billion per year by 2030 i.e., three times the current scenario.

- Plasma gasification is a high-temperature allothermal process that utilizes the combustible fractions into clean syngas and inorganics to inert slag. Even a moderate amount of carbon and hydrogen in the fuel can be utilized by thermal plasma to produce a good heating value of syngas.
- Further, integrating plasma gasification with the emerging technologies of fuel cells, chemical looping, etc., for electricity and hydrogen cogeneration is beneficial from a thermodynamic and ecological perspective. Combining the environmental strength of the processes could bring down the specific emissions of carbon on a large scale.

1.8. Organization of the thesis

The current thesis comprises of eight (8) chapters and the organizational structure is represented in Fig. 1.7. The principal content of these chapters is described below:

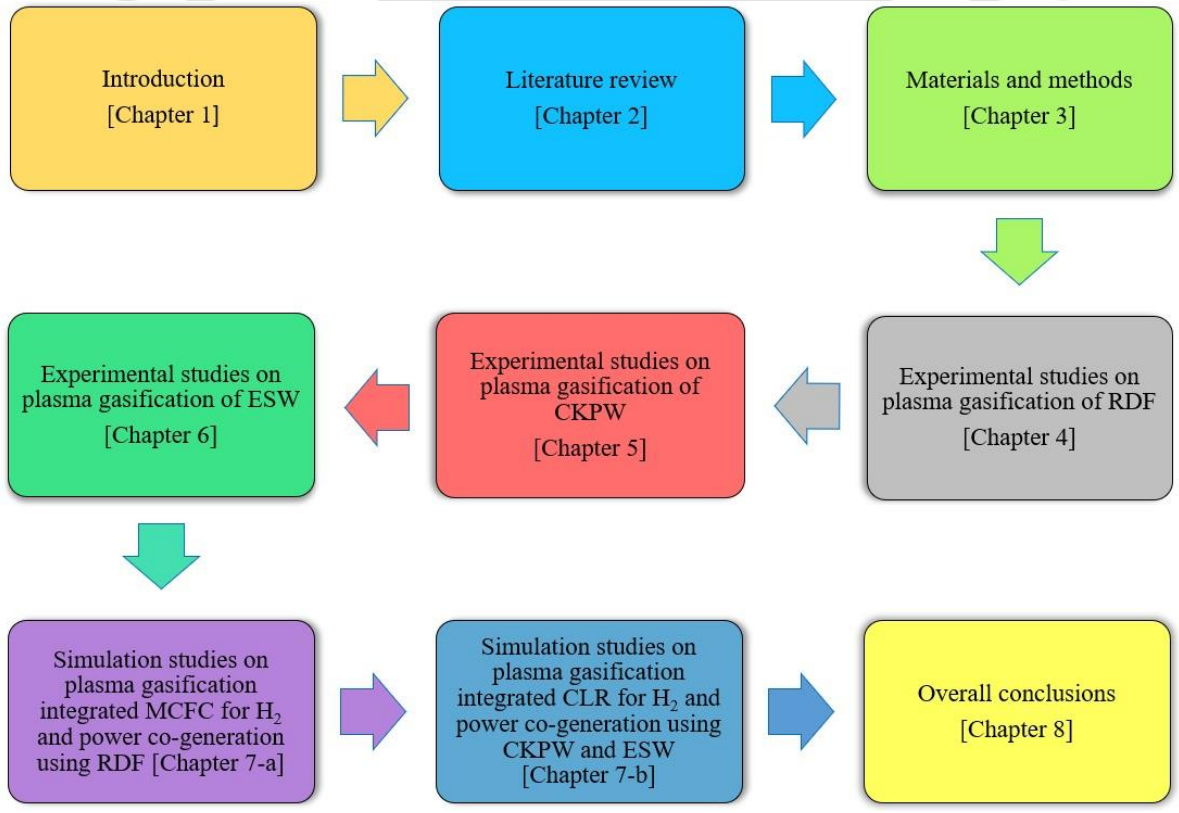

Fig. 1.7. Graphical representation of the thesis.

Chapter 1 gives a layout of the solid waste generation and management issues worldwide and their effects on the environment. The prospect of energy recovery from waste through the plasma gasification route is discussed with potential downstream applications for H_2 and power cogeneration.

Chapter 2 presents a detailed literature review of the plasma gasification process. The properties of different feedstocks, technologies involved, factors affecting the product and end-use real-scale applications are thoroughly discussed.

Chapter 3 emphasizes the materials and methods considered in the current study. The various characterization techniques employed pre- and post-plasma gasification processes, such as GC, TGA, FTIR, etc., are explained. The key factors including the feedstock, experimental set-up description and parameters, are presented. In addition, the method to estimate 3-E (Energy, Exergy and Economic) analysis is explained. Further, the methodology for electricity and hydrogen cogeneration using Aspen Plus based on 4-E analyses (3-E plus Environmental) is detailed.

Chapter 4 presents the experimental findings obtained under plasma gasification of refused derived fuel (RDF) with CO_2 as a gasifying agent. The effect of feed rate, CO_2 gas flow rate and torch power on the products are studied to estimate the optimum operating conditions based on the 3-E analysis. Moreover, a correlation and reaction mechanism are developed centered on the different product characterization.

Chapter 5 investigates the experimental results of CO_2-based plasma gasification using computer keyboard plastic waste (CKPW) comprising acrylonitrile butadiene styrene (ABS). An inclusive analysis centered on 3-E is conducted to determine the feasibility of the process, followed by the analogy and reaction mechanism.

Chapter 6 discusses the experimental outcomes of plasma gasification using bakelite-based electrical switch waste (ESW) under CO_2 atmosphere. The resultant products are analyzed to estimate the optimum operating conditions based on the findings of 3-E analysis. Lastly, a reaction mechanism and relationship are proposed that correlates the actual and measured values.

Chapter 7 focuses on the 4-E (Energy, Exergy, Economic and Environmental) analyses of plasma gasification integrated with molten carbonate fuel cell (MCFC) and chemical looping reforming (CLR) using RDF, CKPW and ESW feedstocks for cogeneration of H_2 and electricity. The effect of different syngas ratios to pressure swing adsorption (PSA) unit and MCFC on the 4-E results is studied using RDF feed. On the other hand, the influence of excess oxygen carrier (Fe_2O_3 in this case), steam and air in the CLR unit on the 4-E analyses is studied using CKPW and ESW.

Chapter 8 summarizes the overall conclusions drawn from the above chapters and the scope of future works.

Chapter 2

Literature review

CHAPTER 2

LITERATURE REVIEW

This chapter provides a comprehensive literature review and emphasizes on the types of fuel properties, followed by a short description about the associated technologies in the present study. Several key parameters that influence the compositions of syngas like feedstock, torch power, gasifying medium, etc., are discussed based on the literature. The usage of residue (slag) of plasma gasification is discussed. Finally, the application of the product gas obtained by plasma gasification is reviewed for electricity generation with a major focus on real-scale industrial developments by simulation studies.

2.1. Fuel properties

Fuel characteristics such as proximate analysis, elemental composition and calorific value possessed by the various types of waste are presented in Table 2.1. It can be noticed that waste in general, has a very low heating value (LHV), which can be attributed to the high amount of moisture content (maximum of ~58%). Moreover, due to lower fixed carbon and higher volatile matter, the thermal cracking process plays a vital role in the reaction as a low amount of carbon (solid) remains for the reduction/oxidation reaction. The elemental C, H and O are profound in all cases except the derivatives of sludge, which also depend on the source point and result in either a high amount of moisture or ash content. Refused derived fuel (RDF), an enhanced form of municipal solid waste (MSW), and medical waste are the better-quality fuel for the waste-to-energy process due to their higher calorific value. Therefore, it becomes critically imperative to characterize the waste before implementing it for the energy conversion process.

2.2. Short outline of the technologies involved in the study

2.2.1. Plasma

Plasma is the fourth state of matter, which American Chemist and Physicist Irving Langmuir first defined in 1927 as an ionized gas under a definite electric field (Fitzpatrick Richard, 2014). It is both electrically and thermally conductive and can be partially or completely ionized (Bogaerts et al., 2002). The gas is under electric polarization as the electric current strains further beyond its dielectric limit, causing electrical breakdown and transforming the gas to conduct. The collisions between the electrons and the nucleus produce more electrons and generate heat. This largely raises the temperature of the gas and turns into a thermal plasma. The collisions could be elastic (kinetic energy is conserved) or inelastic (loss of kinetic energy into heat) in nature (Samal, 2017; St and Braithwaite, 2000).

For better conversion of solid particles, volumetric interaction with plasma is highly necessary. The heat transfer involved between plasma and the particle is the energy exchange through the mode of conduction and convection from plasma to the particle. Also, there is a radiative energy loss transported from the surface of the particle to the surroundings, as presented in Fig. 2.1 (Gomez et al., 2009). The net energy required (Q) for heating and melting of the particle is given as:

$$Q = h_{\infty} A(T_{\infty} - T_S) - \sigma \varepsilon A(T_S^4 - T_{\alpha}^4) \quad (1)$$

where h_{∞} is the heat transfer coefficient between plasma-particle, A is the surface area of the particle, T_S is the surface temperature of the particle, T_{∞} is the plasma temperature, σ is Stefan-Boltzmann constant, ε is the emissivity of the particle and T_{α} is reactor temperature.

Table 2.1

Properties and characteristics of different types of fuels.

Feed		Proximate analysis (wt.%)				Ultimate analysis (wt.%)						HHV (MJ/kg)	Reference
		MC	FC	VM	Ash	C	H	N	S	Cl	O		
Industrial	MSW	26.61	10.82	81.58	7.60	54.98	7.43	1.87	0.35	0.67	34.70	16.41	(Montiel-Bohórquez et al., 2021)
Residential	MSW	57.90	12.36	77.53	10.11	53.01	6.91	2.65	0.34	0.24	36.85	8.55	(Montiel-Bohórquez et al., 2021)
Mixed	MSW	51.33	11.90	78.49	9.61	53.64	7.03	2.38	0.32	0.26	36.37	10.12	(Montiel-Bohórquez et al., 2021)
Commercial	MSW	32.95	10.19	81.38	8.43	56.05	7.47	1.47	0.26	0.15	34.60	15.10	(Montiel-Bohórquez et al., 2021)
Institutional	MSW	37.92	10.92	80.73	8.35	55.04	7.04	1.41	0.26	0.09	36.16	13.42	(Montiel-Bohórquez et al., 2021)
RDF		4.6	8.6	69.3	22.1	46.8	5.7	1.25	0.26	1.60	22.3	22.37[a]	(Agon et al., 2016)
Medical waste		0.29	18.89	78.52	2.30	64.21	9.77	0.72	0.21	-	22.49	28.37[a]	(Peng et al., 2021)
Sewage sludge[c]		68	-	-	15	9.1	1.1	0.7	-	-	6.1	3.51	(Kalinci et al., 2011)
Textile dyeing sludge		5.62	1.85	45.91	46.62	22.54	3.55	0.96	1.18	-	19.53	10.45	(Wang et al., 2019)
Kitchen waste		12.3	0.01	87.15	0.55	40.03	6.88	1.99	0.01	-	47.59	15.64	(Li et al., 2020)
E-waste		0	8.54	45.29	46.17	35.28	3.95	1.11	0.13	-	13.36	19.43[a]	(Hao et al., 2014)
Sawdust		34.9	0.7	64.4	49.8	6	0.5	0.02	-	-	43.7	10.95[b]	(Hlina et al., 2014)
Wood		0	2.35	97.65	47.1	6.4	0.3	0.5	-	-	46.5	20.57[a]	(Tang and Huang, 2005)
Shenhua coal		5.17	5.8	89.03	75.77	5.57	1.16	0.8	-	-	16.69	27.03[b]	(Shin et al., 2013)
Rice straw		0	12.8	87.2	41.8	5.9	0.4	0.2	-	-	51.6	16.90[a]	(Tu et al., 2009)

[a] LHV_{dry}; [b] LHV; [c] %w/w; MC-Moisture content; FC-Fixed carbon; VM-Volatile matter.

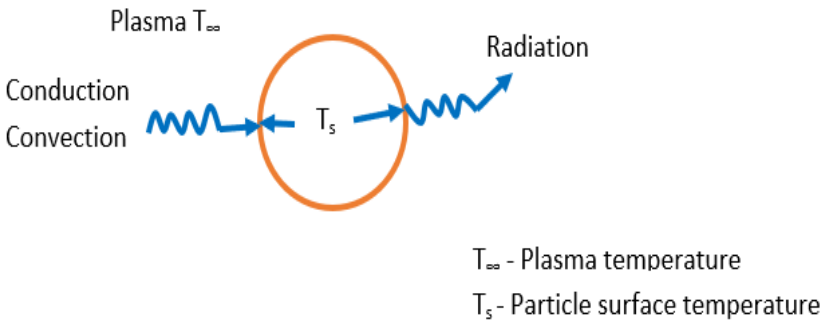

Fig. 2.1. Heat transfer mechanism in the particle by plasma.

Industrial processes include two major modes of plasma technology such as thermal (hot plasma) and non-thermal plasma (cold plasma). Specific thermal plasmas include those created by alternating current (AC) or direct current (DC) plasma torches, microwave (MW), or radio frequency (RF) inductively coupled (Kogelschatz, 2004). While the non-thermal plasmas (NTP) are dielectric barrier discharge (DBD), pulse discharge (PD), gliding arc discharge (GAD) and corona discharge (CD) produced at a normal gas temperature (Sun et al., 2018).

2.2.1.1. Thermal and Non-thermal Plasma

A plasma to be classified as thermal plasma should operate at a temperature above 10,000 °C and the ions, atoms, electrons and neutral species are generated in the plasma. They are characterized by high energy density and temperature (Samal, 2017). The diagnostic tools to regulate the operating parameters of plasmas are shown in Fig. 2.2. These can measure the flux of the plasma particle through a metallic probe inserted in the discharge locally such that capacitive effects are ignored.

In the generation of thermal plasma, electrodes with higher electrical conductivity are used to transfer electrons between the cathode and anode. These electrodes can be constructed using many materials, in particular copper, tungsten, thorium, graphite, etc. The dissociation of carrier (plasma) gas such as N_2, Ar, Air, CO_2, etc. into radical species by the electrodes

increases the reaction rates (Rutberg et al., 2011). Despite several improvements over the past years, the major drawback that remains is the decay of the electrodes, especially the cathode as compared to the anode (Szente et al., 1992). As per the literature, the analysis of electrode erosion revealed that the lifetime of copper rod electrodes using air is between 300 and 350 hours. Under the steam atmosphere, the rate of erosion was 2-3 times higher than other plasma forming gases like air, CO_2, CH_4, etc. or mixtures thereof without any electrode protection agent (Rutberg et al., 2013; Surov et al., 2017). CO_2 as a plasma gas mixed with methane, acts as a protective agent for graphite electrodes against erosion (Rath et al., 2012). There occurs a mass loss in the electrode by the expansion of metal under vacuum, however by increasing the pressure, the eroded substance gets re-deposited at the electrode (Szente et al., 1992). While for microwave and RF plasmas, the absence of electrodes offers the advantage of non-contamination of plasma, lower power consumption and flexibility for a wide range of operating conditions (Samal, 2017).

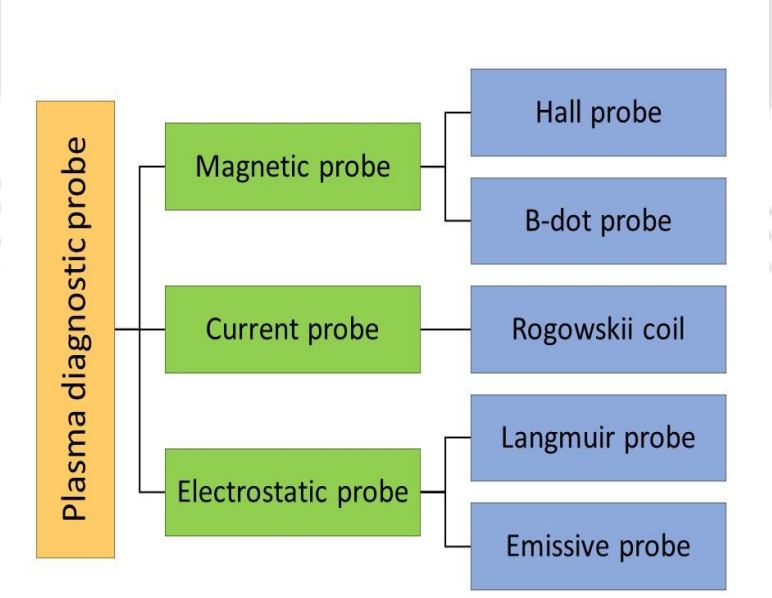

Fig. 2.2. Diagnostic tools for the measurements of plasma parameters.

2.2.2. Molten carbonate fuel cell (MCFC)

In a standard fuel cell, the building block of the cell comprises an electrolyte layer in contiguity with a porous anode and cathode, as shown in Fig. 2.3. The gaseous fuel enters the anode and, the cathode is charged with an oxidant, progressing electrochemical reactions to generate electric current (Cooper et al., 2021). In the MCFC, the porous surface of the electrodes provides a site for ionic conduction imparted by the carbonate ions at 600-700 °C. An added advantage is the use of Nickel catalysts rather than any more expensive noble metal catalysts such as platinum to promote reactions aiding the internal or external reforming. The flexibility of fuel is also another advantage where CO and CO_2-containing fuels can be used directly in the reaction. However, due to the mobility and corrosivity of the electrolyte, CO_2 injection should be done on the cathode side (Hirschenhofer et al., 1998). The reactions shown in Table 2.2 occur in anode and cathode.

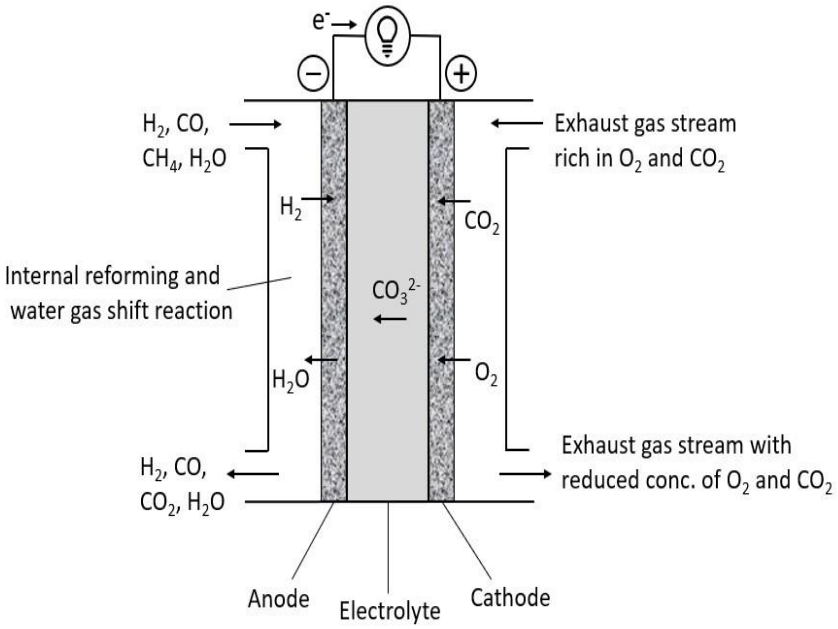

Fig. 2.3. Schematic diagram of an operating MCFC.

Table 2.2

Reactions occurring in the processes.

Reaction number	Chemical reaction	Heat of reaction (kJ/mol)	Reaction
R1	H_2 (g) + CO_3^{2-} → H_2O (g) + CO_2 (g) +2e^-	-	Anode
R2	O_2 (g) + 2CO_2 (g) + 4e^- → 2CO_3^{2-}	-	Cathode
R3	H_2 + CO + 2Fe_2O_3 → H_2O + CO_2 +4FeO	+ 35.53	Fuel reactor
R4	H_2O + 3FeO → H_2 + Fe_3O_4	- 60.42	Steam Reactor
R5	O_2 + 4Fe_3O_4 → 6Fe_2O_3	- 471.6	Air Reactor
R6	C(s) + H_2O (g) ↔ CO (g) + H_2 (g)	+ 131	Steam reforming
R7	C(s) + 0.5 O_2 (g) → CO (g)	- 112	Char partial oxidation
R8	C(s) + 2H_2 (g) → CH_4 (g)	- 75	Methanation
R9	C(s) + CO_2 → 2CO (g)	+ 172	Boudouard reaction
R10	H_2 (g) + 0.5 O_2 (g) → H_2O (g)	- 242	Hydrogen combustion
R11	CO (g) + 0.5 O_2 (g) → CO_2 (g)	- 283	CO oxidation
R12	CO (g) + H_2O (g) ↔ CO_2 (g) + H_2 (g)	- 41	Water-gas shifting
R13	CH_4 (g) + H_2O (g) ↔ CO (g) + 3H_2 (g)	+ 206	Steam-Methane reforming

2.2.3. Chemical looping reforming (CLR)

Chemical looping reforming (CLR) method provides an alternative for the production of high-purity hydrogen (H_2) with high energy efficiency and integral CO_2 capture. The process consists of three reactors, namely fuel, steam and air reactors, coupled with each other. In the fuel reactor (FR), the syngas reacts with oxygen in metal oxides known as oxygen carrier (OC). The end product mainly consists of CO_2, H_2O and reduced OC. The reduced OC undergoes partial oxidation in the steam reactor (SR), producing H_2. Then, the partially oxidized metal particles get completely oxidized in the air reactor (AR) by the exothermic nature of the reaction (Khan and Shamim, 2019). Therefore, the fully oxidized metal particles from the AR

are then transferred to FR, followed by SR. However, a noted ability of the oxygen carrier (OC) to convert the steam into H_2 is very essential. Further, the OC should be low-cost and environmentally friendly. The regular problems encountered by the OC are sintering due to high temperatures in the reactor, attrition loss due to low mechanical strength, etc. (Khan and Shamim, 2016). Among the oxygen carriers (OC), Fe_2O_3 is mostly used due to its various reducing states (FeO, Fe and Fe_3O_4) (Surywanshi et al., 2021) as shown in Fig. 2.4. The reactions that takes place in the respective reactors are shown in Table 2.2 (Yang et al., 2021).

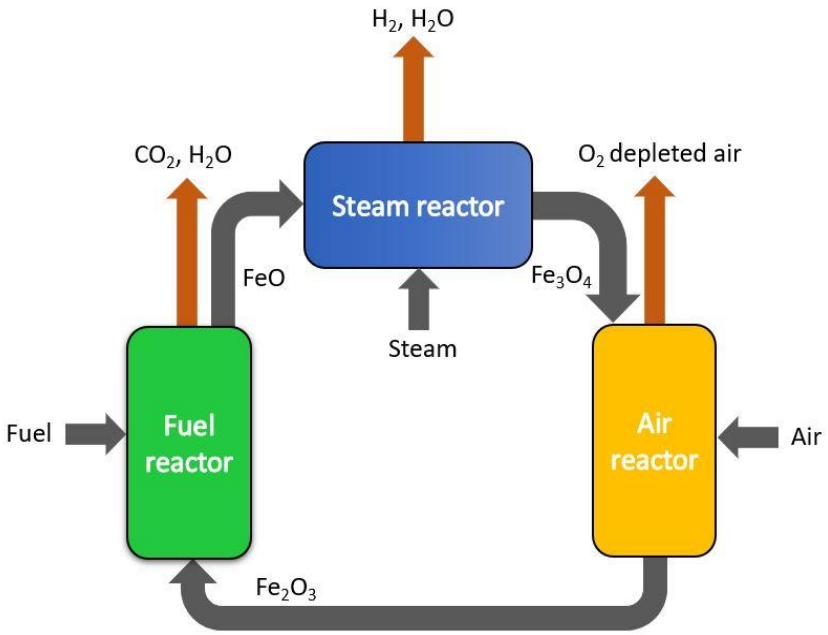

Fig. 2.4. Schematic representation of the CLR process.

2.3. Plasma gasification versus conventional processes

Table 2.3 compares the plasma gasification technology with other thermochemical methods, such as incineration and gasification, based on energy and environmental factors. It can be seen that the capital investment is higher with a shorter service lifecycle and requires proper waste sorting before wet waste handling. However, due to higher power generating capacity and production potential, the net annual revenue is more than the other process and therefore the

Table 2.3

Comparison of the different thermochemical processes based on energy, economic and environmental factors.

Process parameter	Incineration	Conventional gasification	Plasma gasification	Reference
Service life and treating requirements				
Plant service life (year)	30	30	25	(Chen et al., 2022)
Wet waste handling	Limited	Limited	No	(Munir et al., 2019)
Land requirement (acres)	9-10/MW	10/MW	1/MW	(Saini et al., 2012)
Energy analysis				
Power generation capacity (MW/100 TPD of Waste)	1.2	2	4.5	(Saini et al., 2012)
Net energy production potential (kWh/ton of Waste)	544	685	816	(Munir et al., 2019)
Cost assessment for a plant capacity of 500 tons Waste/day (TPD)				
Capital investment (US$M)	116	80	101	(Munir et al., 2019)
Operational and maintenance costs (US$M/year)	11.6	8	10.1	(Munir et al., 2019)
Environmental impact				
Residue (ton/ton of Waste)	0.22	0.2	0.18	(Munir et al., 2019)
Particulate emissions ($\mu g/Nm^3$)	20	14.1	12.5	(Wilson et al., 2013)
SO_x emissions ($\mu g/Nm^3$)	40	19	26	(Arena, 2012)
NO_x emissions ($\mu g/Nm^3$)	40-100	40-70	150	(Tan, 2013)
Dioxins/furans emissions ($\mu g/Nm^3$)	<0.0983	-	<0.00925	(Tan, 2013)

payback period decreases to a few years on average, as discussed in the literature (Chen et al., 2022; Peng et al., 2021). From an ecological view, the plasma gasification process has a lower impact on the environment and requires less area for installation to generate the same energy as compared to other thermochemical methods.

Gasification found a strategic way as an alternative to replace incineration for the thermal processing of waste and recover energy. The limitation in cleaning the emitted harmful gases during gasification is a drawback to produce clean energy (Ayol et al., 2019). The solid fuel conversion into syngas takes place using gasifying agents such as air, steam, O_2 and CO_2 at high temperatures. The composition of the generated syngas depends on the types of feedstocks, type of gasifying medium, reactor type, temperature, residence time, etc. (Cai and Du, 2021). In Fig. 2.5, the contrasting features between the conventional and plasma gasification are described. Plasma gasification efficiently decomposes the higher hydrocarbons and toxic compounds into simpler ones at extremely high temperatures.

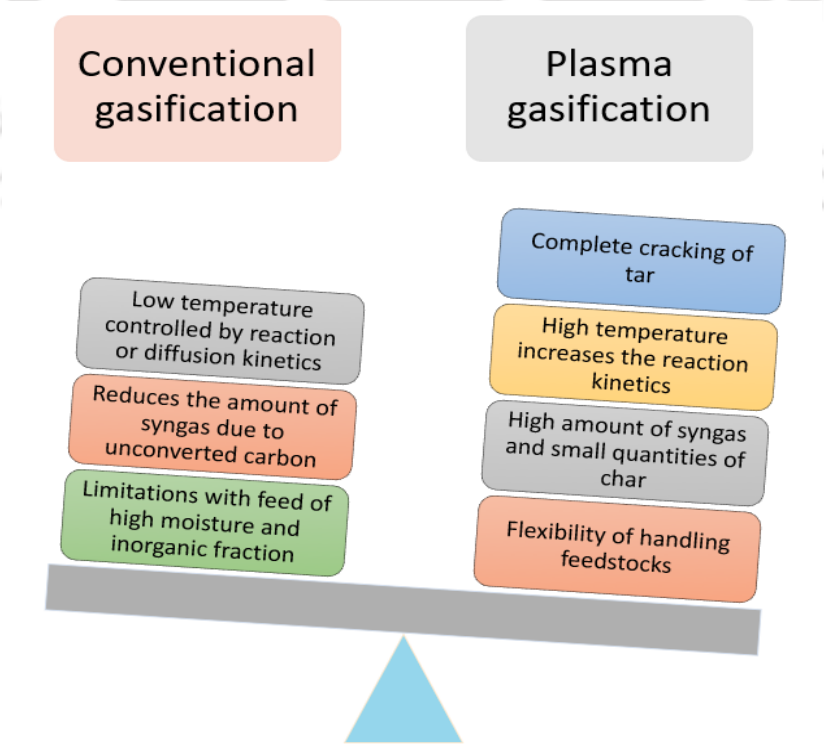

Fig. 2.5. Comparison between conventional and plasma gasification.

One of the noteworthy advantages offered by the plasma method is the higher decomposition rate even with high melting point materials (Tang et al., 2013). However, certain shortcomings in plasma process for industrial applications include the requirement of (i) higher initial investment cost including the expensive plasma generation gas (Argon), (ii) electrical energy-intensive plasma, (iii) steep temperature gradient and (iv) small processing zone.

2.4. Factors that influence the plasma gasification process

A typical layout of the plasma gasification process is shown in Fig. 2.6. The dependent variables (syngas composition, yield, etc.) and independent variables (pressure, temperature, etc.) possibly have an impact on the fuel conversion efficiency. Some of the major operating parameters of plasma pyrolysis/gasification that affect the quality of syngas in terms of valorization include the type of feedstock, particle size, reactor design, reaction temperature, source and power of plasma torch and carrier gas. The application of plasma increases the throughput (H_2/CO ratio) of the syngas thermodynamically compared to conventional gasification as discussed below in this section (Rutberg et al., 2011; Zhang et al., 2012).

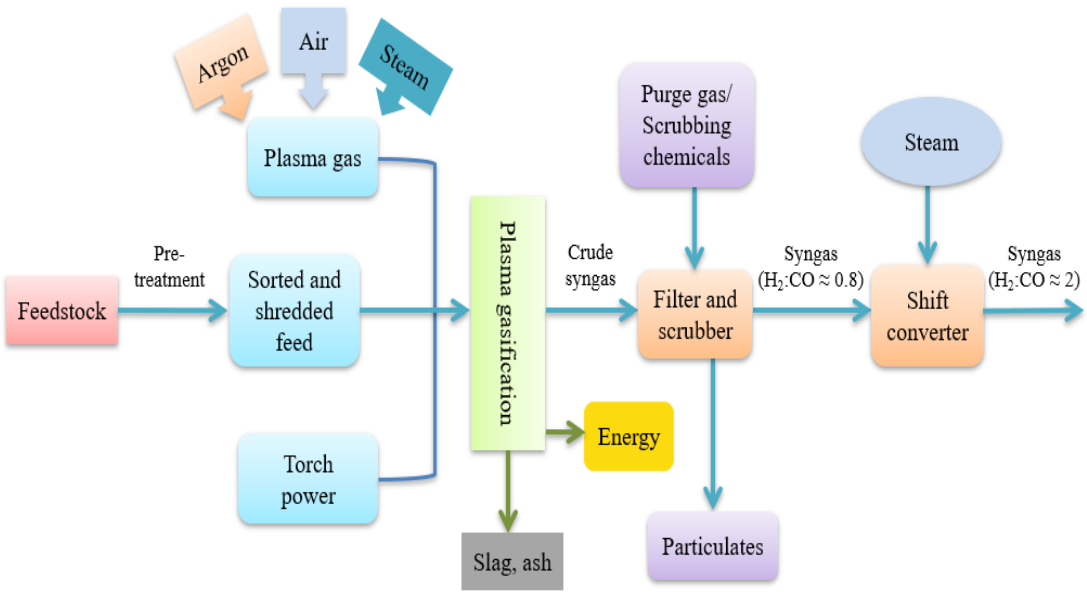

Fig. 2.6. Process diagram of the conversion of feedstock based on plasma gasification.

2.4.1. Feedstock

2.4.1.1. Biomass as a feedstock

A significant amount of moisture and volatile matter with high carbon and oxygen are the major components of biomass. The existence of moisture (> 10%) in feed has a significant impact on gas yield, carbon conversion, CO selectivity and H_2/CO ratio. The increase in drying rate reduces moisture content in the feed and leads to the reduction of syngas yield and carbon conversion except for CO selectivity due to suppression of water-gas shift reaction (Du et al., 2015). Table 2.4 shows the gas composition reported in the literature using various feedstocks. Even for wood sawdust and pellets with high moisture, a carbon conversion of >85 % can be achieved. Due to the distinguishing properties of plasma gas, the syngas has almost 90% of H_2 and CO by total volume with a negligible tar content of less than 10 mg/Nm^3 (Hlina et al., 2014; Hrabovsky et al., 2017). Almost complete gasification was reported even at higher feeding rates due to intensive gasification using plasma (Hrabovsky et al., 2006; Van Oost et al., 2008). In the process, 1 kg of wood having a moisture content of 20% and LHV of ~ 13.9 MJ/kg can produce ~ 13.5 MJ of chemical energy with electric energy consumption of ~ 2.16 MJ/kg (Rutberg et al., 2011). Thus, the introduction of biomass in plasma gasification can produce high-quality syngas with a greater amount of H_2 and CO, low content of tar and makes it desirable for energy recovery.

2.4.1.2. Coal as a feedstock

Coal with high moisture and fixed carbon requires a considerable amount of energy to activate gasification reaction between carbon and plasma gas/gasifying media like petro-coke, which is a low reaction fuel. The percentage of H_2 and CO (85-98%) increases at a lower material feeding rate due to the presence of excess energy for reactions under controlled moisture (Galvita et al., 2007). The higher ash content in the coal leads to an increase in the

Table 2.4

Results obtained by authors for various feedstock in thermal and non-thermal plasma gasification.

Feedstock	Power (kW)	Carrier gas	Gasifying agent	Syngas comp. (vol. %)				Gas yield (Nm^3/kg_{feed})	LHV (MJ/m^3)	Reference
				H_2	CO	CO_2	CH_4			
Municipal solid waste (300 kg/h)	240	Air	Air	19.6	14.2	58.[a]	-	1.06	5.95	(Zhang et al., 2012)
Municipal solid waste (300 kg/h)	260	Air	H_2O + Air (5.38:1)	24.2	14.8	51[a]	-	1.27	7.21	(Zhang et al., 2012)
Bony tissue (10 kg)	70	Air	Air	6.2	63.4	-	-	-	8.68	(Messerle et al., 2018)
Household waste (10 kg)	72	Air	Air	44.6	26.5	-	-	1.45	8.16	(Messerle et al., 2018)
Waste glycerol (20.16 kg/h)	56	Air	Air	29.0	27.0	-	-	0.856	7.32	(Tamošiūnas et al., 2019)
Carpet waste (23.1 kg/h)	90	Air	Air + H_2O	12.8	19.9	-	0.71	-	4.15	(Vaidyanathan et al., 2007)
USAF BEAR Waste (10.7 kg/h)	74-85	Air	Air + H_2O	16.8	27.3	-	0.13	-	5.31	(Vaidyanathan et al., 2007)
Coal (33.51 kg/h)	59	(H_2O, Air, CO_2 etc.)	Air + H_2O (12.7:1)	20.5	23.0	7.42	-	1.03	4.68	(Surov et al., 2017)
Corn cob (0.2g)	0.025	Ar	-	42.3	21.1	27.7	9.0	74.4[b]	10.46	(Du et al., 2015)
Corn cob (0.2 g)	0.025	N_2	-	48.2	24.9	21.5	5.4	79.0[b]	10.29	(Du et al., 2015)

Wood pellets (4 kg)	12.6	N_2	N_2	45.4	45.2	4.1	2.9	1.23	11.65	(Muvhiiwa et al., 2018)
Waste glycerol (20.16 kg/h)	62.4	H_2O	H_2O + Air (4.88:1)	51.2	24.7	-	-	0.93	9.82	(Tamošiūnas et al., 2019)
Wood sawdust (41.4 kg/h)	138	Ar & H_2O	CO_2	41.5	42.5	14.9	1.0	1.55	10.2	(Hrabovsky et al., 2010)
Polyethylene (5.3 kg/h)	140	Ar & H_2O	CO_2 +O_2 (2.6:1)	29.9	41.3	27.1	0.0	1.16	8.5	(Hrabovsky et al., 2010)
Plastics (11.2 kg/h)	131	Ar & H_2O	O_2	41.6	49.7	7.4	0.0	2.85	10.8	(Hrabovsky et al., 2010)
Sawdust (30 kg/h)	100-110	Ar & H_2O	CO_2	41.6	50.9	4.3	2.3	1.92	11.75	(Hlina et al., 2014)
Pyrolytic Oil (9.1 kg/h)	100-110	Ar & H_2O	H_2O	59.5	30.2	4.2	4.5	1.98	18.5	(Hlina et al., 2014)
Refuse Derived Fuel (29 kg/h)	120	Ar & H_2O	H_2O	52.8	30.0	3.9	4.2	1.84	10.9	(Agon et al., 2016)
Pyrolytic Oil (8.8 kg/h)	160	Ar & H_2O	H_2O	57.7	32.7	4.1	4.9	2.04	12.1	(Hrabovsky et al., 2017)
Pyrolytic Oil (10.6 kg/h)	160	Ar & H_2O	O_2	47.9	47.0	2.9	2.0	1.6	11.8	(Hrabovsky et al., 2017)
Wood (0.2 kg/h)	0.9	H_2O	N_2	39.6	32.2	18.0	10.8	-	12.21	(Pang et al., 2019)
Textile dyeing sludge (2.16 kg/h)	15	Ar	CO_2	27.5	48.6	2.3	-	0.84	8.91	(Wang et al., 2019)

[a] CO_2+ N_2; [b] Gas yield in %; in bracket indicates the feed rate.

specific energy consumption and some mineral content gets converted to carbides at higher temperatures in the range of 2800-2900 °C. Likewise, coal with higher oxygen content reduces the dependence on external oxygen for the process. The oxygen in coal participates via the partial oxidation (R7) of char and assists the steam reforming reaction (R6), resulting in the reduction of the total energy consumption (Rutberg et al., 2013; Surov et al., 2017).

2.4.1.3. Waste as a feedstock

Wastes including municipal solid waste (MSW), refuse-derived fuel (RDF), etc. are difficult to handle in gasification process due to the presence of heavy metals and halogen compounds. In fact, the moisture content in waste offers a negligible effect on overall conversion of plasma gasification as the drying process is external and fast (Lopez et al., 2018). Household waste (paper and paper board, food waste, glass, etc.) from healthcare facilities containing 32.31% moisture increases H_2 production with an H_2:CO ratio as high as ~1.68 (Messerle et al., 2018).

A stream of RDF (22 kg/h) generates syngas with a higher amount of CH_4 as compared to coal and biomass due to the decomposition of plastic content in waste (Aznar et al., 2006; Lemmens et al., 2007). However, the examination of semi-volatile compounds during plasma gasification shows a trace amount of other chemicals such as benzene, toluene, ethyl benzene, etc. (Vaidyanathan et al., 2007). RDF based on MSW (51%) and industrial waste (IW) (49%) produced tar in the syngas varying from 132 to 543 mg/Nm^3. The tar content is lower than that obtained by conventional gasification but higher than biomass-based plasma gasification (<10 mg/Nm^3). This is due to the heterogeneous nature and coarser size of RDF (Jeremiáš et al., 2017). In addition, the dioxins measured at the wet scrubber outlet was 0.021 ng-TEQ/Nm^3 and found to be well below the emission regulation, indicating effective destruction of waste at high temperatures by thermal plasma (Zhao et al., 2001).

2.4.2. Particle size

The influence of particle size on the performance of gasification is also crucial. With an increase in particle size, the rate of heat transfer from the reactive environment to the particle becomes slower. It is associated to the shielding of the particles by volatile gases released from the material and reduces the carbon yield to <1 (Hlina et al., 2014; Hrabovsky et al., 2010). This was also demonstrated by the results of wood plasma gasification using various-size particles with 123-355, 355-500, and 500-710 μm. Low carbon conversion was found (~ 0.58, ~ 0.51 and ~ 0.42, respectively) with an increase in the particle size at a specific temperature. The linear dependence of particle size on the produced gas justifies the increase in H_2 and CO concentration in syngas with plasma gasification (76.9 vol.%) as compared to thermal gasification (71.7 vol.%) process (Pang et al., 2019). In the case of coal, due to the rapid release of volatiles at the initial stage of gasification, a decrease in the particle size was noticed for coals with low ash, while the reverse effect occurred for high ash coals (carbon conversion of ~ 60-70%) (Georgiev and Mihailov, 1992; Kalinenko et al., 1993). However, for MSW, the syngas quality was found less sensitive towards the changes in the particle size due to the presence of a high-temperature gasification agent and low fixed carbon content. The heterogeneous mixture of particles with different sizes in MSW could result in fluctuations in the feed rate (Agon et al., 2016; Zhang et al., 2012). Overall, it can be inferred that the influence of feed particle size remains significant in biomass and coal, compared to waste feedstock.

2.4.3. Reactor design

Moving bed reactor, either updraft or downdraft, spouted/fluidized bed and entrained flow reactor are used for thermal plasma pyrolysis/gasification processes. The configuration of these reactors is presented in Fig. 2.7 (Tang et al., 2013). It is highly probable to have an enhanced

tar steam-reforming reaction at high temperatures of the plasma regime along with the water-gas shift reaction (R12 and R14).

$$C_mH_n + aH_2O \rightarrow bCO + cH_2 + dC_xH_y \quad \text{(R14)}$$

Where C_mH_n denote tar and C_xH_y is light hydrocarbons.

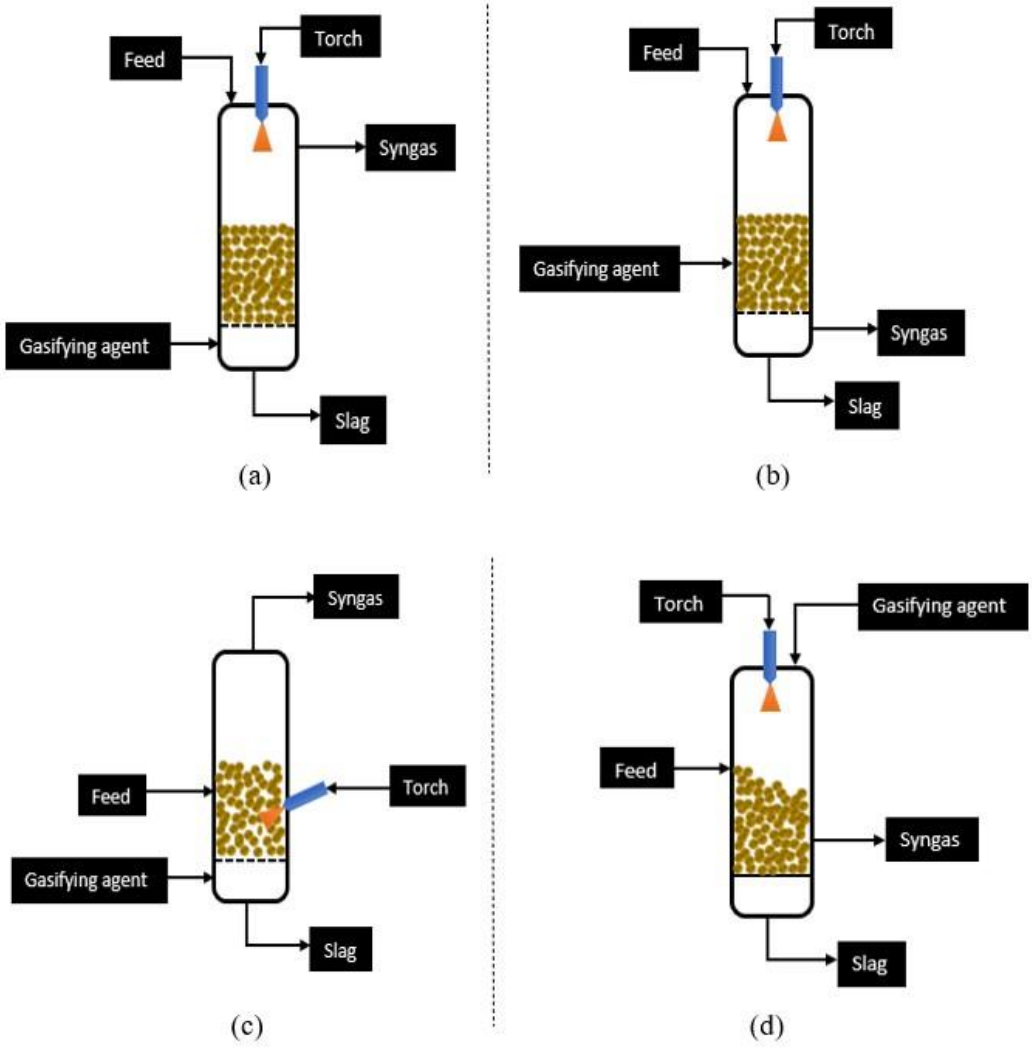

Fig. 2.7. Different types of plasma reactors used in gasification (a) updraft (b) downdraft (c) fluidized bed and (d) entrained flow.

In the case of an updraft fixed-bed reactor using steam-air plasma, the energy loss is mainly because of the chemical energy involved in tar formation (Zhang et al., 2012). Whereas, in a downdraft gasifier, the tar content is lower as the syngas leaves through the high-temperature

gasification zone (bottom). Thus, using steam-air plasma is more effective in downdraft gasifier because steam reforming takes place at a higher temperature but yields soot of 125 mg/Nm^3 due to dependence on the method of supplying plasma heat and flow rate of gases into the discharge medium (Rutberg et al., 2013; Surov et al., 2017). Plasma-based entrained flow reactor utilizing biomedical waste produces syngas with higher CO (63.4 vol.%) and inorganic fraction (67 wt.% of CaO) that accumulates in the bottom slag zone. This design of the reactor produces a lower content of tar than the updraft fixed bed gasifier (Messerle et al., 2018).

2.4.4. Operating temperature

To produce syngas with low undesired product content, the plasma reactors utilizing biomass are to be operated above 900 °C and thus, the overall gas yield increases from 30% at 400 °C to 82% at 1000 °C (Muvhiiwa et al., 2018; Van Oost et al., 2008). At very high temperatures of ~2700 °C, the hydrogen in the syngas may decrease due to the generation of atomic hydrogen (H), which decreases hydrogen in the syngas to 10.3-11.3% (Messerle et al., 2018; Pang et al., 2019). Another important factor in the handling of waste comprising chlorine is the formation of toxic organic compounds (dioxins, furan, hexachlorobenzene, etc.) in the presence of carbon and free chlorine radicals. At temperatures higher than 1200 °C in the plasma reactor, these compounds split the chlorine molecules and couple with hydrogen ions, forming hydrochloric acid (HCl) when the gas cools down (Messerle et al., 2018).

Gasification of high ash coal near its softening point creates higher resistance for the diffusion of gasifying agent into the internal pores of the coal. This leads to a slight change in the coal particle temperature with the liberation of volatiles due to the endo-thermal pyrolysis process (Georgiev and Mihailov, 1992). During the release of volatile matter, the secondary pyrolysis of tar favors H_2 production, which is sensitive to the reaction temperature. On the other hand, the influence of copper (Cu) or palladium (Pd) catalyst temperature on H_2/CO ratio

becomes prominent at high temperatures (~ 250 °C) due to the strong activity of the catalyst (Kroker et al., 2012).

2.4.5. Power of assisted technique

Plasma carries a high amount of energy even at low power and thus the high reaction temperature reaches very fast. Hence, the plasma helps to decompose material faster due to the increase in process enthalpy as the ratio of supplied energy to feed energy input increases (Hrabovsky et al., 2017, 2006). The influence of discharge plasma power ranging from 9 to 25 W of a non-thermal plasma arc indicates an increase in the gas yield from 57% to 79% in the order of H_2>CO>CO_2 (Du et al., 2015). With an increase in the operating power by ~20 W, the conversion of toluene into simpler compounds was enhanced by 23% and naphthalene by 1.6 times. This increases the H_2 and CO yield from the conversion of tar to ~ 78%. Increasing discharge power gives rise to the formation of more active species by cracking tar model compounds augmenting conversion (Tamošiūnas et al., 2019).

In the case of MSW, the increase in power of thermal plasma by 20 kW with a feeding rate of 300 kg/h promotes the cracking of tar to light hydrocarbons (LHCs) through the reforming reaction, improving the yield of H_2 (~ 25%) as given in R15 (Zhang et al., 2012).

$$C_xH_y + xH_2O \rightarrow xCO + \left(x + \frac{2}{y}\right)H_2 \qquad \text{(R15)}$$

The thermal energy of plasma is also utilized for the reduction of the feed gas CO_2 into CO and radicals by the endothermic reaction (Galvita et al., 2007). Power consumption for coal with high ash content is relatively less because the gasification of organic matter requires more power than melting the inorganic fraction of coal (Georgiev and Mihailov, 1992). Hence, high-ash coal may consume less power in plasma gasification.

2.4.6. Type of carrier gas, gasifying medium and their flow rate

2.4.6.1. Carrier gas

The typical impact of carrier gas on gas yield is found in the order of Air >Nitrogen > Argon due to the higher ionization potential of argon. Under the same conditions, the carbon conversion rate is lowest for air (66.2%) and highest for nitrogen (82.9%), while CO selectivity is lowest for argon. Relatively, a small difference exists between air and N_2 due to the influence of excited oxygen and nitrogen present in the air. A marginal effect of carrier gas is found on the H_2/CO ratio in the order of air (2.24) > Ar (2.00) > N_2 (1.95) (Du et al., 2015).

2.4.6.2. Air as a gasifying medium

Application of plasma requires a smaller amount of oxidizer (either nascent or molecular) for the gasification of the solid materials. A low flow rate of air ensures high syngas quality, but too low a supply cannot provide enough oxygen to convert solid char into CO and CO_2. This results in a lower carbon conversion and gas yield. The amount of H_2 remains relatively unchanged (~ 20 vol.%) with airflow, but the LHV decreased due to the dilution of syngas by nitrogen in the air (Tamošiūnas et al., 2019; Zhang et al., 2012). The percentage of CO_2 gas (~ 7 vol.%) is low with the view of favoring partial oxidation over complete oxidation reaction (Messerle et al., 2018).

2.4.6.3. O_2 as a gasifying medium

When RDF is supplied with a reduction of 25 standard liters per minute (slm) of O_2 from 118 to 93, it results in lower CO_2 (~1.9 vol.% by diff.) and slightly higher CO (~1.6 vol.% by diff.) concentrations because lack of O_2 reduces the production of CO_2 via oxidation reaction (R11) and increases the CO content in the syngas (Agon et al., 2016).

Subsequently, the use of stoichiometric O_2 increased both the temperature of the reactor and the LHV value of the syngas due to an increase in the calorific valuable gases (84 vol.% of H_2 and CO) while CO_2 content also rises to 15 vol.% (Hrabovsky et al., 2017).

2.4.6.4. CO_2 as a gasifying medium

Reducing the flow rate of CO_2 by ~18% in the input stream, the CO_2 content decreased by 32%, while CO and H_2 increased by 4.5% and 15.2%, respectively. It is most likely due to the shift in the equilibrium of the water-gas shift reaction towards the product side. Hence the feed rate of CO_2 should be optimized to produce significant levels of H_2 and CO (Agon et al., 2016). However, CO_2 as the gasifying medium, requires additional energy for its dissociation. When O_2 is replaced by CO_2 as a gasifying agent, almost double the inlet feed rate is required to achieve similar quantity of syngas and their LHV (Lee et al., 2014; Lopez et al., 2018). CO_2 feed enhances the CO content but lowers the carbon conversion efficiency under the same reaction time and temperature (Tamošiūnas et al., 2019).

2.4.6.5. Steam as a gasifying medium

The absence of oxidizing medium for steam-based plasma gasification shifts the reaction towards the progress of reduction reactions rather than oxidation/combustion reactions. But it is also likely that a fraction of H_2 is produced from the thermal decomposition of steam (Georgiev and Mihailov, 1992; Pang et al., 2019). Adding steam indicates a favorable steam-reforming reaction of tar and increases the syngas yield but the reaction is limited to occur only at high temperatures. The progress of water-gas shift reaction at a lower temperature (R12) improves the H_2/CO (~ 2.1) ratio except when the reaction gets suppressed due to the insufficient quantity of steam and by the progress of tar-steam reforming (R15) (Agon et al., 2016; Tamošiūnas et al., 2019). On the other hand, the inclusion of steam erodes copper electrodes 2 to 3 times faster than the other plasma-forming mediums such as air, CO_2, CH_4,

etc. To prevent erosion, a small amount of air (10-17%) or nitrogen needs to be supplied as a shielding gas. The major concern is that N_2 favors pyrolysis reaction (R16) at high temperatures and reduces the heating value of syngas (Rutberg et al., 2013; Surov et al., 2017).

Cracking (pyrolysis): $C_xH_yO_x + zN_2 \rightarrow xCO + yH_2 + zN_2$ (R16)

2.4.6.6 Mixture of gases

In the case of a mixed gasifying medium of H_2O and CO_2, the H_2 and CO in syngas are found lower with an H_2/CO ratio of 0.88 due to the endothermic heterogeneous gasification reaction (R6 and R9). The enthalpy of steam is three times higher than air at a particular temperature, causing a significant effect on gasification performance (Agon et al., 2016; Tamošiūnas et al., 2019). Moreover, the specific power consumption of steam-CO_2 plasma reforming is lower than CO_2 reforming alone (Surov et al., 2017).

2.4.7. Two-stage plasma gasification

The two-stage plasma gasification model physically separates the gasifier and plasma converter unit (PCU). The tar compounds, such as heavy poly-aromatic hydrocarbons (PAHs) in the syngas, are exposed to plasma in the PCU. PAHs get converted to non-condensable gases and results in an increase in the syngas content. The first stage can be an electrolytic cell that performs under glow discharge for the generation of steam or the traditional gasifier that operates in the temperature range of 650-800 °C. In the second stage, the plasma converter scrubs the raw syngas at a temperature of ~1200 °C and collects the molten inorganic fraction of ash in the form of slag. The major advantage of connecting the gasifier followed by plasma converter (illustrated in Fig. 2.8**)** is that the flow rate of oxidant and power input can be independently controlled (Diaz et al., 2015; Materazzi et al., 2016).

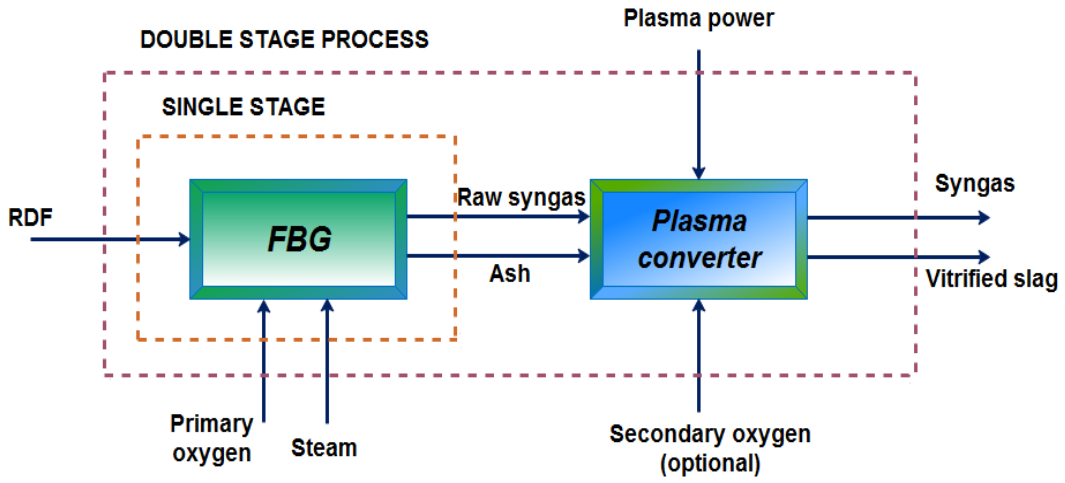

Fig. 2.8. Representation of a two-stage fluidized bed thermal plasma process.

Almost no organic carbon was left downstream of the converter (2nd stage) due to plasma reforming and cracking of tars and organic compounds. The fraction of H_2 and CO almost doubled, with an H_2/CO ratio of 1.62 and CO/CO_2 ratio of 1.61, as shown in Table 2.5. The energy efficiency increased as high as 82% due to the high temperature, turbulence and high residence time in the plasma converter (Materazzi et al., 2016). Higher air flow rate in the second stage decreases the methane (CH_4) concentration, which is associated to the partial oxidation of the produced gas (Striūgas et al., 2017). From Fig. 2.8, it is more efficient to use an oxidant in a two-stage process as compared to a single fluidized bed gasifier (FBG) due to the unnecessary requirement of additional oxygen for ash vitrification. This can be done in the second stage with the aid of plasma (Materazzi et al., 2016). Overall, in both the processes (single and two) of plasma, due to high temperatures, the tar amount in the syngas is reduced to low levels.

Table 2.5

Comparison of experimental data collected from the two-stage plasma gasification process.

Reference	(Materazzi et al., 2016)		(Striūgas et al., 2017)		(Diaz et al., 2015)	
Feed	Refuse Derived Fuel (40-60 kg/h)		Sewage sludge (19 kg/h)		Almond hulls (3.7 kg/h)	
Plasma gas	O_2		Air		H_2O and few $H_2 + CO_2$	
Operating conditions	Fluidized bed gasifier	Plasma converter	Downdraft gasifier	Plasma reactor	Glow discharge electrolytic cell	Plasma reactor
Temperature (°C)	770	1200	800-850	1100	Saturated steam	910
Equivalence ratio	-	0.37	0.36	0.58	-	-
Syngas composition (vol. %)						
H_2	[a]16.5	32.3	14.62	13.19	-	52.4
CO	13.7	27.2	22.2	23.42	-	11.7
CO_2	19.3	9.9	10.3	8.72	-	28.3
CH_4	11.15	0.15	2.37	1.17	-	1.8
Clean syngas						
H_2/CO	-	[b]1.62	0.75	0.56	-	4.5
CO/CO_2	-	1.61	2.15	2.68	-	0.41
LHV (MJ/Nm^3)	-	[c]11.9	5.28	4.82	-	7.99

[a] mol. %; [b] argon-free basis, received from cleaning section; [c] MJ/kg.

2.5. Combination of non-thermal plasma and catalysis

Due to the high energy consumption of plasma, its practices are limited to an extent from a thermodynamic perspective. To avoid such apprehensive applications, catalysis was used. However, with the rapid deactivation of the catalyst due to poisoning, sintering and carbon deposition, the performance of the process deteriorated. Non-thermal plasma (NTP) reforming is another promising method because of its fast heating and reactions, but the process has the disadvantage of coke deposition and low pollutant conversion. Therefore, the NTP process combined with catalytic reforming shows a positive synergistic effect and higher selectivity towards syngas by converting complex tar to energy gas. This is due to changes in the physicochemical characteristics of the catalyst by plasma that increase its activity and durability (Liu et al., 2019, 2017).

The plasma reactor provides an option to use catalysts by two mechanisms: the catalyst kept downstream of the discharge region (after the plasma zone) or the catalyst in contact with the discharge zone (with plasma), as shown in Fig. 2.9. The representation of the former is similar in the two-stage plasma gasification process where the feed and volatile organic carbons (VOCs) are reduced in the plasma converter exiting the gasifier more efficiently. While for the latter, the reactive radicals, electrons and excited-state atoms modify the surface of the catalyst (Pham Huu et al., 2015). Moreover, by employing catalysts such as MnO_2, CuO, Al, Ni and TiO_2 with NTP, the removal efficiency of benzene, toluene, 2-heptanone, etc. can be increased up to 95% (Delagrange et al., 2006; Van Durme et al., 2008). These catalysts can also be prepared from the calcination and reduction of hydrotalcite-like materials (Li et al., 2011). On the other hand, polycyclic aromatic tar compound i.e., naphthalene, which is difficult to decompose because of more thermal stability than toluene, was removed almost 100% with TiO_2 packing (Cimerman et al., 2018). Further, the plasma-assisted technique is also useful in devising the catalyst for the reforming of CH_4 with CO_2 to yield syngas with positive

synergistic effects (Chung and Chang, 2016; Wang et al., 2013). Although the VOCs removal process needs improvement, the presented information demonstrates the potential of plasma catalysis in the low-temperature conversion process.

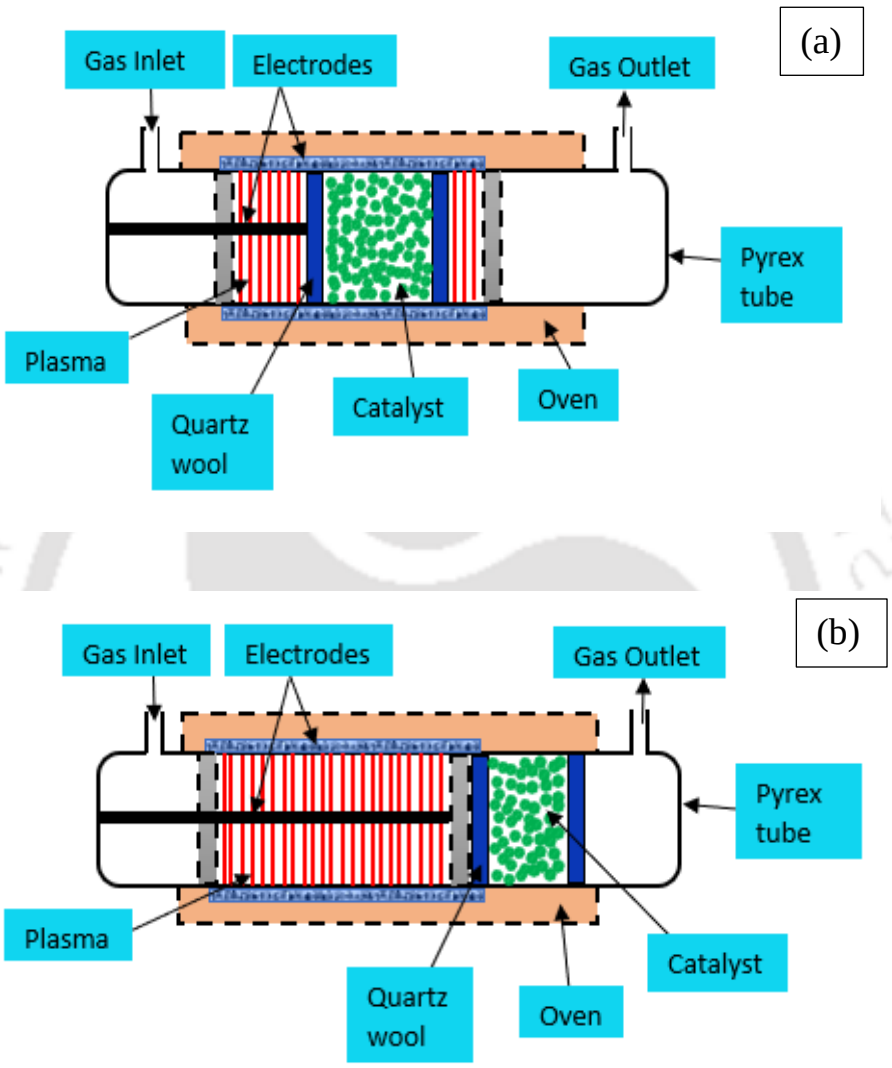

Fig. 2.9. Overview of the plasma-catalytic reactor, (a) in-line plasma catalysis and (b) after plasma catalysis.

2.6. Treatment of plasma-based residual slag

The plasma converts the inorganic portion of the feed into either a glassy slag of low leachability, high strength and high-volume fraction. Depending on the sources of waste generated (medical, e-waste, municipal, etc.), the properties of the slag vary considerably. The

composition of slag for different waste streams in terms of elements and compounds is shown in Table 2.6. Discarded e-waste contains both metallic and non-metallic substances in a weight proportion of 80:20 and produce a loss in weight of 60% (Lee and Huffman, 1996; Rath et al., 2012). The energy dispersive spectroscopy (EDS) analysis of vitrified slag showed the presence of Si, Ca, Na, Mg, Cr, etc. X-ray diffraction (XRD) test showed the amorphous form of slag, verifying the presence of SiO_2 as the major constituent. Scanning electron microscopy (SEM) image confirmed the microstructural variation with the formation of an irregular dispersed second phase that changes with feed composition. This is probably due to the higher melting point of the metals during vitrification, which was entrapped within the slag matrix after solidification (Chu et al., 2006, 1998). The major advantage related to plasma vitrification remains in the cost savings compared to landfill tax avoidance and the value addition of the end products under regulatory conditions (Samal, 2017).

2.7. Applications of product gas and vitrified slag from plasma gasification

Amongst the feasible energy recovery routes, thermochemical conversion method can be better implemented due to the production of H_2, chemicals, energy and syngas from different feedstocks (Puig-Gamero et al., 2018). The main valorization path of syngas conversion and slag to useful products through plasma gasification is summarized in Fig. 2.10. Companies like Alter NRG, CHO-Power, InEnTec, PEAT etc. have already installed plants for thermal plasma gasification of waste focusing on the end-use of syngas to electrical output and vitrification of solid residue. The medium-sized plants working under plasma technology are detailed in Table 2.7. The plants generate low electric power within a few megawatts (MW) due to limitations of the shorter lifetime of electrodes (discussed in Section 2.2.1.1) and high investment costs. Hence, the development of durable plasma torches is required to promote their applications at a larger industrial scale for economical operation (Fabry et al., 2013).

Table 2.6

Analysis of plasma-based slag compositions from different waste reported in the literature.

Authors	(Tzeng et al., 1998)	(Chu et al., 2006)	(Messerle et al., 2018)		(Lemmens et al., 2007)		(Chu et al., 2006)	(Rath et al., 2012)
Feed	Radioactive waste	Fiber-reinforced plastic, gill net & glass	Household waste		Refuse Derived Fuel		Medical waste	Electronic waste
Slag compositions								
Compounds	Wt. %	Wt. %	Compounds	Wt.%	Elements	mg/kgdm	Atomic %	Wt.%
SiO_2	57.37	68.14	SiO_2	13.0	Fe	53,800	1.2	11.64
Na_2O	8.86	21.97	$CaSiO_3$	21.0	Cr	99	8.8	-
CaO	23.43	15.96	Fe_3C	63.0	Cu	28	-	55.7
K_2O	0.88	1.18	Fe	3.0	Co	33	-	1.1
MgO	3.11	6.97			Al	-	4.1	9.98
Al_2O_3	4.88	2.42			Ni	17	-	0.98
Fe_2O_3	0.14	0.29			Zn	7.2	2.8	-
					Sb	26	2.8	-
					Ba	358	-	-
					O	-	46	-
					V	109	4.1	-
					Si	-	21	-
					Ca	-	12.8	-

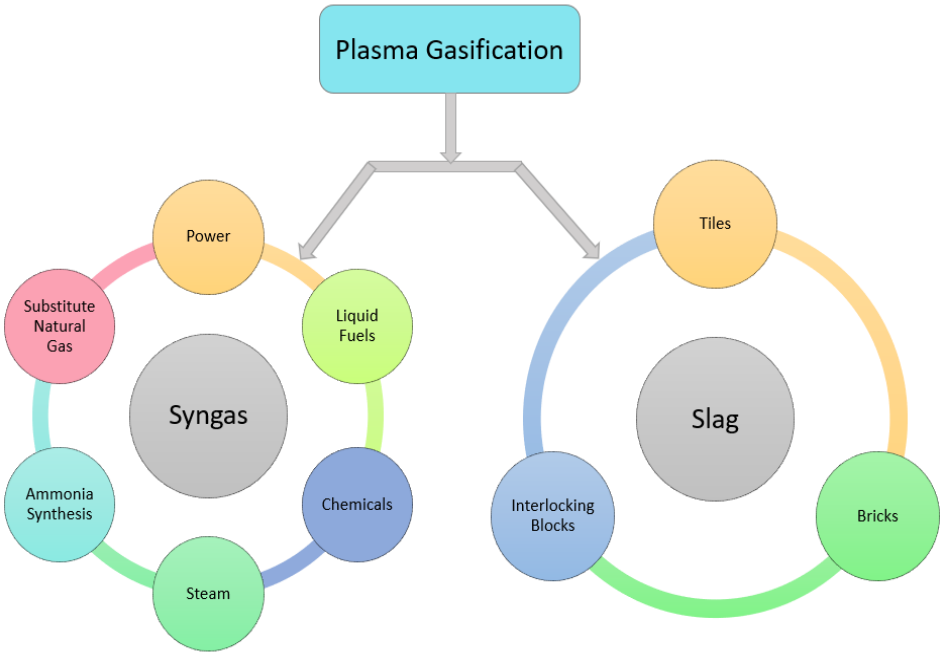

Fig. 2.10. Applications of syngas from plasma gasification and vitrification of the slag.

2.7.1. Plasma syngas to power generation studies

The plasma gasification reactor can be integrated with power generation systems, which include either combined cycles (gas turbine and steam turbine) or fuel cells (SOFC, MCFC, etc.). Fig. 2.11 presents the comparison of energy and exergy efficiencies from literature based on the different power generating systems and feedstocks. The schematic of simulation studies on RDF feedstock (LHV of 16.3 MJ/kg) based plasma gasification combined cycle (IPGCC) is shown in Fig. 2.12. Also, RDF-based plasma integrated with solid oxide fuel cell (IPGFC) systems was reported. Despite the large power consumption in plasma torches, the net efficiency of IPGCC (31%) and IPGFC (32.7%) is still higher than the conventional waste incineration process (20%). The gross power output of the steam turbine for IPGCC (~ 40%) is larger than that of IPGFC (~ 18%). Harmful pollutants such as dioxins and furans are not produced in the plasma-employed system, however, undesired compounds of sulfur, chlorides and particulate matter are to be removed in the clean-up system to meet turbine specifications (Galeno et al., 2011; Minutillo et al., 2009).

Table 2.7

Some of the medium size plants under thermal plasma technology for processing of waste around the world.

Company	Raw material	Capacity (TPD)	Applications	Plasma technology	Location	Reference
Maharashtra Enviro Power Ltd.	Hazardous waste	68	Power (1.6 MW)	Westinghouse plasma corporation	Pune and Nagpur, India	(SMS Maharashtra Enviro Power Ltd.)
PEAT International	Medical waste	1.45	-	PTDR-100 system	Shanghai, China	(PEAT International)
PEAT International	Hazardous waste	0.48	-	PTDR, Lab size unit	Kaohsiung, Taiwan	(PEAT International)
PEAT International	Industrial waste	3-5	-	PTDR system	Tainan, Taiwan	(PEAT International)
Hitachi Metals Ltd.	MSW & Sewage sludge	28	-	Westinghouse plasma corporation	Mihama & Mikata, Japan	(National Energy Technology Laboratory)
Hitachi Metals Ltd.	Auto Shredder Residue	165	Power (7.9 MW)	Westinghouse plasma corporation	Utashinai, Japan	(Orlando, 2010)
Plasco Energy Group Inc.	MSW	85	Power (1 MW)	Phoenix Solutions Co	Ottawa, Canada	(Phoenix Solutions Co.)

Kobelco Eco-Solutions Co. Ltd.	Poly Chlorinated Biphenyls	-	-	Phoenix Solutions Co	Tokai, Japan	(Phoenix Solutions Co.)
CHO-Power	Industrial waste	137	Power (12 MW)	Europlasma	Morcenx, France	(CHO Power)
Pyrogenesis	Municipal/Medical waste	8.5	Power (420 kW)	Plasma Resource Recovery System	Hurlburt Field, USA	(PRRS-Pyrogenesis)
Pyrogenesis	MSW	0.5-2	-	Plasma Resource Recovery System	Montreal, Canada	(PRRS-Pyrogenesis)
Dow Corning Corporation	Industrial waste	-	Syngas/Synglass	InEnTec	Michigan, USA	(InEnTec)
Global Plasma Technology Limited	Medical waste	-	Power	InEnTec	Taipei, Taiwan	(InEnTec)
Kawasaki Plant Systems	Poly Chlorinated Biphenyls/Asbestos	-	Syngas/Power	InEnTec	Harima, Japan	(InEnTec)
Sunbay Energy Corporation	MSW	400	Power (26 MW)	Europlasma	Port Hope, Canada	(Fabry et al., 2013)
EnviroParks Limited	MSW/Industrial	750	Power (20 MW)	Europlasma	Hirwaun, UK	(Fabry et al., 2013)

Green Power Systems	MSW	1000	Power (32 MW)	Westinghouse plasma corporation	Tallahassee, USA	(Chemeurope)
Advanced Plasma Power	MSW	250	Power (16 MW)	Tetronics	Swindon, UK	(Tetronics)
Advanced Plasma Power	MSW	250	Power (17 MW)	Tetronics	South West England, UK	(Tetronics)
Advanced Plasma Power	Residual waste	-	Bio Substitute Natural Gas	Tetronics	Swindon, UK	(Fabry et al., 2013)
Advanced Plasma Power	Landfill waste	1230	Power (100 MW)	Tetronics	Belgium	(Jones et al., 2013)

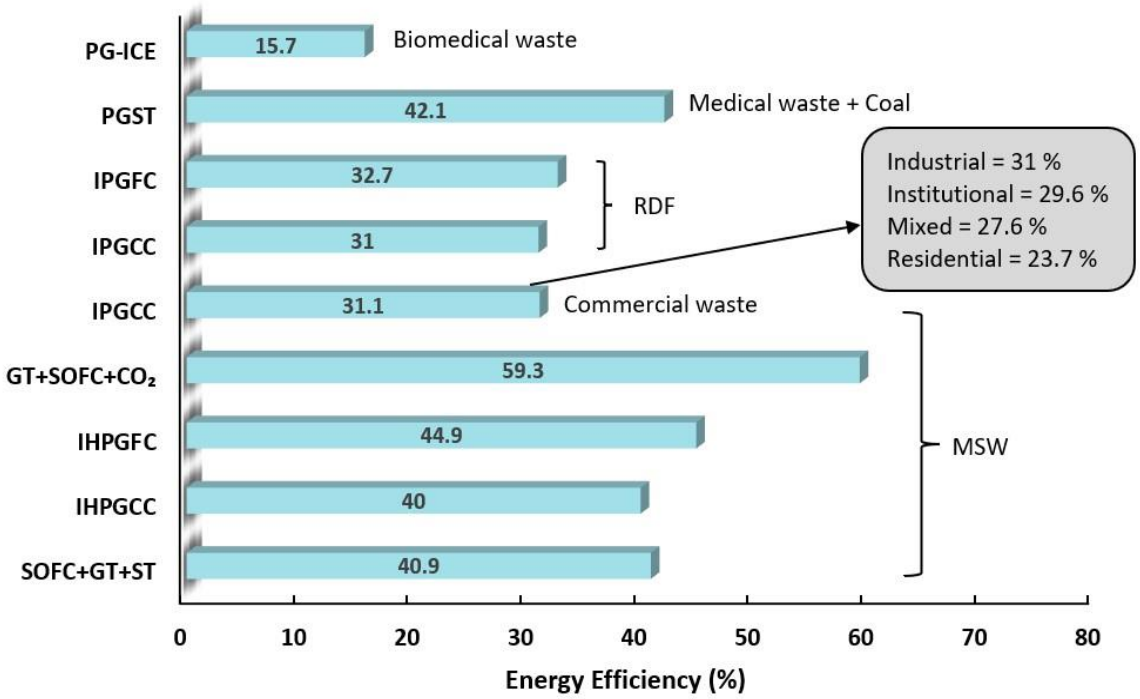

(a)

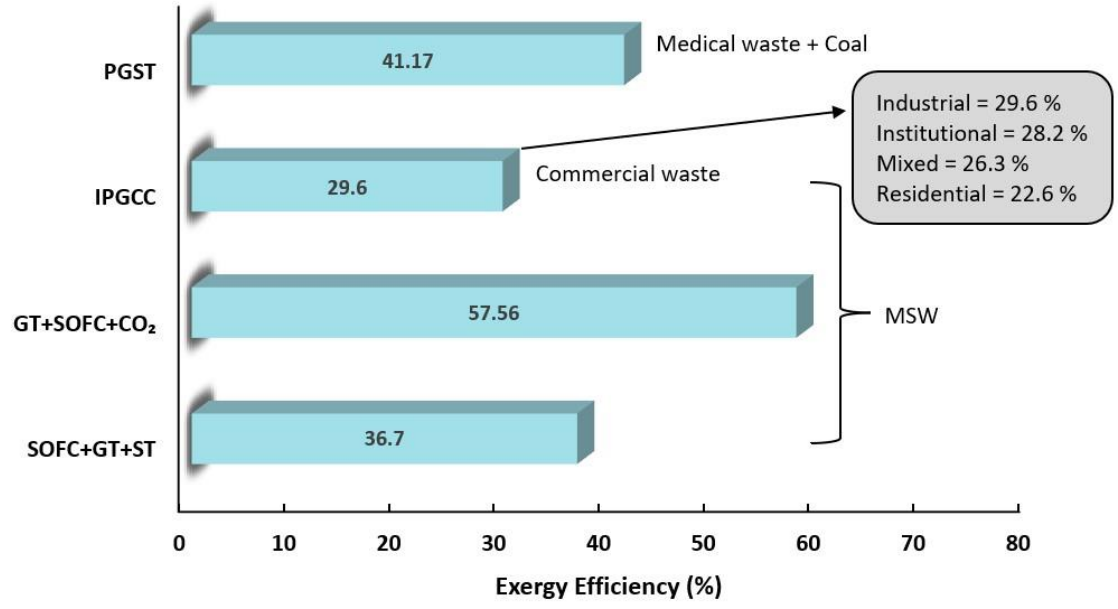

(b)

Fig. 2.11. (a) Energy and (b) exergy efficiencies obtained by authors in their respective power plant studies (Galeno et al., 2011; Jiang et al., 2021; Minutillo et al., 2009; Montiel-Bohórquez et al., 2021; Pan et al., 2022; Peng et al., 2021; Perna et al., 2018, 2016).

The concept of a hydrogen-based EES (Electric Energy and Storage) system allows to store and generate electric energy using SOFC (Perna et al., 2018). The plant consists of: (1) a renewable and storage section based on a solid oxide electrolysis cell (SOEC) unit that consumes wind power, (2) the plasma gasification section which utilizes MSW under hydrogen and air medium and (3) the power generation section based on SOFC unit. The net electric efficiencies were reported as 44.9% for hydrogen-based plasma gasification (IHPGFC) and 35% to 40% (ratio of O_2 changed from 40-100 vol. %) under air medium (IAPGFC). (Perna et al., 2016) also studied the application of hydrogen gas produced from conventional and plasma gasification systems using MSW based on a combined cycle power generation system (IHGCC and IHPGCC). In both configurations, the system shows a better performance in terms of energy output with electric efficiencies of 43% and 40% for IHGCC and IHPGCC, respectively. Hence, hydrogen-based clean energy technologies perform better due to their higher heating value of the fuel.

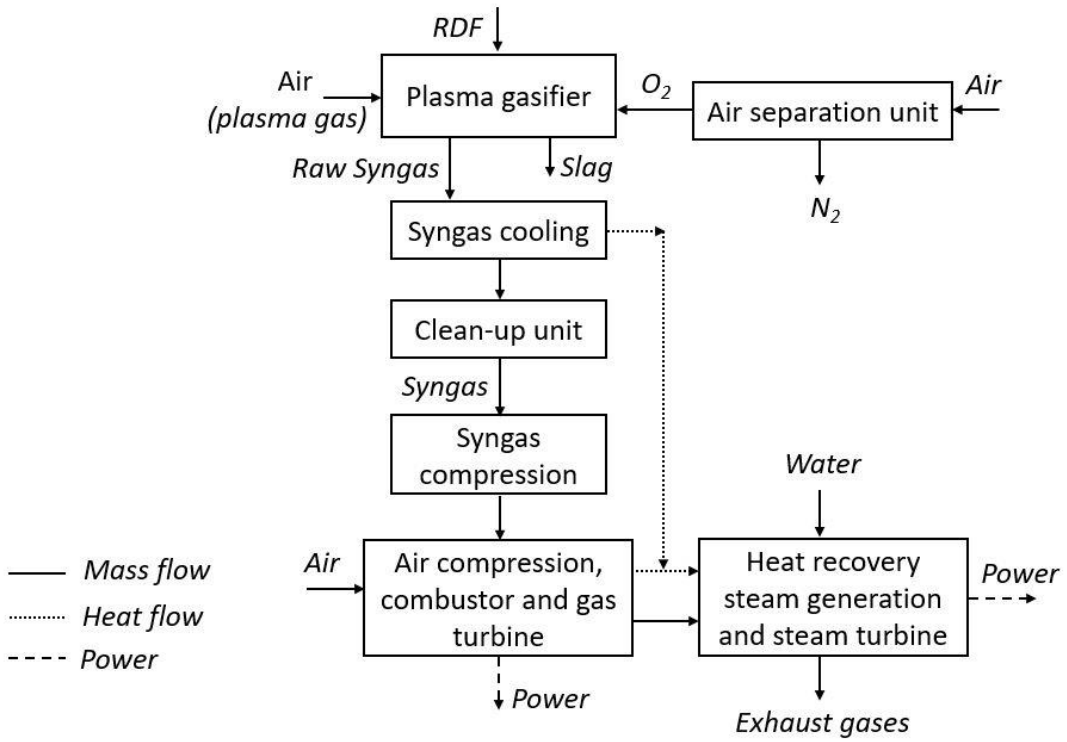

Fig. 2.12. Schematic representation of an IPGCC power plant using RDF feedstock.

The analysis of the effect of moisture content (MC) based on the origin of MSW, such as residential, industrial, etc. on exergo-economic performance helps to assess the improvement potential of the system. As the MC content decreased from 57.9 wt.% to 26.6 wt.% (based on waste type), the plant efficiency of IPGCC increases from 23.7 to 31% (energy), and 22.6-29.6% (exergy). The plasma gasifier has the highest exergy destruction rate due to the irreversible nature of the chemical reactions taking place to convert waste into syngas. It is followed by the MSW-associated drying. The unit exergo-economic cost of electricity, without including the MSW treatment fee, ranged from 117-156 US$/MWh, which is generally higher than the market price by 50 US$/MWh on average (Montiel-Bohórquez et al., 2021). Similarly, the thermodynamic analysis of MSW plasma gasification integrated with chemical looping combustion (CLC) and SOFC power plant results in the net energy and exergy efficiencies of 40.9% and 36.7%, respectively, with 99.3% CO_2 capture. The largest rate of exergy destruction occurs in the BFB-plasma gasification unit, similar to the result reported by Montiel-Bohórquez et al., 2021. The plasma gasifier contributes 33.62% of exergy destruction, followed by SOFC and CLC with 15.45% and 14.72%, respectively (Jiang et al., 2021). Furthermore, the mixture of syngas generated from MSW and coal for power generation, entirely via steam turbine unit, reduces the overall net efficiency (with waste-to-energy efficiency of 35.16%) from 42.36% to 42.14% (referred coal power plant). This is attributed to the auxiliary power consumption of the proposed power plant design. The total exergy efficiency (41.17%) also decreases slightly by 0.27% from the reference plant. With a life span of 25 years of the proposed system, the net present value (NPV) of 40,341 k$ can be achieved with a payback period of 4.58 years by implementing the proposed power plant approach (Pan et al., 2022).

In another novel technique of combined heat and power (CHP) generation through plasma gasification of medical waste, SOFC has been integrated with a gas turbine and CO_2 supercritical turbine cycle, and the waste heat is recovered as domestic hot water (DHW). The

waste-to-electric efficiency of the hybrid system reaches up to 59.3% and the combined CHP efficiency attained 87.8%. In the exergy analysis, the plasma gasifier, SOFC and combustion chamber contributed to irreversibilities in the order of 21.97%, 21.32% and 19.16%, respectively, with an overall exergy efficiency of 57.56%. Despite the high medical waste treatment fee of 466.2 $/t, the annual income due to waste treatment, electricity sale, slag sale and heat supply is 9790.2 k$, 9470.51 k$, 26.6 k$ and 3992.28 k$, respectively, in 20 years with a payback period of only 3.77 years (Peng et al., 2021). Hence the plasma-based system can be commercialized for treating high calorific values waste feedstocks.

2.7.2. Uses of discarded slag

Vitrified slag in the form of granulated aggregates has been reused in roadbeds as an asphalt mixture and concrete cluster while cast slag is used as a secondary product for interlocking bricks, tiles and blocks, as shown in Fig. 2.10. Granular slag is used to produce pavement brick for supplementing cement or gravel (Jimbo, 1996). By appropriate heat treatment of the slag at different temperatures after vitrification and with the addition of nucleation agents such as TiO_2, Cr_2O_3, Fe_2O_3, etc., glass-ceramics with enhanced properties can be produced (Gomez et al., 2009; Rawlings et al., 2006). In addition to the value-added product from waste disposal, which accounts for nearly 42% of the total income, slag sales can fetch up to ~ 27-800 k$ annually by treating 21-100 MT of wastes (Pan et al., 2022; Peng et al., 2021).

2.8. Summary

Although plasma gasification is not a new technology, in the last decade, several studies have been conducted due to its potential as an alternative gasification technique for clean fuel generation. The main advantage of plasma gasification technology is the utilization of a wide variety of waste as feedstocks other than coal and biomass. Significant research has taken place over the years to eliminate the issue of tar formation through the inclusion of primary and

secondary catalysts, high-reacting gasifying medium (steam), modification of reactor, etc., and therefore, plasma-assisted gasification is one of the suitable options for tar-free syngas. Even in the case of steam-plasma gasification of RDF, which is highly endothermic, an operating temperature of 1100-1220 °C can be reached with higher production of H_2 up to 53 vol. % with hot-gas efficiencies of 95% and LHV of 10.9 MJ/Nm^3. Even sawdust-based plasma gasification produces a higher H_2 content of 41.5 vol.% with a heating value of 10.2 MJ/Nm^3 under the CO_2 atmosphere. But in a small-scale system, the structure of the gasification chamber and stability of the plasma torch are crucial to reduce heat dissipation, low tar formation and higher carbon conversion.

Due to its flexibility, the plasma gasifier could be integrated with multiple hybrid power generation systems such as gas turbine combined cycle (η ~ 23.7-31%) or fuel cells (η ~ 35-45%). Low organic content feedstocks such as MSW (with moisture content up to 58%), biomedical waste, carpet waste, etc., which are difficult to decompose even under higher operating temperatures, can be decomposed up to 90% without any release of harmful gases. Some medium-scale companies like Alter NRG, InEnTec, PEAT etc. installed a plasma gasification system for a total cost of $30 to $300 million, processing 30-100 TPD of waste that generates electrical output from 5-50 MW. Now, for scaling to the industrial level, a standard model is required to be established with the theoretical model that can help future researchers and policy-makers. In countries like India, the plasma method requires attention, where the generation of waste is increasing rapidly without any formal treatment process. Moreover, the intense release of carbon emissions from fossil fuels and the expensive usage of electricity, especially in rural areas, call for sustainable methods. If modifications to the existing thermal plasma technique are considered to improve efficiency and cost, microwave-induced plasma may do it with less power consumption and utilize the moisture content in waste to generate heat internally. However, non-uniform heating of the feedstocks is the biggest

disadvantage of microwave application, due to which the temperature remains unstable. Studies on a novel approach to understand the thermodynamics through heat distribution will help increase the process's yield and efficiency.

Every approach discussed above found a possibility of using the plasma gasification process as an alternative to conventional gasification that yields a clean gas stream and has the potential for green energy production. Hence, it is clear that in the energy recovery sector, the system performs rationally in the usage of waste materials and environmental pollution, however, it finds some challenges in terms of the initial cost and returns on investment which is longer as compared to existing industrial facilities.

2.9. Research gaps

Waste management through plasma gasification is studied extensively in the above literature review. The wastes such as MSW, RDF, kitchen waste, etc. are treated to yield moderate and high calorific syngas. Further, the application of clean syngas towards electricity production is conducted as an end-use. Considering the stated literature, the following research gaps are identified as described.

- The thermal decomposition of complex compounds such as butadiene, styrene, phenolic resin, etc., through this route has not yet been studied. The presence of such compounds makes the plastic difficult to recycle or undergo other thermal conversion methods without pollutant generation. Thus, the feedstocks consisting of plastic mixtures (RDF) and specific plastic material like acrylonitrile butadiene styrene (ABS), bakelite are considered in this study.
- For any thermochemical conversion process, the pathway of the chemical reactions is crucial. This can be predicted with the aid of characterization of the feedstock and the

products (residue, oil, syngas) obtained after the plasma gasification process. The pathway of the plasma gasification process is not reported in the literature.

- The usage of CO_2 as plasma gas for the gasification of complex polymer waste is not yet explored. As the complex polymers have high calorific value, their decomposition under plasma condition is beneficial for economic operations.
- Due to high power consumption and initial investment in a plasma gasification process, the thermo-economic analysis of the system becomes essential. In the literature, only energy analysis in terms of cold gas efficiency is reported. Therefore, a 3-E (Energy, Exergy and Economic) analysis of the plasma gasification unit is essential to determine the efficiency of energy utilization, source of losses, and cost-benefits.
- Most of the findings reported in the literature are based on the production of electricity through the integration of plasma gasification (PG) with different routes of power generating systems such as standalone steam turbine units, combined cycles, CLC, etc., using various wastes. However, the integration of plasma gasification unit with advanced systems such as fuel cells (MCFC) and CLR processes to co-produce hydrogen and electricity is not yet unexplored. Moreover, a collective comparison based on 4-E analyses involving the cost to the environment is not yet studied.

2.10. Objectives and scope of the thesis

The main objective of this study is to valorize complex waste using CO_2 plasma gasification for the production of clean syngas to co-generate hydrogen and electricity. This brings down the ecological footprint on a large scale by (i) minimizing waste accumulation, (ii) effective CO_2 utilization, (iii) producing clean energy and (iv) generating more energy per unit mass of feed. To the best of our knowledge, no study on plasma gasification of waste was reported based on a detailed assessment of 4-E (energy, exergy, economic and environmental) analyses

with product characterization. Based on the state-of-the-art survey and research gap, the following objectives are framed.

- Laboratory scale experimental investigation on plasma gasification of biomass, plastic and e-waste derived from solid waste for clean syngas production.
- Product characterization and performance analysis to determine the feasibility of the plasma gasification system for commercial use based on the experimental parameters.
- Effect of integrating plasma gasification with molten carbonate fuel cell (MCFC) and chemical looping reforming (CLR) for the co-generation of hydrogen and electricity.

The scope of the present work is as follows:

- Solid wastes such as refused derived fuel (RDF) based on the Indian scenario, computer keyboard plastic waste (CKPW) and electrical switch waste (ESW) are used for the plasma gasification process under the CO_2 atmosphere.
- Evaluation of the impact of the operational parameters such as feedstock mass flow rate, feed CO_2 gas flow rate and torch power on syngas composition LHV and yield.
- Estimation of the energy intensiveness of the process, exergy distribution and cost involved in the production of syngas.
- Various characterizations of the raw feed, obtained syngas, oil and residue for finding their usage in commercial applications.
- 4-E (energy, exergy, economic and environmental) analyses on the plasma gasification integrated molten carbonate fuel cell (MCFC) and chemical looping reforming (CLR) for the co-generation of hydrogen and electricity using Aspen Plus software.

Chapter 3

Materials and method

CHAPTER 3

MATERIALS AND METHODS

The current chapter provides the materials and methodology considered for this research work. The details of the feedstock used, experimental set-up and operating parameters employed in the plasma gasification process are explained. Then, the characterization techniques for the analysis of feedstock and residues obtained using various analytical instruments are discussed. The 3-E (Energy, Exergy and Economic) analyses based on experimental results to estimate the cold gas efficiency (CGE) and levelized cost of syngas (LCOS) are explained. Then the simulation methodology of plasma gasification integrated molten carbonate fuel cell (MCFC) and chemical looping reforming (CLR) process for hydrogen and power co-generation based on 4-E (3-E plus environmental) analyses of the overall plant is elaborated.

3.1. Feedstocks

This study utilizes refused derived fuel (RDF) comprising mainly of plastic, paper, yard and food waste, computer keyboard plastic waste (CKPW) made of acrylonitrile butadiene styrene (ABS) mixed with polycarbonate (PC) and electrical switch waste (ESW). The photographs of wastes samples shown in Fig. 3.1. are collected from different locations of the Indian Institute of Technology, Guwahati. In case of RDF, the composition of various components is based on the Indian scenario, comprising 35% plastics, 40%-yard waste, 10% paper waste and 15% food waste (Tripathi and Rao, 2022). High-density polyethylene (HDPE), low-density polyethylene (LDPE), polyethylene (PE), polypropylene (PP) and polyethylene terephthalate (PET) are the major contributors in plastic waste (Bhatt et al., 2021). While used paper, newspaper, tissue paper and cardboard contributed to paper waste. Similarly, yard and food waste are garden and kitchen leftovers, respectively. Large chunks of CKPW and ESW feed with an average size of 2 cm are processed to increase the contact between the particles and the plasma arc, which also

reduces the feed pre-treatment cost and time. RDF pellets of 1 cm uniform diameter and 0.5 cm thickness are prepared for plasma gasification. The proximate and elemental analyses of the feedstocks and their lower heating value (LHV) are summarised in Table 3.1. RDF has an average moisture content of 14.57 wt.%., in which food waste has the highest moisture of 67.9 wt.%, followed by paper (10.25 wt.%) and yard (8.41 wt.%), while plastic has no moisture.

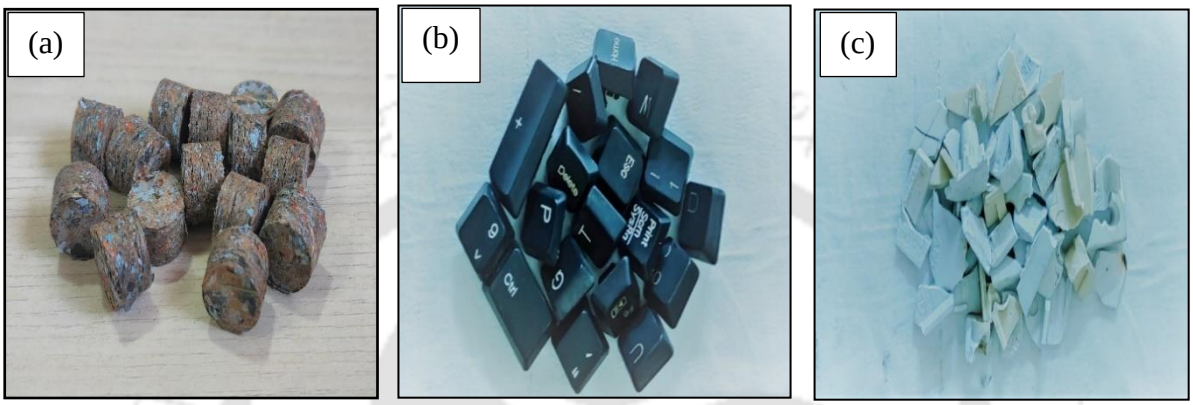

Fig. 3.1. Feed used for the experiments (a) RDF, (b) CKPW and (c) ESW.

Table 3.1

Proximate and ultimate analysis of fuel used in this study.

	RDF[b]	CKPW	ESW
Proximate analysis [wt.%, as received basis]			
Moisture	-	-	1.54
Volatile matter	83.04	93	77.46
Fixed Carbon	3.01	6	17
Ash	13.95	1	4
Ultimate analysis [wt.%, ash free basis]			
C	62.74	78.91	31.53
H	6.69	7.25	5.28
N	3.12	1.65	19.87
S	0.21	-	0.73
O[a]	27.24	11.19	38.59
LHV based on energy [MJ/kg]	22.16	35.31	14.05
LHV based on exergy [MJ/kg]	23.49	37.33	18.51

[a] by difference; [b] dry basis.

3.2. The experimental system

The experiments are performed using a plasma gasification reactor of 5 cm in diameter and 60 cm in length, as shown in Fig. 3.2. The outer shell of the reactor is 20 cm in diameter and made of MS 314 grade, whereas the inner wall has a layer of refractory ceramic coating of 150 mm thickness to prevent heat damage. B-type and k-type thermocouples are used for temperature measurement with a length of 4 cm and 15 cm, respectively, placed away from the plasma arc. The anode and cathode of the DC plasma torch are water-cooled graphite electrodes located perpendicular to the reactor that can operate at currents between 50-200 Amp and arc powers of 0.5-10 kW. Although graphite has a higher rate of erosion, it has the highest melting point of 3600 °C. Further, graphite is low cost among all the possible materials used for the construction of plasma torches (Rath et al., 2012; Szente et al., 1992). The schematic representation of the overall system is shown in Fig. 3.3.

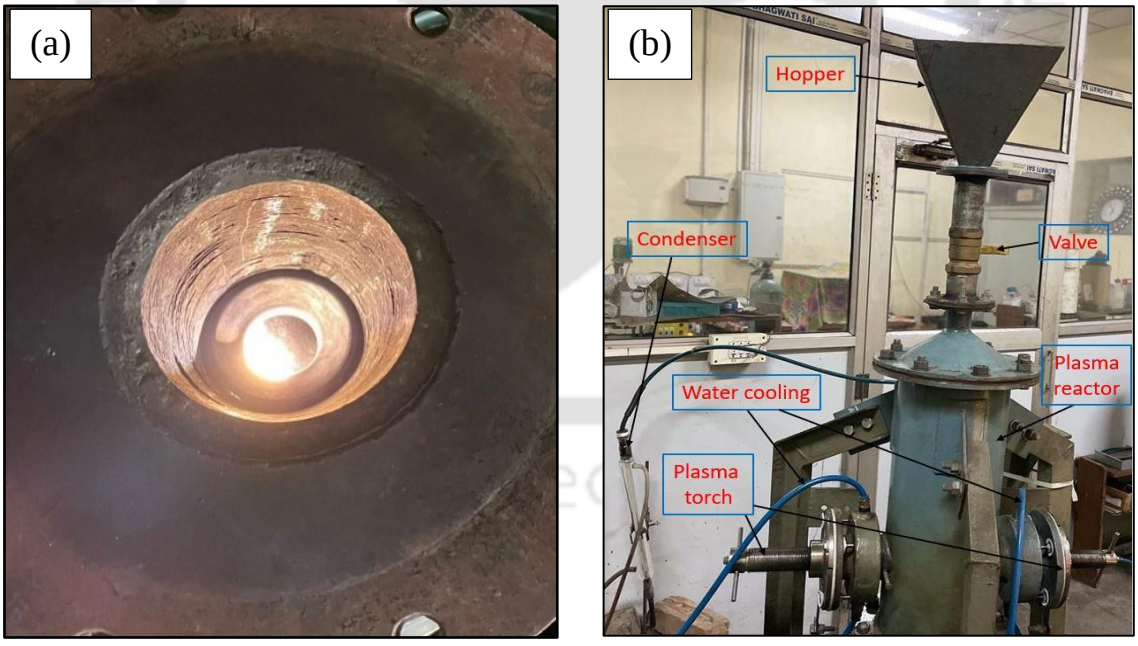

Fig. 3.2. Laboratory set-up of plasma reactor: (a) the plasma zone and (b) the overall plasma gasifier.

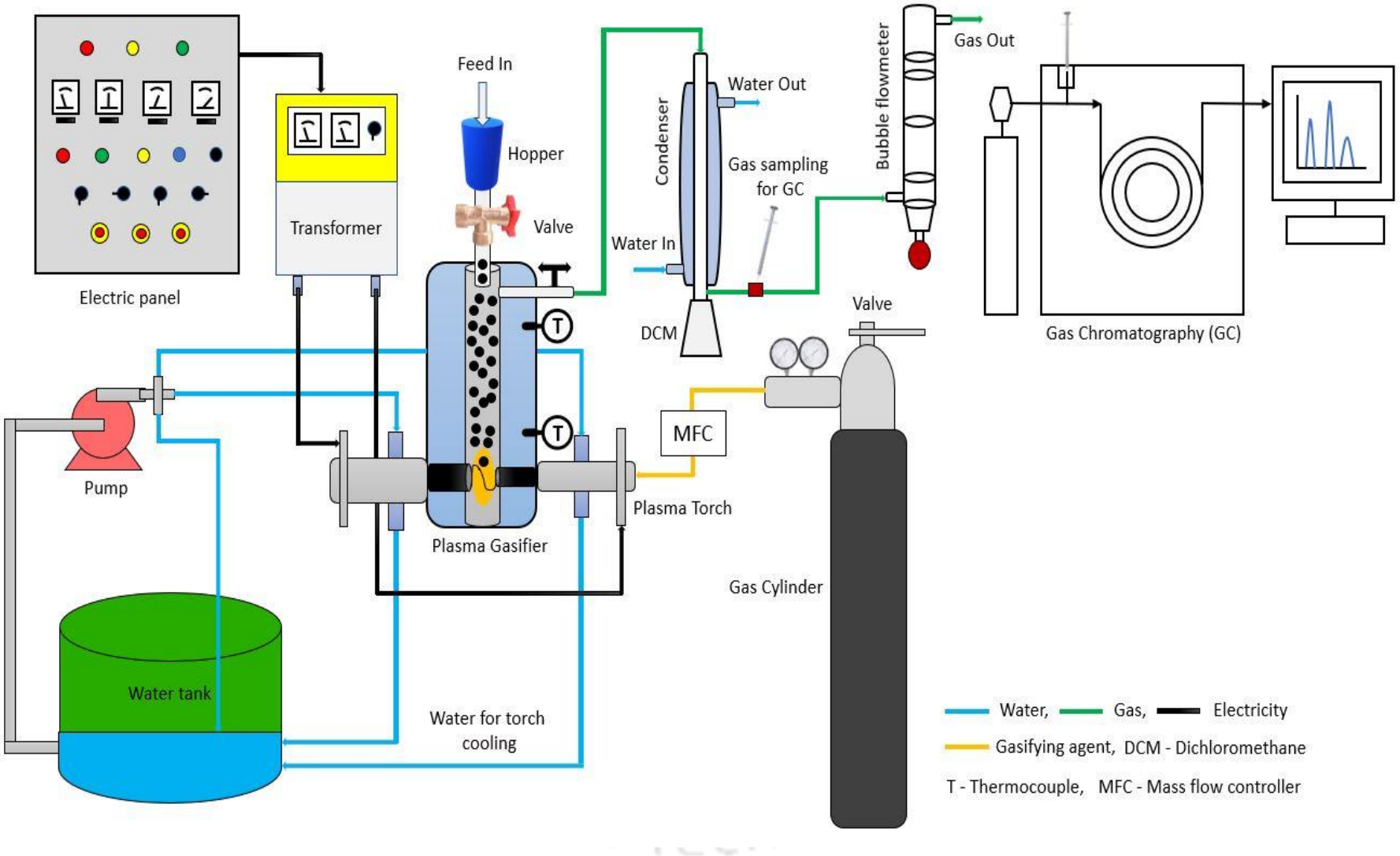

Fig. 3.3. Schematic diagram of the experimental system.

The feed material to be gasified is fed through a hopper from the top and the feed particles fell into the reactor under gravity. Carbon dioxide (CO_2, 99.9% purity) used as both plasma gas and gasifying agent for the experiment is purged through the center of the cathode, which has specifically designed holes that act as a medium for the gas inlet. The volumetric flow rate of the feed gas is controlled using a mass flow controller (MFC, Bronkhorst EL-Flow Select F-201 CV). The outlet of the produced gas is positioned at the top side of the reactor such that the high-temperature syngas exchange heat with the feed before exiting the reactor. Before the collection of syngas for sampling, it is cooled in a water condenser operating at a temperature of 5 °C. A chiller is used to maintain the flow rate and temperature of water in the condenser. In the final step, the cooled syngas is passed through a conical flask filled with 50 ml of dichloromethane (DCM, 99.5% pure) to absorb tar vapors present in the gas. Thereafter, the tar-free syngas are collected at regular intervals in a vacuum container using a needle syringe for their compositional analysis in a gas chromatograph. The volume percentage of H_2, air, CO, CH_4 and CO_2 is detected using a thermal conductivity detector (TCD) and hydrocarbons such as C_2H_4, C_2H_6 and C_3H_6 using a flame ionization detector (FID). The outlet flow rate of the tar-free syngas is measured using a bubble flow meter. The dissolved tar and other particulates in the DCM liquid is filtered using a filter paper to remove the particulates and, then the filtered liquid is sent to a rotavapor (Buchi R 300) for the recovery of DCM from the oil. The separation efficiency of the oil from the DCM solution is around 95-96%. Further, the physical and chemical properties of the obtained oil and the residue are analyzed.

3.3. Experimental conditions and operating parameters

Few preliminary experiments are conducted by batch feeding of the solids in the reactor and almost 80-90% of feed is converted within the first 10 min, as shown in Fig. 3.4. Hence, each experiment is carried out for 40 min, with an equal amount of feed introduced at every 10 min intervals, as shown in Table 3.2. The feed is introduced at the mass flow rate of 20 to 60 g per

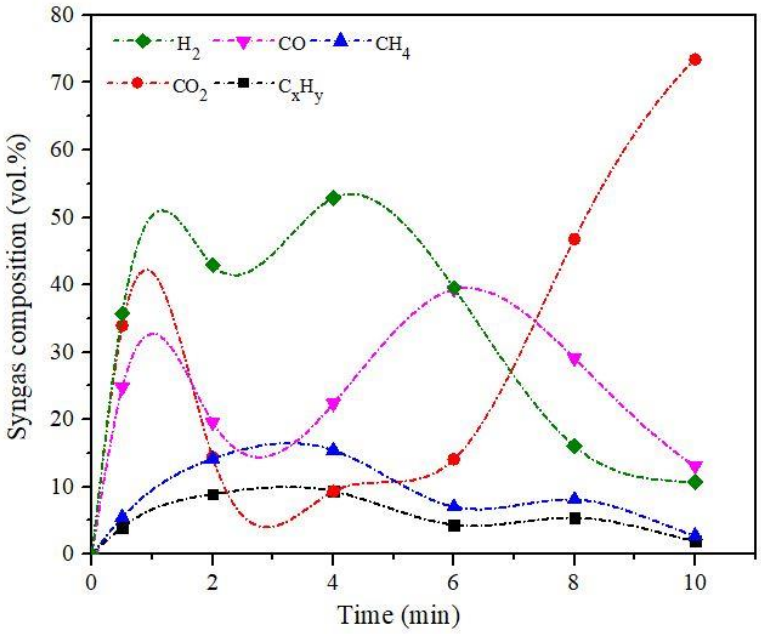

Fig. 3.4. Variation of syngas compositions for 10 min.

Table 3.2

Operating process parameters of the experiments conducted in this study.

	RDF			CKPW			ESW		
Case number	$\dot{m}_F$	CO_2	Power	$\dot{m}_F$	CO_2	Power	$\dot{m}_F$	CO_2	Power
1	20	0.4	0.75	20	0.5	1.12	20	0.5	0.75
2	30	0.4	0.75	30	0.5	1.12	30	0.5	0.75
3	40	0.4	0.75	40	0.5	1.12	40	0.5	0.75
4	50	0.4	0.75	50	0.5	1.12	50	0.5	0.75
5	30	0.2	0.75	60	0.5	1.12	60	0.5	0.75
6	30	0.3	0.75	40	0.3	1.12	40	0.4	0.75
7	30	0.5	0.75	40	0.4	1.12	40	0.6	0.75
8	30	0.4	0.5	40	0.6	1.12	40	0.7	0.75
9	30	0.4	1.12	40	0.7	1.12	40	0.8	0.75
10	30	0.4	1.6	40	0.5	0.75	40	0.5	0.5
11	-	-	-	40	0.5	1.6	40	0.5	1.12
12	-	-	-	40	0.5	2	40	0.5	1.6

$\dot{m}_F$ = feed flow rate (g/10 min); CO_2 = gas flow rate (lpm) and power in kW.

10 min interval, while the CO_2 flow rate is maintained in the range of 0.2 to 0.8 liters per minute (lpm). On the other hand, to observe the effect of temperature, the plasma torch power is maintained between 0.5 and 2 kW for the given set of experiments. The syngas is continuously collected at regular intervals of every 2 min and 4 min for the total run period of 10 and 40 min experiments, respectively. Due to high mechanical routine of the experiments, only 3 cases for each feed was repeated and the error (%) is calculated as a difference between the actual and repeated values, taking the actual result as a reference.

3.4. Characterization techniques

The raw feed and the products obtained after plasma gasification are characterized using various analytical tools and techniques as follows:

(i) Fourier-transform infrared spectroscopy (Make-Perkin Elmer and Model-Spectrum Two) (FTIR) analysis of raw feed, oil and residue is done in the wavenumber of 400-4000 cm^{-1}.

(ii) Thermogravimetric analysis (TGA) (Make-Netzsch and Model-Libra TG 209) of raw feed is carried out in the temperature range of 25-1000 °C with a heating rate of 10 °C/min under CO_2 (40 ml/min) atmosphere.

(iii) Proximate and ultimate analyses (Make-Thermo Fisher Scientific and Model-Flash smart V CHNS/O) of raw feed, oil and residue are performed as per ASTM standards D3172-75.

(iv) Gas chromatography-Mass spectrometry (GC-MS) (Make-Perkin Elmer and Model-Clarus 680 GC/600C MS) analysis of the obtained oil, which is dissolved in hexane, is conducted with helium as carrier gas to detect organic compounds such as alkanes, alkenes, aromatics, etc.

(v) Field emission scanning electron microscopy (FESEM) (Make-Zeiss and Model-Sigma) of the raw feed and the residue is performed at 5kX magnification to capture the morphological changes of the materials.

(vi) Density, viscosity and pH of the obtained oil are determined using a pycnometer by ASTM D891 standards, a rheometer (Anton Paar, Physica MCR301) and a pH meter (Labman, LMPH-10), respectively. These tests are conducted to measure the suitability of the oil for vehicles related to diesel properties.

(vii) X-ray diffraction (XRD) (Make-Rigaku Technologies and Model-Smartlab) with Cu-Kα radiation is performed in the 2θ range of 10-80° with a scanning rate of 10°/min. It provides the material's chemical composition (oxides) and physical properties.

(viii) Energy dispersive spectroscopy (EDS) (Make-Zeiss and Model-Sigma 300) of the ash samples obtained from the ESW feed is conducted at 3kX magnification to estimate the percentage composition of the elements.

3.5. Experimental methodology

3.5.1. 3-E (Energy, Exergy and Economic) analysis

. The syngas, oil and residue yield of the plasma gasification is estimated as follows (Bhui et al., 2021):

$$\text{Residue yield (\%)} = \frac{\text{Weight of residue (g)}}{\text{Initial feed weight (g)}} * 100 \quad (1)$$

$$\text{Oil yield (\%)} = \frac{\text{Weight of oil (g)}}{\text{Initial feed weight (g)}} * 100 \quad (2)$$

$$\text{Gas yield (\%)} = 100 - [Residue\ yield\ (\%) + Oil\ yield\ (\%)] \quad (3)$$

3.5.1.1. Energy analysis

The cold gas efficiency (η_{CGE}) of the plasma gasifier is the main parameter to evaluate the system performance based on Eq. 6. The energy input ($\dot{E}_F$) from the fuel feedstock to the plasma gasifier is found by multiplying the chemical energy of the fuel (LHV_F) and the mass flow rate of fuel ($\dot{m}_F$), moisture removal energy ($\dot{E}_m$, in case of RDF) and $\dot{E}_{plasma}$ is the input

plasma power to the reactor. The syngas energy ($\dot{E}_{syngas}$) is estimated based on the LHV of the individual gases in syngas (Agon et al., 2016; Alipour Moghadam et al., 2014).

$$LHV_{syngas}(MJ/Nm^3) = [(107.98 * xH_2) + (126.36 * xCO) + (358.18 * xCH_4) + (639.8 * xC_2H_4) + (930.5 * xC_2H_6) + (834.03 * xC_3H_6)]/1000 \quad (4)$$

Where 'x' denotes the volume percentage of respective species in the syngas.

The specific energy consumption required to dry 1 kg of material using a convective hot-air drier equipped with blower fans is given by Eq. (5) (Kumar et al., 2022).

$$E_t = A * v * \rho_a * C_{pa} * D_t * \Delta T \quad (5)$$

Where, E_t is specific energy consumption (kWh/kg), A is the area of the sample tray (m^2), v is drying air velocity (m/s), ρ_a is density of air (kg/m^3), C_{pa} is the specific heat of drying air (kJ/kg°C), D_t is drying time (h), ΔT is the temperature difference between drying and atmosphere (°C).

$$\eta_{CGE} = \left(\frac{\dot{E}_{syngas}}{\dot{E}_F + \dot{E}_m + \dot{E}_{plasma}}\right) * 100 \quad (6)$$

3.5.1.2. Exergy analysis

The estimation of exergy is based on the second law of thermodynamics and exergy is defined as the amount of energy available to do work when the system is brought to the dead state, i.e., the environmental conditions (Dincer and Rosen, 2021). The rate of kinetic and potential exergy is assumed to be negligible. The two major terms to calculate total exergy rate are physical ($\dot{E}_{ph}$) and chemical ($\dot{E}_{ch}$) exergy, which are given in Eq. 7-8 (Kalinci et al., 2011).

$$\dot{E}_{ph} = \dot{m}_{pdt} * [(h - h_0) - T_0(s - s_0)] \quad (7)$$

$$\dot{E}_{ch} = \sum_i y_i e_{i,ch} + RT_0 \sum_i y_i ln y_i \quad (8)$$

The specific exergy of fuel ($\dot{E}_{ch,fuel}$) is calculated based on the correlation given by Szargut and Styrylska and implemented by the reference (Ptasinski et al., 2007) as:

$$e_{ch,fuel} = \beta * LHV_F \quad (9)$$

$$\dot{E}_{ch,fuel} = \dot{m}_F * e_{ch,fuel} \quad (10)$$

The factor β is calculated for various fuels by the developed correlation as:

$$\beta = \frac{1.044+0.0160(H/C)-0.3493(O/C)[1+0.0531(H/C)]+0.0493(N/C)}{1-0.4124(O/C)} \quad (11)$$

where H/C, O/C and N/C are atomic ratios in the fuel.

The exergy efficiency (η_{ex}) of the plasma gasifier is estimated by using the following equation (Eq. 12):

$$\eta_{ex} = \left(\frac{\dot{E}_{syngas}}{\dot{E}_{ch,fuel}+\dot{E}_{plasma}}\right) * 100 \quad (12)$$

3.5.1.3. Economic assessment

The levelized cost of syngas (LCOS) obtained from plasma gasification is estimated to examine the commercial feasibility of the process. The following few assumptions are considered for calculating the syngas cost based on experimental results:

- Electricity tariff = 5.48 INR/kWh (India Energy, 2023)
- Annual rate of interest (r) = 4 %
- Equivalent period of utilization (P) = 2000 h/year
- Payback period (k) = 4 years

The LCOS (INR/kWh) (Eq. 19) is determined using the methodology considered by Paulino et al., 2020 and the investment cost (C_{system}) of plasma gasification unit (INR), including all the accessories such as chiller, mass flow controller, etc., is given by:

$$C_{system} = (C_{plasma\ gasifier} * 1.25 * \dot{m}_F) \quad (13)$$

The annuity factor (f), depending on the payback period (k) and annual interest rate (r) is given in Eq. (14) and (15).

$$f = \frac{q^k(q-1)}{(q^k-1)} \quad (14)$$

$$q = 1 + \frac{r}{100} \quad (15)$$

The variable operating cost ($OC_{var,gp}$) is a function of the electricity tariff (E_{tariff}), syngas energy and power of the plasma torch, whereas the maintenance cost (MC_{gp}) of the plasma system is considered as 3% of the plasma investment cost (Silveira and Tuna, 2003), as shown below.

$$OC_{var,gp} = \frac{E_{tariff} * \dot{E}plasma}{\dot{E}_{syngas}} \quad (16)$$

$$MC_{gp} = 0.03 * \left(\frac{C_{system} * f}{P * \dot{E}_{syngas}}\right) \quad (17)$$

In the model, the net cost (C_{total}) of the gasifying agent is estimated by Eq. (18):

$$C_{total} = C_{capex} + \frac{C_{opex}}{r}\left(1 - \frac{1}{1+r^P}\right) \quad (18)$$

where, C_{capex} is the capital cost (INR) of the CO_2 gas cylinder, including the gas flow regulator and C_{opex}, the operating cost (INR) is the gas refilling cost. As the costs are associated with the size of the units and therefore, the capital cost of plasma gasification and gasifying agent depends on the gas flow rate used.

$$LCOS = \left(\frac{C_{system} * f}{P * \dot{E}_{syngas}}\right) + OC_{var,gp} + MC_{gp} + C_{total} \quad (19)$$

3.5.2. Correlation developed for experimental and measured variables

The measured product gas compositions are strongly dependent on the feed mass flow rate (g/min), CO_2 flow rate (lpm) and torch power (kW), hence these are chosen as independent variables. The syngas composition (H_2, CO, CH_4, CO_2 and C_xH_y), LHV (MJ/m^3) and energy efficiency (%) are considered as dependent variables. The obtained values of these parameters are fitted in a polynomial curve of order 2 as per the given correlation in Eq. 20. Based on the experimental data, the constants are estimated by using the SPSS software provided by the institute (IBM, 2021). The software is a platform to implement statistical and text analysis, including data preparation and management.

$$Y = \beta_0 + \beta_1 X_1 + \beta_2 X_2 + \beta_3 X_3 + \beta_4 X_1^2 + \beta_5 X_2^2 + \beta_6 X_3^2 + \beta_7 X_1 X_2 + \beta_8 X_1 X_3 + \beta_9 X_2 X_3 \quad (20)$$

where, Y represents the general form of all the dependent variables, β is the constant assigned with the parameter and X_1, $X_2$and X_3 are the independent variables such as feed flow rate, CO_2 gas flow rate and torch power, respectively.

3.6. Simulation methodology

3.6.1. 4-E (Energy, Exergy, Economic and Environmental) analyses

3.6.1.1. Energy analysis

Table 3.3 provides the assumed operating parameters considered in the simulation for both the MCFC and CLR plants. The overall performance of the plant is estimated in terms of net energy efficiency ($\eta_{en,net}$), which is defined as the ratio of the sum of net hydrogen energy and electric power output ($\dot{W}_{net}$) to the input chemical energy of fuel (product of mass flow rate and LHV of the feed) of the plant as given in Table 3.4. The hydrogen output is estimated by multiplying the mass flow rate of H_2 ($\dot{m}_{H_2}$) with its LHV i.e., 120 MJ/kg (Khan and Shamim, 2016).

Table 3.3

Specifications of the proposed power-generating system by integrating plasma gasifier with MCFC and CLR (Duan et al., 2015; Minutillo et al., 2009; Ryzhkov et al., 2018; Cormos et al., 2020; Khan and Shamim, 2016; Surywanshi et al., 2021).

Unit	Operating conditions
Gasification pressure	1.013 bar
Syngas temperature	1250 °C
Combustor outlet temperature	1550 °C
Fuel reactor operating pressure and temperature	15 bar & 900 °C (Case 1); 1 bar & 900 °C (Case 2)
Steam reactor operating pressure and temperature	15 bar & 600 °C (Case 1); 1 bar & 580 °C (Case 2)
Air reactor operating pressure and temperature	15 bar & 1000 °C (Case 1); 1 bar & 1000 °C (Case 2)
Steam turbine pressures [HP/MP/LP]	120 bar / 34 bar / 3 bar
Steam turbine temperatures [HP/MP/LP]	530 °C / 560 °C / 240 °C
Fuel utilization factor	75 %
CO_2 utilization factor	80 %
MCFC reaction temperature	650 °C
MCFC current density	1500 A/m^2
H_2 compression	60 bar at 25 °C
CO_2 compression	110 bar at 25 °C
Isentropic efficiency (compressors, pumps, etc.)	90 %
Mechanical efficiency (compressors, pumps, etc.)	90 %

Table 3.4

Equations used for 4-E analyses.

Analysis	Equation	Reference
Energy		
	$\eta_{elec,net} = \frac{\dot{W}_{elec,net}}{\dot{m}_{F} * LHV\ of\ solid\ fuel} * 100$	(Surywanshi et al., 2021)
	$\eta_{H_2} = \frac{(\dot{m}_{H_2} * LHV_{H_2})}{(\dot{m}_{F} * LHV\ of\ solid\ fuel)} * 100$	(Surywanshi et al., 2021)
	$\eta_{overall} = \frac{\dot{W}_{elec,net} + (\dot{m}_{H_2} * LHV_{H_2})}{\dot{m}_{F} * LHV\ of\ solid\ fuel} * 100$	(Cormos et al., 2020)
Exergy		
	$\dot{E}_{xd} = \sum \dot{E}_{xin} - \sum \dot{E}_{xout}$	(Surywanshi et al., 2021)
	$\eta_{ex,overall} = \frac{\dot{W}_{overall}}{\dot{m}_{F} * Specific\ exergy\ of\ fuel}$	(Surywanshi et al., 2021)
Economic		
	$C_{plasma\ gasifier} = (4800 * 1.25 * \dot{m}_{F} * \left(\frac{Quot_{US\$}}{Quot_{EURO}}\right))$	(Paulino et al., 2020)
	$C = C_0 * (S/S_0)^{f}$	(Duan et al., 2015)
	$CO_2 avoided\ cost = \frac{COE_{Capture} - COE_{Non-capture}}{\ddot{E}_{CO_{2,Non-capture}} - \ddot{E}_{CO_{2,Capture}}}$	(Cormos et al., 2020)
	$CO_2 removal\ cost = \frac{COE_{Capture} - COE_{Non-capture}}{CO_2\ removed}$	(Cormos et al., 2020)
Environment		
	$\ddot{E}_{CO_2} = \frac{(\dot{m}_{CO_{2,emit}})}{\dot{W}_{net}}$	(Surywanshi et al., 2019)
	$\varepsilon^{a}_{f,CO_2} = \frac{(\dot{m}^{a}_{CO_2})}{(3.6 * E^{a}_{chf})}$	(Surywanshi et al., 2019)
	$GWP = \sum PP_i * \dot{m}_i$	(Sun et al., 2021)
	$SI = \frac{1}{(1 - \frac{\dot{E}_{xd}}{\dot{E}_{xin}})}$	(Dincer and Rosen, 2021)

$$\eta_{en,net} = \frac{\dot{W}_{net}}{(\dot{m}_F * LHV\ of\ solid\ fuel) + (\dot{m}_{CH_4} * LHV\ of\ methane)} \quad (21)$$

The output power of the fuel cell system is determined based on the current and applied voltage. The ideal cell voltage of MCFC can be calculated by Nernst Potential (E_{Nernst}) in terms of partial pressures (p):

$$E_{Nernst} = E_0 + \frac{RT}{n_e F} \ln\left(\frac{p_{H_2,an} * (p_{O_2,ca})^{0.5} * p_{CO_2,ca}}{p_{H_2O_{an}} * p_{CO_2,an}}\right) \quad (22)$$

$$E_0 = \frac{\Delta G}{n_e F} \quad (23)$$

$$\Delta G = 242{,}000 - 45.8 * T \quad (24)$$

Where E_0 is ideal standard potential (volt), ΔG is Gibbs free energy change (J/mol), T is the operating temperature (°C), R is the universal gas constant (J/mol °C), n_e is the number of electrons released in the dissociation of H_2 molecule (equal to 2), F is the Faraday constant (96487 C/mol).

The actual voltage (V_{cell}) is calculated following Ohm's law:

$$V_{cell} = E_{nernst} - (r_{an} + r_{ca} + r_{ohm}) * i_c \quad (25)$$

$$i_c = \frac{I}{A} \quad (26)$$

$$r_{an} = 2.27 * 10^{-9} * \exp\left(\frac{E_{act,an}}{RT}\right) * p_{H_2,an}^{-0.42} * p_{CO_2,an}^{-0.17} * p_{H_2O_{an}}^{-1.0} \quad (27)$$

$$r_{ca} = 7.505 * 10^{-10} * \exp\left(\frac{E_{act,ca}}{RT}\right) * p_{O_2,ca}^{-0.43} * p_{CO_2,ca}^{-0.09} \quad (28)$$

$$r_{ohm} = 0.5 * 10^{-4} * \exp\left[3016\left(\frac{1}{T} - \frac{1}{932}\right)\right] \quad (29)$$

Where, r_{an}, r_{ca} and r_{ohm} are the resistances of the anode, cathode and ohmic polarization, respectively (Ohm m^2), i_c is the current density (A/m^2), I is the current flowing in the system,

A is the total active surface area (m^2), p_x is the partial pressure of species 'x' (atm), $E_{act,an}$ and $E_{act,ca}$ are the anode and cathode activation energy, respectively, $E_{act,an}$ = 53,500 J/mol , $E_{act,ca}$ = 77,229 J/mol (Campanari et al., 2014).

The power output of the stack ($\dot{W}_{mcfc}$) is estimated by:

$$\dot{W}_{mcfc} = V_{cell} * I \quad (30)$$

Other indicators such as current density, fuel utilization factor, CO_2 utilization factor greatly determine the performance of the MCFC system (Leto et al., 2011):

Fuel utilization factor (FU) is defined as the ratio of the molar flow rate of the hydrogen utilized at the anode to that of hydrogen fed at the inlet,

$$FU = \frac{n_{H_{2,in}} - n_{H_{2,out}}}{n_{H_{2,in}}} = \left(1 - \frac{n_{H_{2,out}}}{n_{H_{2,in}}}\right) \quad (31)$$

CO_2 utilization factor (CU) is defined as the ratio of the molar flow rate of CO_2 utilized as carbonate ion to the flow rate of CO_2 at the cathode inlet.

$$CU = \frac{n_{CO_{2,in}} - n_{CO_{2,out}}}{n_{CO_{2,in}}} \quad (32)$$

3.6.1.2. Exergy analysis

The exergy analysis can identify the process irreversibilities and deduce the contribution of individual components towards exergy destruction as well as overall process efficiencies. The methodology to estimate the input fuel exergy and output exergy distribution is given in Section 3.5.1.2. The exergy destruction ($\dot{E}_{xd}$) in terms of exergy inflow ($\dot{E}_{xin}$) and outflow ($\dot{E}_{xout}$) of the unit, and the net exergy efficiency ($\eta_{ex,net}$) is specified in Table 3.4.

3.6.1.3. Economic analysis

Economic analysis has been considered based on the principle of dividing the overall process into individual components for calculating the costs of equipment, operation and maintenance (Q&M), fuel, metal oxide, etc. (Duan et al., 2015; Leto et al., 2011). Meanwhile, the cost of electricity (COE) and the cost of CO_2 avoided and removed are estimated as per the methodology adopted by the International Energy Agency (IEA) (Duan et al., 2015). The levelized cost of hydrogen (LCOH, $/kg) is calculated based on the total plant cost and the mass flow rate of H_2 leaving the steam reactor, as given in the literature (Khan and Shamim, 2016). The cost assumptions based on literature to estimate the cost of electricity are shown in Table 3.5. The equipment cost of a plasma gasifier using steam as plasma gas is calculated based on the equation given in Table 3.4. Also, the annuity factor (f) is estimated using Eq. (14, 15) in terms of the annual interest rate and payback period (Paulino et al., 2020).

Table 3.5

Assumptions of parameters for COE calculations.

	Value	Reference
RDF cost [M$/year]	4.06	(Ministry of Housing and Urban Affairs, 2018)
Natural gas cost [M$/year]	6.76	(Duan et al., 2015)
ESW and CKPW cost [M$/year]	7.38	(Lavee and Nardiya, 2013)
Iron oxide cost [$/kg]	0.056	(Surywanshi et al., 2021)
Process water cost [$/$m^3$]	1.09	(Khan and Shamim, 2016)
MEA cost [$/ton]	2200	(Sahu and V, 2021)
Interest rate [%]	8.00	(Duan et al., 2015)
First year operating hours [h]	5700	(Duan et al., 2015)
Rest of the lifetime operating hours [h]	7500	(Duan et al., 2015)
Operating lifetime [years]	25	(Campanari et al., 2014)
CO_2 transport and storage cost [$/$ton_{CO2}$]	11.22	(Mishra et al., 2019)
CO_2 emission tax [$/$ton_{CO2}$]	27.22	(Mishra et al., 2019)

The cost of a plasma gasifier includes: $\dot{m}_F$ is the mass flow rate of fuel (kg/h), $Quot_{US\$}$ is the dollar-to-euro quotation (US$), $Quot_{EURO}$ is the euro quotation (1 Euro), k is the payback period (years) and r is the annual interest rate (%). The capital cost (C) of the equipment is determined by the capacity factor method based on a scaling parameter and reference component cost given by the relationship in Table 3.4. Where, C_0 is the related cost from reference plants, S is the size of the designed equipment, S_0 is the reference size and f is the scaling component (Campanari et al., 2014; Zang et al., 2018). The specific cost of MCFC assumed here is adopted according to the ranges given in the literature (Spinelli et al., 2020).

The exchange rate of the prices is calculated based on the purchasing power of the countries i.e., purchasing power parity index (PPPI) and power capital cost index (PCCI) (Adams et al., 2017):

$$C_{country} = C_{knowncurrency} * \left(\frac{PCCI\ for\ current\ year}{PCCI\ for\ original\ year}\right) * PPPI_{country} \quad (33)$$

Finally, the procedure for determining COE, including all the factors of plant investment, O&M, etc., are shown in Fig. 3.5.

3.6.1.4. Environmental analysis

The specific CO_2 emission rate ($\ddot{E}_{CO_2}$) is measured in kg of CO_2 per MWh and the annual CO_2 emission or avoided (kg/s) for 7500 operation hours per unit of fuel ($\mathcal{E}^a_{f,CO_2}$) is calculated using annual energy input to the power plant (E^a_{chf}) in MWh. Whereas, the global warming potential (GWP) factor is estimated based on the pollution potential of CO_2 (1), CH_4 (28) and N_2O (265) in $kgCO_{2eq}/kg_{substance}$. GWP measures the amount of heat that the greenhouse gases trap in the atmosphere in equivalence to CO_2. The method is based on the CML (Centrum voor Milieukunde Leiden) baseline technique describing the impacts of the emitted compounds in Table 3.4 (Sun et al., 2021). While the sustainability index (SI) is related to the exergy loss in

the overall system caused due to the use of energy sources associated with emissions and resource depletion (Dincer and Rosen, 2021).

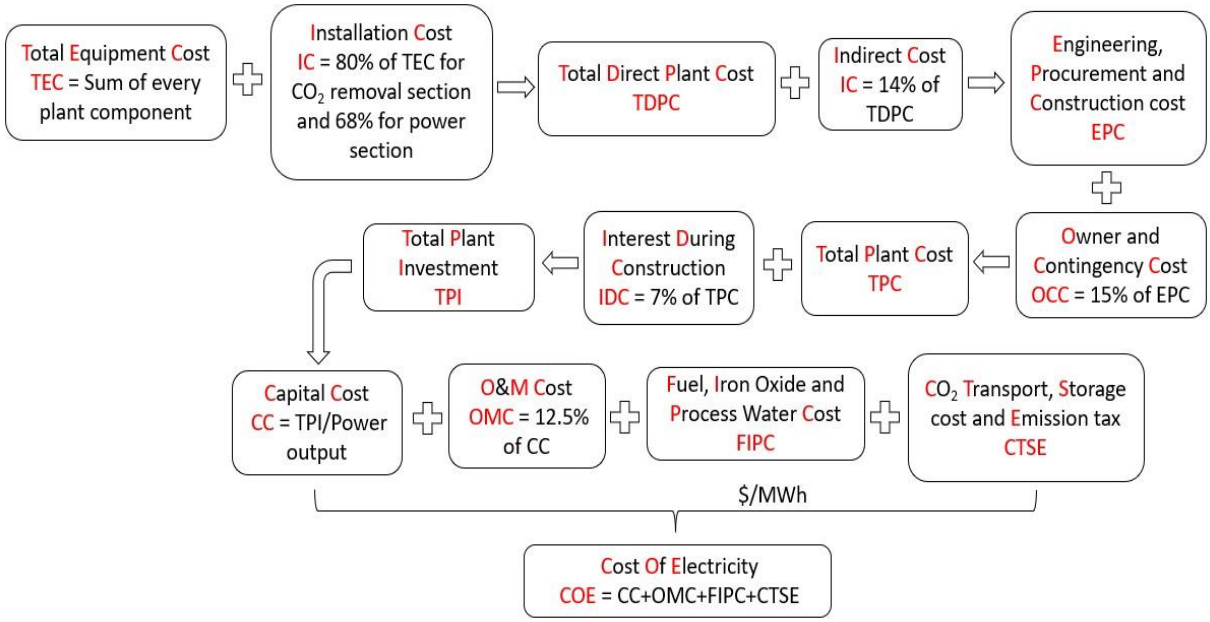

Fig. 3.5. Schematic sequence of the cost estimation parameters.

Chapter 4

Experimental studies on utilizing refused derived fuel as feedstock by CO_2 thermal plasma gasification process

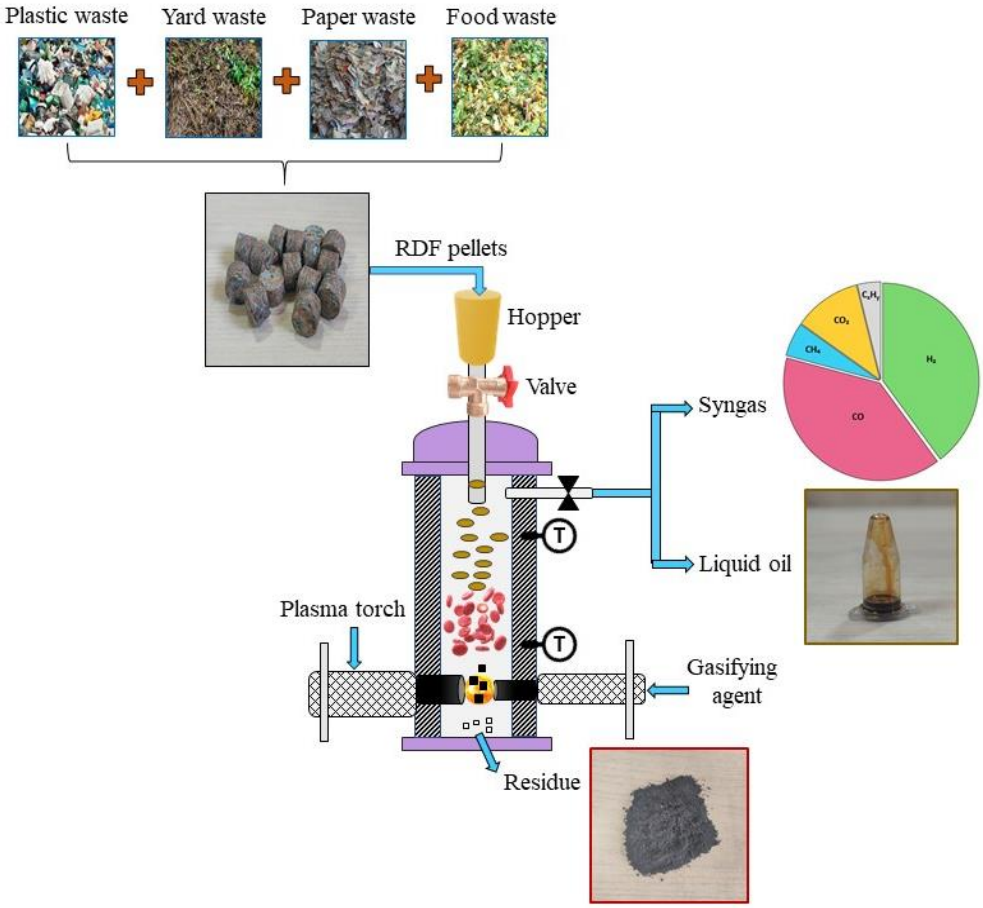

CHAPTER 4

EXPERIMENTAL STUDIES ON UTILIZING REFUSED-DERIVED FUEL AS FEEDSTOCK BY CO_2 THERMAL PLASMA GASIFICATION PROCESS

This chapter presents the experimental investigation on CO_2-plasma gasification of refused derived fuel (RDF), an offshoot of municipal solid waste. Carbon dioxide is chosen for two primary reasons: (i) to reduce net CO_2 emissions in the environment through consumption and (ii) the ability to liberate oxygen-free radicals for producing syngas-rich gaseous products. In this regard, an in-depth analysis is required to establish a correlation between refused-derived fuel and its constituent parts. The characteristics of RDF (physical and chemical properties, ash content, etc.) and the optimization of operating parameters (mass flow rate, CO_2 gas flow rate and plasma torch) of the plasma gasifier are performed. A comprehensive analysis involving 3-E (energy, exergy and economic) is performed to evaluate the key performance of the system in terms of energy distribution to examine the commercial viability of the process. Besides, the characterization of the products i.e., oil and residue, are found to predict the reaction mechanism of the overall process. Empirical correlations to predict the syngas compositions, lower heating value (LHV) of syngas and energy efficiency of the process are developed and validated.

4.1. Experimental parameters

To obtain the desired temperature for each experiment with respect to the set point of torch power, the plasma gasifier is slowly heated for around 1-1.5 h. The introduction of RDF pellets is considered at an interval of every 10 min for a total run 40 min of experiment and this has

resulted in almost 85-98% degradation of RDF. The method followed for making the RDF pellets of size 1 cm diameter and 0.5 cm thickness is shown in Fig. 4.1. The gas samples are collected every 2 min and 4 min, respectively, for a total run of 10 min and 40 min experiments. The RDF feed rate ($\dot{m}_F$) is varied in the range of 20-50 g per 10 min, with the feed CO_2 gas flow rate ranging from 0.2 to 0.5 liters per minute (lpm). The plasma torch power in the range of 0.5-1.6 kW is used in the experiments and these process parameters for each experiment are shown in Table 4.1.

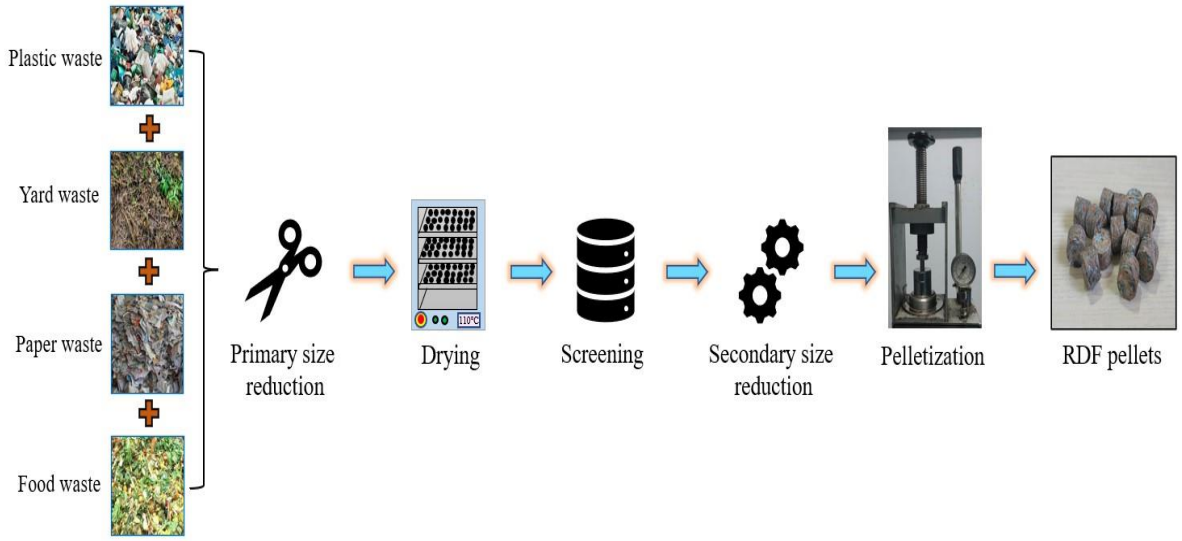

Fig. 4.1. Process followed in the preparation of RDF pellets as feedstock for plasma gasifier.

4.2. Results and discussion

4.2.1. Characterization of raw RDF feed

The component-wise proximate and ultimate analysis of RDF is shown in Table 4.2. Food waste has the highest moisture content of 67.9 wt.%, followed by paper (10.25 wt.%) and yard waste (8.41 wt.%), while plastic has no moisture. RDF has a higher fraction of volatile matter content (on a dry basis) that favors the generation of high-quality syngas with a lower amount of oil and solid residue. However, an ash content of ~ 14 wt.% reduces the energy density per

unit mass of feed. On the other hand, a moderate value of carbon and hydrogen content (mainly due to the plastic content) provides a better calorific value of RDF (22.16 MJ/kg), which is found in the range between high ash and low ash coal. Hence, RDF feed is suitable for converting waste to energy under plasma conditions.

Table 4.1

Process parameters used for the RDF experiments.

Case number	$\dot{m}_F$ (g/10 min)	CO_2 gas flow rate (lpm)	Torch power (kW)	Temp. (°C) at 4 cm away from plasma
1	20	0.4	0.75	1114
2	30	0.4	0.75	1139
3	40	0.4	0.75	1097
4	50	0.4	0.75	1084
5	30	0.2	0.75	1128
6	30	0.3	0.75	1136
7	30	0.5	0.75	1125
8	30	0.4	0.5	1024
9	30	0.4	1.12	1177
10	30	0.4	1.6	1225

Table 4.2

Proximate and ultimate analysis of RDF based on the type of waste.

Waste type (% in RDF)	Proximate analysis (wt.%, dry basis)			Ultimate analysis (wt.%, dry, ash-free basis)					LHV_{dry} (MJ/kg)
	VM	FC	Ash	C	H	N	S	O[a]	
Plastic (35)	98	1	1	85.31	7.86	5.28	-	1.55	37.1
Paper (10)	73.41	10.59	16	54.95	5.81	0.32	-	38.92	11.32
Yard (40)	72.38	2.52	25.1	53.52	5.99	2.02	0.14	38.33	13.96
Food (15)	83.02	3.98	13	39.87	6.42	2.92	0.07	50.72	16.41

[a] by difference; VM-Volatile matter and FC-Fixed carbon.

4.2.1.1. XRD and EDS analysis

Fig. 4.2 displays the XRD plot of different types of waste considered in the RDF. Ash recovered from each component of RDF feed is used to determine the mineral compounds in the form of oxides. Moreover, FESEM-EDS, as shown in Table 4.3, is performed to confirm and quantify the elements. The plastic waste consists primarily of calcium titanate ($CaTiO_3$), calcium aluminate ($CaAl_4O_7$) and haematite (Fe_2O_3). Due to the opacity and stability nature of $CaTiO_3$ and $CaAl_4O_7$ and radiation shielding property of Fe_2O_3, these components are added as fillers in the plastics. Titanium oxide (TiO_2) and $CaAl_4O_7$ are the white pigments in the paper added to increase the quality and brightness of the material. While yard waste has a higher amount of calcium oxide (CaO) and magnesium carbonate ($MgCO_3$), which can neutralize the acidity of soil and increase the effectiveness of photosynthesis, respectively. Similarly, food waste also contains a large quantity of $MgCO_3$ in addition to potassium sulfate (K_2SO_4) and these components are the basis of macronutrients to manufacture fertilizers (National Center for Biotechnology Information, 2023).

Correspondingly, the EDS analysis showed that the highest percentage of elements in the RDF are Ca, K, Fe, C, Ti and O (Table 4.3), which is analogous to the XRD plot. The other elements, such as Mg, Si and Al are also found in the RDF. Due to the presence of more minor elements (not shown in Table 4.3), the sum of the elements is less than 100%. This illustrates that the residue of the RDF (~14 wt.% ash) after plasma gasification can find some potential applications in healthcare, paints, the cement industry, etc.

4.2.1.2. TGA analysis

Prior to the plasma gasification, the different waste that constitutes the RDF is analyzed under non-isothermal conditions using CO_2 as a gasifying agent. Thermogravimetric analysis

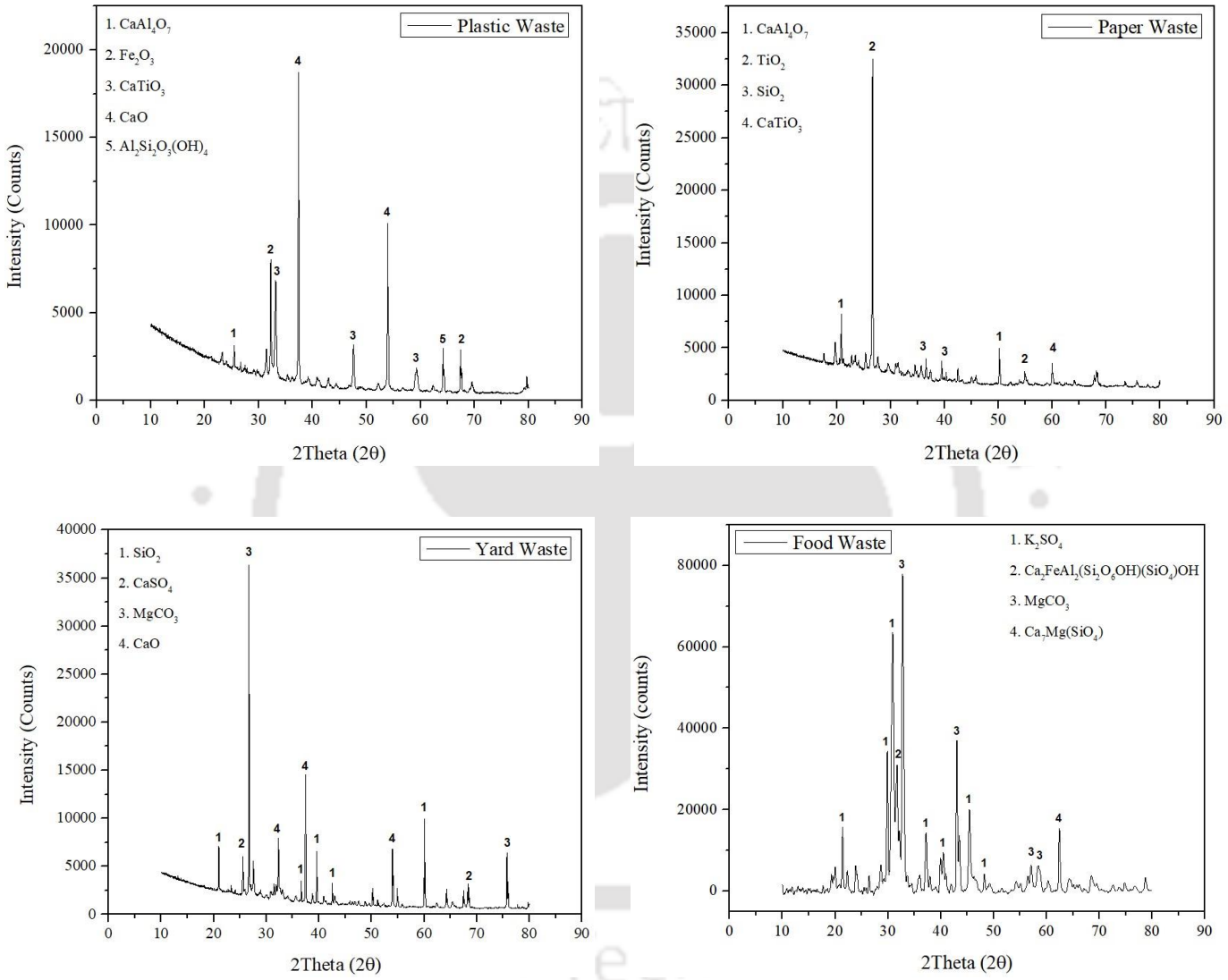

Fig. 4.2. XRD plot of ash from various waste considered in RDF.

Table 4.3

FESEM-EDS analysis of the RDF ash sample.

Element (wt.%)	Si	Al	Ca	Fe	K	Mg	C	P	S	Ti	O
Plastic ash	5.14	10.28	19.96	7.54	3.28	2.27	-	-	-	4.36	46.42
Paper ash	2.22	1.2	39.04	1.87	0.1	1.64	5.3	-	-	10.56	37.16
Yard ash	2.6	0.24	22.5	0.96	0.9	3.08	24.76	1.1	4.34	-	39.12
Food ash	5.13	1.45	5.36	3.33	19.85	4.23	18.46	4.56	1.91	-	32.7

(TGA) is performed from 25 to 1100 °C at a heating rate of 10 °C/min. Fig. 4.3 shows the mass loss (%) curve and its derivative (DTG) form as a function of temperature. The initial loss in weight at around 100-120 °C denotes the evaporation of moisture in the sample. Nearly 10%, 6% and 3% of moisture in the paper, yard and food waste, respectively, is lost in the drying region of the TGA curve. Since the food waste is already dried, it shows a lower loss as compared to paper and yard waste. On the other hand, plastic waste showed no moisture loss. The maximum loss for plastic waste (97%) occurred between 404-507 °C, followed by 932-963 °C (2%). These are associated with the release of volatile matter (pyrolysis region) and gasification of fixed carbon in the high-temperature zone, respectively. While for biomass-based waste such as paper, yard and food waste, the pyrolysis zone shifts left towards the lower temperature. The decomposition of paper waste is observed between 230-380 °C, 260-390 °C for yard waste and 237-492 °C for food waste. The wide range of temperatures are attributed to the cellulose, hemicellulose and lignin content in the biomass sample. Although the degradation of hemicellulose starts at around 300 °C due to lower thermal stability, the breakdown of lignin happens simultaneously at a temperature range of 200-500 °C. The second mass loss curve of food waste in the pyrolysis zone indicates the release of cellulose in the gas phase (Babinszki et al., 2021). Only paper waste showed a drastic loss (~9%) in the gasification zone because of the reaction concerning high fixed carbon content with CO_2.

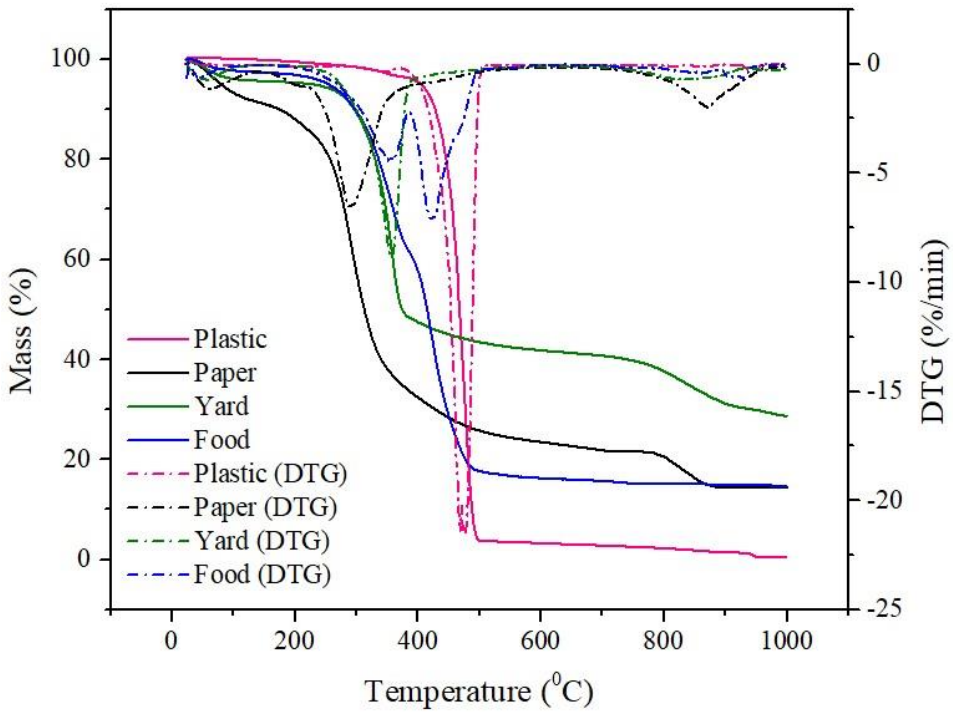

Fig. 4.3. TGA curve of the different waste in RDF.

4.2.2. Gasification performance

In this section, the impact of the feed flow rates of RDF and CO_2 plasma gas and plasma torch power on the composition of syngas is analyzed. The yields of various products of plasma reactions are shown in Table 4.4. The volume percentage of gas compounds such as H_2, CO, CH_4, CO_2 and lower hydrocarbon (LHCs) gases such as C_2H_4, C_2H_6 and C_3H_6 are estimated. The methodology for estimating the gas, oil and residue yield is given in Section 3.5.1 from Eq. (1-3). Ten experiments are conducted with respect to RDF feed rate (Case 1-4), followed by CO_2 flow rate (Case 5-7) and torch power (Case 8-10). The error deviation of the repeatability experiments in syngas volume percentage is found in the range of 1.4 to 5.31%.

4.2.2.1. Effect of feed flow rate on the syngas composition, LHV and yield distribution

It can be seen that for Case 1-4, the highest H_2 (37.71 vol.%) and CO (38.2 vol.%) content are observed for 30g/10 min (Case 2), CO_2 flow rate of 0.4 lpm and torch power of 0.75 kW. This is attributed to various possible reasons: (1) suitable conditions for interactions between

feed and high-temperature plasma, which generates simpler compounds from tar cracking (2) governance of the Boudouard reaction and (3) partial oxidation with free O_2 radical. The influence of the Boudouard reaction is low as the plasma chemistry enhances the interaction between oxygen radicals and volatile matter, activating partial oxidation (R7 and R17). The low C_xH_y content indicates the thermal cracking of tar compounds into simpler ones of H_2, CO and CH_4 as per reaction R18. Keeping the other parameters constant, the lower and higher feed rates of RDF and plasma gas cause either dilution of the syngas with CO_2 or incomplete degradation of RDF feed due to insufficient plasma power. In Table 4.4, the concentration of LHCs increases with an increase in the RDF feed rate (20 to 50 g). This could be due to the inefficient thermal cracking reactions by the fast plasma pyrolysis. Syngas with a maximum LHV of 13.62 MJ/m^3 is obtained under the operating conditions of Case 2 despite a slightly lower feed conversion than Case 1. Agon et al., 2016 reported a similar CO (~ 46 vol.%) concentration using RDF feed with CO_2 and O_2 as gasifying agents. The reported H_2 content (~30 vol.%) is lower than the results of the present study. It is most likely due to the generation of more reactive species of CO_2 to break the LHCs into simpler molecules (Zhang and Harvey, 2021) and thus, the LHV of syngas is also higher than the stated literature.

Partial oxidation: $Fuel + 0.5O_2 \rightarrow CO + H_2$ (R17)

Tar cracking: $Tar \rightarrow H_2 + CH_4 + H_2O + C_xH_y$ (R18)

A maximum yield of gas and solid residue (including ash content) is obtained with almost 73-81% and 18-25%, respectively, while the oil yield is reduced to the least in the range of 0.76-2.12%. The increase in the feed rate increases the solid carbon content in the residue and as a result, the gas yield reduces. However, the oil yield showed an alternate increase and decrease trend because of the retention of condensable gases in the residue matrix at higher feed rate. A detailed assessment of the oil and residue is shown in Section 4.2.6.

Table 4.4

Results of syngas compositions, LHV and yield based on different parameters using RDF feed.

Case number	$\dot{m}_F$ (g/10 min)	Power (kW)	Feed CO_2 flow (lpm)	Syngas composition (vol. %)					LHV (MJ/m^3)	Gas yield (%)	Oil yield (%)	Residue yield (%)
				H_2	CO	CH_4	CO_2	C_xH_y				
1	20	0.75	0.4	27.54	29.22	3.37	33.27	2.4	9.67	81.03	0.92	18.05
2	30	0.75	0.4	37.71	38.2	5.4	10.86	3.76	13.62	79.45	2.12	18.43
3	40	0.75	0.4	31.72	34.34	6.48	19.17	4.51	13.42	76.96	0.76	22.28
4	50	0.75	0.4	23.03	26.59	8.44	32.07	5.7	13.04	73.33	1.43	25.24
5	30	0.75	0.2	27.06	30.46	6.61	28.3	3.58	11.86	75.10	1.20	23.70
6	30	0.75	0.3	30.04	32.17	6.12	24.8	3.1	11.88	77.63	1.71	20.67
7	30	0.75	0.5	29.47	31.11	5.12	27.4	2.99	11.13	82.85	1.45	15.70
8	30	0.5	0.4	23.91	26.29	4.67	38.19	2.01	9.01	71.87	0.87	27.27
9	30	1.12	0.4	40.43	41.59	4.87	5.8	3.36	13.89	82.12	1.85	16.03
10	30	1.6	0.4	42.6	44.06	4.42	2.14	2.91	13.95	83.77	1.63	14.60

C_xH_y includes C_2H_4, C_2H_6 and C_3H_6 compounds; LHV = lower heating value.

4.2.2.2. Effect of CO_2 flow rate on the syngas composition, LHV and yield distribution

In comparison to cases 1-4, the increase in the flow rate of feed CO_2 (Case 5-7) shows a lower quality of syngas and their corresponding LHV with a negative deflection of around 2 MJ/m^3. For these series of experiments, the optimum feed rate of 30 g/10 min and input power of 0.75 kW are maintained. Both the H_2 and CO concentrations rise with the increase in CO_2 flow rate, reaching a maximum value of 37.71 vol.% and 38.2 vol.%, respectively, at 0.4 lpm (Table 4.4) and then drops suddenly at 0.5 lpm. A deficient CO_2 feed flow (0.2 and 0.3 lpm) increases the solid residue yield (with ash) to 23.70% due to the lower conversion of RDF. However, at an optimum flow rate of 0.4 lpm, the enhanced reactivity of the various components in the RDF occurred with the generation of the reactive species of CO, O and O_2. This directs the governance of partial oxidation of organic compounds and delays the usual Boudouard reaction to occur. On the other hand, with higher values of CO_2, the reactor gets overloaded with excess CO_2 and eventually, the syngas is diluted and the low percentage of H_2 and CO in the syngas reduces the LHV of the product gas. From Table 4.4, it is observed that the increase in oil and residue yield (on average) led to a decrease in gas yield and further LHV of the syngas. This is due to the impact of a higher CO_2 flow rate, and this effect is found higher in the syngas composition compared to the impact of an increase in the solid feed rate. The literature result on the variation of CO_2 feed gas flow rate for plasma gasification of sewage sludge showed a similar impact of the gasifying agent on the syngas composition. Moreover, the LHV of syngas of about 13.62 MJ/m^3 in this study is found higher than the literature results reported for the syngas composition with 8.91 MJ/m^3 (Wang et al., 2019).

4.2.2.3. Effect of torch power on the syngas composition, LHV and yield distribution

Plasma gasification is an energy-intensive process due to the external supply of electricity for the plasma torch. Therefore, it becomes imperative to adjust the input power of the torch at

such a level that high energy density plasma gas at high temperature converts the fuel to high-quality syngas and improves the production of H_2 and CO. Compared to the impact of gasifying agent flow rate on syngas composition, the H_2 (42.6 vol.%) and CO (44.06 vol.%) content in the syngas (Table 4.4) increased with the increase in torch power level (Case 8-10), reaching the maximum calorific value of 13.95 MJ/m^3 for Case 10. At power less than 0.75 kW, the unconverted solid residue yield rises to ~ 28% and thereby, the energy output of the process in terms of the calorific value of syngas is reduced. However, a substantial increase in the torch operating power (1.12-1.6 kW) enhanced the progress of the thermal cracking reaction and resulted in the reduction of C_1-C_3 compounds in the syngas with an increase in H_2 and CO concentration. At higher temperatures, the Boudouard reaction becomes prominent to produce more CO. But the rise in H_2 and CO content is not in similar proportion with the increase in torch power and hence, energy is unused. The excess supply of plasma torch beyond 0.75 kW for the specified RDF flow rate could increase the energy loss, leading to a reduction in the thermal efficiency of the system. Thus, the highest H_2 and CO concentration in the syngas with the maximum LHV of 13.95 MJ/m^3 is obtained at the torch power of 1.6 kW (Case 10) among all the cases. It is clearly evident (Table 4.4) that the syngas (90% on average, excluding ash content) contribute the largest share of the products quantitatively.

4.2.3. Energy and exergy analysis

As discussed in the above section, plasma torch power brings a high amount of energy in the gasification process; therefore, evaluating the performance of the system is important from the point of view of optimum energy utilization. Here, the cold gas efficiency (η_{CGE}) is defined as the ratio of chemical energy of the syngas ($\dot{E}_{syngas}$) to that of the chemical energy of the RDF feedstock input ($\dot{E}_F$) to the system, moisture removal energy ($\dot{E}_m$) and the supplied plasma power ($\dot{E}_{plasma}$), whereas the exergy analysis is broadly defined in Section 3.5.1.2.

With an increase in the operating parameters (RDF feed and CO_2 flow rate and torch power), the energy efficiency increased to a certain extent and declined attaining a maximum efficiency of 49.90% at 30g/10 min and 0.4 lpm, as shown in Fig. 4.4. This is ascribed to a lower LHV value of syngas and hence the reduction in CGE. The values are quite adjacent with a study on single-stage plasma gasification of RDF using a mixture of CO_2 and O_2 as gasifying agents. However, the composition of RDF is dissimilar (Agon et al., 2016). On the other hand, the energy efficiencies decrease (39 to 44%) despite the increase in the calorific value of syngas for 1.12 kW and 1.6 kW as compared to 0.75 kW. It indicates that a higher amount of energy is supplied to the system by the plasma torch, which is not efficiently utilized. On average, 3.5% of the total energy is consumed for removing moisture (68%) from food waste during the feed preparation. As discussed in the experimental methodology, the process requires cooling of both the hot syngas generated and hot plasma torch. The high-temperature product gas exits the plasma gasifier at an average of 250 °C, which is then suddenly quenched through the condenser working at 5 °C. Therefore, a huge amount of sensible heat can be extracted from the cooling water (~25%) and the syngas (~8%). Moreover, a small fraction of chemical energy is found in liquid oil (~1%) and the solid residue (~7%), while the rest (~10%) may have been lost to the environment as heat. Considering the recovery of energy from all the gas and solid streams exiting the reactor except the radiation loss, the overall energy efficiency of the process for the optimum case (Case 2) can increase up to ~ 90%. Scaling the process to an industrial capacity, the part of the energy from the sensible heat of syngas can be recovered and used externally for combined heat and power (CHP) while the water at 51 °C can be sent to the local residents for providing domestic hot water (DHW) (Agon et al., 2016; Peng et al., 2021).

The exergy efficiency is found to be 1-2% lower than the energy efficiency (Fig. 4.4). This is mainly due to the irreversibilities caused by the chemical reaction between the gas-solid and gas-gas, whereby entropy is generated.

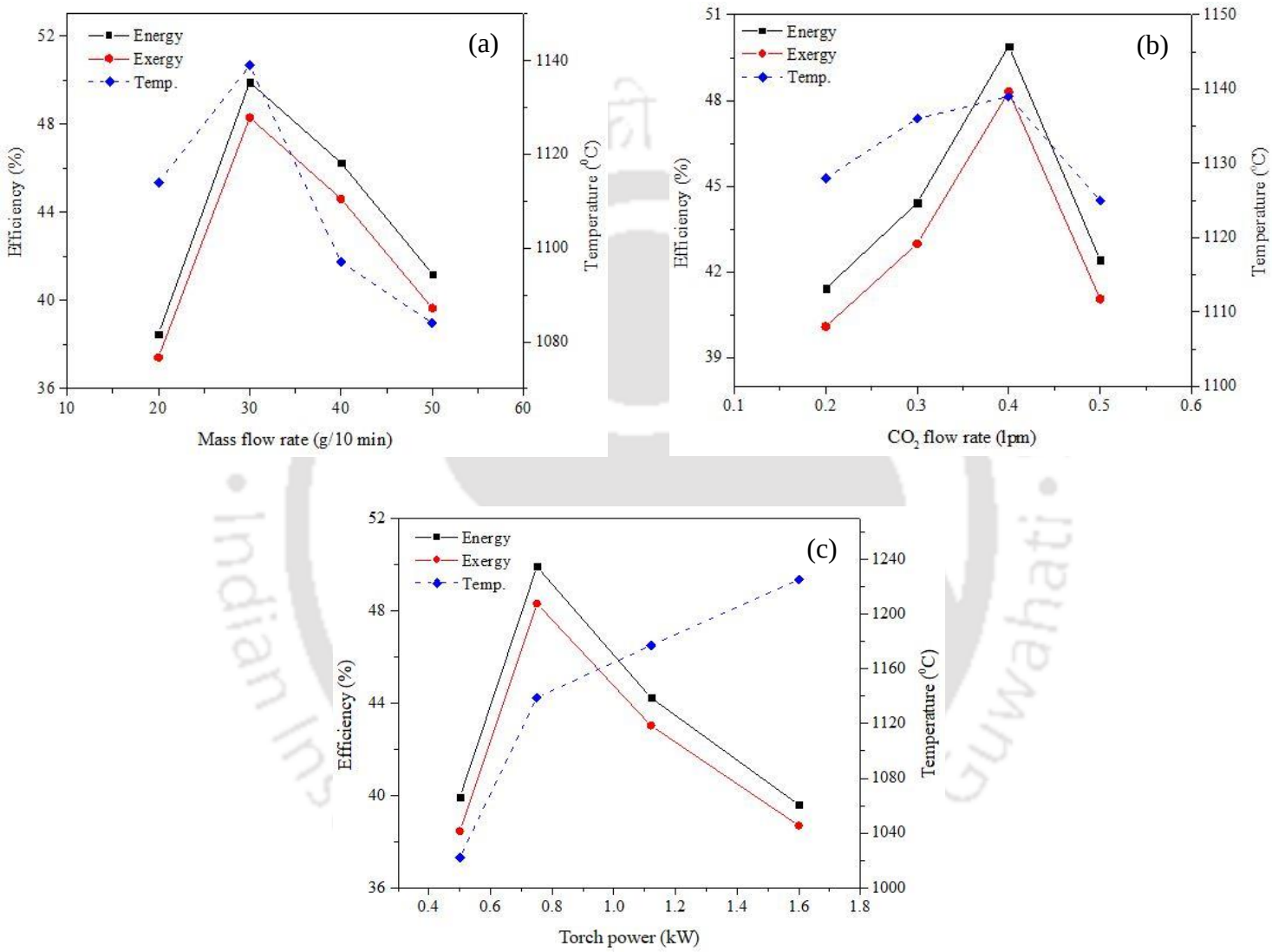

Fig. 4.4. Energy and exergy efficiencies as a function of (a) feed rate, (b) CO_2 flow rate and (c) torch power.

4.2.4. Economic analysis

The levelized cost of syngas (LCOS) in Indian rupee (INR) is calculated based on the methodology described in Section 3.5.1.3. Nominal discount rate (*r*) of 4%, annual utilization period (*P)* of 2000 h/year and payback period (*k*) of 4 years are considered for the analysis. Table 4.5 summarizes the complete cost analysis, including the plasma gasifier cost, which varies with capacity related to the mass feed rate ($\dot{m}_F$). Whereas the operating and maintenance cost depend on the plasma power and energy output from the system. The LCOS values vary in the range of 27-38 INR/kWh. The lowest value of 27.83 INR/kWh is obtained for Case 2 i.e., the optimum conditions based on the thermodynamic analysis. It shows that the energy output had a strong influence in determining the LCOS, such that Case 10 has an LCOS value of 28.39 INR/kWh despite producing the highest LHV. On that note, Case 8 has a relatively higher syngas cost of 37.97 INR/kWh, which runs at the low torch power of 0.5 kW. At this power, the gas yield is reduced and similarly, the CGE decreases. At the optimum conditions, the LCOS results are fairly promising as compared with the literature values of 8.5-32.3 INR/kWh (Paulino et al., 2020), but can be minimized further by reducing the energy losses.

4.2.5. Model development and validation

To validate the system, a model is developed to predict and compare the syngas composition of the plasma gasification process using Aspen Plus software as shown in Fig. 4.5. The syngas composition of Case 2 i.e., the optimum scenario based on 30 g/10 min, 0.4 lpm of CO_2 flow rate and torch power of 0.75 kW is considered. Fig. 4.6 compares the experimental syngas results with those obtained from simulation. The blocks used for modeling are followed from the literature (Minutillo et al., 2009). The plasma is generated (in block H2) by heating the feed CO_2 at 4000 °C such that enough energy is provided to break the gas molecules apart. The results obtained from stream G5 present the final syngas concentration. It can be seen that the

Table 4.5

Results of the syngas production cost for the considered experimental conditions.

Case number	C_{system} (INR)	$OC_{var,gp}$ (INR/kWh)	MC_{gp} (INR/kWh)	C_{capex} (INR)	C_{opex} (INR)	C_{total} (INR/kWh)	LCOS (INR/kWh)
1	109477.5	6.15	0.74	27000	1001.83	1.27	32.89
2	164216.25	3.75	0.68	27000	1001.83	0.78	27.83
3	218955	3.35	0.81	27000	1001.83	0.69	31.78
4	273694.75	3.21	0.97	27000	1001.83	0.66	37.06
5	164216.25	4.52	0.82	27000	1000.91	0.94	33.53
6	164216.25	4.21	0.76	27000	1001.37	0.87	31.27
7	164216.25	4.41	0.80	27000	1002.29	0.91	32.74
8	164216.25	3.57	0.97	27000	1001.83	1.11	37.97
9	164216.25	5.33	0.65	27000	1001.83	0.74	28.26
10	164216.25	7.08	0.60	27000	1001.83	0.69	28.39

C_{system} = Plasma gasification unit cost; $OC_{var,gp}$ = Variable operating cost of plasma gasifier; MC_{gp} = Maintenance cost of plasma gasifier;

C_{capex} = Capital cost of gasifying agent; C_{opex} = Operating cost of gasifying agent and C_{total} = Net cost of gasifying agent.

percentage composition (simulation) of H_2 (39.59 vol.%) and CO (43.64 vol.%) in the syngas is found higher by ~2 vol.% than the corresponding experimental values. While the CH_4 is reduced to 1.49 vol.% and CO_2 (6.01 vol.%) gets consumed in the reaction, and LHCs (C_xH_y) is completely converted into CO and H_2 due to the chemical equilibrium approach. Therefore, the H_2 and CO in the simulated syngas are found to be higher than the experimental results.

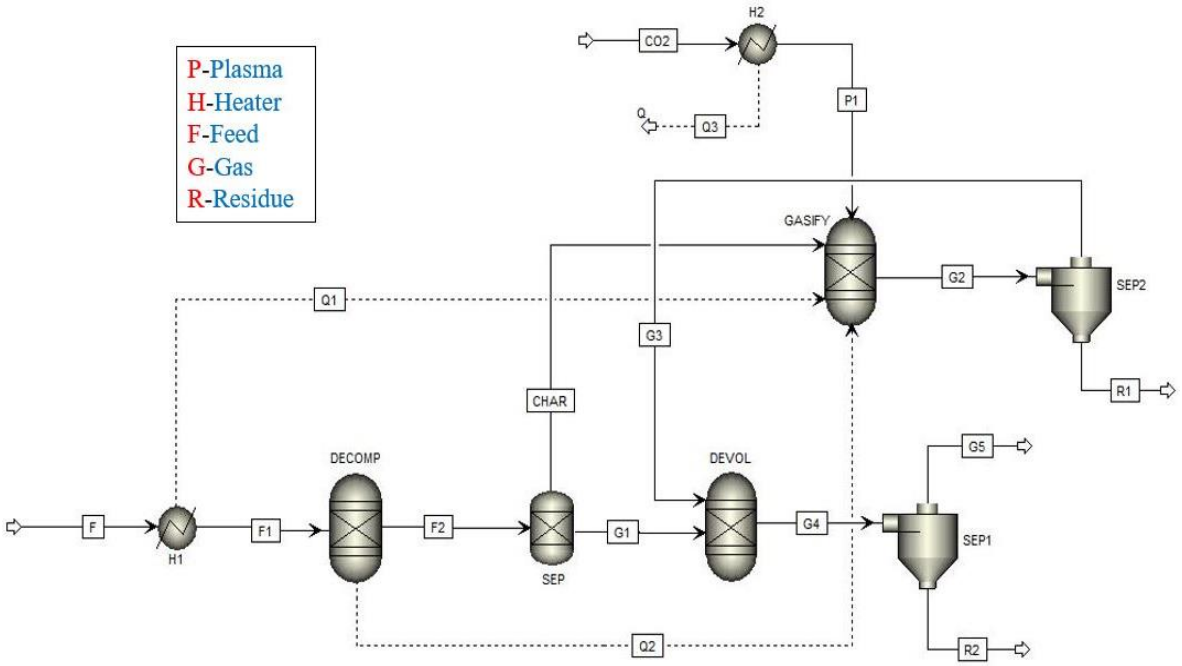

Fig. 4.5. Aspen plus flowsheet of the model adopted in the plasma gasification process.

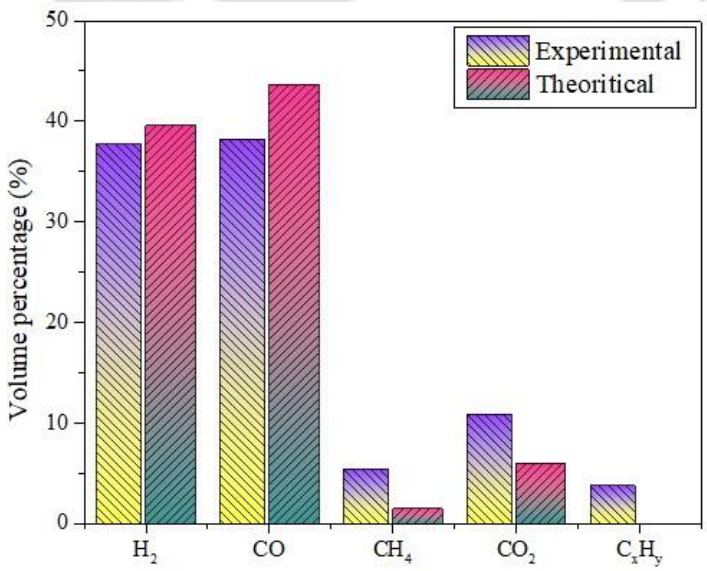

Fig. 4.6. Comparison between experimental and theoretical syngas composition (Case 2).

4.2.6. Post-plasma gasification characterization

4.2.6.1. Proximate and ultimate analysis

Fig. 4.7 shows the liquid oil and solid residue obtained from the plasma gasification process of RDF. Their ultimate and proximate analyses are given in Table 4.6. The solid residue contains a mixture of fixed carbon (20%) and ash (80%) in the ratio of 1:4, which is analogous to the composition of raw RDF in Table 4.6, whereby the ash content is ~ 75% (without volatile matter). At such a high temperature, it is expected to convert almost 100% of the RDF feed, however, due to low residence time and structural arrangement of the reactor, 20.08 wt.% of fixed carbon in the solid residue is obtained along with some oil by-product. Additionally, the increase in the residence time of the feed is not beneficial in terms of energy efficiency, as less energy is produced than consumed from a plasma torch. From Table 4.4, it can be noticed that only a small fraction of oil (1.5% on average) is obtained from the process. This is analogous to the literature on gasification (Lopez et al., 2018; Cao et al., 2020) utilizing plastics and biomass at high pressure and temperature under steam and catalyst medium. A similar percentage of elemental oxygen and carbon is found in the liquid product and raw RDF and these are attributed to the oxides in ash and fixed carbon, respectively. Concentrated minerals in the form of ash of the solid residue can be effectively recovered through float-sink and froth floatation methods. On the other hand, liquid oil has a high H/C ratio of 2.05, which is in the range of diesel fuel. However, due to the presence of aldehydes, ketones, etc., a large proportion of oxygen (27.14 wt.%) is found in the liquid product. Therefore, further refining via hydrotreating and deoxygenation process is necessary to improve the quality and make it applicable for usage in diesel engines, boilers, etc. A calorific value of 30.59 MJ/kg and 7.97 MJ/kg of liquid oil and residue, respectively, is estimated. It is important to note that the measured values are highly dependent on the influencing parameters such as gas flow rate, temperature, etc. used in this study (Czernik and Bridgwater, 2004).

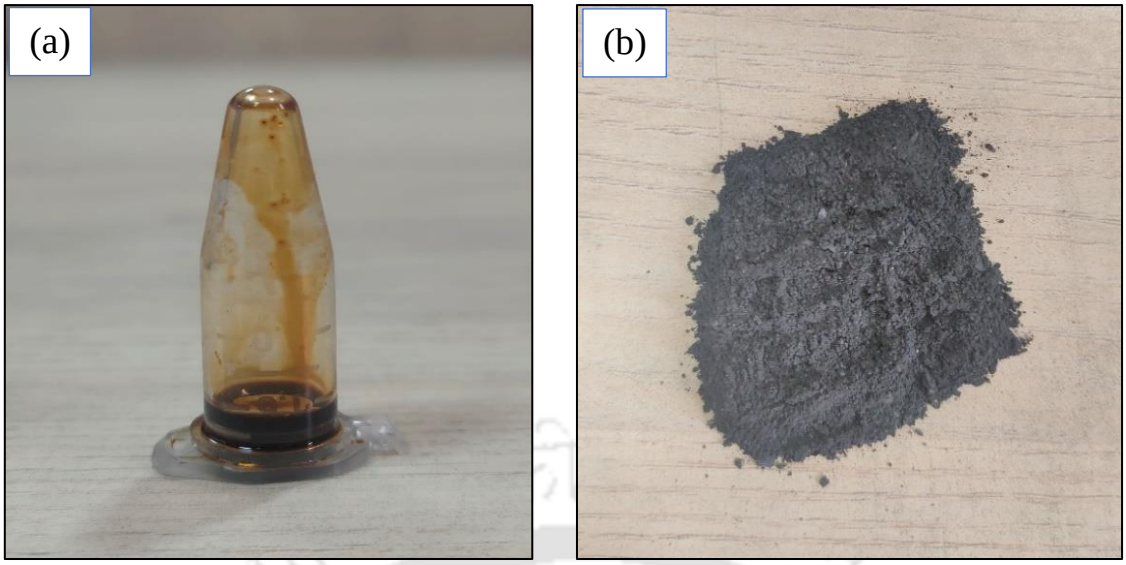

Fig. 4.7. Images of (a) oil and (b) residue obtained after CO_2 plasma gasification.

Table 4.6

Proximate and ultimate analyses of raw RDF, oil and solid residue obtained after plasma gasification.

	Raw RDF	Oil	Residue
Proximate analysis [wt.%, dry basis]			
Moisture	14.57	-	-
Volatile matter	83.04	-	-
Fixed Carbon	3.01	-	20.08
Ash	13.95	-	79.92
Ultimate analysis [wt.%, dry-ash free basis]			
C	62.74	60.04	21.46
H	6.69	10.26	1.87
N	3.12	2.56	0.69
S	0.21	0.13	-
O[a]	27.24	27.01	75.98
LHV based on energy [MJ/kg]	22.16	30.59	7.97

[a] by difference.

4.2.6.2. FTIR analysis

The FTIR plot of various components of raw RDF along with the obtained oil and residue is shown in Fig. 4.8. The major functional groups such as C-H stretch at 2915 cm^{-1}, 2845 cm^{-1}, 3024 cm^{-1}, CH_2 bend at 1472 cm^{-1}, 1462 cm^{-1}, 1451 cm^{-1}, CH_2 rock at 730 cm^{-1}, 808 cm^{-1} and aromatic CH out-of-plane bending at 720 cm^{-1}, 694 cm^{-1} verifies the presence of high and low density polyethylene (HDPE, LDPE), polypropylene (PP), polystyrene (PS), etc. in the plastic waste. Moreover, C=O stretch at 1713 cm^{-1} and C-O stretch at 1241 cm^{-1} suggest the existence of PET (Jung et al., 2018). Whereas paper, food and yard waste have broad bands from 3000-3500 cm^{-1}, which are associated with O-H stretching of cellulose or moisture content. While the O-H bending around 1620 cm^{-1} indicates the amide in protein. The strong bands from 900-1200 cm^{-1} are due to the C-O-C stretching, C-O, C=C stretching, which shows the presence of hemicellulose, cellulose and lignin. Bands ranging from 1400-1750 cm^{-1} are attributed to aromatic ring stretching (C=O, C=C) in lignin subunits. The aliphatic bonds in the form of CH_2 stretching are visible at 2800-2950 cm^{-1} (Arif et al., 2021; Lazzari et al., 2018). Due to the difficulty in depolymerization of lignin subunits, the bands show a higher intensity of aromatic and aliphatic compounds in the case of liquid oil and C-O and C=C stretching in the solid residue (Pavlostathis, 2011). Oils from biomass waste are assumed to contain a large amount of phenols. However, due to the rigorous thermal degradation under the plasma atmosphere, the weak bands of O-H stretching depict a minimal presence of such compounds (Lazzari et al., 2018).

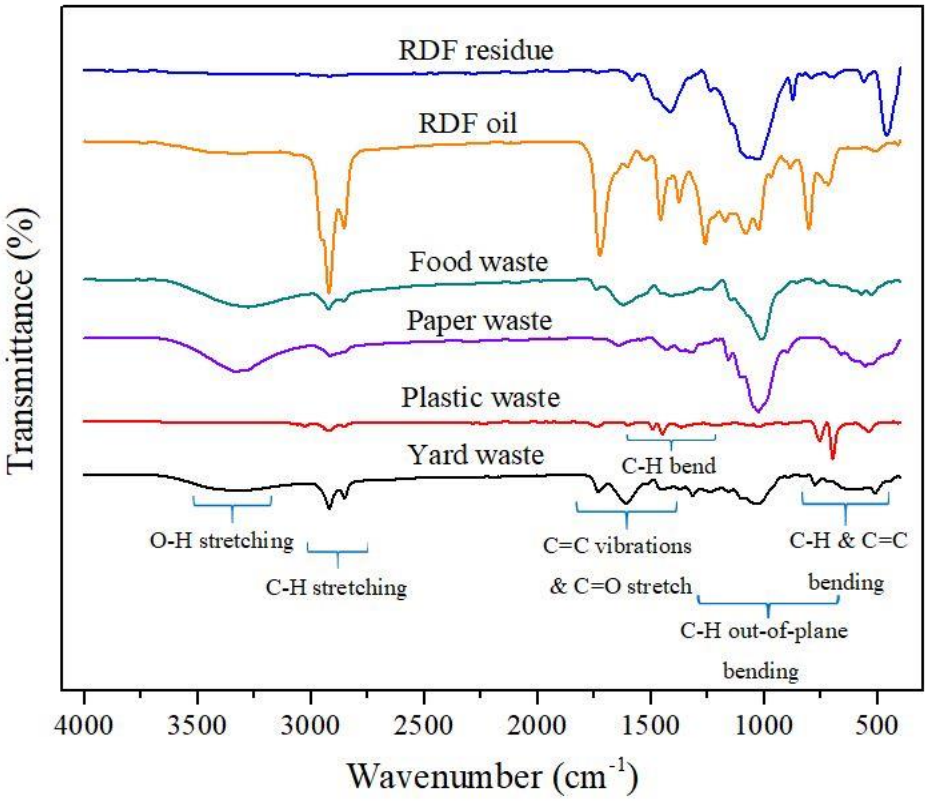

Fig. 4.8. FTIR curve of various waste in RDF, oil and residue after plasma gasification.

4.2.6.3. FESEM analysis

Due to the combination of various components in the RDF, the FESEM images of the raw RDF (Fig. 4.9(a)) showed a partially smooth and non-uniform surface. The different size fragments in the image can be due to the presence of biomass particles, which is distributed randomly on the sticky and strong polymer plastic material (Suman et al., 2017). On exposure to thermal plasma, abundant tiny particles with a large number of internal pores are created, as shown in Fig. 4.9(b). It shows the intense release of volatile matter, which creates a void for CO_2 gasification through the diffusion mechanism. The gasification process further breaks the porous matrix into unorganized patterns of crystals and flakes. Moreover, the visible bright flake like substance is the ash particles deposited on the unconverted carbon or situated freely. These flakes can function as catalysts to drive the gasification reaction (Assad Munawar et al., 2021), but the superior influence of thermal plasma gasification overrides the catalytic activity.

The intricate process of plasma depolymerizes the material despite the large particle size of the feed, which is a major factor influencing the gasification performance significantly.

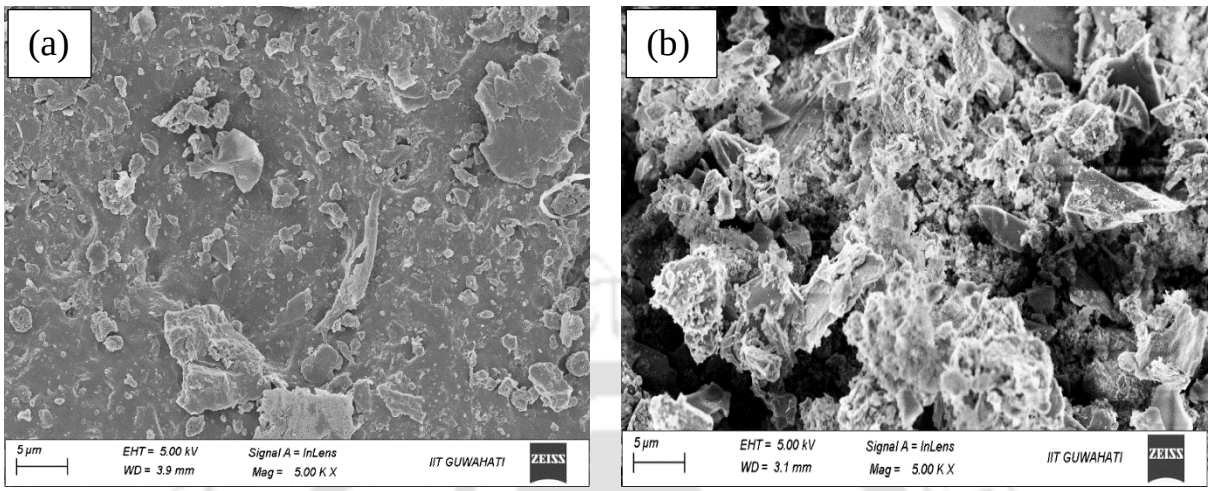

Fig. 4.9. FESEM image of (a) RDF feed and (b) after CO_2 plasma gasification.

4.2.6.4. Viscosity, pH and GC-MS analysis of oil

Upon further examination of the liquid oil for suitable applicability in the transport or energy sector, the viscosity, density and pH are found to be 5.97 cP (centipoise), 924 kg/m^3 and 9.01, respectively. The oil obtained from the optimal operating conditions (Case 2) is considered for the analysis. Nevertheless, it is assumed that the deviation among the cases is minimal. The LHV of the oil is given in Table 4.6. The higher values of viscosity, density and pH are due to the condensation of more nitrogen and oxygen-related compounds from the gas phase to the oil. As almost 70% of the feed is biomass, the obtained oil has good amount of N, O and S. The detailed study to classify the compounds is provided in the GC-MS analysis below. Several process involving the enrichment of the oil, such as hydrogeneration or hydrotreating, is imperative for its use in engines and boilers or run in vehicles (Ahmad et al., 2020).

Table 4.7 shows the GC-MS analysis of oil showing the main chemical constituents present in it Dimethyl heptadecane (iso-alkane) and 1-Pentene, 3-methyl- (monomer from polyolefin production) are the two most abundant compounds found in the oil obtained in Case 2 and Case

5. For Case 8, dimethyl heptadecane is found significantly, followed by a saturated aliphatic compound known as tetramethyl pentane. These are produced from the breaking of complex aromatic structures and thus, the benzene derivatives have a major contribution in the oil. In addition, ketones in the form of methyl hydroxy heptanone and azetidine carboxylic acids, which are plant-based non-protein amino acids, also have a moderate presence in the oil. The remaining compounds are mostly esters, unsaturated carboxylic acids and mono-cycloalkanes. The mixture of pyrrolidine and s, s-dioxide in the oil contains some portions of sulfur (S) and nitrogen (N), respectively, while the remaining N and S have escaped in the gas phase. The existence of saturated hydrocarbons indicates the presence of polyaromatic hydrocarbons (PAHs) in the form of Benz[a]anthracene. However, it is relatively low (0.1-1.12%) compared to other organic compounds due to the high-temperature plasma environment.

4.2.7. Reaction mechanism

A reaction mechanism is proposed for CO_2-plasma based RDF gasification as shown in Fig. 4.10. RDF is a mixture of various types of wastes such as plastics, paper, yard and food waste. In the first stage, all the four wastes are considered to undergo thermal degradation (release of volatiles) or depolymerization to form intermediates such as paraffins and oligomers in the case of plastics, and other intermediates such as phenols, carboxylic acids, and furans in the case of biomass (Huang et al., 2023). Cellulose and hemicellulose in the biomass have a high and moderate degree of polymerization, respectively, and therefore, upon degradation, carboxylic acids, esters and ketones are released. On the other hand, the degradation of lignin content favors the formation of high molecular weight phenolic compounds (Akhtar et al., 2018; Anca-Couce, 2016). Also, the gases like H_2, CO, CO_2 and lower hydrocarbons (LHCs) are produced. The release of CO and CO_2 is mainly due to the degradation of lignin and hemicellulose, while CH_4 is formed from the methoxy group of lignin (Guo et al., 2020; Müsellim et al., 2018). During the release of volatile matter, the aromatization or hydrogenation of alkanes with

Table 4.7

Major compounds identified from the GC-MS analysis of oil obtained from RDF.

Case 2			Case 5			Case 8		
Retention time (min)	Compound name	Area (%)	Retention time (min)	Compound name	Area (%)	Retention time (min)	Compound name	Area (%)
7.4	3,3-Dimethylheptadecane	23.1	7.4	3,3-Dimethylheptadecane	22.7	7.4	3,3-Dimethylheptadecane	23.1
7.71	Pyrrolidine,1-methyl-3,2`-spiro-benzo-1,3-dioxolane	5.03	7.71	Pyrrolidine,1-methyl-3,2`-spiro-benzo-1,3-dioxolane	6.60	7.71	Pyrrolidine,1-methyl-3,2`-spiro-benzo-1,3-dioxolane	8.60
7.75	6-Hepten-3-one,5-hydroxy-4-methyl-	8.71	7.75	6-Hepten-3-one,5-hydroxy-4-methyl-	9.36	7.75	6-Hepten-3-one,5-hydroxy-4-methyl-	5.72
7.79	2-Heptene,5-methyl	8.24	7.79	2-Heptene,5-methyl	6.04	7.79	2-Heptene,5-methyl	8.33
8.03	Pentane,2,2,4,4-tetramethyl-	10.3	8.03	Pentane,2,2,4,4-tetramethyl-	8.48	8.03	Pentane,2,2,4,4-tetramethyl-	15.9
8.10	L-azetidine-2-carboxylic acid	12.3	8.10	L-azetidine-2-carboxylic acid	14.8	8.10	L-azetidine-2-carboxylic acid	7.79
8.18	But-2-en-1-yl 2-methylbutanoate	2.69	8.18	But-2-en-1-yl 2-methylbutanoate	3.38	8.84	1-Pentene, 3-methyl-	9.74
8.84	1-Pentene, 3-methyl-	23.8	8.84	1-Pentene, 3-methyl-	24.8	37.44	Benz[a]anthracene	1.12
9.65	Cyclohexane	1.23	9.65	Cyclohexane	1.68			
26.25	8-Heptadecene	0.10	37.44	Benz[a]anthracene	0.10			
30.01	Chloroacetic acid, tetradecyl ester	0.11						

33.34	2-methyl-4-n-pentylthiane, s,s-dioxide	0.12				
34.79	Decalin, 2-methyl-	0.18				
36.34	Hexacosylacetate	0.10				
37.44	Benz[a]anthracene	0.15				
39.33	Distearyl thiodipropionate	0.11				
	Total	96.3	Total	97.9	Total	80.3

C_6-C_{10} atoms may occur to give PAHs (liquid at room temperature), aromatics, cyclic olefins, H_2, etc. (Cao et al., 2020). But, the intense plasma reactive atmosphere containing electrons (e^-) and radicals (O) prevents the formation of aromatics and saturated hydrocarbons. It reduces them to iso-alkanes and monomers, as detected in the GC-MS analysis of the oil sample (Table 4.7) (Saleem et al., 2019). This initiates the cracking of primary tar to secondary and tertiary tar consisting of phenols, cresols, BTX/PAHs, etc. The breaking of tar begins at the particle pores and ends up either in the formation of permanent gas or secondary phenolics or holocellulose fracture at the pore walls via different pathways (Anca-Couce, 2016). Fragmentation reaction plays an imperative role in char formation through solid-gas interaction, which further improves the progress of Boudouard reaction via the conversion of char to CO under the ambiance of CO_2 (Guo et al., 2020). The suggested mechanism (Fig. 4.10) takes place by intra and inter-molecular activities of the species in the presence of high-energy electrons. The overall experimental analysis showing high syngas yield, low solid residue and unsaturated derivatives in the oil supports the proposed reaction mechanism.

4.2.8. Quantitative relationship between experimental parameters and obtained results

It is evident that the assessed product gas compositions are strongly dependent on the process parameters and therefore, the feed mass flow rate (g/min), CO_2 flow rate (lpm) and torch power (kW) are chosen as independent variables and the resultant volume percentage of individual species (H_2, CO, CH_4, CO_2 and C_xH_y) in the syngas, LHV (MJ/m^3) and energy efficiency (%) are considered as dependent variables. Table 4.4 shows that 90% (without ash) of the feed is converted under the optimum operating conditions. On that note, the specified three independent variables (feed and CO_2 flow rate and torch power) are chosen to develop a correlation between the input and output parameters. The developed correlation attained a polynomial fit of order 2 and an R^2 of ~ 0.92-0.98.

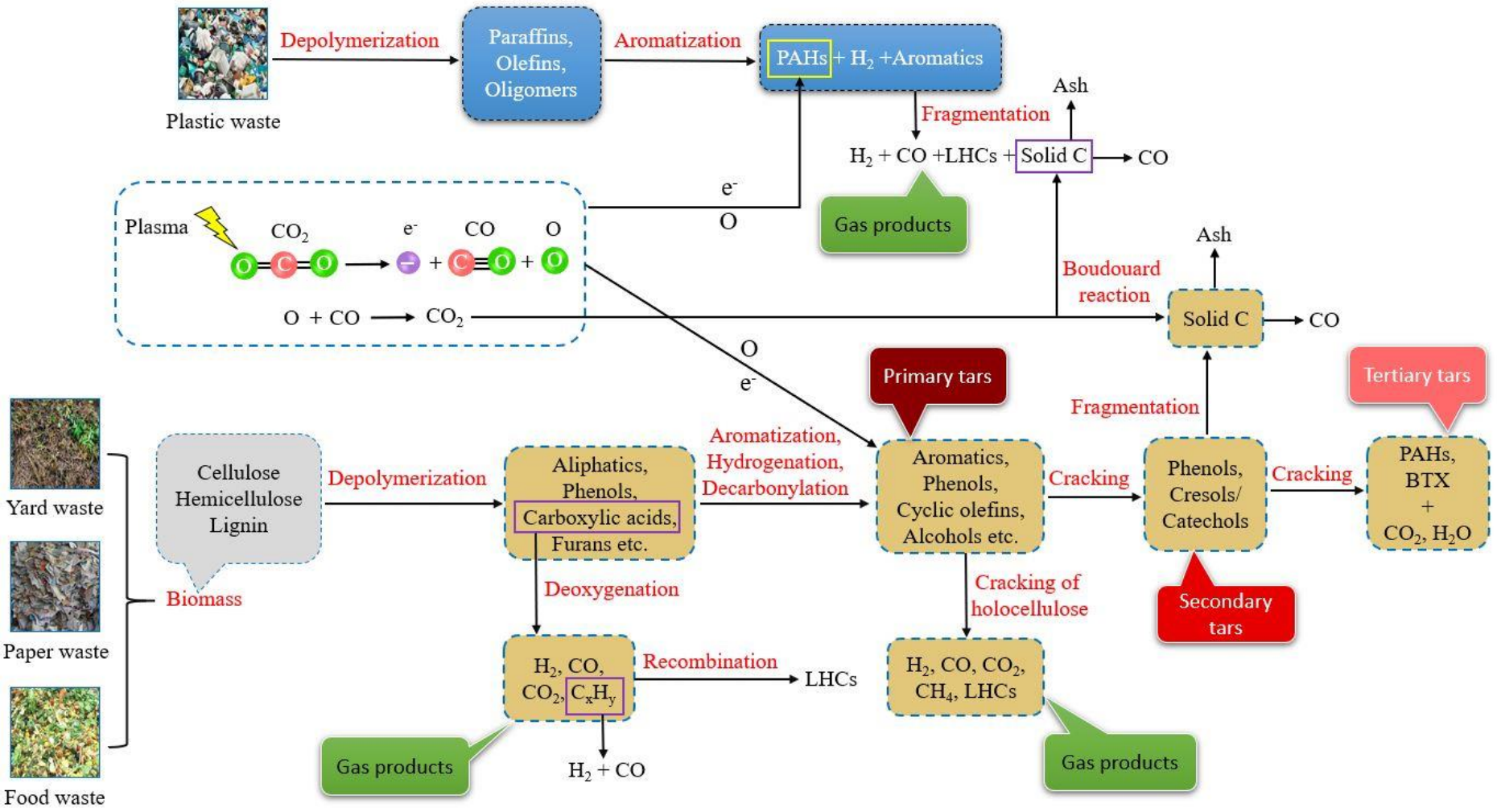

Fig. 4.10. Reaction mechanism of CO_2-plasma gasification of RDF.

The experimental data are fitted as per Eq. 20 of Section 3.5.2 and the constant values are predicted. Table 4.8 shows the constant values of the equation, which is estimated by using SPSS software (IBM, 2021). Similarly, Fig. 4.11 illustrates the parity plot that associates the experimental syngas concentration with their corresponding measured values for all the cases. The reliability of the fit between the values is adequate to propose a substantial correlation for the quick estimation of the syngas composition for the plasma gasification of RDF.

Table 4.8

Empirical constants required to predict the correlated values.

	H_2	CO	CH_4	CO_2	C_xH_y	LHV	η_{CGE}
β_0	223249.29	10405.44	-137650.88	-82699.15	46820.75	-45158.46	199962.36
β_1	-839.47	3157.79	1474.14	-569.55	4133.80	845.60	2993.57
β_2	-360548.76	-245967.81	12656.11	-101910.82	-179444.21	-134067	-561874.41
β_3	-377146.87	172444.89	553979.23	647526.70	-207674.35	413783.62	-170685.46
β_4	-0.038	-0.033	0	0.069	0.001	-0.007	-0.034
β_5	-23.29	-20.24	-1.90	47.06	-3.862	-8.79	-23.05
β_6	-234.08	-194.0	21.80	410.20	0.928	-41.99	-85.41
β_7	3217.54	3528.31	3730.93	7831.29	-1610.95	5349.34	5852.87
β_8	-3928.01	-14504.43	-10680.40	-13271.92	-7313.93	-12142.43	-18451.78
β_9	660218.71	350440.96	-311451.09	-332892.34	569453.75	-65976.87	965832.04

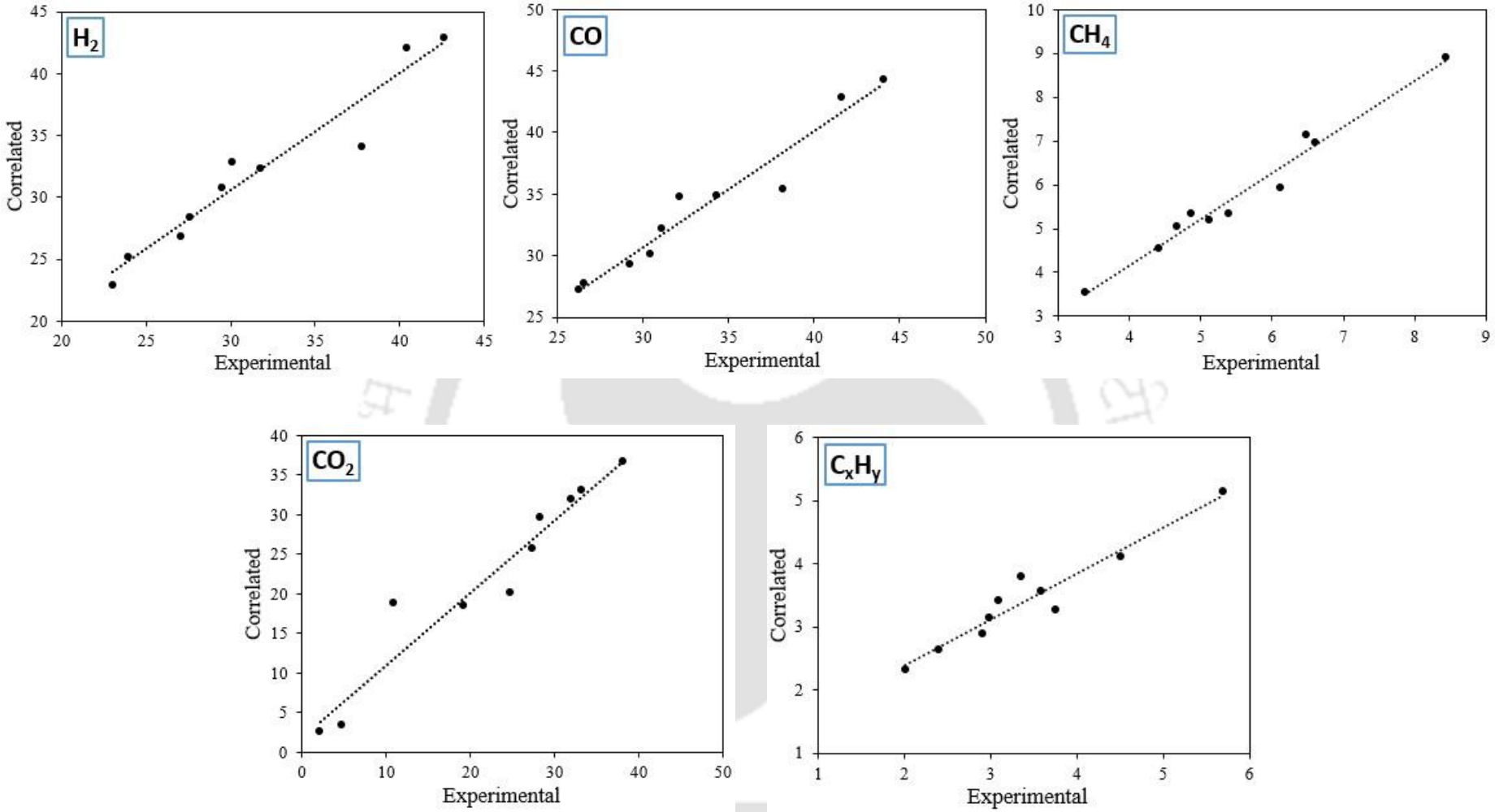

Fig. 4.11. Parity plot between actual and measured values for syngas compositions.

4.2.8.1. Experimental validation of the developed correlation

Table 4.9 provides the syngas compositions and their LHV along with the CGE of three random experiments conducted at different operating conditions. These are performed to validate the proposed correlation. It is to be noted that the developed relationship is highly dependent on three values of independent variables such as 30g/10 min, 0.4 lpm and 0.75 kW. This is because the maximum number of experiments are carried out using the stated parameters, as summarized in Table 4.1. Therefore, while predicting the outcome at least two values among them need to be fixed and a change in one parameter is suggested. The error percentage between the calculated values from the correlations and the experimental values is shown in Table 4.10. The maximum error of 21% is estimated, which may be attributed to mixing multiple wastes in RDF, causing large variations of small values. This relationship offers a good quantitative relationship to predict the syngas composition within the range of operating parameters fixed in the experimental study.

Table 4.9

Results of syngas compositions with LHV and CGE for validated RDF experiments.

$\dot{m}_F$ (g/10 min)	Power (kW)	Gas flow (lpm)	Validated syngas composition (vol. %)					LHV (MJ/m^3)	η_{CGE} (%)
			H_2	CO	CH_4	CO_2	C_xH_y		
30	0.75	0.35	35.24	36.47	4.92	16.18	3.33	12.65	44.38
35	0.75	0.4	34.94	37.11	5.54	15.59	3.08	12.78	47.62
30	1	0.4	38.67	38.89	4.62	8.16	3.19	13.24	42.29

Table 4.10

Comparison of syngas compositions, LHV and CGE between the validated experiments and correlated results.

$\dot{m}_F$ (g/10 min)	Power (kW)	Gas flow (lpm)	Correlated syngas composition (vol. %)					LHV (MJ/m^3)	η_{CGE} (%)	Error (%) between the validated and correlated results						
			H_2	CO	CH_4	CO_2	C_xH_y			H_2	CO	CH_4	CO_2	C_xH_y	LHV	η_{CGE}
30	0.75	0.35	34.09	35.56	5.58	18.52	3.33	12.80	44.38	-3.27	-2.5	13.32	14.43	0.09	1.19	5.23
35	0.75	0.4	34.19	35.98	6.23	16.98	3.66	13.51	47.62	-2.14	-3.04	12.44	8.9	18.74	5.72	8.75
30	1	0.4	40.22	41.06	5.39	7.04	3.73	14.40	42.29	4.00	5.57	16.7	-13.8	17.02	8.75	21.37

4.3. Conclusions

The impact of the operating parameters such as feed flow rates of RDF and CO_2, and torch power on the syngas composition is evaluated. The reaction mechanism of RDF-CO_2-plasma gasification and a correlation are proposed based on the experimental results. The following conclusions can be drawn from the present study:

- The syngas with the highest percentage of H_2 (42.6 vol.%), CO (44.06 vol.%) and LHV (13.95 MJ/m^3) can be achieved at a feed RDF flow rate of 30 g/10 min, 0.4 lpm of CO_2 at 1.6 kW torch power.
- The highest cold gas efficiency of 49.90% and exergy efficiency of 48.30% (Case 2) can be achieved in the RDF-plasma process. However, the system's overall efficiency may rise up to 90% with proper recovery of sensible heat from syngas, cooling water, etc. Further, the LCOS value of 27.83-37.97 INR/kWh is obtained for all the cases.
- The characterization of oil and solid residue from plasma gasification indicated their potential applications upon further upgradation. Oxygen (27 wt.%) and fixed carbon (20 wt.%) in oil and residue, respectively, need to be reduced, such that oil can be used as an alternative to diesel while higher ash content (14 wt.%) in the solid residue favors the recovery of metals for cement industry, healthcare, etc.
- The developed quantitative correlations provide a good accuracy between the actual and predicted values. These correlations are valid for an RDF flow rate of 20-50 g/10 min, a CO_2 flow rate of 0.2-0.5 lpm and a torch power of 0.5-1.6 kW conditions.

The application of high-temperature CO_2-plasma for the gasification of RDF generated high-quality syngas, showing an alternative for energy production. Integrating the plasma system with downstream processing units in the co-generation of hydrogen, electricity, or chemicals can be studied further for end-use.

Chapter 5

Experimental studies on plasma gasification of computer keyboard plastic waste under CO_2 atmosphere for syngas production

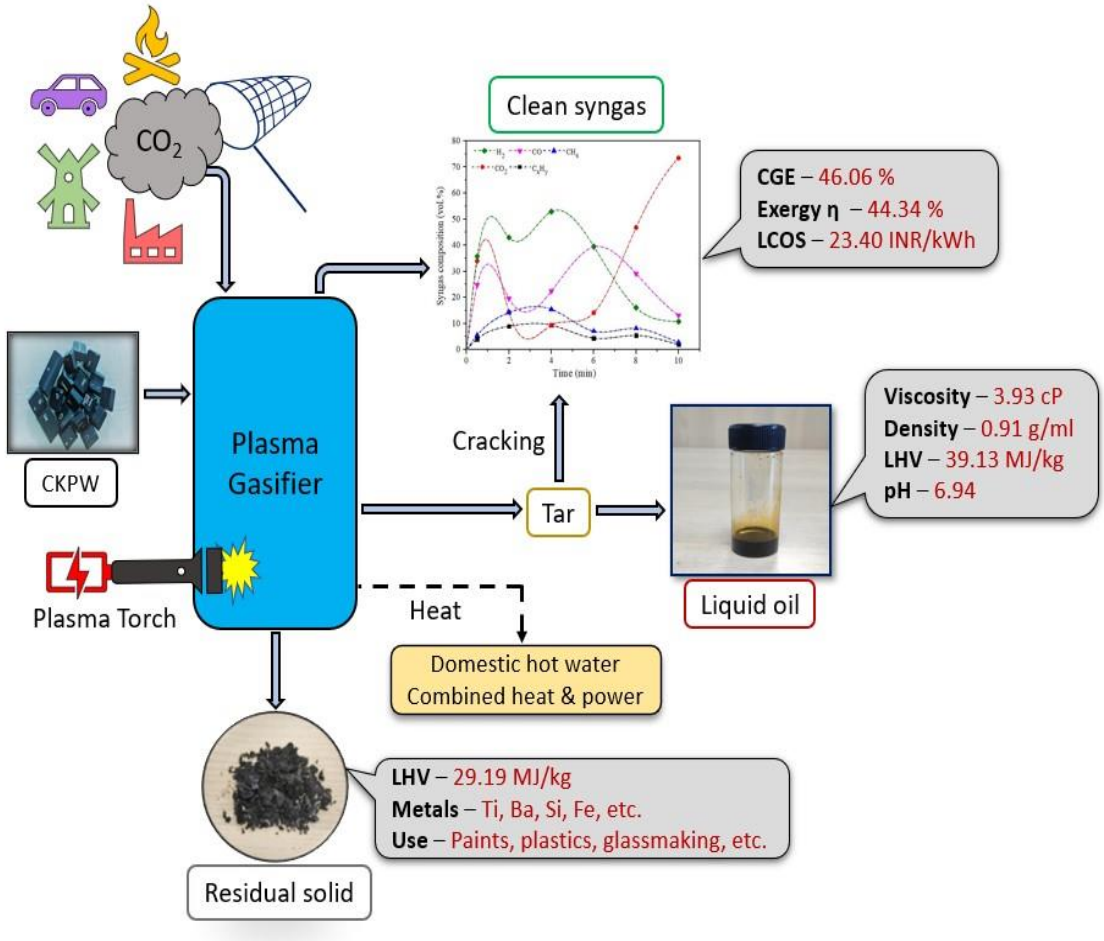

CHAPTER 5

EXPERIMENTAL STUDIES ON PLASMA GASIFICATION OF COMPUTER KEYBOARD PLASTIC WASTE UNDER CO_2 ATMOSPHERE FOR SYNGAS PRODUCTION

In this novel study, the single-stage plasma gasification of computer keyboard plastic waste (CKPW) is carried out in a CO_2 atmosphere using a non-transferred plasma torch. Even though the CO_2 gasification process has slow reaction kinetics, highly endothermic and energy-intensive nature, the increase in mean electron energy in the plasma activates the CO_2 molecules to initiate chemical reactions. Here, the effect of plasma power, feed, and CO_2 flow rate on the syngas composition is studied to optimize the gasification performance for efficient production of high-quality syngas. The potential characterization of feed, product, and residue is performed and the results are interpreted in detail. Further, energy, exergy and economic analyses are performed to understand the thermodynamic balance of the system and commercial feasibility. It intends to locate the losses in the system and improve the overall plasma gasification efficiencies and reduce the cost of syngas production. Besides, a reaction mechanism of CO_2 plasma gasification is proposed based on the results obtained during product analysis and their characterization. Finally, a correlation is developed based on the operating parameters to estimate the syngas composition, LHV and CGE.

5.1. Experimental parameters

The plasma reactor is gradually heated with the plasma torch for around 1 h to reach the maximum temperature at the corresponding power set for each experiment. After several trials in batch feeding, it is observed that the gasifier could degrade more than 90% of wastes within

the initial 10 min. Therefore, all the experiments are conducted for a period of at least 40 min, with the introduction of the sample at every 10 min. The feed rate ($\dot{m}_F$) is varied between 20-60 g per 10 min and the CO_2 flow rate between 0.3-0.7 liters per minute (lpm). On the other hand, a power level of 0.75-2 kW is maintained for the given set of experiments based on the stated temperatures, as shown in Table 5.1. The gas sampling period is kept at an interval of 2 min and 4 min for the 10 min and 40 min experiments, respectively.

Table 5.1

Process parameters used for the CKPW experiments in this study.

Case number	$\dot{m}_F$ (g/10 min)	CO_2 gas flow rate (lpm)	Torch power (kW)	Temp. (°C) at 4 cm
1	20	0.5	1.12	1133
2	30	0.5	1.12	1244
3	40	0.5	1.12	1172
4	50	0.5	1.12	1186
5	60	0.5	1.12	1177
6	40	0.3	1.12	1164
7	40	0.4	1.12	1206
8	40	0.6	1.12	1145
9	40	0.7	1.12	1138
10	40	0.5	0.75	982
11	40	0.5	1.6	1238
12	40	0.5	2	1312

5.2. Results and discussion

5.2.1. Raw CKPW characteristics and its thermogravimetric behavior

The physicochemical characteristic of CKPW feed is presented in Table 3.1. It has a high volatile matter of 93 wt.% and low content of fixed carbon and ash of 6 wt. % and 1 wt. %, respectively, with no moisture. A high amount of volatiles and low fixed carbon favors the

generation of more condensable gases and tars for oil formation than the production of syngas alone. However, the gas yield can be maximized under controlled operating environments of high-temperature and suitable gasifying atmosphere. The high carbon and hydrogen content in raw feed is desirable for higher LHV when the fuel is burnt. The ash content of >5 wt.% in the feed material increases the possibility of slag formation during high-temperature gasification (Ayol et al., 2019). Therefore, the proximate and ultimate analyses (Table 3.1) of CKPW indicate the presence of 78.91 wt.% of C and 7.25 wt.% of H, and hence the fuel is suitable for the plasma gasification process.

The mineral components such as solid oxides present in the ash of the CKPW feed, are shown in the XRD plot (Fig. 5.1), whereby the elements on average, are affirmed with the help of FESEM-EDS as depicted in Table 5.2. Titanium (Ti) and Barium (Ba) are found to be the most abundant metals in oxide forms, which are usually added to increase the resistance to weather and heat, improve mechanical and electrical properties etc., among others. Silica (SiO_2) has the ability to control the rheology of plastics by making the granulates flow freely.

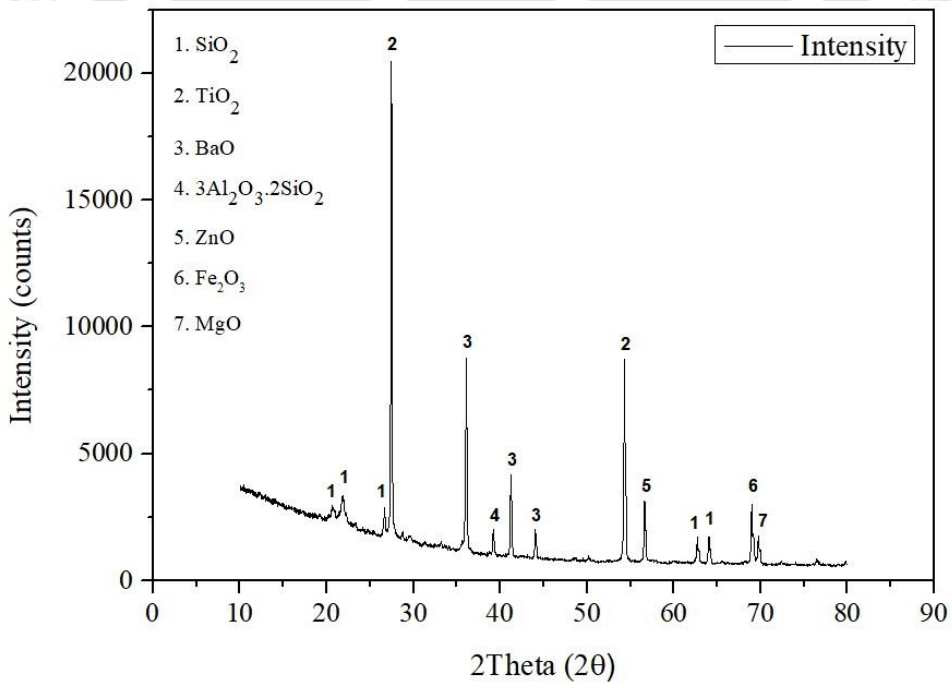

Fig. 5.1. XRD plot of the ash recovered from CKPW.

Table 5.2

FESEM-EDS analysis of the CKPW ash sample.

Element	Ti	Ba	Si	Mg	Fe	Zn	Na	Al	O
wt.%	32.8	22.55	3.42	2.55	4.65	0.46	0.81	0.82	31.83

Whereas other elements such as Mg, Zn, Al, etc. are included to increase the strength and durability of the material. Ti may find application in joint replacements, tooth implants and sunscreens, preventing UV lights from entering the skin. The largest use is in the form of titanium oxide (TiO_2) as a vivid white pigment in paints, plastics, etc. Moreover, Ba is not an extensively used element due to its toxic nature but is generally used in paints and glassmaking process ("Periodic Table," 2022; "Titanium Dioxide Market Size, Share & Trends Analysis Report," 2023).

To understand the gasification behavior of the CKPW feed, thermogravimetric Analysis (TGA) is performed from 25-1100 °C under a CO_2 atmosphere. The thermogram displaying the mass loss with respect to temperature and its derived form (DTG) is shown in Fig. 5.2. The absence of mass loss at 100-150 °C indicates no moisture in CKPW. Approximately 91-92 % of the decomposition is observed in the temperature range of 350-550 °C, which is the pyrolysis zone i.e., the release of the volatile matter. In the high-temperature region (800-1060 °C), the rest of the weight loss (6.5%) occurred due to the gasification of fixed carbon with CO_2.

5.2.2. Syngas composition, LHV and yield

In this section, the product gas composition obtained for different experimental cases is shown and compared. The percentage composition of H_2, CO, CH_4, CO_2, C_2H_4, C_2H_6 and C_3H_6 are measured. Table 5.3 presents the syngas concentration on a volume basis with respect to

changes in feed flow rate, gasifying agent (CO_2) flow rate and power level. The compound C_xH_y involves the lighter hydrocarbons (LHCs) such as C_2H_4, C_2H_6 and C_3H_6.

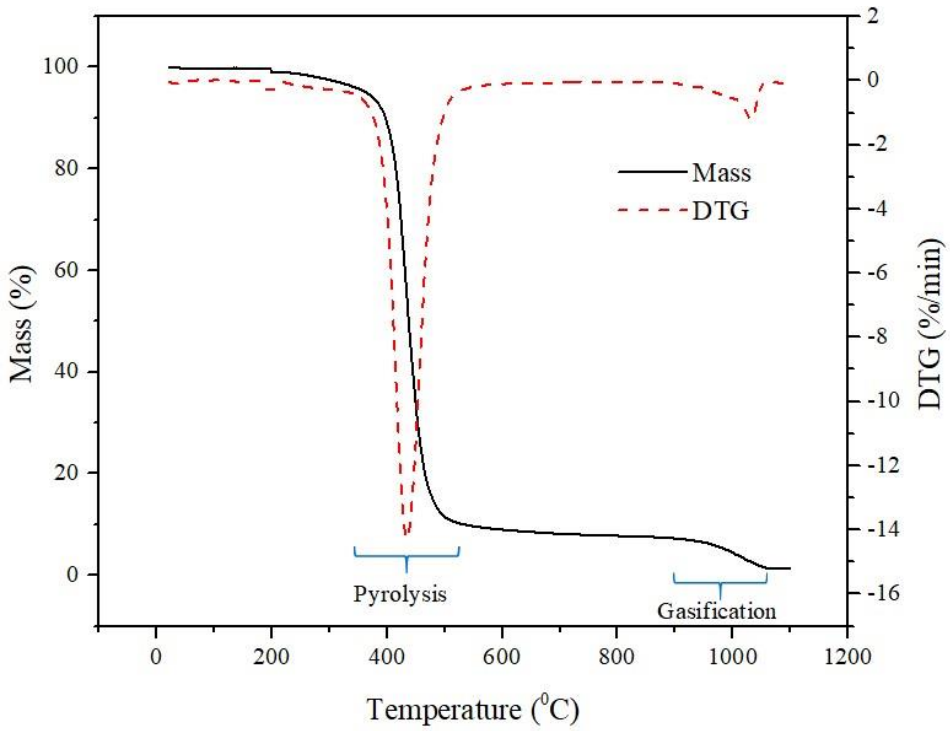

Fig. 5.2. TGA curve of CKPW feed.

5.2.2.1. Effect of mass flow rate of feedstock on syngas concentration, LHV and yield

With an increase in the feed rate of CKPW, the H_2 and CO concentration (Table 5.3) increases up to 30.16 vol.% and 46.09 vol.%, respectively for 40 g/10 min (Case 3) and then decreases. The total content of H_2 and CO is almost 60-76 vol.% for all the feed rates, with an average molar ratio of H_2/CO = 0.7. The repeatability of the performed experiments exhibited a deviation of 0.1-3.2% on average with respect to the outlet syngas composition. A higher CO observed in the product gas is attributed either to the partial oxidation of carbon/fuel with the free oxygen radical produced from CO_2 dissociation (R7 and R17) or the role of the Boudouard reaction (R9). The dominance of partial oxidation (R7) is highly probable due to two reasons (i) low fixed carbon (6 wt.%) and (ii) plasma chemistry hinders the governance of the

Table 5.3

Results of syngas compositions, LHV and yield using CKPW feed based on different parameters.

Case number	$\dot{m}_F$ (g/10 min)	Power (kW)	Gas flow (lpm)	Syngas composition (vol. %)					LHV (MJ/m^3)	Gas yield (%)	Oil yield (%)	Residue yield (%)
				H_2	CO	CH_4	CO_2	C_xH_y				
1	20	1.12	0.5	25.03	36.19	6.23	29.51	3.04	11.64	92.83	6.44	0.73
2	30	1.12	0.5	27.32	40.02	8.07	21.48	3.11	13.10	91.90	7.08	1.02
3	40	1.12	0.5	30.16	46.09	8.54	10.12	5.09	15.80	90.48	7.67	1.85
4	50	1.12	0.5	28.47	41.34	9.01	14.76	6.42	16.16	88.16	7.75	4.09
5	60	1.12	0.5	24.07	35.02	9.09	24.92	6.90	15.29	82.59	10.19	7.23
6	40	1.12	0.3	21.35	36.17	7.45	28.72	6.31	14.13	91.10	1.88	7.03
7	40	1.12	0.4	23.80	45.17	7.89	17.34	5.80	15.27	88.97	8.43	2.60
8	40	1.12	0.6	19.86	35.27	7.30	32.33	5.24	12.96	95.26	3.38	1.36
9	40	1.12	0.7	16.78	31.18	6.96	39.68	5.40	12.07	96.55	2.26	1.29
10	40	0.75	0.5	24.48	38.09	6.21	27.84	3.38	12.23	88.54	0.97	10.49
11	40	1.6	0.5	31.17	49.29	6.96	7.43	5.15	15.89	91.70	6.38	1.93
12	40	2	0.5	32.23	51.98	7.29	3.28	5.22	16.46	92.53	6.34	1.13

C_xH_y includes C_2H_4, C_2H_6 and C_3H_6 compounds; LHV = lower heating value.

Boudouard reaction. Moreover, the presence of O radicals and the impact of electrons on C-H molecules from volatile matter (93 wt.%) are inclined toward the progress of partial oxidation (Agon et al., 2016; Saleem et al., 2019; Zhang and Harvey, 2021). As shown in Table 5.3, some fractions of fixed carbon are also found in the solid residue. Due to low residence time in the plasma gasifier, high particle size and insufficient energy (1.12 kW) provided by the plasma torch, the concentration of CH_4 and C_xH_y also increases with feed rate. The volatiles released by the pyrolysis process (R16) and CO_2 gasification (R9) are heavier hydrocarbons, which require a high amount of energy to break into CO and H_2, especially under fast-heating pyrolysis conditions in the plasma method. The process gives rise to a higher temperature gradient inside the particles, leading to incomplete gasification and tar cracking (R18). Thus, the plastic waste-to-energy conversion process at a higher feed rate minimizes the gas yield with more volume of light hydrocarbons and consequently increases the yield of oil (condensable gases and compounds soluble in DCM solvent) and residue (unconverted carbon excluding ash) yield.

The LHV of syngas increases with an increase in the feed rate to a maximum value of 16.16 MJ/m^3 for Case 4 (50 g/10 min) despite its lower H_2 and CO content as compared to Case 3 (15.80 MJ/m^3), which is related to the added contribution of LHCs in calorific value. The results are quite analogous to those reported in the literature on fluidized bed gasification of ABS, regarding LHCs and tar content (Jeong et al., 2022). The percentage of feed conversion (96%) and quality of syngas related to H_2 and CO content (84 vol.%) in this study is higher than the stated literature (non-plasma system) of 91% and 32 vol.%, respectively, mainly due to the dilution of air in the product gas. Correspondingly, using supercritical water and high-pressure ABS gasification conditions under non-plasma conditions, the syngas have a high CH_4 content and equivalent mole fraction of H_2. At the same time, the shift in equilibrium consumes CO to produce more CO_2 compared to the present study (Bai et al., 2019; Cao et al., 2020).

5.2.2.2. Effect of CO_2 flow rate on syngas concentration, LHV and yield

Table 5.3 shows the changes in the syngas composition due to CO_2 flow rate variation from 0.3 lpm to 0.7 lpm and simultaneously its impact on the LHV and product yield. The concentration of H_2 and CO increases first and then decreases with the increase in the CO_2 flow rate, attaining a maximum at 0.5 lpm with values as reported in Section 5.2.2.1. A deficient supply of CO_2 (at 0.3 and 0.4 lpm) will increase the residue yield to 7.03% (without ash), as observed in the analysis (Table 5.3), because of the fuel leaving the plasma gasifier unreacted. With the increase in CO_2 flow rates, the generated reactive species such as CO, O and O_2 enhanced the conversion of plastic waste, since more energy is accumulated by the generation of reactive species and utilized in the gasification process (Wang et al., 2019). On the other hand, with a higher flow rate of CO_2 (at 0.6 and 0.7 lpm), the reactor gets overloaded with excess CO_2, which eventually exits with the syngas, diluting the percentage of H_2 and CO and thereby reducing the LHV of the product gas. The higher LHCs in the syngas are due to the bigger particle size and lower time spent by the volatile gases inside the reactor. Comparing the effect of CO_2 flow rate, the average CO content produced is lower in the syngas than the effect of increase in the solid feed rate (cases 1-5) due to the dominance of partial oxidation over Boudouard reaction. It can be seen from Table 5.3 that the influence of CO_2 flow rate becomes less significant than the changes in solid feed rate in terms of the calorific value of the syngas and percentage of gas yield. A reported literature observed maximum CO and H_2 content of 48.58 vol.% and 27.5 vol.% at a CO_2 flow rate of 0.43 Nm^3/h and 0.34 Nm^3/h, respectively, using sewage sludge as a fuel for plasma gasification (Wang et al., 2019). The CO concentration is higher by 2.49 vol.% and H_2 lower by 2.66 vol.% than the present study. Besides, the LHV (15.80 MJ/m^3) is higher using CKPW feed as compared to sewage sludge (8.91 MJ/m^3). (Hlina et al., 2014) reported that the CO_2 plasma gasification of HDPE feedstock yields an H_2 and CO percentage of 41.6 vol.% and 49.7 vol.%, respectively. Almost complete

degradation of feedstocks such as HDPE, and sewage sludge is reported, whereas a significant amount of LHC is generated in the present study due to the complexity in the ABS degradation.

5.2.2.3. Effect of torch power on syngas concentration, LHV and yield

For a given feed rate of solid fuel (40 g/10 min) and CO_2 (0.5 lpm), when the torch power is lower (0.75 kW), the feed material gets accumulated in the reactor, increasing the residue yield to 10.49 % and thus decreasing both the gas and oil yield. Since all the volatiles and fixed carbon could not be utilized in the process, the content of H_2 and CO is also found the lowest, around 24.48 vol.% and 38.09 vol.%, respectively. Similarly, the C_1-C_3 compounds are only around 3-6%. Moreover, an increase in the torch power by 0.37 kW increases the gas yield to ~ 91%, with a total yield of CO and H_2 by 16%. Further, increasing the input power to 2 kW increases the H_2 and CO to ~ 84 vol.%; hence, the LHV is also higher (16.46 MJ/m^3) with high gas yield. On the other hand, the total amount of H_2 and CO does not substantially improve with an increase in every power level after 1.12 kW, indicating that the excess amount of energy from the plasma torch is not utilized. Similar influences of torch power on kitchen waste are reported in the literature with a maximum CH_4 of 2.5 vol.%) and C_xH_y of 1 vol.%) content. The lower values of CH_4 and C_xH_y content are due to the efficient thermal degradation of kitchen waste, which is not complex in nature. Moreover, the feed's low C, H and calorific value results in lower H_2 and CO content in the syngas (Li et al., 2022).

5.2.3. Energy and exergy analysis

Other parameters that measure the performance of the plasma gasification process besides syngas composition and heating value are the energy and exergy efficiencies. The cold gas efficiency (η_{CGE}) (Table 5.4) is calculated as given in Section 3.5.1, which is the ratio of the chemical energy of the syngas and the sum of input chemical energy from fuel and power consumed by the plasma torch. Similarly, the estimated exergy efficiencies are shown in Table

5.4. The energy efficiency increases and then decreases with the feeding rate, achieving a maximum of 46.06 % for 40 g/10 min. It is attributed to the higher calorific value of the syngas of 15.80 MJ/m^3. However, the highest LHV (16.16 MJ/m^3) is observed for a 50g/10 min feed rate, however, the CGE decreased due to the poor consumption of solid fuel at higher input rates. The same results are obtained with the increase in the torch power level i.e., the LHV increases, but at the input power of 1.12 kW, the CGE starts decreasing for analogous reasons. The inlet CO_2 flow rate impacts the energy efficiencies and is found optimum at 0.5 lpm, and then the efficiency decreases at a higher flow rate. On the other side, the exergy efficiencies (~44%) show a negative deflection of around 1.5% from energy efficiencies (~46.5%) considering all the cases. This illustrates the lower loss in entropy generation due to the chemical reactions' irreversibilities. Based on the reported literature on plasma gasification, RDF and kitchen waste can achieve a CGE of 48% and 28%, respectively (Agon et al., 2016; Li et al., 2020). The drop in efficiency is ascribed to the heat losses from the system and structure of the plasma gasifier that reduces plasma-feed interaction.

It is important to note that the lower energy and exergy efficiencies values do not include the sensible heat of syngas, energy loss in cooling the plasma torch, energy in oil and residual energy. Table 5.4 also presents the percentage distribution of energy and exergy among various products based on the input (fuel and plasma power) to the system. It can be seen that the share of the sensible heat of the gas varies in the range of 4-7 % while the maximum share is occupied by the radiative losses (heat dissipation to the environment) between 23-34%, which is deduced after subtracting all the other losses. However, the energy captured by the plasma torch cooling water, increases the water temperature to around 51 °C on average and is highly significant (14-26 %) among the energy distributed in other streams. Further recovering the sensible heat is beneficial to produce hot water for domestic usage. Similarly, the oil and the residual slag can be utilized in their respective field of interest, which is discussed below in Section 5.2.7.

Table 5.4

Results of energy and exergy efficiencies and their distribution based on the various experimental factors.

Case number	Energy output (kW)	Energy η_{CGE} (%)	Exergy η_{ex} (%)	Sensible heat (%)	Energy in water (%)	Energy in oil (%)	Residual energy (%)	Radiative losses (%)	Exergy in water (%)	Exergy in oil (%)	Residual exergy (%)
1	0.86	37.44	36.37	6.69	25.60	3.75	0.32	26.20	18.76	3.80	0.47
2	1.17	40.55	39.18	6.40	21.83	5.85	0.51	24.86	16.00	5.91	0.74
3	1.6	46.06	44.34	5.19	17.41	5.01	1.04	25.29	12.76	5.04	1.50
4	1.79	44.06	42.31	4.37	15.51	5.27	1.56	29.23	11.37	5.28	2.25
5	1.84	39.56	37.91	3.52	14.27	8.34	4.41	29.90	10.46	8.35	6.68
6	1.41	40.59	39.07	4.39	18.62	7.51	5.65	23.24	13.65	7.55	8.10
7	1.55	44.62	42.95	4.82	18.13	7.06	1.62	23.75	13.29	7.09	2.36
8	1.36	39.15	37.69	4.25	18.38	1.91	2.77	33.55	13.47	1.92	4.02
9	1.31	37.71	36.30	4.08	18.10	3.17	4.21	32.73	13.26	3.19	6.12
10	1.12	36.08	34.58	4.65	20.30	2.48	7.95	28.54	14.88	2.48	11.40
11	1.63	41.22	39.87	4.84	17.01	4.26	0.96	31.71	12.46	4.30	1.40
12	1.7	39.04	37.87	4.89	17.17	4.39	0.58	33.93	12.59	4.44	0.85

5.2.4. Economic Analysis

The syngas production cost or levelized cost of syngas (LCOS) based on the total capital cost of the plasma gasifier and its accessories required during the experiments is estimated in the Indian scenario. Table 5.5 shows the LCOS value calculated based on the various operating parameters considering interest rate (r) of 4 %, equivalent period of utilization (P) of 2000 h/year and payback period (k) of 4 years. The syngas cost varies in the 23-36 INR/kWh range, with the lowest value found for 40 g/10 min of solid feed rate with a CO_2 flow of 0.5 lpm and torch power of 1.12 kW (Case 3). From the energy analysis, the maximum cold gas efficiency (η_{CGE}) is obtained for the stated operating conditions of Case 3; thus, the relatively optimum energy output decreases the syngas cost. Similarly, the highest LCOS of 35.24 INR/kWh is for the case when the gasifier functions at a plasma power of 0.75 kW (Case 10). At this condition, the torch power is not sufficient to maximize the syngas yield, and thus the energy output decreases with the lowest CGE. The higher LCOS values are still in good agreement with the reported literature (Paulino et al., 2020), taking into account the same assumptions.

5.2.5. Model validation

From the above analysis, the optimum conditions of solid feed rate, CO_2 flow rate and input power are found to be 40 g/10 min, 0.5 lpm and 1.12 kW, respectively i.e., Case 3. A model is developed using Aspen Plus software in Fig. 4.5 of Chapter 4, to predict the composition of syngas by the plasma gasification process of the current experimental study. In Fig. 5.3, the simulated syngas compositions (stream G5) is compared with that of the results obtained in the experiment. As the theoretical model assumes thermodynamic equilibrium, the concentration of H_2 and CO in the syngas is found higher than the experimental results process, which is due to the complete conversion of CKPW feed and left with no solid carbon. Subsequently, CH_4 formation is drastically suppressed to 2.67 vol. % with no LHCs in the product gas.

Table 5.5

Results of the syngas production cost for the considered experimental conditions.

Case number	C_{system} (INR)	$OC_{var,gp}$ (INR/kWh)	MC_{gp} (INR/kWh)	C_{capex} (INR)	C_{opex} (INR)	C_{total} (INR/kWh)	LCOS (INR/kWh)
1	109477.5	6.59	0.53	27000	1002.29	0.91	25.78
2	164216.25	4.79	0.58	27000	1002.29	0.66	25.36
3	218955	3.50	0.57	27000	1002.29	0.49	23.40
4	273694.75	3.13	0.63	27000	1002.29	0.43	25.26
5	328432.5	3.09	0.75	27000	1002.29	0.43	29.27
6	218955	4.55	0.74	27000	1001.37	0.63	30.44
7	218955	3.61	0.58	27000	1001.83	0.50	24.16
8	218955	4.59	0.74	27000	1002.74	0.64	30.69
9	218955	4.91	0.79	27000	1003.20	0.68	32.84
10	218955	3.71	0.90	27000	1002.29	0.77	35.24
11	218955	5.99	0.54	27000	1002.29	0.47	25.06
12	218955	4.91	0.56	27000	1002.29	0.48	24.44

C_{system} = Plasma gasification unit cost; $OC_{var,gp}$ = Variable operating cost of plasma gasifier; MC_{gp} = Maintenance cost of plasma gasifier; C_{capex} = Capital cost of gasifying agent; C_{opex} = Operating cost of gasifying agent and C_{total} = Net cost of gasifying agent.

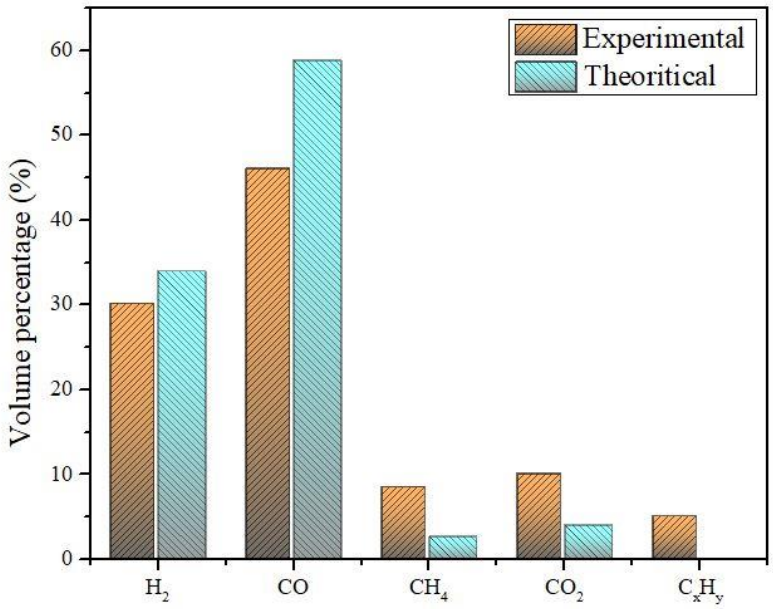

Fig. 5.3. Comparison between experimental and theoretical syngas composition (Case 3).

5.2.6. Characteristics comparison between raw feed, liquid oil, and residue

Based on the optimum operating parameters of $\dot{m}_F$ = 40 g/10 min, CO_2 flow of 0.5 lpm and power = 1.12 kW (Case 3), Case 7 and Case 10 i.e., taking one case from each independent variable, the different characterization techniques are adopted for more detailed assessment.

5.2.6.1. Proximate and ultimate Analysis

The images of the residue and liquid oil obtained are shown in Fig. 5.4, and their corresponding physicochemical characteristics are given in Table 5.6. Fixed carbon (FC) and ash are the only components present in the residue with a ratio of ~ 2:1 and are in accordance with the mass balance provided in Table 3.1. Carbon and hydrogen (97.6 wt.%) are the most abundant elements present in oil, with a negligible fraction of oxygen (0.46 wt.%), usually the standard maintained in a liquid fuel (diesel). Whereas the residue is enriched with carbon and oxygen of 69.67 wt.% and 29.13 wt.%, respectively, associated with FC and ash. The higher nitrogen content in oil (1.94 wt.%) than in the residue (0.5 wt.%) may be due to the thermal cracking of acrylonitrile monomer to condensable nitrogen compounds. Moreover, the LHV of

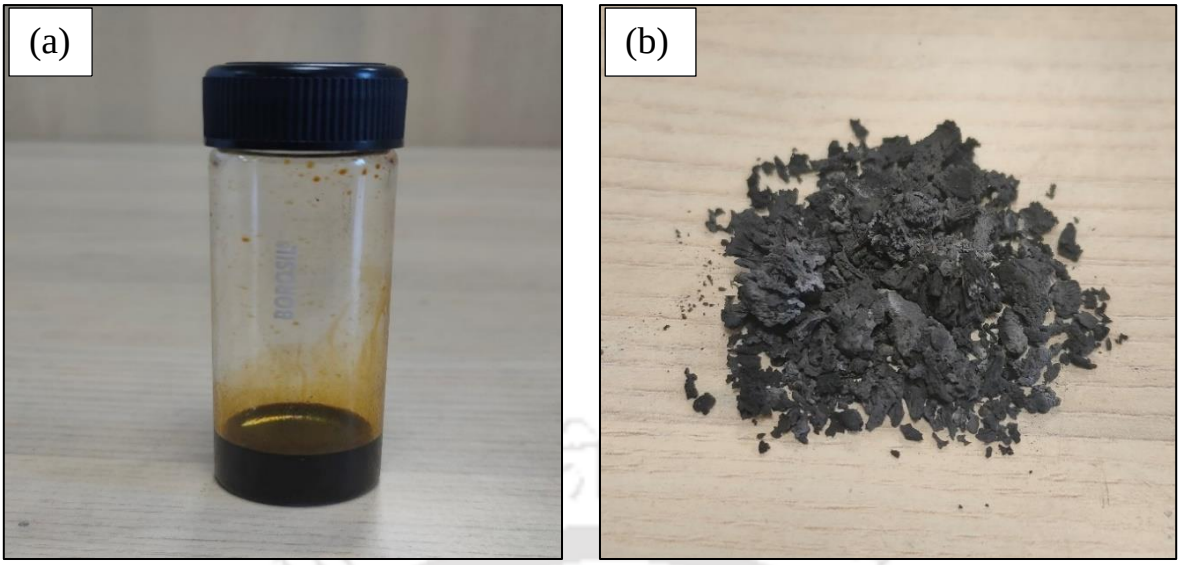

Fig. 5.4. Images of (a) oil and (b) residue obtained after CO_2 plasma gasification.

Table 5.6

Proximate and ultimate analysis of raw CKPW, oil and solid residue.

	Raw CKPW	Oil	Residue
Proximate analysis [wt.%, as received basis]			
Moisture	-	-	-
Volatile matter	93	-	-
Fixed Carbon	6	-	68.59
Ash	1	-	31.41
Ultimate analysis [wt.%, ash free basis]			
C	78.91	90.8	69.67
H	7.25	6.8	0.7
N	1.65	1.94	0.5
S	-	-	-
O[a]	11.19	0.46	29.13
LHV based on energy [MJ/kg]	35.31	39.13	29.19

[a] by difference.

oil (39.13 MJ/kg) is found higher than the oil obtained by ABS liquefaction (Areeprasert and Khaobang, 2018), while the LHV of char in the residue (29.19 MJ/kg) is on the lower side compared to ABS feed due to higher carbon conversion in the plasma gasification process.

5.2.6.2. FTIR analysis

The residue and oil obtained from three cases (considering one from each independent variable), such as Case 3, Case 7 and Case 10, are used for comparison with the CKPW feed. Fig. 5.5 shows the FTIR spectra stating functional groups at different wavenumbers. The spectra of raw feed are verified for the identification of probable plastics i.e., ABS and PC, with the FTIR curves as reported in the literature (Jung et al., 2018). The presence of aromatic and aliphatic groups is quite evident in the raw feed and liquid oil, while no such major compound is detected in the residue, mainly fixed carbon and ash. The lower intensity of the peaks between 1000-1250 cm^{-1} observed in the oil is due to the chemical reaction of single-ring aromatic compounds i.e., C-H out-of-plane bending and tertiary alcohols to LHCs, H_2 and CO under CO_2 atmosphere. Similarly, the peaks obtained in the range of 555-780 cm^{-1} indicate aromatics and alkenes with C-H bending and C=C vibrations, whereas alkanes (C-H stretching) are identified between 2850-3180 cm^{-1}. The functional groups of the liquid oil and residue of all the cases indicate almost a similar profile except for the residue of Case 10. It is attributed to the lowest feed conversion and shows aliphatic and aromatic groups identical to the feed spectra. Moreover, other studies focused on liquefaction and slow pyrolysis of packaged plastic waste and polystyrene using ethanol solvent for liquid fuel production obtained the same functional groups (Ahmad et al., 2020; Das and Tiwari, 2018).

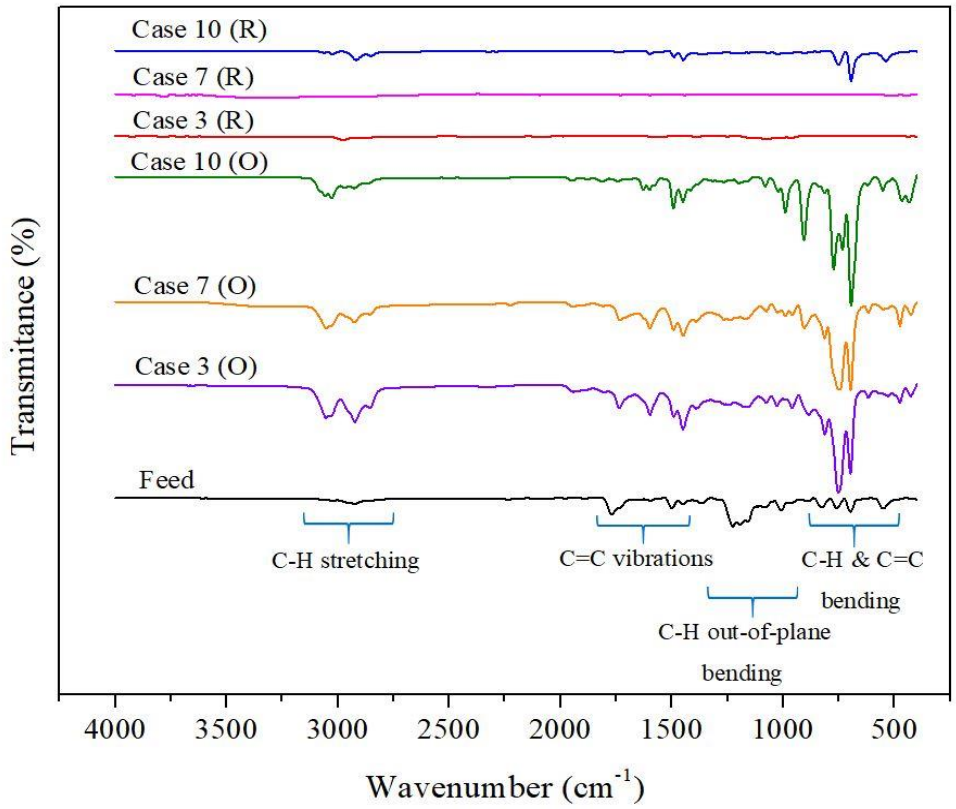

Fig. 5.5. FTIR spectra of raw feed, oil (O) and residue (R) for different cases.

5.2.6.3. Analysis of oil

Viscosity, density and pH of the oil product obtained in Case 3 are found to be 3.93 centipoise (cP) at 40 °C, 910 kg/m^3 and 6.94, respectively. When compared with diesel fuel, the pH and LHV of 39.13 MJ/kg (given in Table 5.6) are lower than that of diesel fuel, however, the viscosity and density are on the higher side (Ahmad et al., 2020; Zhao et al., 2022). Hence, reduction in viscosity and increase in pH are necessary to enhance the oil flow through the injecting system of diesel engines and prevent corrosion as low pH fuel destroys metal components. Therefore, the obtained oil requires further treatment or upgradation for commercial use.

GC-MS analysis is carried out for the selected samples considered in FTIR analysis to determine the chemical components present in the oil sample. Table 5.7 reveals that

monocyclic ring compounds such as toluene, ethylbenzene and styrene, and polycyclic aromatic hydrocarbons (PAHs) like naphthalene and anthracene are the main detected compounds. Styrene, a monomer of ABS, finds little share among the major compounds in the oil as most of it decomposes into ethylbenzene (an intermediate of styrene) and toluene in Case 3 (Liu et al., 2019). In a reported study conducted under catalytic reforming conditions, the portion of styrene and its derivatives, such as ethylbenzene and methylstyrene is found mainly in the oil, similar to found in the present study (Areeprasert and Khaobang, 2018). However, at a low power of 0.75 kW (Case 10), the supplied energy is insufficient to depolymerize the feed, whereby styrene and PAHs (naphthalene and anthracene) are found to be maximum in the oil. Due to the high reactivity under the plasma environment, the other two monomers, such as acrylonitrile and butadiene, are detected in a very small amount as benzenebutanitrile. On the other side, decreasing the CO_2 gas flow rate (Case 7), the saturated aliphatic (paraffins) and unsaturated aliphatics (olefins) are found to increase in the oil while a low quantity of cyclic hydrocarbons and aromatics is detected (Chen et al., 2019). Further, the low flow rate of CO_2 feed also resulted in the incomplete destruction of styrene monomer. PAHs are difficult to decompose into simple compounds; therefore, they are stable and remain in the oil product. It is also reported in the literature that PAHs are detected in the tar content obtained by the plasma gasification of RDF and ABS using supercritical water (Agon et al., 2016; Bai et al., 2019).

Table 5.7

Main components identified from the GC-MS analysis of oil after CKPW plasma gasification.

Case 3			Case 7			Case 10		
Retention time (min)	Compound name	Area (%)	Retention time (min)	Compound name	Area (%)	Retention time (min)	Compound name	Area (%)
8.23	Toluene	20.1	7.34	3,3-Dimethylheptadecane	16.4	7.39	Isobutyl isopentyl carbonate	12.8
10.67	Ethylbenzene	63.6	7.65	6-Hepten-3-one,5-hydroxy-4-methyl-	20.5	8.82	2H-pyran,3,4-dihydro-	15.2
12.25	Alpha-methylstyrene	0.61	8.02	Hexane,2,2,5,5-tetramethyl	15.3	9.64	Pyridine-d5-	4.83
13.58	Styrene	0.34	8.76	3-Ethyl-2-methyl-1-heptene	17.3	11.95	Toluene	2.99
16.67	Naphthalene	1.12	8.81	1H-1,2,4-triazole-3-carboxaldehyde,5-methyl-	6.65	14.18	Ethylbenzene	1.65
20.60	Biphenyl	0.35	9.58	Cyclohexane	1.26	15.02	Styrene	18.3
26.68	Ethylene 1,1-diphenyl	0.88	14.91	Styrene	5.08	17.19	Alpha-methylstyrene	1.24
28.13	Anthracene	1.77	17.14	Alpha-methylstyrene	0.33	22.84	Naphthalene	2.36
29.03	Naphthalene, 1-phenyl	0.52	19.08	Benzene,1-Propynyl-	0.36	26.92	Biphenyl	0.80
30.84	Naphthalene, 2-phenyl	1.13	22.80	Naphthalene	1.37	33.03	Stilbene	1.03
34.25	Benzenebutanitrile	0.11	34.94	9H-fluorene	1.12	34.82	Anthracene	4.09
36.54	3-methyl-2-(2-oxopropyl)furan	0.52				37.50	Naphthalene, 2-phenyl	2.32
	Total	91.1		Total	85.7		Total	67.6

5.2.6.4. FESEM analysis

SEM investigation is conducted to study the topographical behavior of CKPW obtained under the pre and post-plasma gasification process. CKPW (combination of ABS and PC), being a thermoplastic polymer, does not have strong polymer chains bonded chemically to each other, due to which it can be untangled when exposed to thermal heating. From Fig. 5.6(a), it can be seen that the surface of raw CKPW feed is smooth and non-uniform. Under non-plasma conditions, the gasification may occur only on the surface due to the condensation and absorption of the volatiles in the internal pores (Li et al., 2022). However, no such phenomenon is observed under the reactive plasma atmosphere, and many pores with high surface area are created, as shown in Fig. 5.6(b), which depicts the intense release of volatiles and favors the gasification by reducing the diffusional resistance of CO_2 molecules. The thermo-chemical interaction due to thermal plasma not only enlarged the pores but also increased the depth of the pores. The porous structure is due to the existence of unconverted carbon in the residue matrix. A higher ash content or agglomeration of the ash would cause the sample surface to be smooth and compact. The findings are consistent with the stated literature on printed circuit board gasification (Bhui et al., 2021; Bhui and V, 2021).

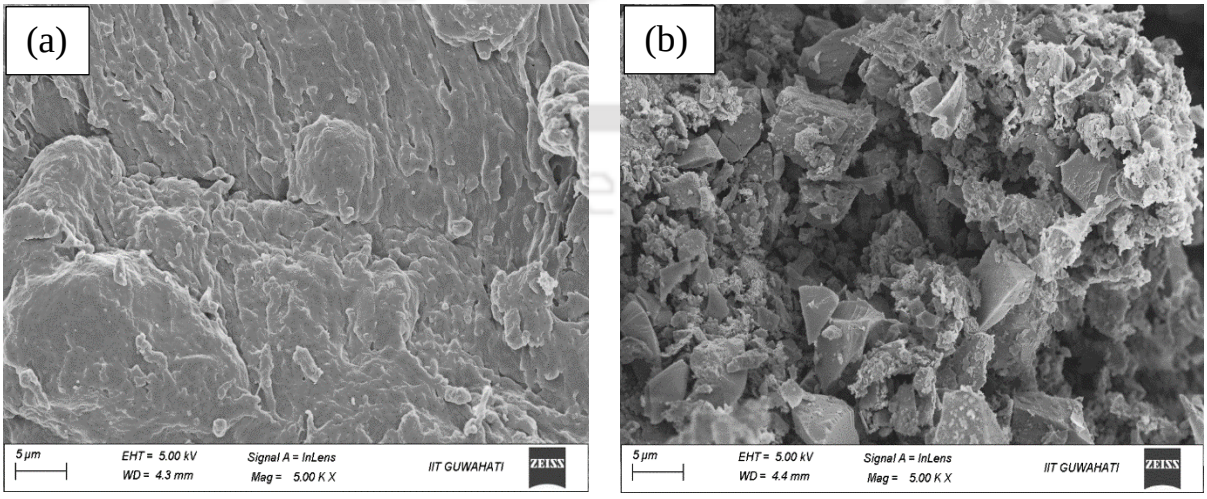

Fig. 5.6. FESEM images of (a) CKPW feed and (b) after CO_2 plasma gasification.

5.2.7. Reaction mechanism

Based on the results and analysis, the decomposition mechanism of ABS in CKPW under plasma conditions is proposed and summarized as shown in Fig. 5.7. In the first step, the long-chain ABS polymer goes through depolymerization or thermal cracking under heat whereby the volatiles release from the internal pores of the material. During the pores formation, some volatile compounds may undergo rearrangement within the residue matrix while the remainder continues to endure secondary reactions due to their instability (Collard and Blin, 2014). This results in the production of paraffins, olefins and oligomers with some intermediates further transformed into gas products (Cao et al., 2020). The gases such as H_2, CO and CH_4 are formed after the decomposition and reforming of the aliphatic chain compounds in ABS (Bai et al., 2019). The breaking of bonds allows to form new chain ends and the produced molecules are identified in the liquid fractions in the GC-MS analysis (Table 5.7) in the form of derived monomer (ethylbenzene and toluene) or dimer (benzenebutanitrile). Aromatic compounds, including PAHs, find special mention in the products due to their presence in the oil and increase with the drop in CO_2 gas flow rate and plasma power. Though the aromatization of olefins and paraffins occurs at the intermediate pathway of ABS gasification, it is restricted to minimal progress, which can be observed with fewer aromatics present in the oil and gas (Table 5.3 and 5.7). The maximum proportion of gas yield under a reactive plasma atmosphere showed the rigorous gasification reactions of PAHs into LHCs such as C_1-C_3 olefins and simpler compounds. Moreover, the production of LHCs is compensated with the higher values of CH_4 from the decomposition of the organic portion. In fact, sometimes the higher amount of LHCs in the gas product of plastic gasification is seen as an indicator of tar presence or PAHs in the oil (Lopez et al., 2018). The impact of electron or radical species (O) through CO_2 dissociation on the PAHs, including the aromatic ring and cyclic components, promotes the generation of more gaseous products (Saleem et al., 2019; Zhang and Harvey, 2021). On the other hand,

fragmentation and charring take place to result in the formation of solid carbon named char and condensable and non-condensable gases of small chain organic compounds. The pathway is generally through a series of intra and inter-molecular arrangements accompanied by a high thermal stable environment (Collard and Blin, 2014). Finally, the solid carbon in CO_2 ambiance produces CO as per reaction R9 and the remaining is collected as a residue. Therefore, due to the presence of high energy electrons, nascent oxygen and independent CO_2 molecules in the plasma gasification process, the intermediate products are able to enhance the syngas production (H_2 and CO) with lower oil and residue yield.

The presence of metallic minerals in the feed (Ti, Ba, etc.), as illustrated in Table 5.2, shows a negligible effect on the plasma gasification reactions. The formation of molten slag is avoided due to the low ash content (1 wt.%) in the CKPW feed. This leads to the reduction of a number of active sites on the metal surface for the adsorption of reactive species for catalytic activity. The absence of significant amounts of alkali and alkaline metals, such as K, Na, Ca, etc., in the ash reduces the dependence of gasification reactivity on ash (He et al., 2023; Yu et al., 2021). The agglomeration of the ash or synergistic influence of ash on the syngas composition is highly susceptible to the presence of optimal ash quantity and suitable catalyst minerals in the fuel feedstock e.g., high ash coal (33 wt.%), garden waste (15 wt.%), etc. A smooth and dense surface is formed after the gasification of high ash-based residue (Bhui and V, 2021; Fazil et al., 2022). In the present study, due to low ash content in the CKPW feed, a highly porous structure of the residues observed from the FESEM images (Fig. 5.6) is noted. This confirms the non-agglomeration of the ash at higher temperatures, which allows a higher diffusion rate of CO_2 under plasma gasification conditions.

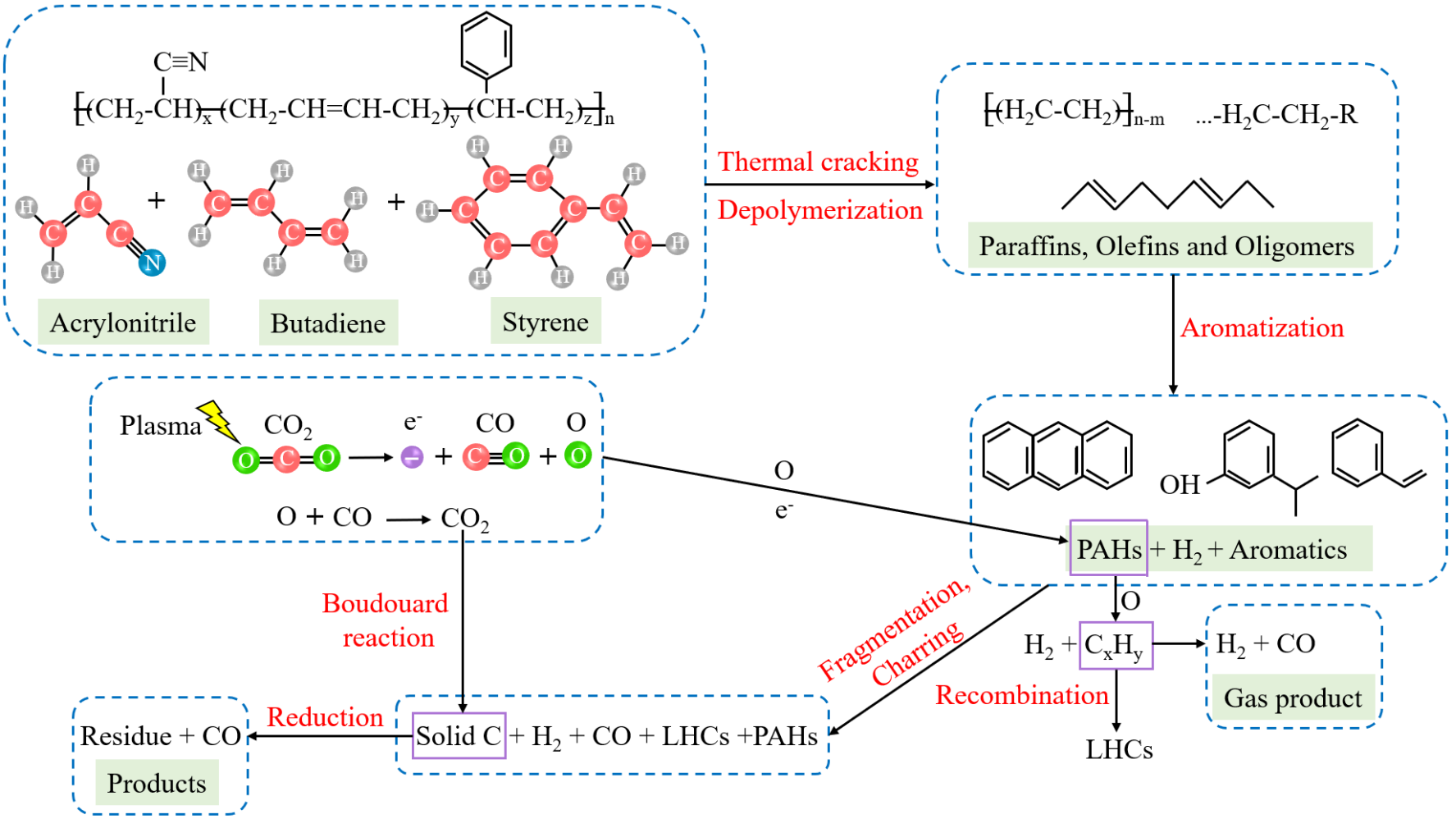

Fig. 5.7. Thermal degradation mechanism of ABS in a plasma gasification process under CO_2 atmosphere.

5.2.8. Quantitative relationship between experimental parameters and obtained results

The developed correlation is applicable to the specific feed mass flow rate (g/min), CO_2 flow rate (lpm) and torch power (kW), as discussed in Section 3.5.2. A polynomial fit is obtained with an R^2 of ~ 0.93 as per the correlation (Eq. 20):

Table 5.8 shows the constants of the equation, which is estimated by using SPSS software. The values of the experimental data are fitted to determine the constants of the correlation with respect to the individual operating conditions. The parity plot shown in Fig. 5.8 compares the predicted values with the experimental data of syngas compositions. This showed good accuracy and quick estimate of the syngas composition with variation in the operating parameters of plasma gasification.

Table 5.8

Empirical constants required to predict the correlated values.

	H_2	CO	CH_4	CO_2	C_xH_y	LHV	η_{CGE}
β_0	-214135.80	-103042.79	-13534.22	442053.67	250590.69	223753.69	175528.13
β_1	11616.20	15792.73	-3477.21	-1556.12	-8315.64	-7209.42	-7033.21
β_2	318559.72	3402.16	105777.77	-350855.21	-137727.40	12326.60	-11422.35
β_3	-786220.72	-858703.10	95393.43	-857711.42	-28594.51	-345824.1	-113713.86
β_4	-0.007	-0.021	0	0.028	0	-0.004	-0.012
β_5	-2.33	-4.52	-3.81	13.55	-2.843	-4.056	-17.81
β_6	-229.99	-254.55	-20.51	479.84	25.28	-46.94	-103.95
β_7	-13556.01	-11885.00	762.50	294.76	5274.68	1134.71	2648.60
β_8	7134.09	4959.77	5246.60	2447.24	4816.22	11877.86	8135.58
β_9	447387.50	944043.31	-272534.53	678016.87	-146501.61	-115401.6	-188943.56

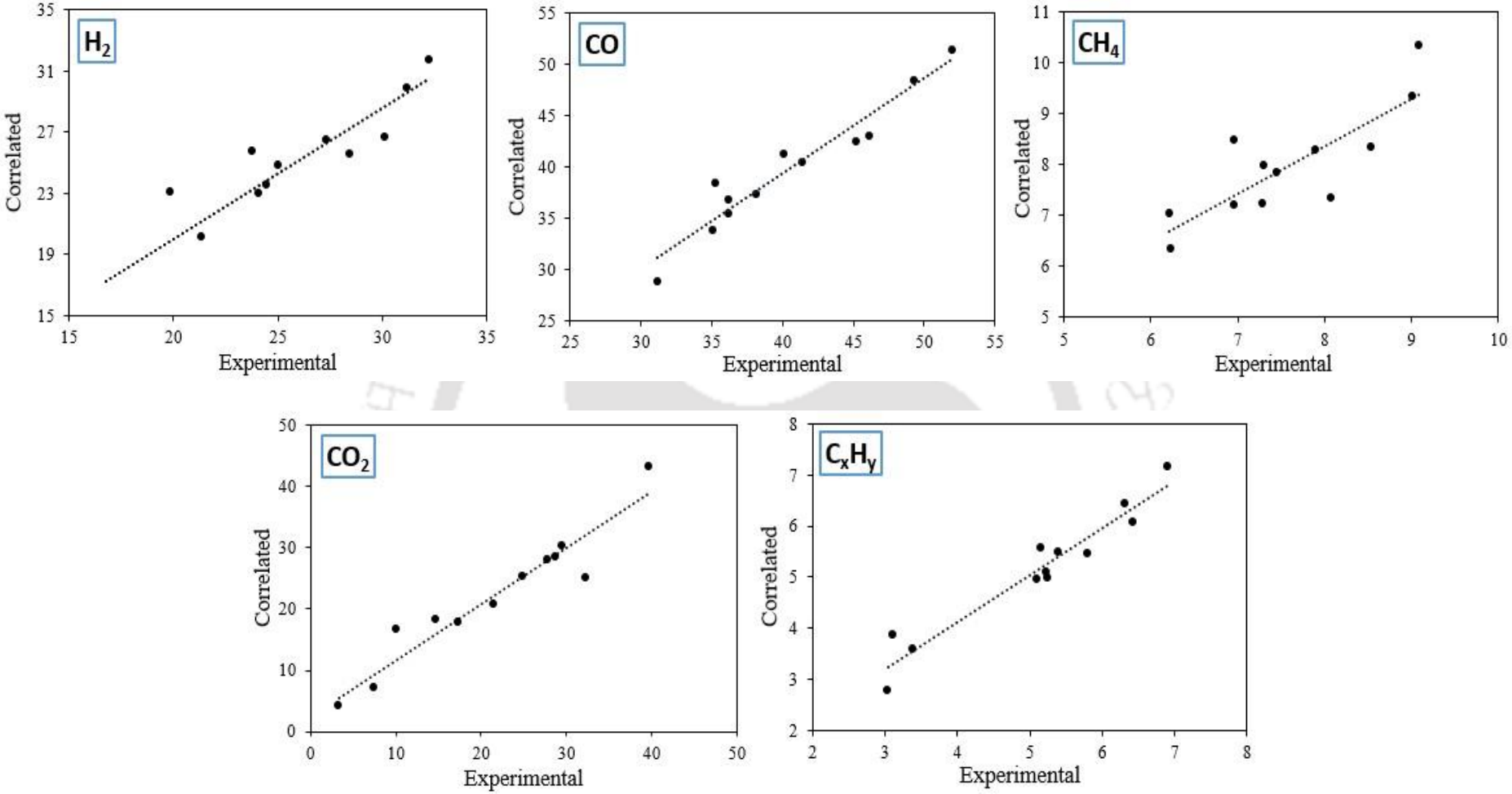

Fig. 5.8. Parity plot between actual and measured values for syngas compositions.

5.2.8.1. Experimental validation

Three experiments are conducted to validate the developed correlation. Table 5.9 provides the syngas compositions, LHV and CGE of the conducted experiments for validation. Table 5.10 shows the calculated values of output variables obtained from the correlations with error percentage (%). The independent variables, such as solid feed rate (40g/10 min), CO_2 feed gas flow rate (0.5 lpm) and torch power (1.12 kW), have a strong influence on the developed correlations. Thus, only one parameter is changed while keeping the other two parameters constant. A maximum value of 16% error is obtained under different scenarios of operational conditions. This estimation offers a quantitative relationship to estimate the performance of the plasma gasification system.

Table 5.9

Syngas compositions with LHV and CGE of the experiments conducted for validation.

$\dot{m}_F$ (g/10 min)	Power (kW)	Gas flow (lpm)	Validated syngas composition (vol. %)					LHV (MJ/m^3)	η_{CGE} (%)
			H_2	CO	CH_4	CO_2	C_xH_y		
40	1.12	0.45	26.47	46.01	7.64	14.27	5.61	15.57	45.19
35	1.12	0.5	28.25	43.16	7.92	15.64	5.03	15.07	41.83
40	1	0.5	24.96	41.72	7.19	22.18	3.95	13.50	38.46

Table 5.10

Comparison of syngas compositions, LHV and CGE between the data validated from experiments and correlated results.

$\dot{m}_F$ (g/10 min)	Power (kW)	Gas flow (lpm)	Correlated syngas composition (vol. %)					LHV (MJ/m^3)	η_{CGE} (%)	Error (%) between the validated and correlated results						
			H_2	CO	CH_4	CO_2	C_xH_y			H_2	CO	CH_4	CO_2	C_xH_y	LHV	η_{CGE}
40	1.12	0.45	26.78	43.39	8.37	16.01	5.14	14.75	43.05	1.17	-5.69	9.57	12.20	-8.44	-5.25	-4.73
35	1.12	0.5	26.75	42.71	7.85	17.99	4.41	14.12	41.83	-5.30	-1.05	-0.94	15.04	-12.41	-6.31	0.85
40	1	0.5	25.74	41.35	8.04	19.98	4.60	13.88	38.46	3.12	-0.89	11.81	-9.92	16.34	2.78	7.42

5.3. Conclusions

In this study, the CO_2-based plasma gasification of CKPW feed is carried out at different feed rates of solid and CO_2 gas with different power levels of torch. The following observations are drawn from this study:

- Case 3 had the best performance with the feed rate of 40 g/10 min, CO_2 flow rate of 0.5 lpm and power level of 1.12 kW, i.e., Higher H_2 (30.16 vol.%) and CO (46.09 vol.%) percentage in the syngas with an LHV of 15.8 MJ/m^3 is obtained.
- At the optimum operating conditions (Case 3), maximum energy (46.06 %) and exergy (44.34 %) efficiency are achieved. However, these could increase beyond 70% if the sensible heat of syngas, cooling water, etc., are recovered for commercial use. Moreover, the LCOS value of 23.40 INR/kWh is the lowest for the given scenario (Case 3).
- The oil product obtained has physicochemical properties similar to diesel, with higher carbon, hydrogen, and LHV values and lower oxygen content. On the other hand, the residue has a high amount of Ti and other useful metals, which can be recovered for potential applications in the healthcare industry.
- The developed correlations suggest a good agreement between actual and theoretical values. These are valid for a feed flow rate of 20-60 g/10 min, a CO_2 flow rate of 0.3-0.7 lpm and a torch power of 0.75-2 kW range of operating parameters.

Therefore, from the overall analyses, it can be inferred that the application of high-temperature CO_2 plasma gasification for waste-to-energy conversion is a feasible route.

Chapter 6

Experimental investigation on CO_2-plasma gasification of bakelite based electrical switch waste

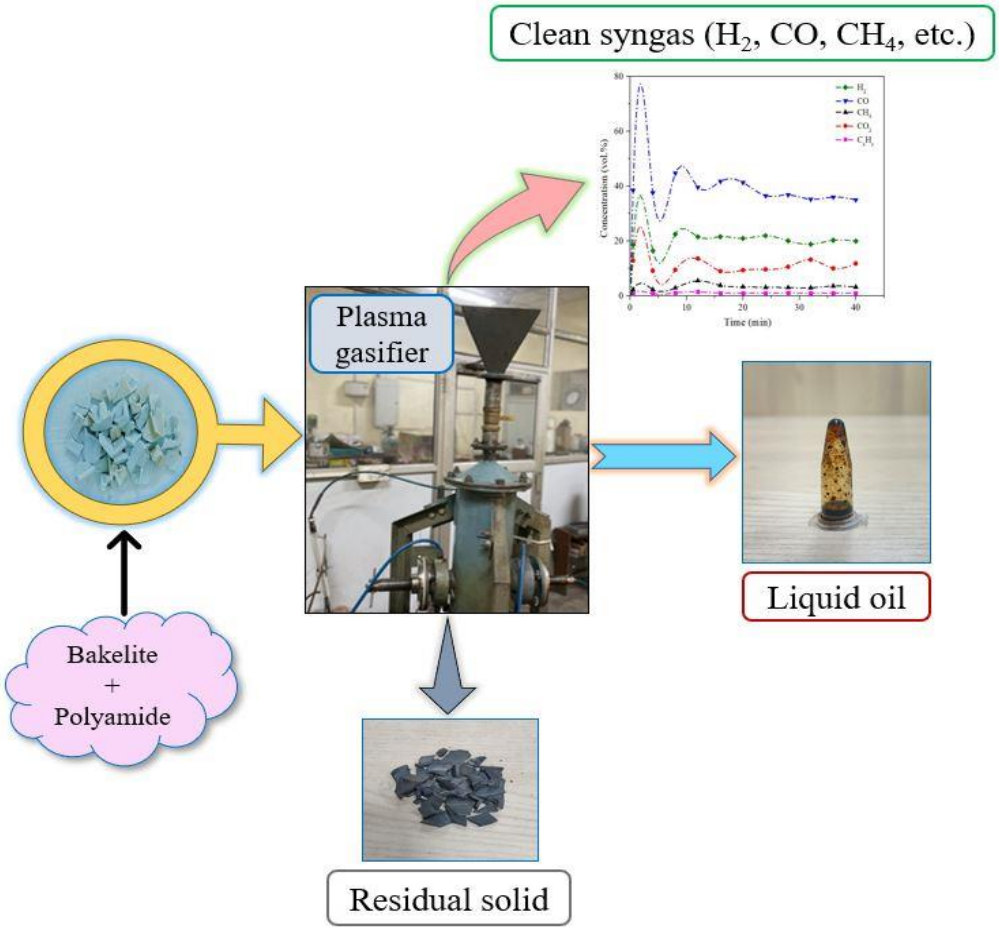

CHAPTER 6

EXPERIMENTAL INVESTIGATION ON CO_2-PLASMA GASIFICATION OF BAKELITE-BASED ELECTRICAL SWITCH WASTE

This chapter demonstrates a viability study on the impact of plasma on the thermal decomposition of thermosetting plastics. In this context, a thermoset fuel i.e., electrical switch waste (ESW) made of bakelite and polyamide, is considered for detailed investigation. ESW has a moderate amount of C and H that can be utilized by thermal plasma to produce syngas with a better heating value. Thus, it is imperative to analyze the plasma gasification behavior of ESW plastics for syngas production. In this study, the effect of feed rate, gasifying agent i.e., CO_2 flow rate and torch power on the syngas composition are explored. Further, energy, exergy and economic (3-E analysis) analyses are conducted to measure the performance of the plasma gasifier based on the lower heating value (LHV) of the product gas. The products obtained after plasma gasification are characterized to observe the implications of the thermochemical conversion on yield. To understand the impact of operating parameters on the formation of products, a reaction mechanism is proposed. Lastly, a developed relationship is put forward to predict the output variables theoretically.

6.1. Experimental parameters

Few preliminary experiments are conducted by batch feeding of the solid in the reactor and almost 80% of feed is converted within the first 10 min. Hence, each experiment is carried out for 40 min with an equal amount of feed introduced at every 10 min intervals. The feed is introduced at a mass flow rate of 20 to 60 g per 10 min interval while the CO_2 flow rate is maintained in the range of 0.3 to 0.8 liters per minute (lpm) as shown in Table 6.1. On the other

hand, to observe the effect of temperature, the plasma torch power is maintained between 0.5 and 1.6 kW for the given set of experiments. The syngas is continuously collected at regular intervals of 2 min and 4 min for the total run period of 10 and 40 min experiments, respectively.

Table 6.1

Process parameters of ESW plasma reaction experiments used in this study.

Case number	$\dot{m}_F$ (g/10 min)	CO_2 gas flow rate (lpm)	Torch power (kW)	Temp. (°C) at 4 cm
1	20	0.5	0.75	1147
2	30	0.5	0.75	1160
3	40	0.5	0.75	1177
4	50	0.5	0.75	1141
5	60	0.5	0.75	1175
6	40	0.4	0.75	1181
7	40	0.6	0.75	1166
8	40	0.7	0.75	1205
9	40	0.8	0.75	1192
10	40	0.5	0.5	1000
11	40	0.5	1.12	1230
12	40	0.5	1.6	1296

6.2. Results and discussion

6.2.1. Characteristics and thermal behavior of raw ESW feed

The proximate and ultimate analyses of the feedstock are shown in Table 3.1. As the moisture (1.54 wt.%) and ash content (4 wt.%) in the feedstock are low, the performance of the gasification process remains unaffected by them. Largely, the share of volatile matter and fixed carbon (~ 94 wt.%) in the feed is imperative to generate high-quality syngas. In addition, the high carbon and hydrogen content in the feed are desirable for the production of high-quality syngas. On the other hand, the crosslinking and rigid behavior of thermoset feedstock creates

operational difficulties in the conventional gasification process. However, the present study showed that under the reactive and hot plasma gas atmosphere, thermoset plastics such as ESW can be decomposed efficiently into syngas.

XRD analysis (Fig. 6.1) shows the presence of various solid oxides in the ash content of ESW feed. Several chemical compounds are detected in the ESW and each of these components plays a major role in improving the rheological properties of the material. Barium sulfate ($BaSO_4$) is found as the most abundant mineral component in the ESW, followed by barium orthotitanate (Ba_2TiO_4), a useful electro-ceramic. These oxides are protective agents to improve the heat resistance and mechanical properties of the ESW. Titanium is found in the form of titanium dioxide (TiO_2), which acts as a pigment, imparting brightness to the plastics. Almost, all thermoplastic and thermosetting material uses TiO_2 to improve electrical properties (Chin Trento, 2023). The presence of zinc ferrite ($ZnFe_2O_4$) in the ESW has the role to increase

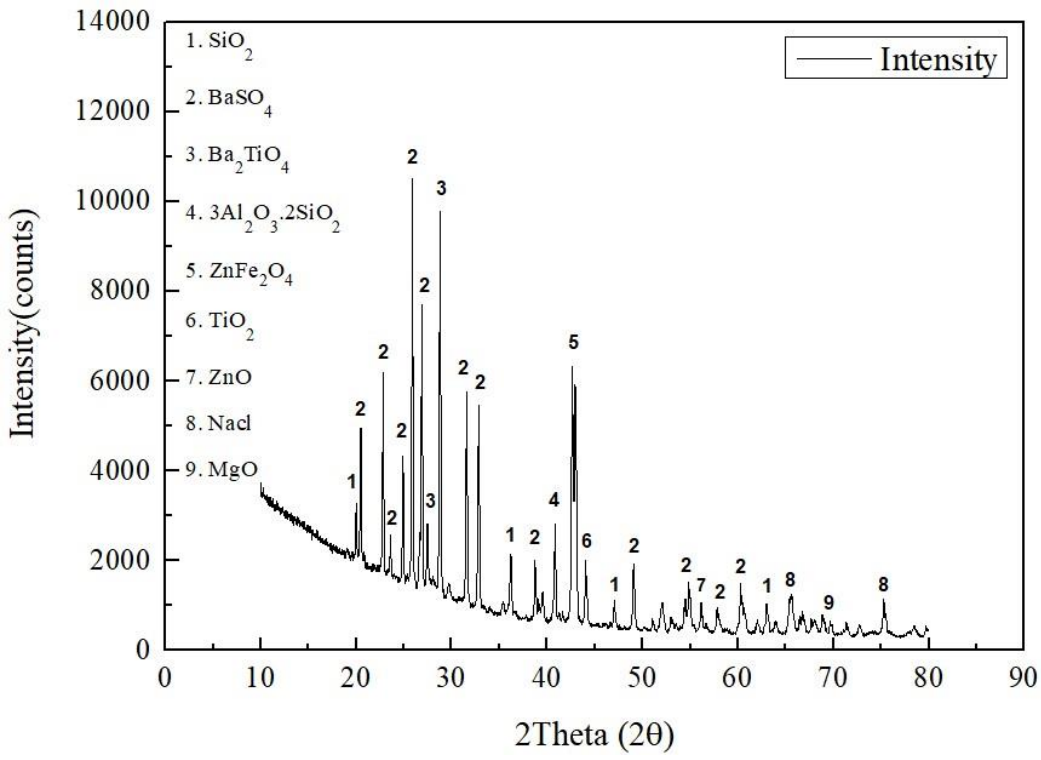

Fig. 6.1. XRD plot of the ash recovered from ESW feed.

the opacity and act as corrosion-resistant (Bhui and V, 2021). Further, the magnesium oxide (MgO) in the ESW could be a thickening agent for molding phenolic resin. Using FESEM-EDS analysis, the elemental composition of minerals in ash is identified and verified with XRD results, as depicted in Table 6.2. Barium (Ba) constitutes ~ 70 wt.% among the metals in the ESW with minor proportions of Ti, Si and Zn. If recovered, these metals can be used for multiple applications in the field of making die-castings, alloys, paints, etc.

Table 6.2

FESEM-EDS analysis of the ESW ash sample.

Element	Ba	Ti	Zn	Si	Na	Mg	Cl	Fe	Al	O
wt. (%)	70.42	3.25	3.87	2.9	0.83	0.65	0.37	0.32	0.12	17.05

Thermogravimetric analysis (TGA) of raw ESW is carried out from 25 to 1000 °C to assess the thermal degradation behavior under the CO_2 environment. Fig. 6.2 shows the mass (%) curve and derivative thermogravimetry (DTG) of ESW. In the moisture removal zone i.e., 100-150 °C, nearly 1.5-2% mass loss is observed. Compared to other plastics, the pyrolysis zone (release of volatile matter) of ESW feed started at a very low temperature of ~230 °C and continued till 480 °C, losing around 64% of mass. Due to the high amount of fixed carbon in the feed, a large drop in mass (~14.5%) is observed in the gasification region between 800 and 1000 °C. In the gasification zone, a mass loss of 14.5% occurs between 800 and 1000 °C and the remaining 3.5% of fixed carbon are left unreacted due to their complex nature. Hence, the plasma environment would be suitable for the effective conversion of bakelite. Thus, the study aids in identifying the thermal decomposition behavior and employs the significance in the plasma gasification process.

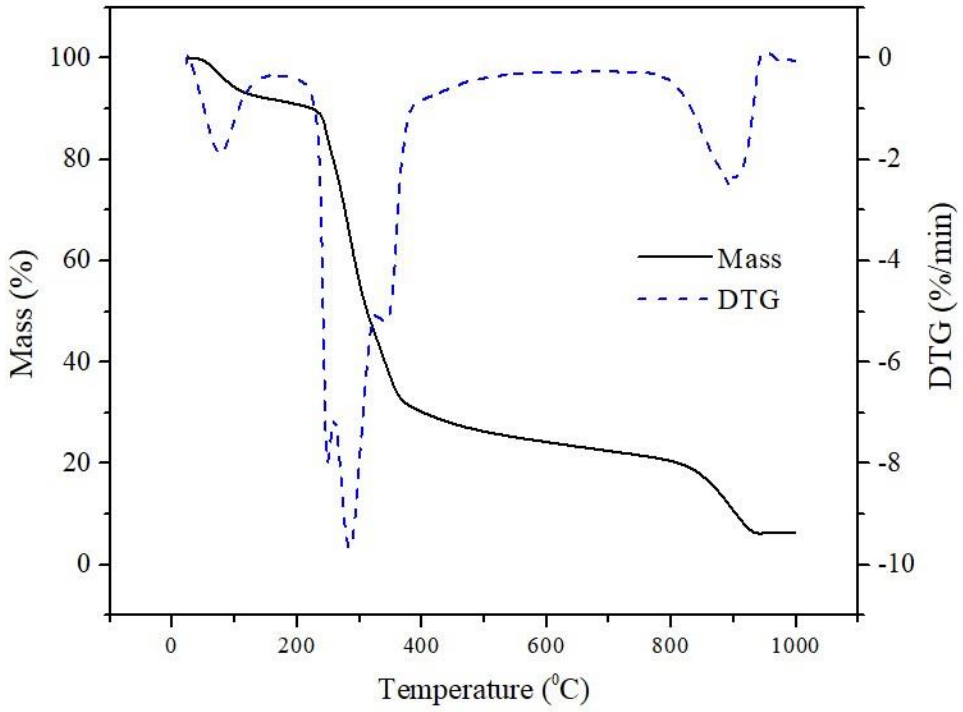

Fig. 6.2. TGA curve of the raw ESW feed.

6.2.2. Syngas composition, yield and LHV

Table 6.3 illustrates the syngas composition (H_2, CO, CH_4, CO_2, C_2H_4, C_2H_6 and C_3H_6) obtained for all the considered parameters with the variation of solid feed rate, CO_2 gas flow rate and torch power in the plasma gasification process. C_xH_y signifies the light hydrocarbons (LHCs) comprising of C_2H_4, C_2H_6 and C_3H_6.

6.2.2.1. Influence of solid fuel (Bakelite) flow rate

This section discusses the impact of feed flow rate (Case 1-5) on the syngas composition and their corresponding LHV. As shown in Table 6.3, the feed rate is varied between 20-60 g/10 min, keeping a constant CO_2 gas flow rate of 0.5 lpm and torch power of 0.75 kW. It is observed that the increase in the solid feed up to 40 g/10 min (Case 3) increases the H_2 and CO content up to 21.01 vol.% and 38.65 vol.%, respectively, with an LHV of 9.68 MJ/m^3. With a further increase in the solid feed rate from 50 to 60 g/10 min, the concentration of hydrocarbons rises with a decrease in CO and H_2 in the syngas. This could be due to the low residence time

of solid feed in the plasma, where there is an inefficient cracking of hydrocarbons into CO and H_2. The maximum LHV (10.20 MJ/m^3) is observed for Case 5 i.e., at a higher feed rate of 60 g/10 min due to the higher content of CH_4 and LHCs in the syngas.

Table 6.3

Results of syngas compositions, LHV and product yield based on different parameters.

Case number	$\dot{m}_F$ (g/10 min)	Power (kW)	Gas flow (lpm)	Syngas composition (vol. %)					LHV (MJ/m^3)
				H_2	CO	CH_4	CO_2	C_xH_y	
1	20	0.75	0.5	17.89	31.97	3.12	22.50	1.04	7.87
2	30	0.75	0.5	18.29	35.17	3.43	19.66	1.51	8.78
3	40	0.75	0.5	21.01	38.65	3.57	15.58	1.65	9.68
4	50	0.75	0.5	18.44	33.64	5.22	18.24	2.44	9.95
5	60	0.75	0.5	16.91	30.58	6.09	21.24	3.06	10.20
6	40	0.75	0.4	18.50	34.53	3.88	19.59	1.73	9.10
7	40	0.75	0.6	23.64	40.82	3.01	12.40	0.89	9.46
8	40	0.75	0.7	16.62	30.50	2.75	24.09	0.63	7.11
9	40	0.75	0.8	14.27	27.10	2.40	28.90	0.45	6.16
10	40	0.5	0.5	15.62	28.77	2.52	31.43	0.55	6.58
11	40	1.12	0.5	22.10	40.27	3.11	9.53	1.54	9.74
12	40	1.6	0.5	24.36	43.61	2.72	7.71	1.14	9.98

C_xH_y includes C_2H_4, C_2H_6 and C_3H_6 compounds; LHV = lower heating value.

A higher content of CO (30-39 vol.%) for all the cases is observed either due to the gasification of fixed carbon (FC) by Boudouard reaction (R9) or by incomplete oxidation (R7) of carbon/fuel with free oxygen (O) producing via. CO_2 dissociation in the plasma gas. A syngas yield in the range of 77-85% (Fig. 6.3) is obtained in all the cases with 15-22% of residue (including FC and ash) and a minor proportion of liquid oil (0.2-0.8%). A higher amount of residue is obtained, although in plasma conditions and this could be due to the complex thermoset structure of bakelite. Thus, the feed rate increase is effective to a certain

degree (40 g/10 min), beyond which the CO and H_2 in syngas decreases. The LHV (10.20 MJ/m^3) of the syngas obtained in this work is higher by 0.3-4.2 MJ/m^3, compared to the CO_2-based plasma gasification of RDF, kitchen waste, etc. reported in the literature (Agon et al., 2016; Li et al., 2022; Wang et al., 2019). To find the optimum conditions, a more detailed assessment in terms of energy performance is required and discussed in Section 6.2.3. Moreover, the comparison between the properties of raw feed, liquid oil and residue is discussed in Section 6.2.5.

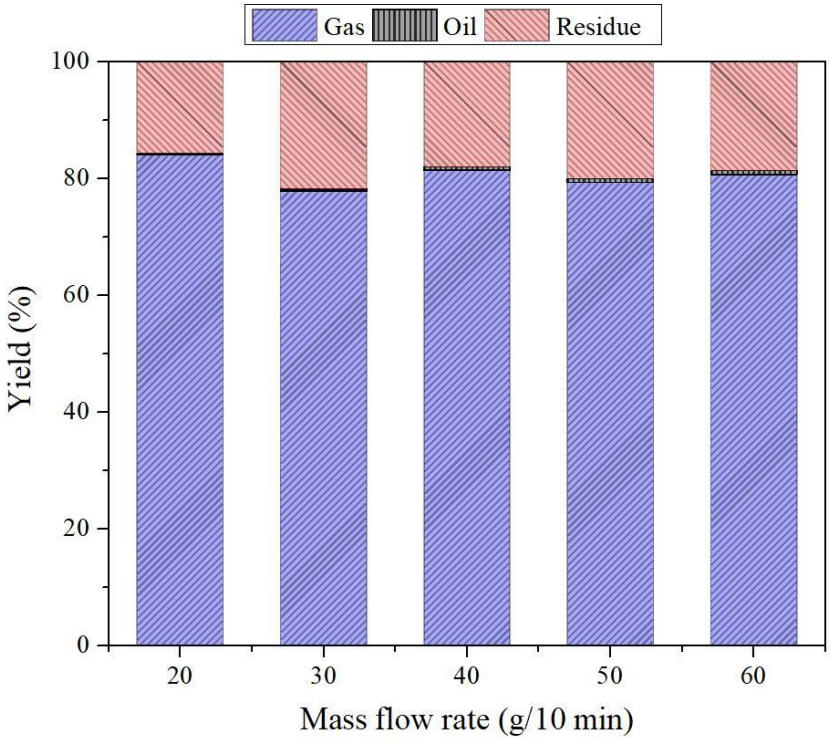

Fig. 6.3. Product yield distribution as a function of feed flow rate.

6.2.2.2. Influence of feed CO_2 flow rate

With an increase in the feed flow rate of CO_2 from 0.4 to 0.8 lpm and at 40g/10 min flow rate of bakelite particles with a torch power of 0.75 kW, the H_2 and CO content first increases, reaching its highest at 0.6 lpm (Case 7) and then decreases, as illustrated in Table 6.3. At this flow rate of bakelite (40g/10 min), the maximum volumetric percentage of H_2 and CO in the

syngas composition is 23.64 vol.% and 40.82 vol.%, respectively. A deficient (0.4 and 0.5 lpm) supply of the gasifying agent results in the decrease of gas yield by ~ 4%, as shown in Fig.6.4. While an increase in the flow rate of feed CO_2 gas (0.7 and 0.8 lpm) leads to a reduction in LHV of syngas from 9 to 6 MJ/kg, which could be due to the dilution of the excess CO_2 feed gas. As reported in the literature (Wang et al., 2019), the low residence time of feed decreases the degree of conversion with surplus feed CO_2. Another possible reason for the drop in H_2 and CO content at a higher CO_2 flow rate may be due to the progress of reverse water gas shift reaction leading to the production of steam (H_2O) and CO from the excess feed CO_2 (Agon et al., 2016). A similar trend is noticed while validating the model with the experimental values in Section 6.2.4. The highest LHV of syngas is achieved at 0.5 lpm of feed CO_2 due to the higher generation of light hydrocarbons in the syngas, as discussed in Section 6.2.2.1. Hence, the effect of the CO_2 flow rate becomes imperative when the solid carbon content in the fuel is relatively high.

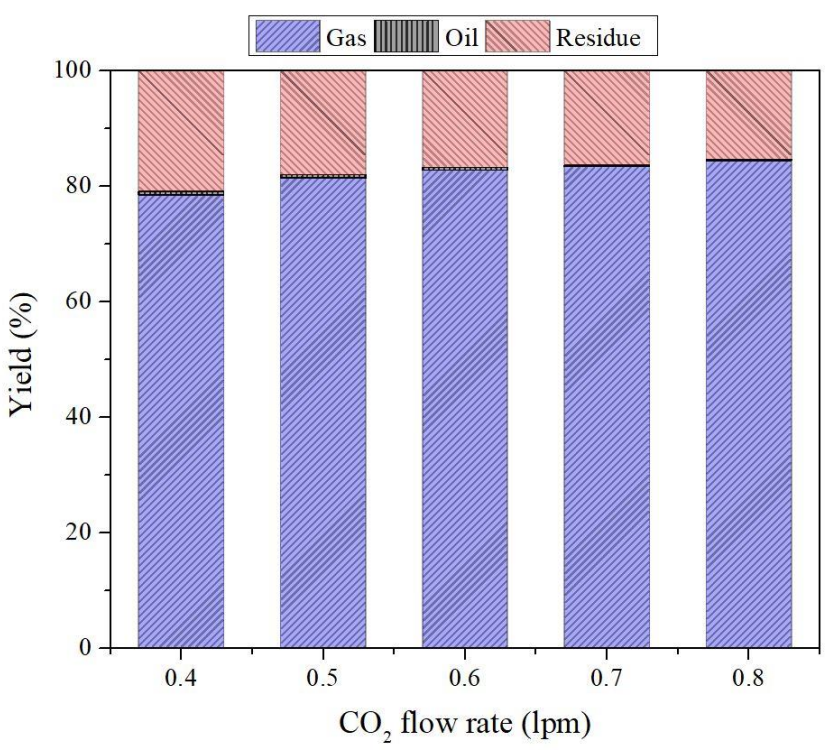

Fig. 6.4. Product yield distribution as a function of CO_2 gas flow rate.

6.2.2.3. Influence of torch power level

The torch power in the plasma gasification process is the most influential factor that impacts the feasibility of commercializing the technology. High energy density plasma gas is utilized effectively to increase the H_2 and CO content in the syngas. Plasma energy ratio (PER) is defined as the ratio of the input power of the plasma torch to that of the chemical energy of the solid feed (Li et al., 2022). Therefore, excess feed (low plasma power in this case) or excess plasma power than required for gasification can reduce the output energy i.e. quality of syngas. As summarized in Table 6.3, the torch power is varied between 0.5 to 1.6 kW for the constant fuel flow rate of 40g/10 min and CO_2 flow rate of 0.5 lpm. When the power is maintained as low as 0.5 kW (Case 10), the major part of the feedstock remains unutilized and gets deposited in the reactor. At such conditions, the gas yield reduces to 74.85%, which leads to an increase in the residue yield to 24.58%, as shown in Fig. 6.5.

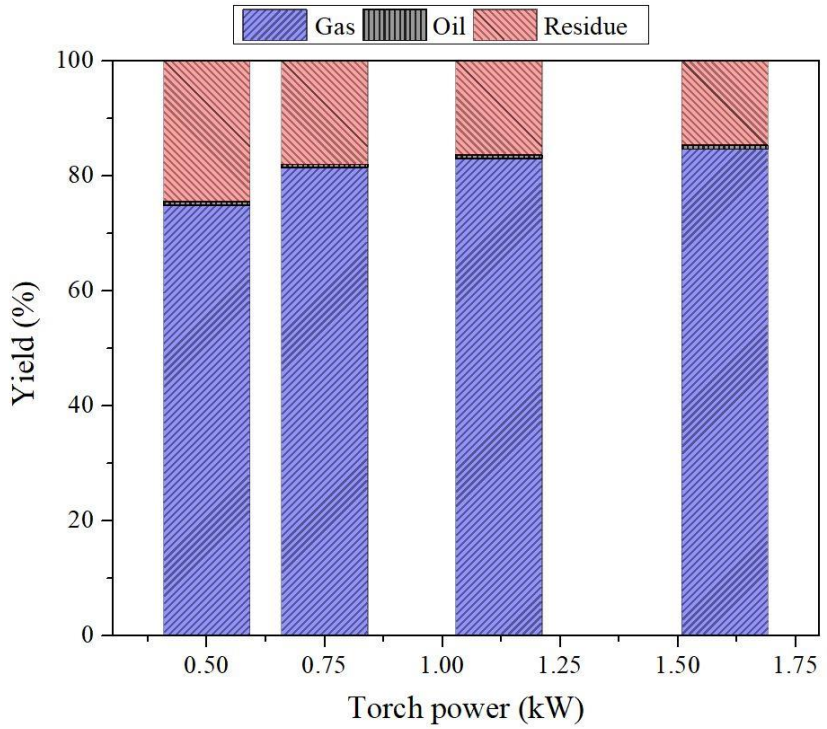

Fig. 6.5. Product yield distribution as a function of plasma torch power.

This also results in the decrease of H_2 (15.62 vol.%), CO (28.77 vol.%) and LHV (6.58 MJ/m^3) of the syngas because of the insufficient energy to exploit the volatiles and FC in the bakelite. With an increase in the torch power to 0.75 kW, 1.12 kW and 1.6 kW, H_2 and CO concentration in the syngas increases subsequently and the gas yield rises to a maximum of 84.58%. But beyond 0.75 kW (optimum torch power), there is no significant rise in average syngas yield and LHV despite the increase in H_2 and CO content. This indicates the excess supply of power beyond 0.75 kW, which may lead to a loss of energy. At high torch power (1.6 kW), the dissociation of nitrogen (escaped in the gas phase) from the bakelite feed might interact with H_2, forming NH radicals and further to NH_3. The dissolution of NH_3 from the syngas in DCM (obtained liquid oil) is confirmed by the GC-MS analysis (Section 6.2.5.4). The produced ammonia, at the first stage, can be adsorbed and recovered using a water wash arrangement or reactive absorber of metal halide salts, followed by the separation of nitrogen in a cryogenic rectification column (Kale et al., 2020; Linde, 2023).

6.2.3. 3-E (Energy, Exergy and Economic) analyses

6.2.3.1. Energy and exergy analysis

This section conducts a 2-E analysis (energy and exergy) for the operating parameters discussed in Section 6.1. It comprises the energy and exergy balance, including the respective efficiencies and losses involved in different components of the process.

A literature (Li et al., 2022) already studied the impact of low values of plasma energy ratio (0.08-0.53) in the gasification process. In the present study, the effect of higher PER (0.53-1.7) on the syngas composition is assessed. With an increase in the solid feed flow rate, the energy efficiency increases and reaches a maximum of 41.80% for 40g/10 min (Case 3) and then decreases despite their relatively higher LHV, as shown in Fig. 6.6(a). This describes the excess energy input to the system in terms of plasma torch power and, hence the drop-in efficiency. If

the specific energy of the feed is lower than the power of plasma, the efficiency decreases due to the loss of the excess energy. Correspondingly, a similar trend is observed while investigating the effect of CO_2 gas flow rate in Fig. 6.6(b). A slight improvement in the maximum energy efficiency (42.33%) is observed for 0.6 lpm (Case 7). On the other hand, the rise in LHV with the increase in torch power does not possibly indicate higher energy efficiency as seen in Fig. 6.6(c). Other plasma gasification studies (Li et al., 2022; Wang et al., 2019; Zhang et al., 2012) reported a similar profile of syngas quality and CGE trends concerning PER and CO_2 flow rate. The exergy efficiencies for all the experimental parameters show a negative deflection of around 3-6% as compared to CGE. This difference is due to the irreversibilities caused by a hot plasma environment. It allows to approach the exergy losses in terms of entropy generation, energy usage and environment (Jain et al., 2023). The exergy loss can be abated by modifying the operating parameters, selecting higher calorific value fuels, etc. In the case of bakelite based feed, optimal PER (minimal torch power and moderate feed rate) is essential to control exergy loss.

The energy and exergy efficiency of the overall process can be increased by utilizing the residual energy in the various streams of the process. By recovering sensible heat of syngas at the reactor outlet, the thermal energy of water used for cooling the plasma torch, the chemical energy of the oil and the solid residue produced. These residual components consist of nearly 42-44% of energy/exergy; the rest (~15-20%) could be radiative losses to the environment. The losses in cooling water has the maximum share of around 25-30%, followed by the chemical energy of residue solid of 6-13% and sensible heat of 5-8% of the syngas. In commercial or industrial scale processes of plasma, the residual energies can be recovered and economically reutilized in the plant and this can significantly reduce the overall energy costs. The thermal energy of hot water from plasma cooling process can be used for domestic purposes and combined heat and power generation (CHP) (Agon et al., 2016; Peng et al., 2021).

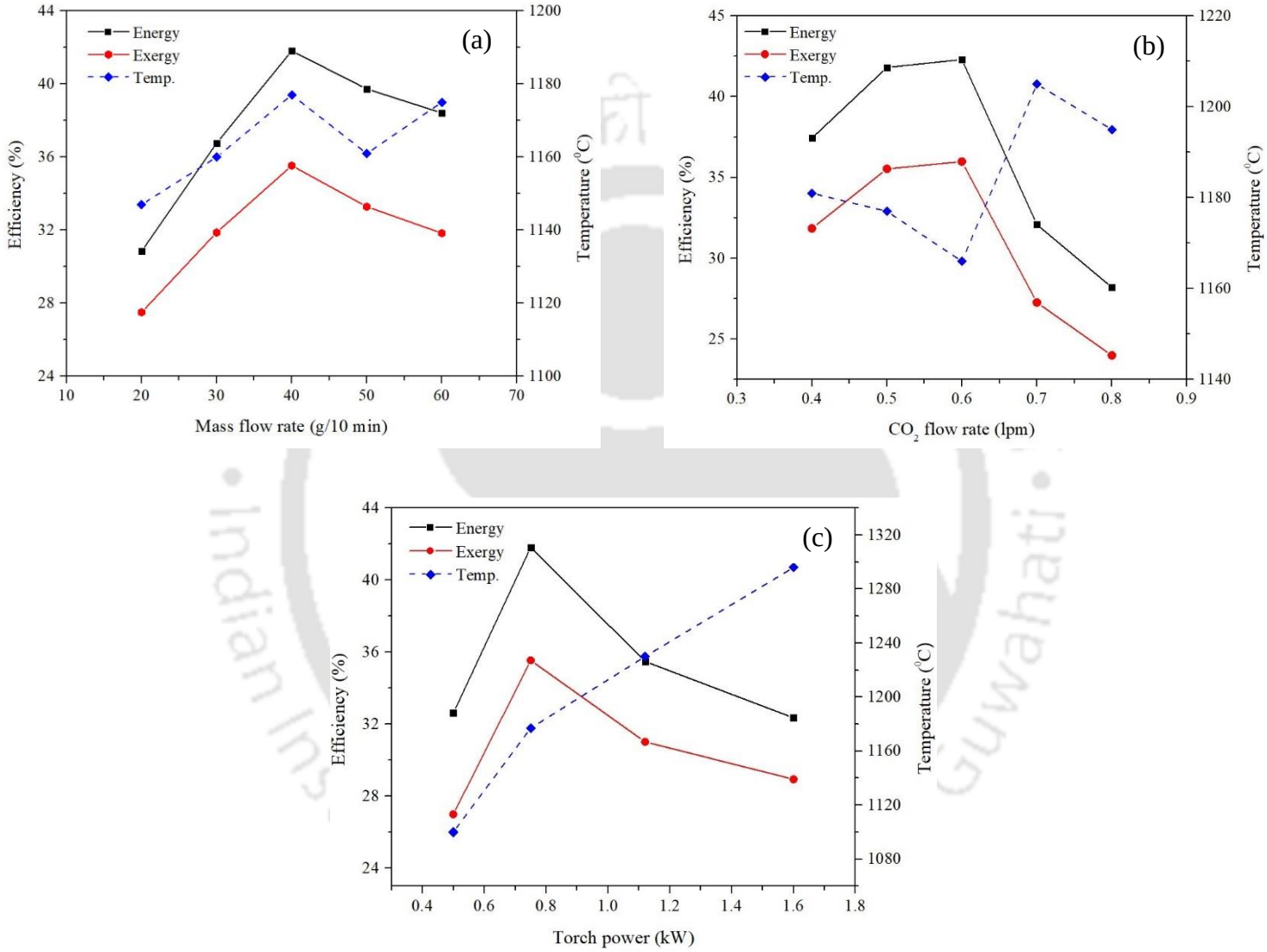

Fig. 6.6. Energy and exergy efficiencies as a function of (a) feed flow rate (b) CO_2 gas flow rate and (c) torch power.

6.2.3.2. Economic analysis

In this section, the levelized cost of syngas (LCOS) based on the total capital cost of the plasma gasifier and its operation and maintenance cost are estimated based on the Indian scenario. The assumptions considering the rate of interest, utilization and payback period are followed as per Section 3.5.1.3 and the operating parameters are given in Table 6.1. The LCOS for all the cases (Table 6.4) is found in between 40 and 63 INR/kWh. It is clearly evident that the syngas cost is highly dependent on the energy output, therefore, the lowest value of 40.91 INR/kWh is achieved for 40 g/10 min, CO_2 flow of 0.6 lpm and torch power of 0.75 kW (Case 7). From the energy analysis, the maximum cold gas efficiency (η_{CGE}) is obtained for the above stated operating conditions. However, the LCOS values are higher than the reported literature (8.5-32.3 INR/kWh) using bio-medical waste (Paulino et al., 2020). Also, it is higher than the LCOS estimated using RDF (Table 4.5) and CKPW (Table 5.5). This is due to the lower calorific value of bakelite-based feedstock with a decrease in the overall energy output. The highest LCOS of 62.44 INR/kWh is observed for a low plasma power of 0.5 kW (Case 10). This is ascribed to the lower feed conversion and gas yield (74.85%) and, therefore, low energy output. Hence, the optimum conditions need to be maintained to negate the energy-intensive consequences of the plasma gasification process.

6.2.4. Model development and validation

A model is developed using Aspen Plus software to predict the composition of the product gas of the plasma gasification process. Fig. 4.5 represents the flowsheet of the plasma gasification process. The syngas composition (stream G5) estimated from the simulation is compared with the results obtained in the experiment, as illustrated in Table 6.5. The simulation has shown a higher percentage of H_2 (24.80 vol.%) and CO (45.63 vol.%) than the experimental results with an error percentage estimated in the range of 3-12%. This is due to the equilibrium

Table 6.4

Results of the syngas production cost for the considered experimental conditions.

Case number	C_{system} (INR)	$OC_{var,gp}$ (INR/kWh)	MC_{gp} (INR/kWh)	C_{capex} (INR)	C_{opex} (INR)	C_{total} (INR/kWh)	LCOS (INR/kWh)
1	109477.5	7.65	0.92	27000	1002.29	1.59	40.94
2	164216.25	5.60	1.01	27000	1002.29	1.16	41.53
3	218955	4.36	1.05	27000	1002.29	0.90	41.39
4	273694.75	4.12	1.24	27000	1002.29	0.85	47.65
5	328432.5	3.87	1.40	27000	1002.29	0.80	52.71
6	218955	4.87	1.18	27000	1001.83	1.01	46.22
7	218955	4.31	1.04	27000	1002.74	0.89	40.91
8	218955	5.68	1.37	27000	1003.20	1.18	53.93
9	218955	6.47	1.56	27000	1003.66	1.34	61.37
10	218955	4.55	1.65	27000	1002.29	1.41	62.44
11	218955	6.22	1.01	27000	1002.29	0.86	41.60
12	218955	8.42	0.95	27000	1002.29	0.82	41.94

C_{system} = Plasma gasification unit cost; $OC_{var,gp}$ = Variable operating cost of plasma gasifier; MC_{gp} = Maintenance cost of plasma gasifier;

C_{capex} = Capital cost of gasifying agent; C_{opex} = Operating cost of gasifying agent and C_{total} = Net cost of gasifying agent

approach of simulation with the complete conversion of ESW into syngas. As a result, methane (CH_4) and other hydrocarbons are dissociated into syngas and a low percentage of methane (2.67 vol. %) is obtained in the product gas. The other gases such as N_2, H_2S and NH_3 are not detected under experimental conditions due to insufficient measuring apparatus. However, the analysis of the liquid oil below anticipated such presence.

Table 6.5

Model validation of plasma gasification process with the ESW experimental values (Case 7).

	Simulation	Experimental work	Error (%)
Feed rate (g/10 min)	40	40	
CO_2 flow rate (lpm)	0.6	0.6	
Torch power (kW)	0.75	0.75	
H_2	24.80	23.64	4.90
CO	45.63	40.82	11.78
CH_4	2.74	3.01	8.97
H_2O	8.19	-	-
CO_2	11.96	12.40	3.54
C_xH_y	-	0.89	-
N_2	6.15	-	-
H_2S	0.20	-	-
NH_3	0.33	-	-
Syngas temperature (°C)	1203	1166	3.07
LHV (MJ/m^3)	9.47	9.46	0.10
Energy efficiency (η_{CGE}, %)	42.34	42.33	0.02

6.2.5. Characterization of raw feed, liquid oil and residue, and their analogy

The variation in the syngas composition with time is shown in Fig. 6.7. The introduction of feed at different intervals does not cause a significant change in the constituent gases. The syngas yield is 82.75% and the rest is obtained as a liquid oil (0.48%) and residual solid (16.78%). The obtained products are characterized for in-depth investigation.

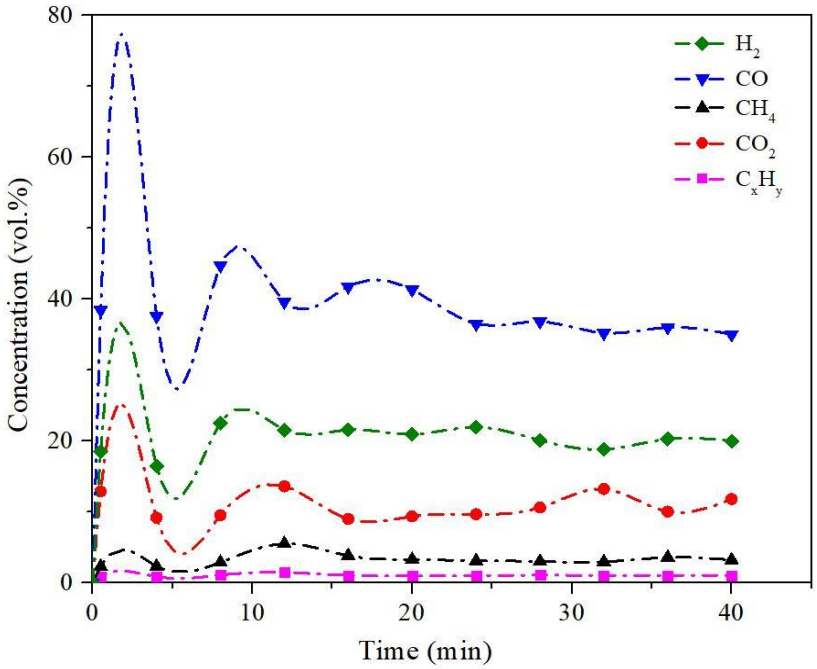

Fig. 6.7. Change in syngas composition as a function of time.

6.2.5.1. Physicochemical properties

Fig. 6.8 displays the images of the liquid oil and residue collected after the plasma gasification. Their respective proximate and ultimate analyses are provided in Table 6.6. The high nitrogen content (19.87 wt.%) in ESW feed can be due to the presence of polyamide, which may contain melamine as a fire-retardant substance. Under thermal treatment, these nitrogen sources convert into N_2, NH_3, etc., in the gas phase or other condensable gases in the liquid oil. The rest of N_2 is retained in the residual solid. In the case of liquid oil, the hydrocarbons i.e., H and C content comprise ~75 wt.%, followed by oxygen (13.39 wt.%) and nitrogen (11.11 wt.%). Oxygen in liquid oil exists in various forms, including aldehydes, phenolic compounds, ketones, etc. In the composition of solid residue shown in Table 6.6, the fixed carbon and ash content share nearly a 3:1 ratio by mass. The presence of N, H and some fractions of C and O in the solid residue is due to the volatile matter, which may be condensed on the residue surface (Li et al., 2022). The distribution of these elements mainly depends on the process factors (residence time, temperature, etc.) (Czernik and Bridgwater, 2004).

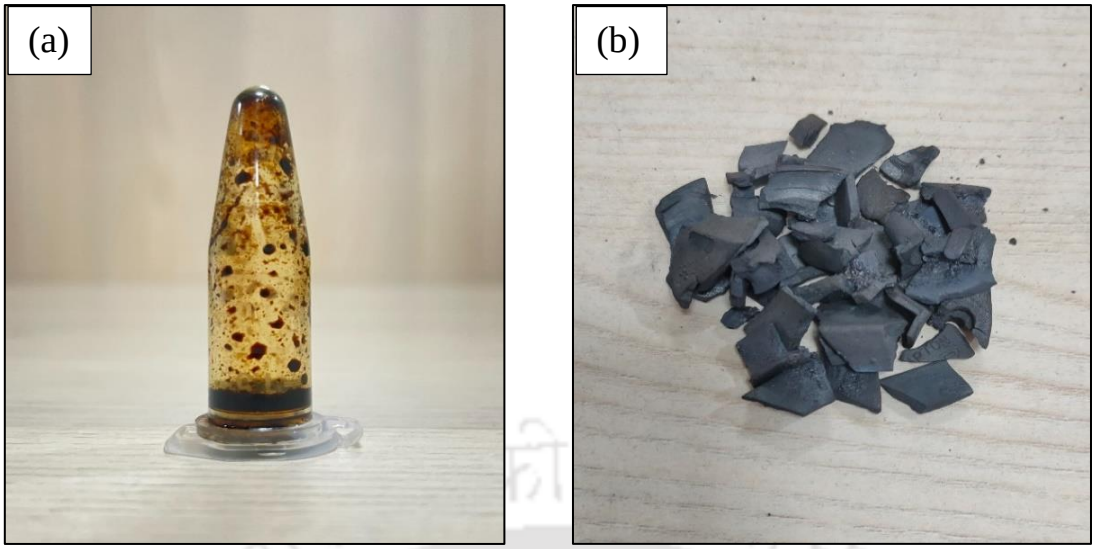

Fig. 6.8. Images of (a) oil and (b) residue obtained after plasma gasification.

Table 6.6

Proximate and ultimate analysis of raw ESW, oil and residue obtained.

	Raw ESW	Oil	Residue
Proximate analysis [wt.%, as received basis]			
Moisture	1.54	-	-
Volatile matter	77.46	-	11
Fixed Carbon	17	-	65.67
Ash	4	-	23.33
Ultimate analysis [wt.%, ash free basis]			
C	31.53	68.08	41.73
H	5.28	7.42	1.15
N	19.87	11.11	8.1
S	0.73	-	2.66
O[a]	38.59	13.39	46.36
LHV based on energy [MJ/kg]	14.05	31.47	15.51

[a] by difference.

Despite the higher content of non-combustible fractions in the fuel, the liquid oil has a higher calorific value of 31.47 MJ/kg, while the residue has 15.51 MJ/kg. The obtained solid residue can be effectively utilized after removing the ash by float-sink separation, froth floatation and oil agglomeration methods. The remaining char residue can be used as a catalyst for tar reforming, adsorbents, etc. (Hwang et al., 2008; Ravenni et al., 2020).

6.2.5.2. FTIR analysis

The functional groups in the ESW feed are compared with the products obtained in the liquid oil and residue for different cases in Fig. 6.9. The presence of bakelite and polyamides in the ESW feed is reported in the literature (Dhunna et al., 2014; Jung et al., 2018). Phenol identified at 3337 cm^{-1} in the bakelite feed completely gets into the oil product as there is no OH group found in the solid residue. Because of low water absorption features, phenolics offer good electrical insulating properties (Rodríguez-Reinoso, 2001). The C-H stretch in the range of 2750-3000 cm^{-1} indicates the presence of alkane or weak aldehydes. Under low torch power (Case 10), the concentration of alkanes in oil decreases and that of phenols in residue increases. It is attributed to the insufficient supply of energy required to break the stable methylene bridges in the phenolics (Bouajila et al., 2003). The peaks intensified between 1261-1455 cm^{-1} in the liquid oil are due to the thermal cracking of CH_2 from polyamides phenol or formaldehyde. The strong bands at 1640-1740 cm^{-1} in the oil are associated with the presence of C=O stretch from carbonyl compounds (carboxylic acids, ketones, esters and aldehydes). In this range, the lower wavenumber from 1640 to 1700 cm^{-1} showed the presence of unsaturated ketones and amide groups. The residue contains mostly C=O and C-N stretch in the range of 1416-1577 cm^{-1} and the C-O stretch and O-H bend at 610-1081 cm^{-1} are due to polyamides and bakelite, respectively. The single bond amine group in the feed converts into a double bond (C=N stretch) nitrile group in the stretch of 2250 cm^{-1} and at low torch power, the intensity of this group increases due to strong bond energy (615 kJ/mol) between the sigma and pi bond

(Y. Du et al., 2023). Moreover, the higher N-H bend (1269 cm^{-1}) in the melamine compound is not distinguished clearly in the residue but in oil. Thus, the formation of primary and secondary amine or amide group compounds involving N-H bend escaped with the syngas before condensing in the oil. This result is validated by the study on the influence of torch power on syngas yield in Section 6.2.2.3 and the GC-MS analysis below.

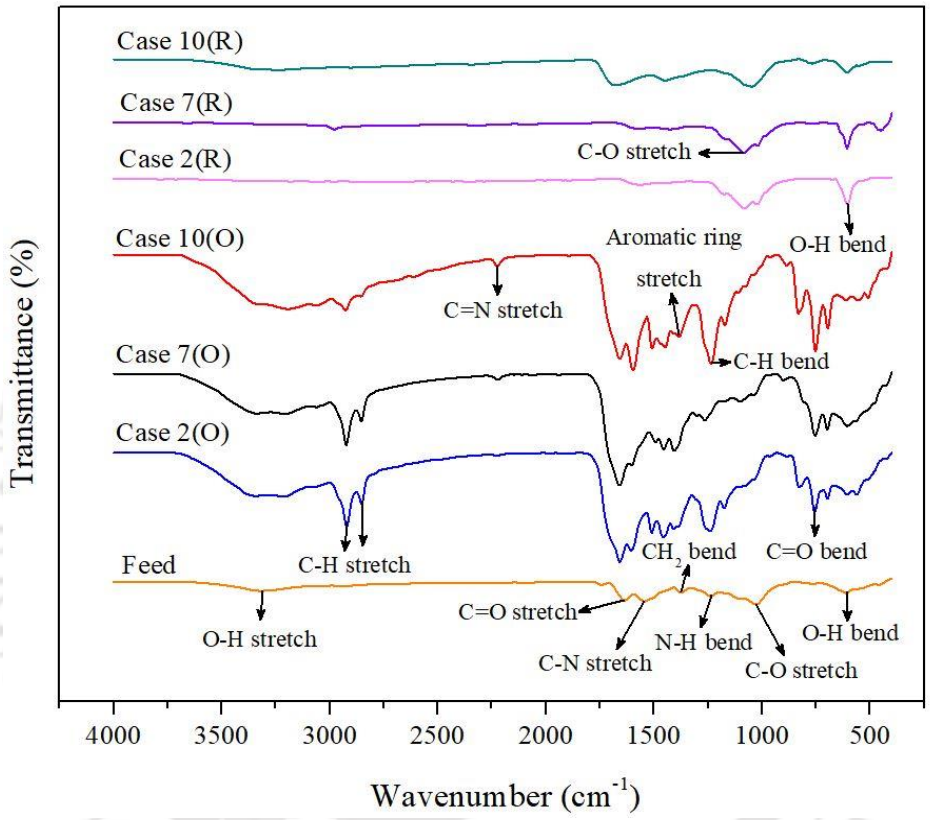

Fig. 6.9. FTIR plot of raw feed, oil (O) and residue (R) obtained for different cases.

6.2.5.3. FESEM analysis

Fig. 6.10 shows the FESEM images of the ESW before and after CO_2 plasma gasification. The thermosetting behavior of phenolic resin (bakelite), such as high thermal stability, low mechanical strength and durability, is evident from the topographical structure and cracks captured in FESEM images (Li et al., 2010). In conventional gasification conditions, the presence of polyamides reduces the number of internal openings (voids) and as a consequence,

these thermosetting plastics undergo inefficient cracking and gasification (Wang et al., 2015). However, under a plasma environment, non-uniform and in-depth pores are created, as shown in Fig. 6.10(b). Even after the plasma heat treatment, the structure has prominent smooth surfaces that indicate the transformation into an intermediate deformed stage. This can be attributed to three possible reasons: (i) the intricate process of polymerization, (ii) a decrease in void formation leading to low pore diffusion of CO_2 gas due to the presence of nitrogen-based substance and (iii) large particles allow the gasification to occur on the surface due to the condensation and absorption of volatiles (Li et al., 2022).

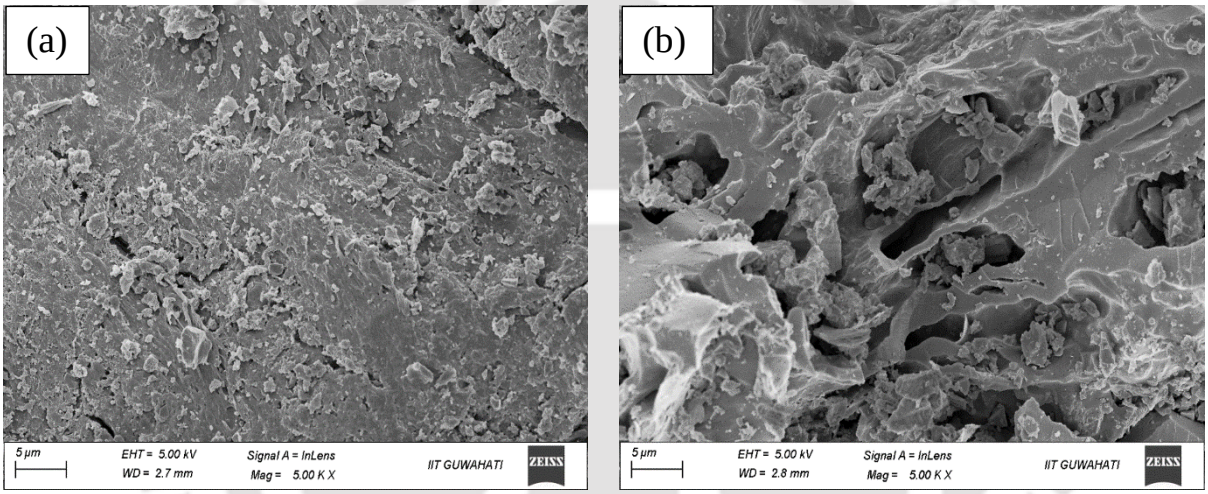

Fig. 6.10. FESEM image of (a) ESW feed and (b) after CO_2 plasma gasification.

6.2.5.4. Viscosity, pH and GC-MS analysis of oil

The oil obtained in the process is characterized to understand its suitability for various applications. The viscosity, density, pH and LHV (for Case 7) of the oil are found to be 6.43 cP (centipoise), 975 kg/m^3, 8.01 and 31.47 MJ/kg (Table 6.6), respectively. In comparison to diesel fuel, the viscosity, pH and density of the obtained oil are on the higher side, whereas the calorific value is lower. This could be due to the higher nitrogen and oxygen content of the oil. Hence, further upgradation of the oil properties is essential to avoid carbon deposition and soot formation in their application to vehicles (Ahmad et al., 2020). Moreover, the obtained oil

could be better used as a waste-derived oil in boilers, gas turbines, diesel engines for CHP, Stirling engines and for producing chemicals (Czernik and Bridgwater, 2004).

Table 6.7 illustrates the major compounds in the obtained oil determined through GC-MS analysis. For Case 7, the highest percentage is shared by a phenethylamine alkaloid compound named ephedrine, which is also commonly used as a drug to treat hypertension. It is followed by heteroaromatic and polyunsaturated compounds, typically benzene derivatives and carboxylic acids. While porphyrin i.e., aromatic macrocyclic structure, has pyrrole subunits coupled with methylene bridges and, hybridized iso-alkanes are found for Cases 2 and 10. The cyclization of polyolefins and nitrogen results in the formation of pyrrolidines. Cyclooctatetraene (an unsaturated derivative of cyclooctane) and alpha-methyl styrene present in the oil belong to the benzene group of compounds, while heptadiene-3-yne is a long-chain alkyne. Although these complexes (C_6-C_9) are weakly desirable but are preferred compared to the polycyclic aromatic hydrocarbons (PAHs) class of organic compounds.

Morpholine, an organic saturated heterocyclic compound, has both amine and ether groups, possessing high volatility and anti-corrosion properties. This compound would decompose slowly at high temperatures in the absence of oxygen. Thus, the experiments conducted at a low torch power of 0.5 kW (Case 10) produced a higher percentage of morpholine. The other most abundant compounds in the oil are the alkenes, with the rest as the small fractions of alkanes, aldehydes and ketones. These result from higher nitrogen and oxygen content in ephedrine and carbonyl compounds (carboxylic acids and ketones) (Ahmad et al., 2020). On the other hand, pyridines are synthesized from nitrile, ammonia and aldehyde. A small amount of organic acids (oleic and erucic acid) is also found in the oil. Due to the lower content of saturated hydrocarbons in the fuel and further due to plasma reactive atmosphere, PAHs like anthracene and naphthalene are not obtained in the liquid oil.

Table 6.7

GC-MS analysis of oil obtained for different cases of ESW experiments.

Case 2			Case 7			Case 10		
Retention time	Compounds	Area (%)	Retention time	Compounds	Area (%)	Retention time	Compounds	Area (%)
7.39	3,3-Dimethylheptadecane	22.65	7.02	3-Methyl-2-(2-oxopropyl) furan	3.5	7.39	3,3-Dimethylheptadecane	21.8
7.7	Pyrrolidine,1-methyl-3,2`-spiro-benzo-1,3-dioxolane	6.64	7.81	Ephedrine	7.96	7.7	Pyrrolidine,1-methyl-3,2`-spiro-benzo-1,3-dioxolane	5.88
7.73	6-Hepten-3-one,5-hydroxy-4-methyl-	15.47	8.2	1,6-Heptadien-3-yne	2.93	7.73	6-Hepten-3-one,5-hydroxy-4-methyl-	15.8
8.02	Hexane,2,2,5,5-tetramethyl	5.33	10.61	1,3,5,7-Cyclooctatetraene	5.72	8.02	Hexane,2,2,5,5-tetramethyl	10.5
8.08	Morpholine	4.99	12.24	Alpha-methyl styrene	2.66	8.08	Morpholine	14.4
8.11	3-Pentanone, O-methyl oxime	8.74	12.61	Bicyclo [2.2.1]-2,5-heptadiene-2,3-dicarboxylic acid	3.6	8.18	But-2-en-1-yl 2-methylbutanoate	4.21
8.18	But-2-en-1-yl 2-methylbutanoate	2.88	14.35	Benzyl alcohol	1.42	8.84	1H-1,2,4-triazole-3-carboxaldehyde,5-methyl-	24.7
8.84	1H-1,2,4-triazole-3-carboxaldehyde,5-methyl-	25.87	16.17	1,2,3,4-Tetramethylcyclohexane	1.44	9.65	Pyridine-d5-	1.6
9.65	Pyridine-d5-	1.78	16.65	1H-Indene,1-methylene or Azulene	0.9			

		17.41	Bicyclo [3.1.0] hex-3-En-2-One,5-(1-methylethyl)-	0.98	
		18.24	4-Undecene, 6-methyl-	0.38	
		19.07	2-Allylphenol	1.05	
		20.59	Biphenyl	0.54	
		23.29	1-(4-Methylphenyl)-6-nitro-1,2,3-benzotriazole	0.69	
		25.58	Benzene,1,1`-(1,3-propanediyl) bis-	0.76	
		26.68	Cyclopropylphenylmethane	1.42	
		26.93	5,7-Dodecadyne-1,12-diol	0.91	
		28.12	9H-Fluorene,9-methylene	1.2	
		29.10	Z, Z-6,28-Heptatriaactontadien-2-one	1.35	
		30.83	Oleic acid	1.15	
		31.96	Erucic acid	1.87	
Total	94.35	Total		42.43	Total 98.9

6.2.6. Reaction mechanism

The plasma gasification of ESW is a complex process because of the following reasons: (i) the mixture of polymers, (ii) the thermosetting behavior of bakelite and (iii) the dissociation of CO_2 under plasma medium to generate different reactive species and their interactions. However, based on the various analyses conducted in this study, a reaction mechanism of the plasma gasification of ESW feed is proposed and summarized in Fig. 6.11. In the first step, the thermal degradation of the fuel occurs and releases the volatiles. As the ESW polymer is a complex and crosslinked structure, the gradual rise in the temperature is not sufficient to break the arrangement bonded with methylene groups formed from the splitting of dimethylene-ether bridges (Bouajila et al., 2003). Hence, the decomposition of phenolic substances requires instantaneous heating and a reactive atmosphere such as plasma for efficient release of volatile species. At higher temperatures, the mixture of bakelite and polyamide degrades into phenol, formaldehyde, CO_2, etc. and forms oligomers (Holland and Hay, 2000; Puglia et al., 2001). In the intermediate stages, the liquid oil exhibited several aromatic and aliphatic compounds, signifying the aromatization of the cyclic oligomers. These compounds are produced from methoxy groups through the rupture of ether bonds. The formation of diphenyl and ketones via condensation reaction liberates simpler compounds of H_2, CO, CH_4 and LHCs (Cao et al., 2020). The cracking of bonds generates molecules with new chain ends. These are identified in the GC-MS analysis of the liquid products (Table 6.7) mostly in the form of benzene derivatives, carbonyls and a small amount of organic acids. The higher yield of syngas clearly shows the conversion of PAHs into LHCs, such as C_1-C_3 olefins. On the other side, the effect of electrons and radical species (O) during CO_2 dissociation on the cyclic aromatic components promotes more gaseous products comprising H_2, CO and straight-chain hydrocarbons (LHCs) (Saleem et al., 2019; Zhang and Harvey, 2021). The carbonization (formation of residual solid) process progresses through four different stages of depolymerization, merging, flattening

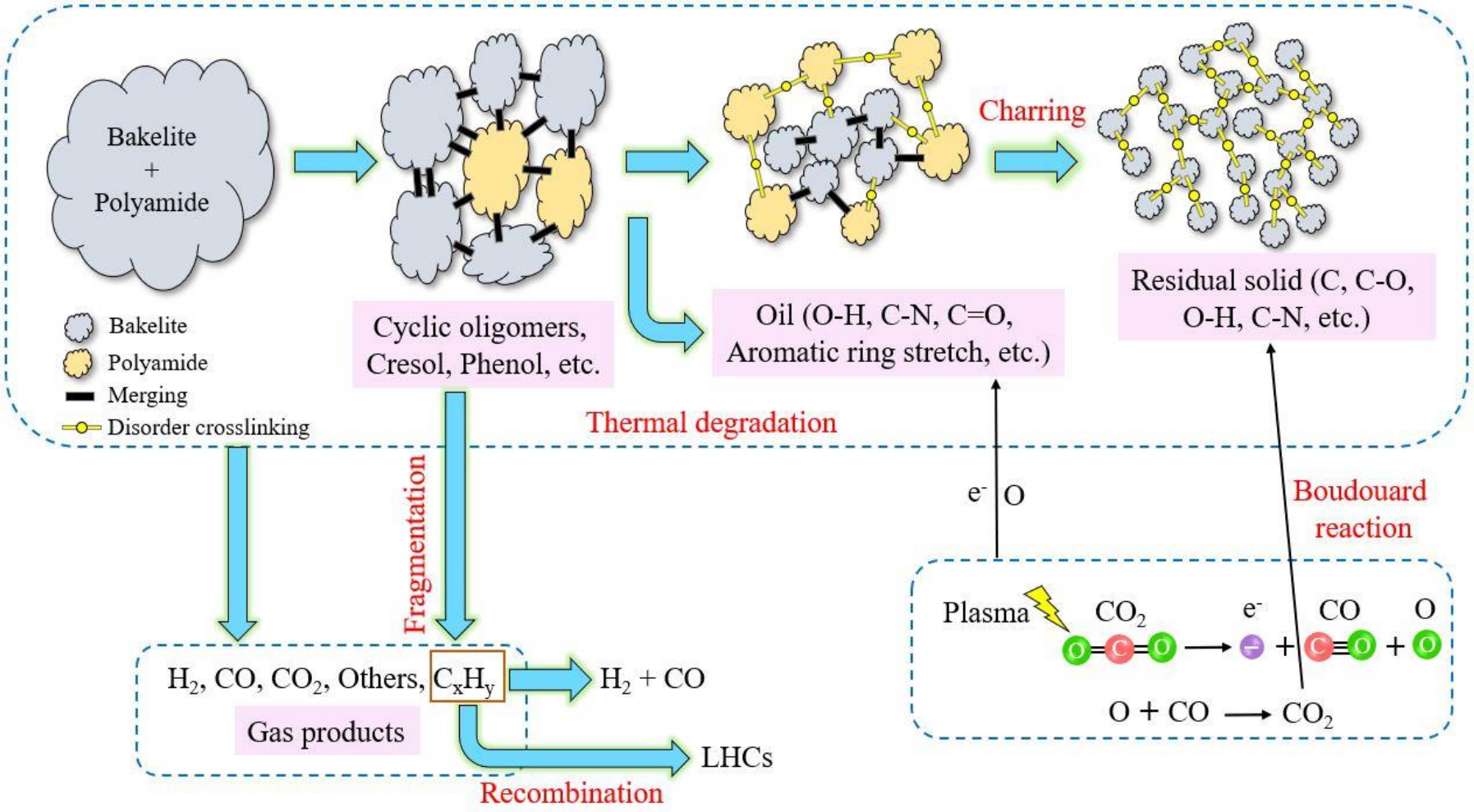

Fig. 6.11. Reaction mechanism of ESW in a plasma gasification process under CO_2 atmosphere.

and charring reactions (Y. Du et al., 2023). The high residual yield is mainly ascribed to the phenyl-associated compounds with barium, silicon, etc., formed during the charring reaction. This can hinder the thermal decomposition of ESW by blocking the release of phenolic hydroxyl groups. Further, the inorganic compounds after gasification may deposit on the residue surface and make it less porous (Wang et al., 2015). Thus, even after these drawbacks in the gasification of ESW, the application of the high-temperature plasma can enhance the overall syngas production with lower oil yield.

6.2.7. Quantitative relationship between experimental parameters and obtained results

Table 6.8 presents the constants obtained as per the developed correlation based on the independent variables such as feed mass flow rate (g/min), CO_2 flow rate (lpm) and torch power (kW). These values are assigned to the individual dependent variables, as discussed in Section 3.5.2. SPSS software is used to fit the polynomial model with an R^2 of ~ 0.92. To understand the reliability of the values, the parity plot in Fig. 6.12 is shown for comparing the experimental and correlated results. The syngas compositions obtained from the experiments are fitted alongside the measured values to determine the constants, considering the individual operating conditions. In the view of providing a rapid estimation of the performance of the plasma gasifier, the correlations are developed.

6.2.7.1. Experimental validation

In addition to the reported experiments in Table 6.1, an additional three experiments are carried out for validation of the proposed correlation. The experimental results obtained for such operating conditions are shown in Table 6.9, comprising the syngas compositions, LHV and CGE. Accordingly, the values are incorporated into the quantitative relationship obtained in Eq. (20) to match the measured values. Table 6.10 presents the desired values from the correlation combined with the error percentage (%). For the given set of parameters, the

operating parameters values such as 40g/10 min, 0.5 lpm and 0.75 kW are employed most number of times. Thus, the developed relationship is strongly dependent on the three independent variables. A maximum error of 14.21% suggests that the established relationship is favorable for estimating the plasma gasification results utilizing ESW. It is to note that the proposed relationship is valid only for the given set of parameters in Table 6.1.

Table 6.8

Empirical constants required to predict the correlated values.

	H_2	CO	CH_4	CO_2	C_xH_y	LHV	η_{CGE}
β_0	-82481.00	235460.87	5067.08	110590.78	142500.02	-6704.93	-243884.16
β_1	-6756.14	567.00	4209.61	-7809.04	-428.21	5092.32	8440.12
β_2	275508.6	-75715.57	-135740.72	98193.71	-201842.31	-171867.3	42550.37
β_3	457202.24	-873528.56	-153417.08	35216.59	-232978.10	-122741.4	236620.59
β_4	-0.008	-0.014	0.003	0.012	0.002	0	-0.011
β_5	-9.19	-18.44	-3.195	36.51	-3.028	-6.725	-22.261
β_6	-113.25	-161.76	1.483	188.74	1.228	-30.51	-154.80
β_7	4869.92	-6711.06	-2388.11	4271.88	867.09	2269.37	4186.9
β_8	6208.57	8934.79	-4837.4	9208.19	-444.38	-6780.44	-10597.77
β_9	-940558.21	688417.22	462543.49	-538329.64	334330.84	525317.4	249937.49

Table 6.9

Results of syngas compositions with LHV and CGE for validated experiments.

$\dot{m}_F$ (g/10 min)	Power (kW)	Gas flow (lpm)	Validated syngas composition (vol. %)					LHV (MJ/m^3)	η_{CGE} (%)
			H_2	CO	CH_4	CO_2	C_xH_y		
40	0.75	0.55	22.24	38.47	3.18	14.56	1.45	9.49	42.09
45	0.75	0.5	19.41	35.22	4.09	17.11	2.12	9.64	40.53
40	1	0.5	21.30	38.98	3.18	9.78	1.71	9.65	37.69

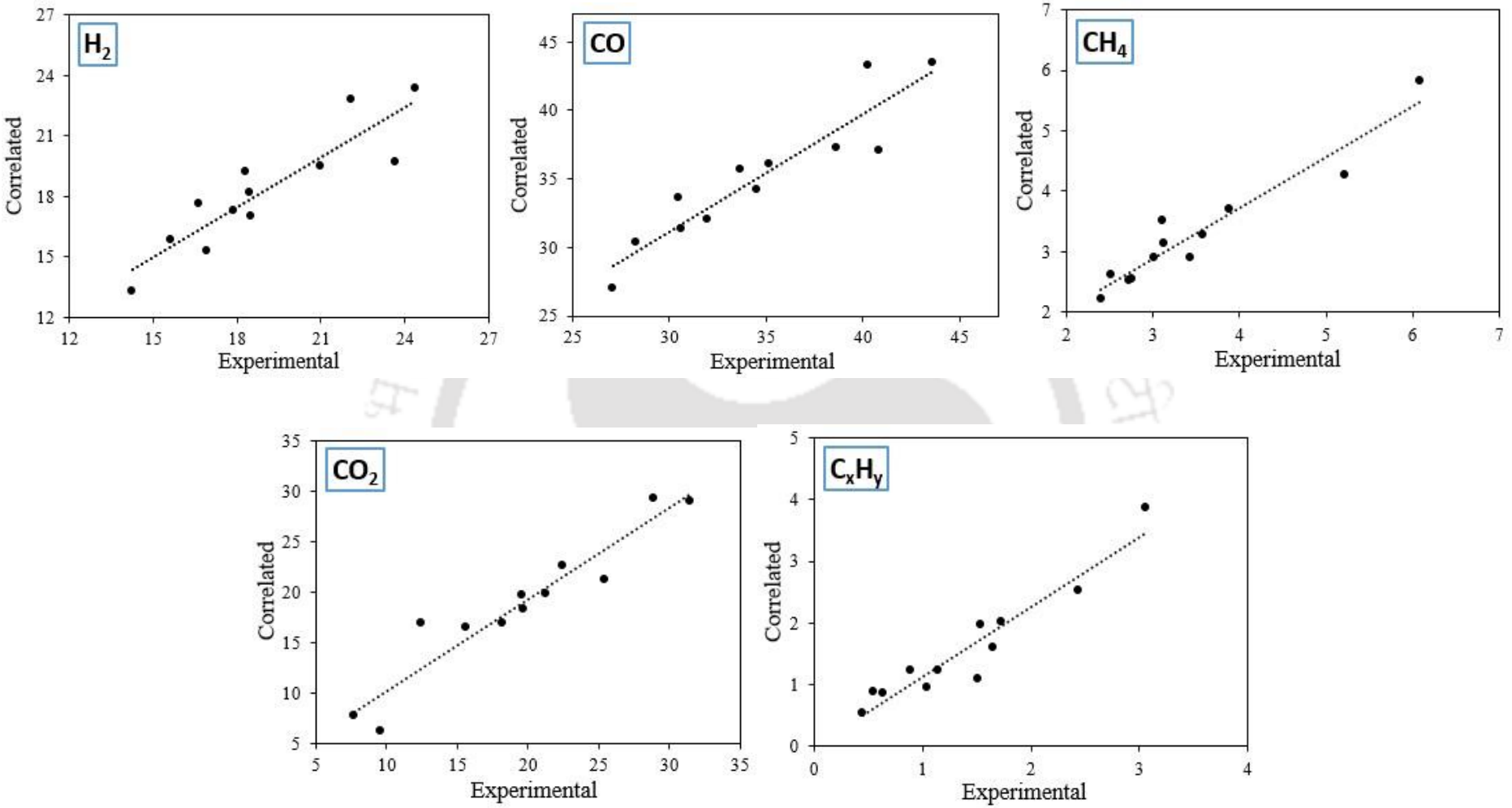

Fig. 6.12. Parity plot between actual and measured values for syngas compositions.

Table 6.10

Comparison of syngas compositions, LHV and CGE between the validated experiments and correlated results.

$\dot{m}_F$ (g/10 min)	Power (kW)	Gas flow (lpm)	Correlated syngas composition (vol. %)					LHV (MJ/m^3)	η_{CGE} (%)	Error (%) between the validated and correlated results						
			H_2	CO	CH_4	CO_2	C_xH_y			H_2	CO	CH_4	CO_2	C_xH_y	LHV	η_{CGE}
40	0.75	0.55	19.89	37.61	3.09	14.56	1.42	9.36	39.14	-10.57	-2.25	-2.92	11.47	-2.27	-1.33	-7.02
45	0.75	0.5	19.05	36.87	3.69	17.11	2.02	9.89	39.74	-1.87	4.67	-9.66	-4.10	-4.48	2.56	-1.94
40	1	0.5	22.02	41.89	3.54	9.78	1.95	10.69	40.15	3.38	7.47	11.34	-13.85	14.21	10.75	6.53

6.3. Conclusions

From the investigation of plasma gasification utilizing ESW, a complex e-waste, under the CO_2 atmosphere, the following conclusions can be drawn:

- The plasma gasification of ESW showed a maximum gas yield of nearly 85% and a lower oil yield (0.21- 0.75%) with a significant solid yield of 14.75-24.58%.
- The feed rate of 40 g/10 min, CO_2 flow rate of 0.5 lpm and power level of 1.6 kW i.e., Case 12 had the best performance in terms of higher H_2 (24.36 vol.%) and CO (43.61 vol.%) content. A medium LHV of 6.16-10.20 MJ/m^3 is found for all cases.
- Case 7 (feed rate of 40g/10 min, CO_2 flow rate of 0.6 lpm and torch power of 0.75 kW) experiment has shown the highest energy (42.33 %) and exergy (35.99 %) efficiency and therefore, considered as the optimum operating conditions. Similarly, the LCOS value of 40.79 INR/kWh is the lowest for Case 7.
- The oil product obtained has a higher LHV (31.47 MJ/kg), but its properties, such as viscosity (6.43 cP), density (975 kg/m^3) and pH (8.01) need to be improved for its applications as fuel for combustion or transportation. In the residue, Ba (70 wt.%), the most abundant element and low proportions of Ti, Zn, etc., can be recovered for applications in die-casting, alloys and paints.
- The established correlation presented a concurrence among the actual and measured values with a maximum error of 14.21%.

Thus, the experimental study on high-temperature CO_2 plasma gasification and the corresponding 3-E analyses inferred that treating electrical switch waste can be a feasible and economical route for waste-to-energy conversion.

Chapter 7

Simulation studies on plasma gasification integrated molten carbonate fuel cell and chemical looping reforming

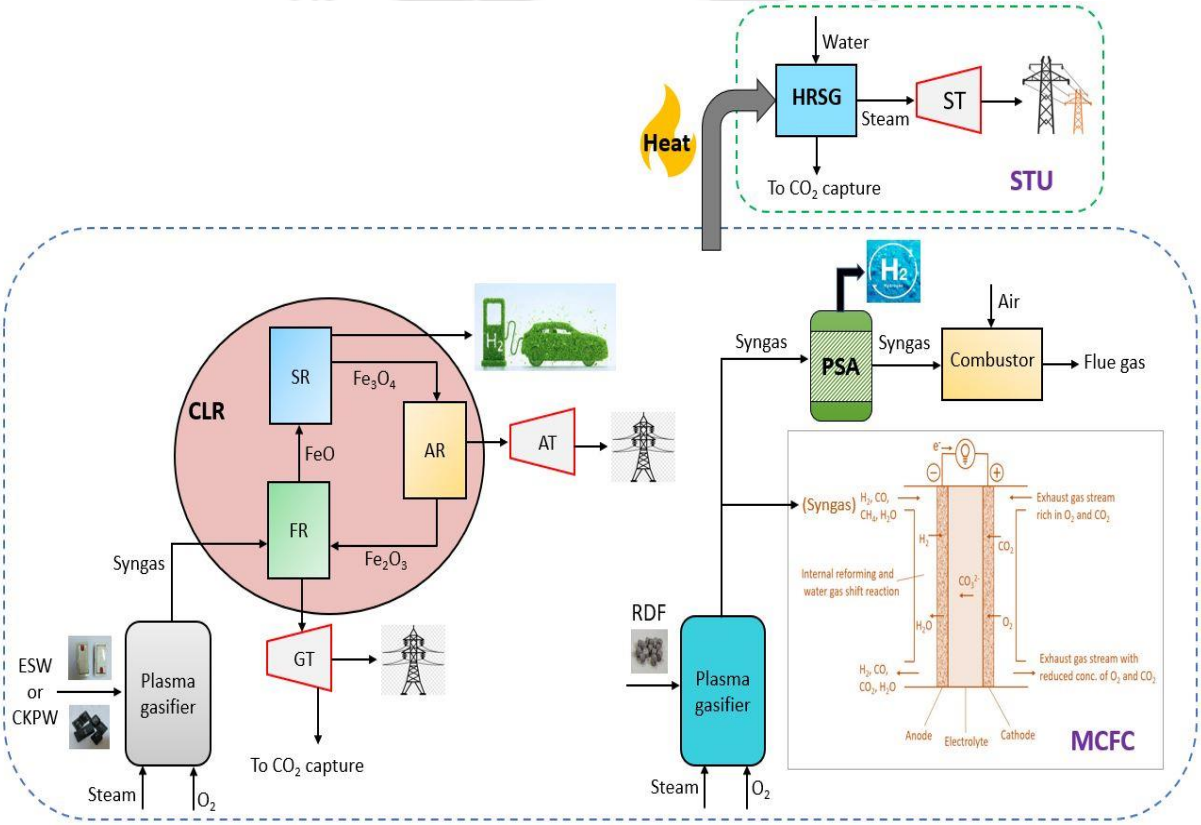

CHAPTER 7

SIMULATION STUDIES ON PLASMA GASIFICATION INTEGRATED MOLTEN CARBONATE FUEL CELL AND CHEMICAL LOOPING REFORMING

This chapter evaluates the feasibility of the plasma gasification process for commercial applications. Thus, the integration of plasma gasification with energy-generating systems for hydrogen and electricity co-production is assessed. The chapter is divided into two sections: Plasma gasification combined with molten carbonate fuel cell (MCFC) (Chapter7 A) and (7B) chemical looping reforming (CLR) (Chapter 7B). Chapter 7A studied the utilization of RDF feedstock for generation syngas, followed by the separation of hydrogen in the pressure swing adsorption (PSA) unit and power generation in the MCFC and steam turbine unit. Chapter 7B assessed the impact of CKPW and ESW feedstock on syngas composition and the syngas utilization in the CLR unit with the use of oxygen carriers (Fe_2O_3 in this case) in the CLR unit. Hydrogen is produced in one of the reactors of the CLR unit, while the electricity is derived from the CLR process with the use of turbines. The plants are simulated using Aspen plus v10 software. Both the studies focused on the 4-E (energy, exergy, economic and environmental) analyses that aim to offer possible ways of integrating plasma gasification with clean and energy-efficient techniques. The key performance indicators such as thermodynamic efficiencies, levelized cost of electricity (COE) and hydrogen (LCOH) and reduction in environmental footprint with CO_2 capture and utilization are evaluated.

CHAPTER 7A

Energy, exergy, economic and environmental (4-E) analyses of plasma gasification steam cycle integrated molten carbonate fuel cell for hydrogen and power co-generation based on refused derived fuel

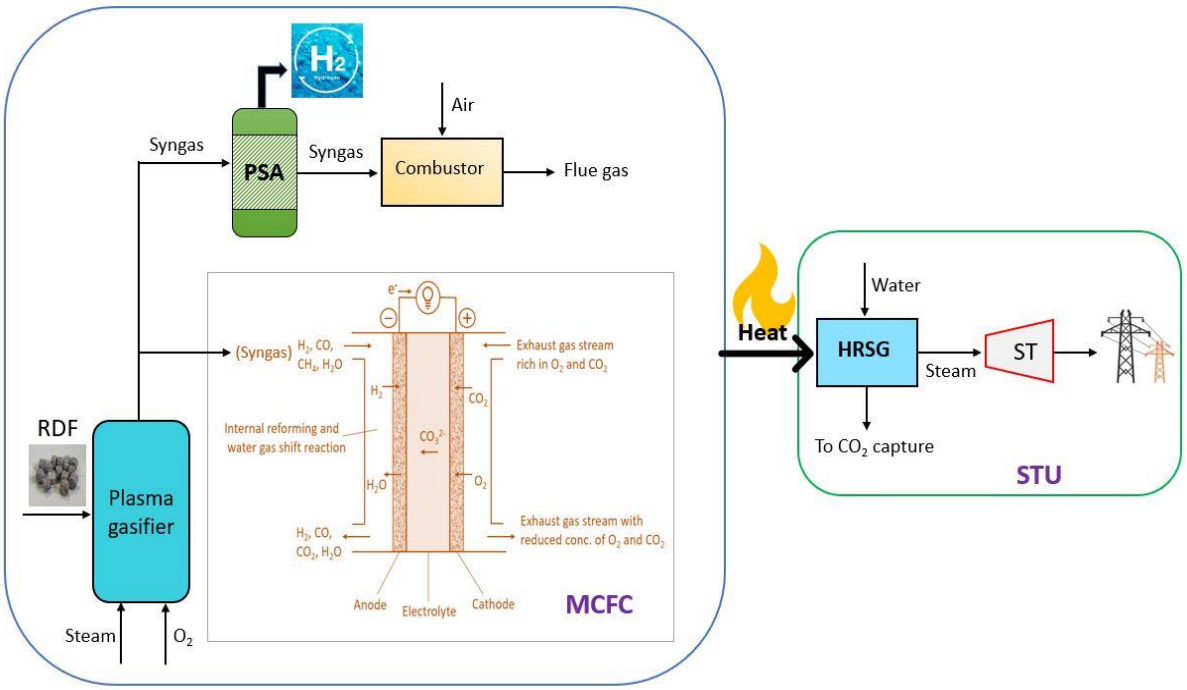

In this chapter, the system description and simulation results based on the 4-E analyses of plasma gasification integrated with molten carbonate fuel cell (MCFC) are discussed. The system co-generates hydrogen and electric power and, subsequently, minimizes the environmental footprint with CO_2 recycle looping. The feedstock considered for the study is refused-derived fuel (RDF), which is the combustible fraction of municipal solid waste. The RDF is prepared according to the composition of the Indian scenario as illustrated in Section 3.1.

7.1. System description

7.1.1. Plasma integrated molten carbonate fuel cell (MCFC)

The performance of plasma-based power plants is evaluated for various systems. A basis of 100 MW of chemical energy of the fuel is chosen as a reference for simulation. The fuel considered here is Refused Derived Fuel (RDF), as shown in Fig. 3.1 and the characteristics are outlined in Table 3.1.

The Aspen Plus simulation focuses on the sensitivity analysis for efficient operation of the co-generation (hydrogen and power) system with RDF feed for the following four (4) cases:

Case 1: Plasma integrated steam turbine cycle (IPGST)

Case 2: Plasma integrated steam turbine (IPGST) with MCFC system

Case 3: IPGST with MCFC system under different syngas ratio to fuel cell

Case 4: Plasma integrated steam turbine (IPGST) with MCFC using CH_4 as secondary fuel

The assumptions made for simulating the MCFC model stack are:

(i) Steady-state conditions

(ii) Temperature is uniform throughout the cell plane and negligible pressure drop

(iii) Stacks are made of the same material and behave identically

(iv) No thermal exchange between the cells

7.1.1.1. Aspen plus model of the overall power plant

All blocks, such as gasifiers, heat exchangers, turbines, compressors, etc are considered for modeling the power plant in Aspen Plus using appropriate thermodynamic methods and operating parameters from various literature. The property method used for the combined cycle is Peng-Robinson (PENG-ROB) based on the equation of state and carbon capture using MEA

absorber/stripper is Electrolyte Non-Random Two Liquid (ENRTL) that correlates activity coefficient with its mole fraction. To simulate the fragmented phase of the organic portion of feed, an RYIELD reactor (DECOMP) is positioned before HTR, as shown in Fig. 7.1. Here, the feed is decomposed into individual elements as specified in the yield distribution of proximate and ultimate analysis. The plasma gasifier is divided into two reaction zones: an HTR (High-Temperature Reactor) at 2500 °C and an LTR (Low-Temperature Reactor) at 1250 °C. An RGIBBS reactor is used for both, where the approach for conversion is based on chemical equilibrium by direct minimization of Gibbs free energy change. The organic fraction of the input feed is processed into synthesis gas in these reactors and the inorganic part is converted to slag. The Aspen plus flowsheet for the IPGST integrated with MCFC (Case 3) is shown in Fig. 7.1 and Fig. 7.2.

The fuel is fed into the plasma gasifier, working under atmospheric pressure with steam as plasma gas and oxygen as a secondary gasifying agent. Oxygen at a purity of 99% is obtained from an air separation plant (ASU) as per the process reported by Aneke and Wang, 2015, and a certain fraction of steam is recycled from the steam turbine (ST) section for plasma generation. The syngas mainly consist of H_2 and CO and small fractions of CO_2, CH_4, and H_2O produced in the gasifier at 1250 °C. This stream enters a heat recovery steam generator (HRSG), where it is cooled to its operating temperature of 250 °C (Minutillo et al., 2009). In the HRSG, the thermal energy of the syngas is converted in the form of steam at subcritical conditions. The syngas, after the removal of pollutants (H_2S, COS, etc.) in the acid gas removal (AGR) unit, gets split into two streams in which one of the streams goes to the fuel cell and the rest to the recovery of H_2. The remainder syngas following H_2 separation is combusted with air at 1 bar to provide heat for steam production. After power generation, the residual heat in the flue gas streams obtained from the outlet of the fuel cell and the combustor is extracted to generate high-pressure steam to drive the ST. The hydrogen in the syngas is separated using

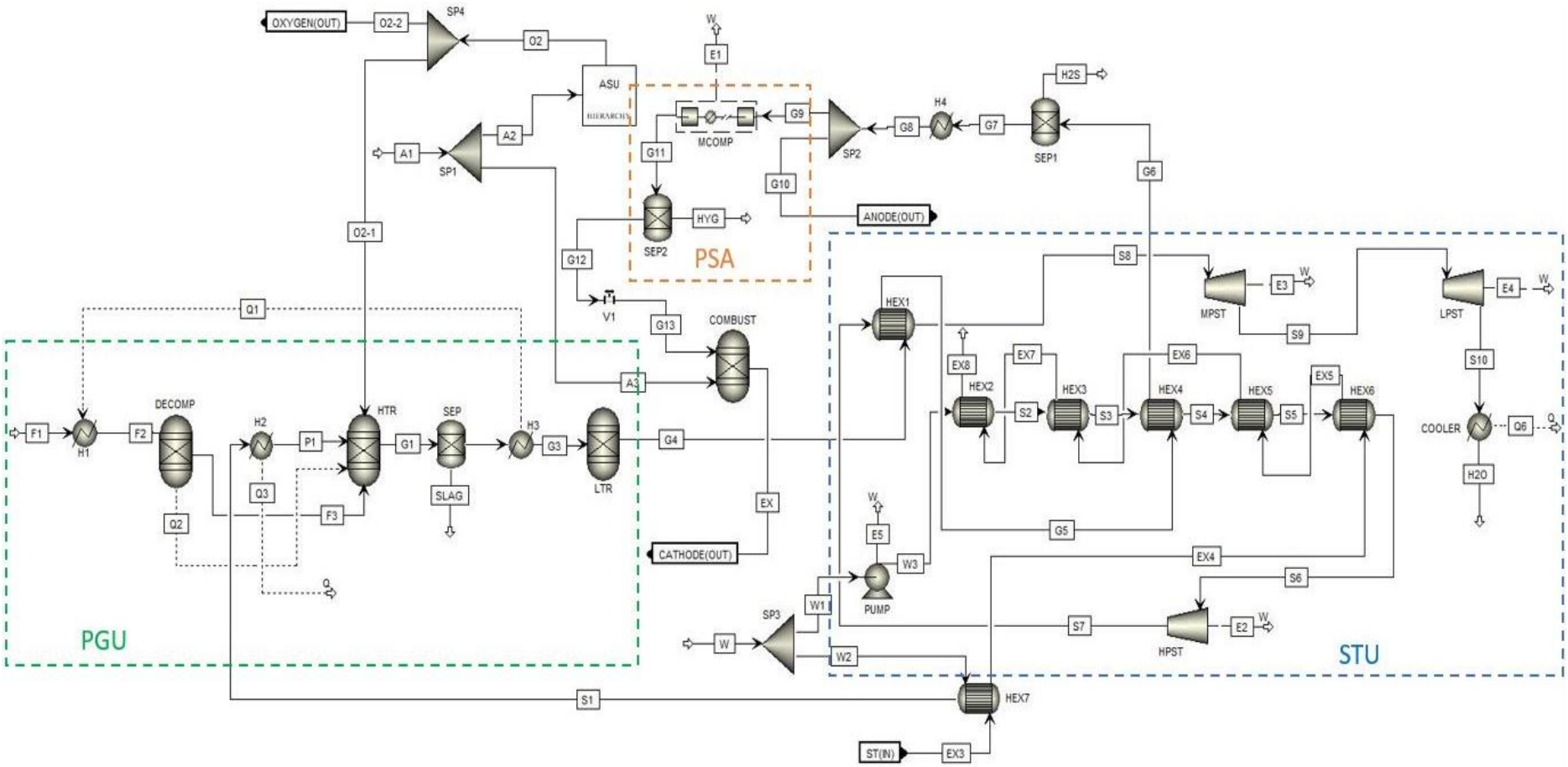

A-Air; **F**-Feed; **P**-Plasma; **SEP**-Phase separator; **G**-Gas; **C**-Compressor; **MCOMP**-Multiple compressor; **V**-Valve; **HYG**-Hydrogen; **W**-Water; **S**-Steam; **E**-Energy produced; **EX**-Exhaust/Flue gas; **PGU**-Plasma gasification unit; **ASU**-Air separation unit; **PSA**- Pressure swing adsorption; **STU**-Steam turbine unit; **HPST**-High pressure steam turbine; **MPST**-Medium pressure steam turbine; **LPST**-Low pressure steam turbine

Fig. 7.1. Aspen flow sheet representation of the IPGST system under different syngas ratios to PSA and MCFC.

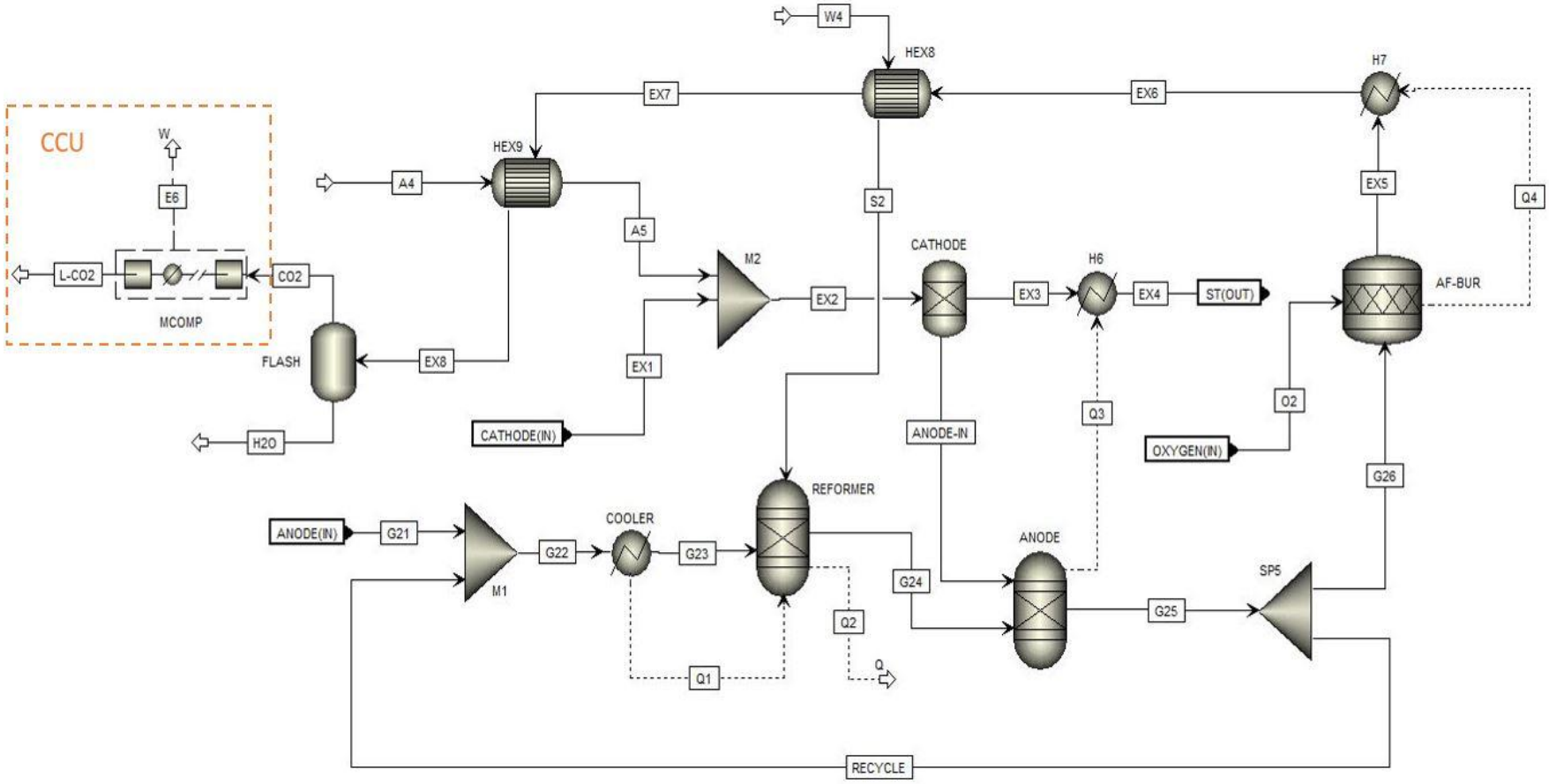

A-Air; **W**-Water, **FLASH**-Flash separator; **G**-Gas; **MCOMP**-Multiple compressor; **E**-Energy; **EX**-Exhaust/Flue gas; **AF-BUR**-After burner; **SP**-Stream splitter; **ST**-Steam turbine; **RECYCLE**-Recycle gas; **O2**-Oxygen; **M**-Mixer; **CCU**-CO_2 compressor unit; **L-CO2**-Liquid CO_2

Fig. 7.2. Aspen flow sheet representation of the MCFC system under different syngas ratios to PSA and MCFC.

the pressure swing adsorption (PSA) method. The electricity is generated using the combined power system of ST and MCFC (Duan et al., 2015; Kalinci et al., 2011).

7.1.1.2. Plasma integrated steam turbine cycle (IPGST)

A steam turbine cycle is employed for the generation of electricity and the conceptual flow sheeting is shown in Fig. 7.3. Before the syngas is being fed into the combustion chamber (CC), 95 vol.% of H_2 is recovered in PSA with high purity. The operating conditions of the PSA unit is fixed at 60 bar and 35 °C using 4 stages of compressors with interconnected cooling step. The H_2 stream generated can be directly stored for commercial applications (Cormos et al., 2020; Puig-Gamero et al., 2018). The syngas is completely burnt in the CC using atmospheric air at 1 bar, and a temperature of 1550 °C is maintained considering the limitation of the constructing materials (Emun et al., 2010). Thereafter, the flue gas from the CC is used to generate high-pressure steam at sub-critical conditions for driving the steam turbine. The final flue gas stream is then passed through a monoethanolamine (MEA) absorption unit, where 91% of CO_2 is captured, compressed and stored (Zang et al., 2018).

7.1.1.3. IPGST integrated MCFC

In this system, the cooled clean syngas after the HRSG is sent to the anode section of the MCFC as the inlet stream. Fig. 7.4 shows the conceptual flow sheeting of the plasma gasifier integrated steam turbine cycle. A reformer is employed before the anode to convert CO in the syngas into H_2 via. water-gas shift reaction (R12) as given in Table 2.2. A portion of the anode outlet gas at 650 °C is recycled to the inlet of the reformer based on the steam-to-carbon ratio of 3 to maintain thermal equilibrium without carbon deposition. The remaining outlet anode gas is sent to an afterburner to burn off the gases using pure oxygen and, the product gas is obtained with only CO_2 and H_2O. The following electrochemical reactions (R1, R2 and R13) take place in the cell, as mentioned in Table 2.2. At the cathode side, the CO_2 and O_2 react to

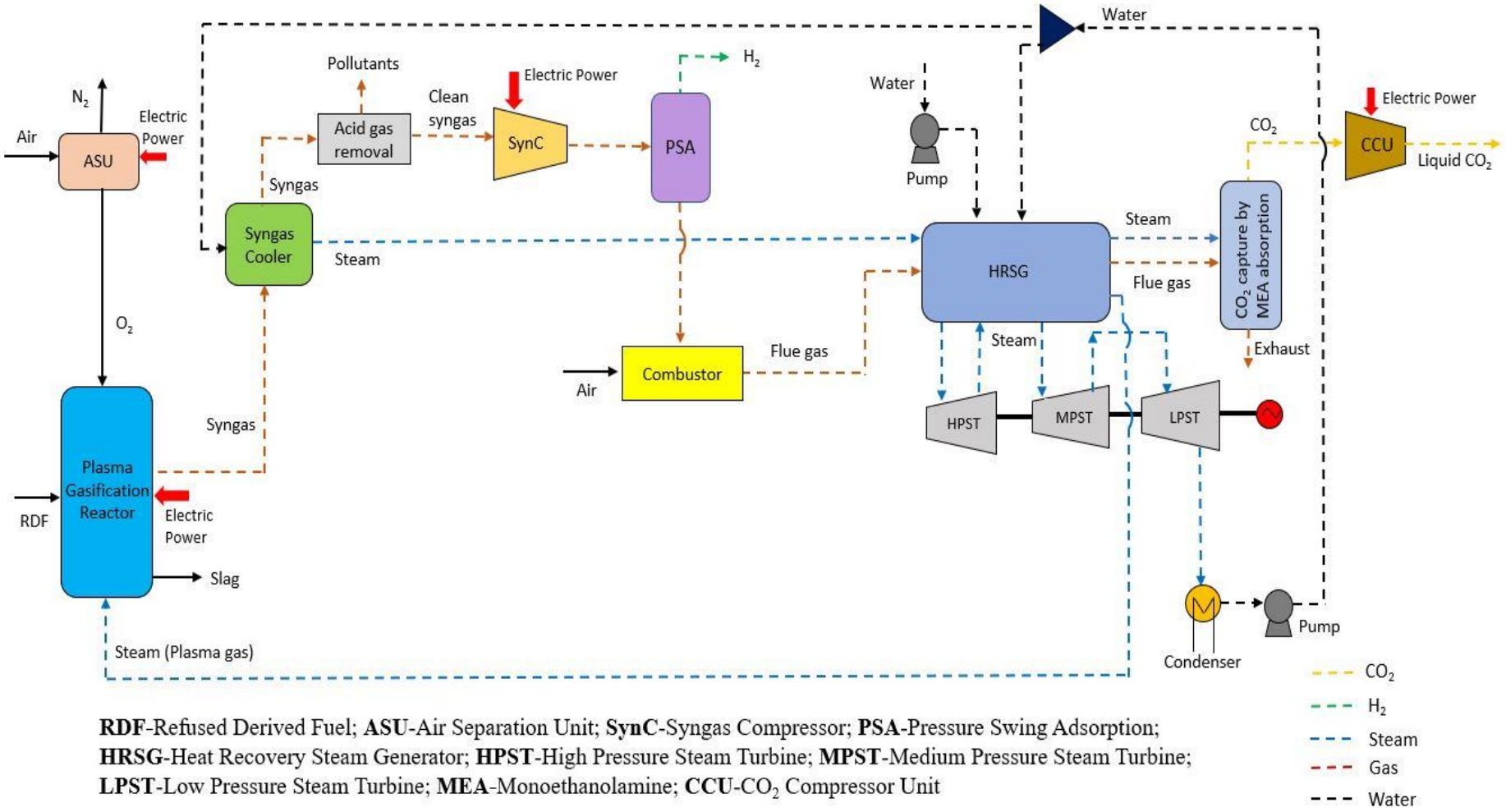

RDF-Refused Derived Fuel; **ASU**-Air Separation Unit; **SynC**-Syngas Compressor; **PSA**-Pressure Swing Adsorption; **HRSG**-Heat Recovery Steam Generator; **HPST**-High Pressure Steam Turbine; **MPST**-Medium Pressure Steam Turbine; **LPST**-Low Pressure Steam Turbine; **MEA**-Monoethanolamine; **CCU**-CO_2 Compressor Unit

Fig. 7.3. Schematic diagram of the integrated plasma gasification steam cycle (IPGST) system.

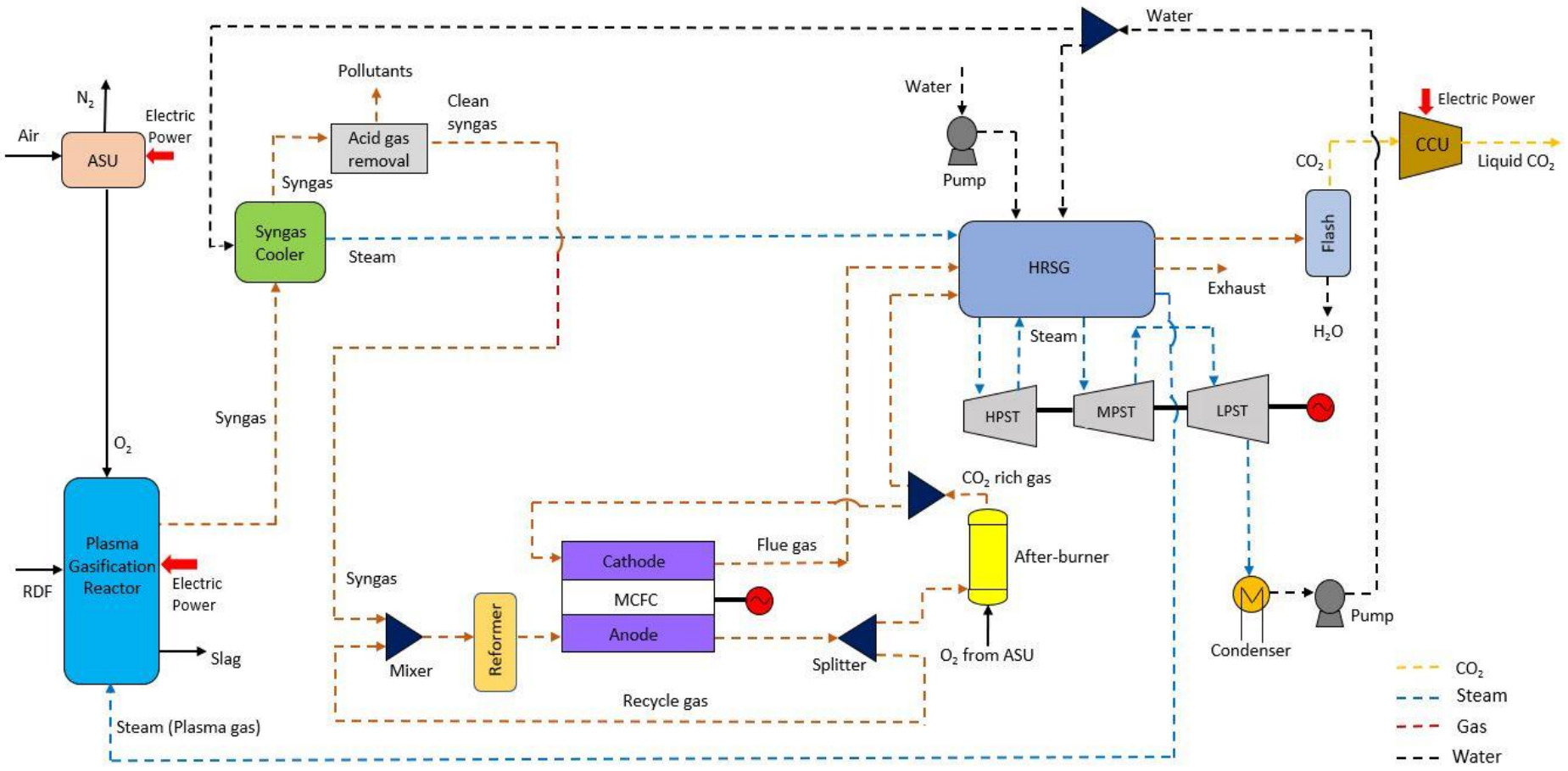

RDF-Refused Derived Fuel; **ASU**-Air Separation Unit; **HRSG**-Heat Recovery Steam Generator; **HPST**-High Pressure Steam Turbine; **MPST**-Medium Pressure Steam Turbine; **LPST**-Low Pressure Steam Turbine; **MCFC**-Molten Carbonate Fuel Cell; **CCU**- CO_2 Compressor Unit; **Flash**- Flash Separator

Fig. 7.4. Schematic diagram of the IPGST integrated MCFC system without PSA unit.

form carbonate ions (CO_3^{2-}), which are then transferred through the electrolyte to the anode of the fuel cell. A portion of CO_2 stream from the afterburner is sent to the cathode side to generate carbonate ions (CO_3^{2-}) and the remaining CO_2 is sent to a condenser to flash out H_2O and the obtained dry CO_2 is compressed to a final pressure of 110 bar using 5 stages of compressors unit for storage (Vairakannu and Kumari, 2016). The residual heat from the MCFC unit is used to generate steam and, the combination of low, medium and high-pressure steam turbines (LPST, MPST and HPST) are used to generate electricity.

7.1.1.4. IPGST integrated MCFC under different syngas ratio to fuel cell

The obtained syngas from the plasma gasifier (shown in Fig. 7.5) is split into two streams and sent to PSA and MCFC at various ratios 25:75, 50:50 and 75:25 (PSA: MCFC). This is to determine the optimum ratio for an efficient process. The process followed for the PSA section is similar to Section 7.1.1.2 and that of MCFC as per Section 7.1.1.3. The flue gas from the CC containing CO_2 enters the cathode of MCFC, which generally acts as a separator for CO_2. Finally, the CO_2 is separated from the gas stream by the condensation of steam.

7.1.1.5. IPGST integrated MCFC using secondary CH_4 fuel

In this method, a secondary fuel such as methane is employed to increase the efficiency of the power system (Campanari et al., 2014; Duan et al., 2015). The schematic flowchart of the system is shown in Fig. 7.6. The methane fuel is used to produce hydrogen (H_2) and carbon monoxide in the reformer. Moreover, the CO energy also gets converted into H_2 through reaction R12. The product gas formed in the anode side is recycled to the inlet of the fuel cell system to avoid the deposition of carbon due to the thermal decomposition of CH_4 (Campanari et al., 2014). The operational mechanism of plasma gasification unit (PGU), PSA and MCFC are similar to the proposed in Section 7.1.1.2 to Section 7.1.1.4.

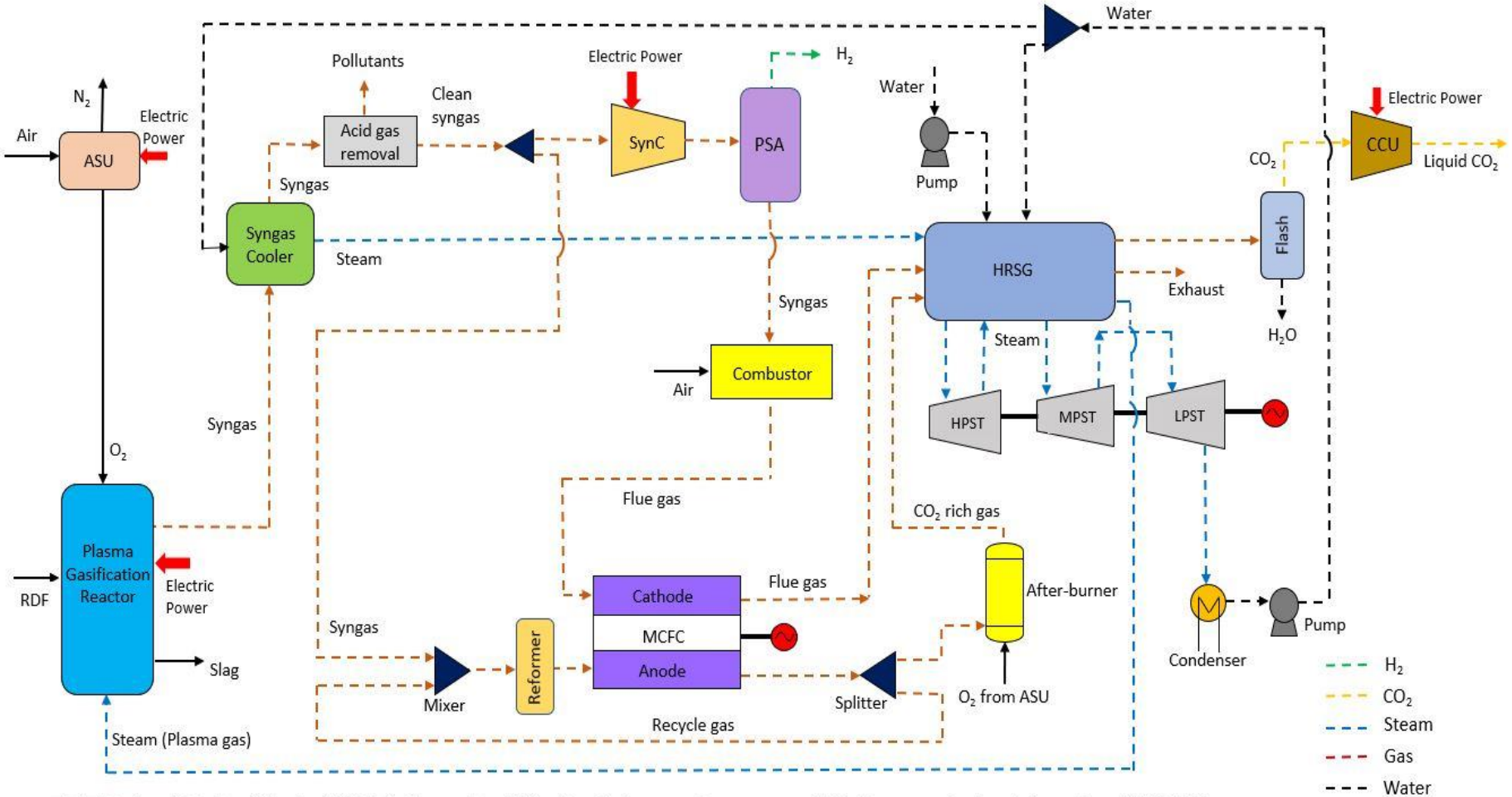

RDF-Refused Derived Fuel; **ASU**-Air Separation Unit; **SynC**-Syngas Compressor; **PSA**-Pressure Swing Adsorption; **HRSG**-Heat Recovery Steam Generator; **HPST**-High Pressure Steam Turbine; **MPST**-Medium Pressure Steam Turbine; **LPST**-Low Pressure Steam Turbine; **MCFC**-Molten Carbonate Fuel Cell; **CCU**- CO_2 Compressor Unit; **Flash**- Flash separator

Fig. 7.5. Schematic diagram of the IPGST system combined with MCFC at various syngas ratio to PSA and MCFC.

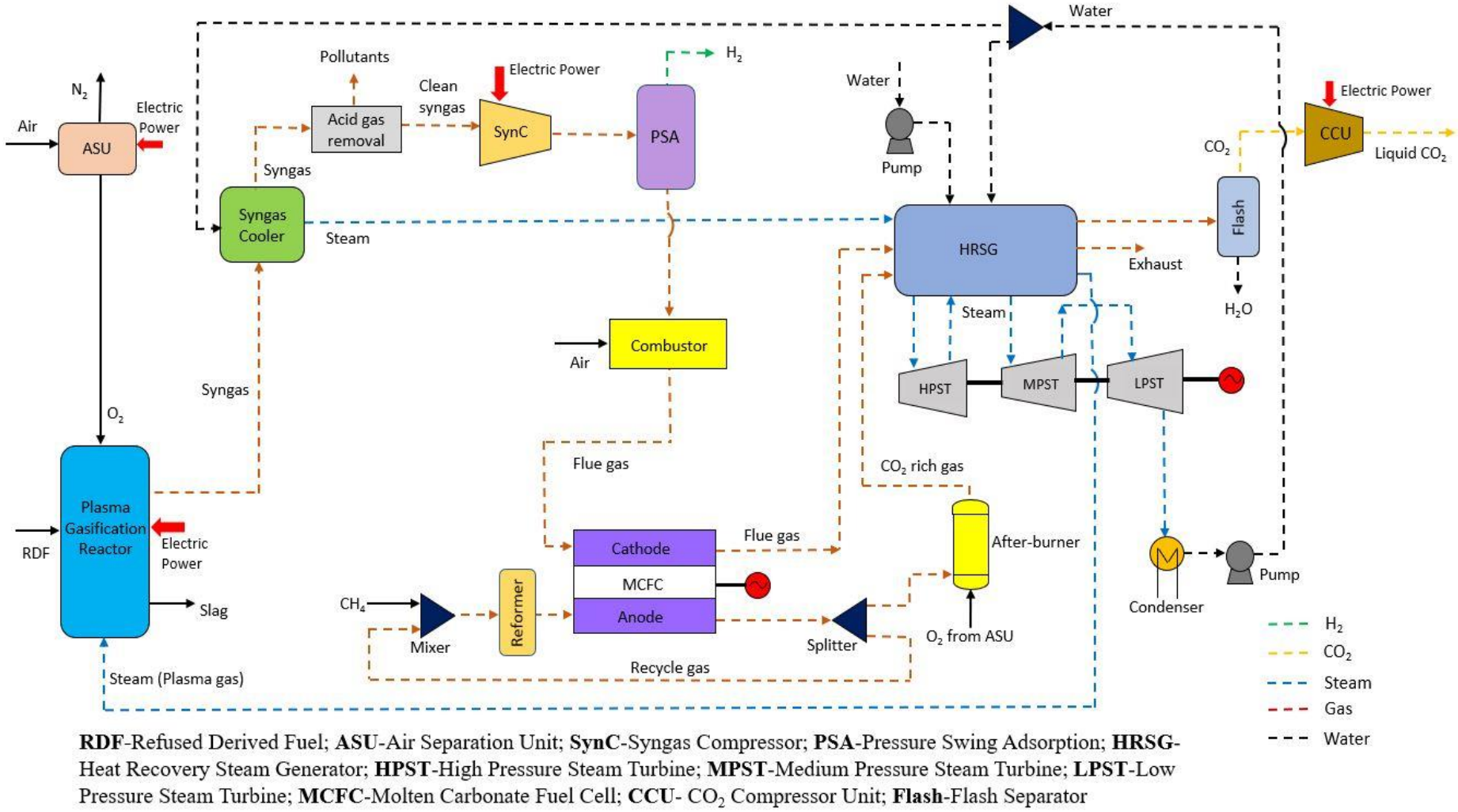

RDF-Refused Derived Fuel; **ASU**-Air Separation Unit; **SynC**-Syngas Compressor; **PSA**-Pressure Swing Adsorption; **HRSG**-Heat Recovery Steam Generator; **HPST**-High Pressure Steam Turbine; **MPST**-Medium Pressure Steam Turbine; **LPST**-Low Pressure Steam Turbine; **MCFC**-Molten Carbonate Fuel Cell; **CCU**- CO_2 Compressor Unit; **Flash**-Flash Separator

Fig. 7.6. Schematic diagram of the IPGST system integrated with MCFC system using secondary CH_4 fuel.

7.1.2. Model validation

The considered model of the plasma gasification unit is validated with the experimental and simulated results obtained by other literature. Table 7.1 presents the design data of the plasma gasifier compared with (Minutillo et al., 2009) and (Agon et al., 2016). It suggests that the results are quite adjacent to the reference values and therefore, based on the accuracy and reliability of the model, this can be used further in the study.

Table 7.1

Model validation of RDF plasma gasification with literature simulation results (Minutillo et al., 2009) and experimental (Agon et al., 2016) values.

	Simulation (Minutillo et al., 2009)	This work	Error (%)	Experimental (Agon et al., 2016)	This work	Error (%)
Composition of syngas (vol.%)						
H_2	28.65	28.71	0.21	~ 44.4	42.98	3.2
CO	37.37	37.42	0.13	~ 36.4	43.81	20.35
CH_4	0	0	0	~ 2.5	0.07	97.2
H_2O	14.91	14.80	0.74	-	0.09	-
CO_2	1.41	1.38	2.13	~ 6.2	1.7	72.58
N_2	17.12	17.13	0.06	-	0.07	-
HCl	0.31	0.32	3.23	-	0.6	-
Ar	-	-	-	~10	10.5	5
H_2S	0.22	0.23	4.55	-	0.1	-
COS	0.01	0.01	0	-	0.08	-
Total	100	100	-	99.5	100	-
Syngas temperature (°C)	1250	1250	-	1217	1250	-
LHV (MJ/kg)	9.2	9.21	0.05	10.4[a]	10.2[a]	1.92
Plasma gasification efficiency (η_{PG}, %)	69.1	69.07	0.04	53	51.98	1.92

[a] MJ/m^3.

7.2. Results and discussion

The parametric evaluation is segregated into two portions: (1) co-generation (hydrogen and power) from plasma gasification integrated steam turbine cycle and (2) the effect of integration of MCFC on the overall process. The simulation is conducted for the cases stated in Section 7.1.1 and an assessment is done based on energy, exergy, economic and environmental factors.

7.2.1. Syngas from the plasma gasification process

The inlet flow rates of the gasifying agent, oxidizing medium, plasma gas and fuel are given in Table 7.2. These flow rates are found to be optimal based on the higher H_2 and CO content in syngas after sensitivity analysis. The flow rate of steam and secondary oxygen is kept at 1.50 kg/s and 0.05 kg/s, respectively, due to the presence of moderate amount of elemental carbon in the feed as per reaction R6 and R7. Steam as the feed gas consumes higher power for plasma generation (16.34 MW) than other gases, which is calculated by the heat stream output (Q3) of the heater H2 in Fig. 7.1 of the Aspen flowsheet. This energy penalty is compensated through the production of the syngas with a higher heating value and lower concentration of toxic by-products (Kim et al., 2003). The molar syngas composition obtained is 59.57% H_2, 37.55% CO, 2.11% CO_2 and 0.59% CH_4, which are close to the experimental values reported by Agon et al. (Agon et al., 2016). It can be seen that using steam as the gasification agent, the concentration ratio of H_2/CO ratio is found high, possibly due to the water-gas shift reaction (R12). This also shows that the Boudouard reaction (R9) is insignificant in producing CO.

7.2.2. Effect of temperature, fuel and CO_2 utilization factor in MCFC

The following observations are found to be identical for all the stated cases in Section 7.1.1 while analyzing the influences of the operating parameters (temperature and fuel and CO_2 utilization factor) involving MCFC. Fig. 7.7 represents the parameter's effect on the current density and cell voltage. When the CO_2 utilization factor is increased from 70% to 95%, the

anode fuel and O_2 input into the fuel cell increase due to the progress of the electrochemical reaction. This resulted in a drop in the cell voltage with an increase in current density, as shown in Fig. 7.7 (a). The increase in the current density is found higher than the decrease in the cell voltage due to the rise in the MCFC power output. Further, with an increase in the CO_2 utilization factor, the requirement of O_2 in the afterburner for combustion also rises and thus, the power consumption in both ASU and CO_2 compression units also increases.

Table 7.2

Thermodynamic performance of the major cases considered.

Process configuration	IPGST-MCFC	IPGST	IPGST-MCFC
Syngas ratio [PSA: MCFC]	[0:100]	[100:0]	[Syngas:CH_4]
Flow rate [kg/s]			
Feed rate	4.51	4.51	4.51
Methane fuel rate	-	-	0.48
Steam plasma flow rate	1.50	1.50	1.50
Oxygen flow rate to gasifier	0.05	0.05	0.05
Oxygen flow rate to MCFC	1.91	-	0.56
Power section [MW]			
ASU power consumption	2.56	0.14	1.12
Syngas compression power	-	6.76	6.76
Plasma power consumption	16.34	16.34	16.34
Auxiliaries power consumption	0.55	0.41	0.44
Hydrogen output	-	56.20	56.20
Steam turbine output power	35.86	21.20	22.67
Natural gas input power	-	-	24.00
MCFC power output	35.79	-	14.28
CO_2 power consumption	0.92	5.43	1.38
Gross power output	71.65	21.20	36.95
Net power output	51.28	-7.88	10.91
Overall energy efficiency [%]	51.28	48.32	54.12
Exergy efficiency [%]	48.72	45.91	52.02

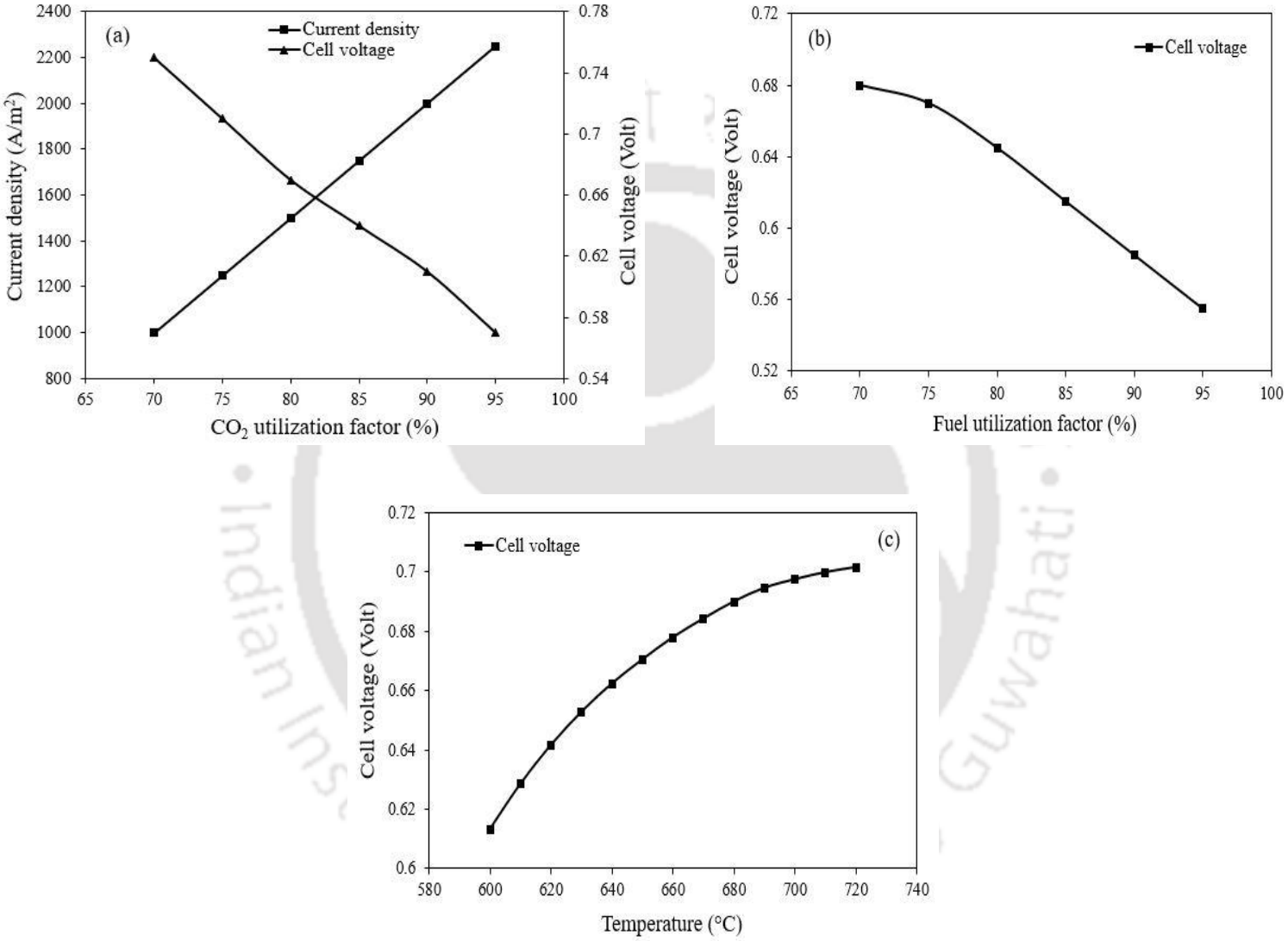

Fig. 7.7. Effect of (a) CO_2 utilization on current density and cell voltage, (b) fuel utilization and (c) temperature on cell voltage.

The waste heat recovered from the high-temperature afterburner exhaust gas is utilized in the steam turbine. The fuel utilization factor (FU) is another essential parameter that strongly influences the system's operation. As the FU increased from 70% to 95%, the anode input fuel decreases according to Eq. (31) in Section 3.6.1.1, and thereby the cell voltage decreases, as shown in Fig. 7.7 (b) due to the increase in anode polarization and excessive concentration losses. This leads to a decrease in MCFC power output as the current density is kept constant. With the increase in the operating temperature of MCFC, the cell voltage increases, as shown in Fig. 7.7 (c), due to the decrease in the internal cell resistance. It further increased the after-burner exhaust gas temperature, MCFC and steam turbine power output, and overall efficiency. However, for a longer life shelf, it is recommended to maintain the temperature around 650°C to avoid acceleration of material corrosion and volatilization of the electrolyte (Hirschenhofer et al., 1998). To obtain high net efficiencies, the optimum values of CO_2 utilization factor (80%), current density (1500 A/m^2), cell voltage (0.67) and FU (75%) in Table 3.3 are determined by considering a correlation between them. It is also reported in a similar manner in other literature and suggested to keep these parameters in the range as estimated in this study for sustaining the electrochemical reactions and proper functioning of fuel cells (Duan et al., 2015; Spinelli et al., 2020).

7.2.3. 4-E analyses of the power system configurations

The plasma gasification process producing hydrogen combined with MCFC is simulated for a chemical energy input of 100 MW. On the basis of the effect of temperature, fuel and CO_2 utilization factor on MCFC provided in Section 7.2.2, the 4-E analyses are conducted. The influences of the operating parameters for all the cases involving the MCFC system are found to be identical.

7.2.3.1. Energy analysis

Table 7.2 summarizes the major cases for hydrogen and power production with the overall net efficiency, whereas the remaining cases are shown in Fig. 7.8. It can be seen that there is a decrease of 2.96% in the overall efficiency when the syngas (G8) sent to the MCFC unit is reduced from 100% to 0% (by mass). This can be attributed to the lower amount of feed flow rate to the MCFC section. The chemical energy of hydrogen separated by the PSA unit considering 95% recovery for the syngas ratio (PSA: MCFC) of 25:75 to 100:0 is found between 14.01 and 56.20 MW. As the fuel utilization factor is set at 75%, therefore the unconverted gas at the outlet of the system is higher for 0:100 (PSA: MCFC) syngas ratio, which subsequently gets consumed under an oxygen atmosphere in the afterburner. This leads to an increase in the oxygen flow rate from 0.21 to 1.9 kg/s. The efficiency of the MCFC system is estimated in the range of 55-60%. In the clean-up section, an energy penalty of 0.3% of gasifier energy output is assumed, as reported in the literature (Peng et al., 2021; Toonssen et al., 2011). The heavy-duty plasma torch uses 22-78% of the gross power output of the overall system for all the cases. The steam turbine power output increased from 19.16 MW at a 75:25 ratio to 35.86 MW at 0:100 ratio (PSA: MCFC).

The energy penalty due to CO_2 compression is found between 1.28-4.5% of the gross power output, which is nearly similar to reported by other authors for MCFC (Campanari et al., 2010; Duan et al., 2015), whereas for 100:0 (PSA: MCFC) the energy penalty for CCU unit is 25.61% due to the diversion of energy for H_2 production (Zang et al., 2018). As MCFC utilizes CO_2 in the reaction, lower amount of CO_2 is generated at the exhaust gas of the plant, whereby low power is needed for its compression. Despite substantial changes in the overall efficiency based on variations in the syngas ratio (51.28% to 48.32%), it is still higher in comparison to the plasma gasification power plant studies reported in the literature using RDF (Galeno et al., 2011; Minutillo et al., 2009). Another new system feeding an additional 0.48 kg/s of methane

gas in the MCFC unit instead of syngas produces 2.84% higher net efficiency as compared to when 100% syngas enters the fuel cell. The addition of methane to the MCFC increases the performance of the overall process due to the extra power generated of 14.28 MW in addition to the steam cycle.

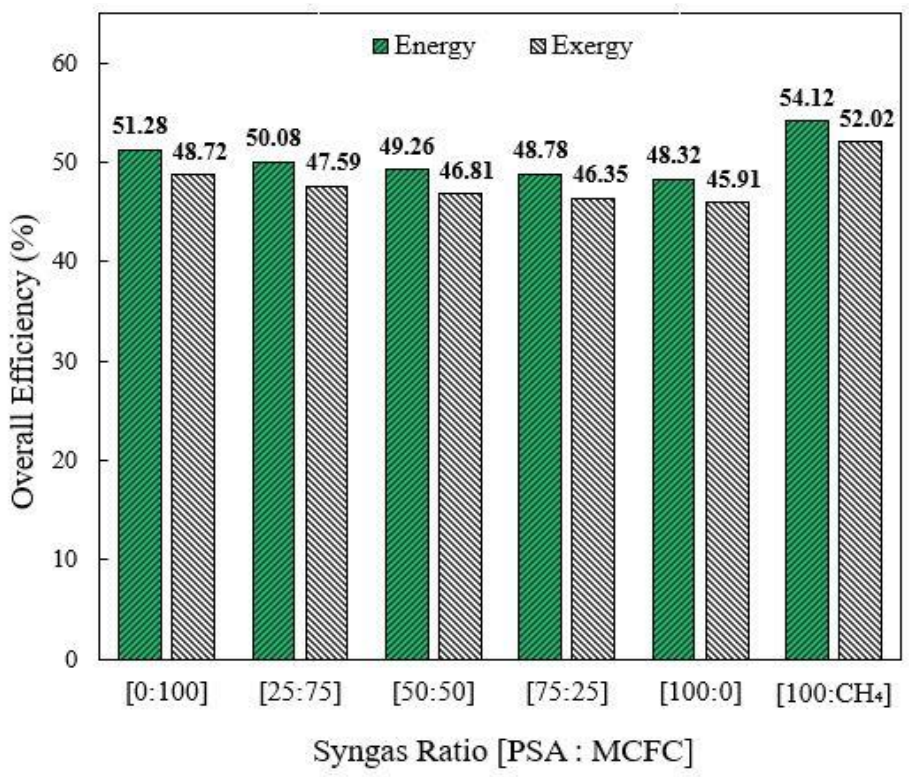

Fig. 7.8. Comparison of net energy and exergy efficiencies for different systems.

7.2.3.2. Exergy analysis

Using Eq. (7) - (11) and Table 3.4, the exergy flow, exergy destruction and efficiencies are estimated. The fuel input exergy of 105 MW is calculated using Eq. (10). This fuel exergy provided to the overall plant process can be related to the exergy destruction of individual components. To recognize the section where most of the exergy destruction takes place, component-wise exergy analysis in all the units present in the power plant is conducted. The maximum destruction rate, as shown in Fig. 7.9, originates in the combustor, plasma gasifier and afterburner, accounting for 20.08 MW, 13.42 MW and 12.26 MW, respectively, for IPGST

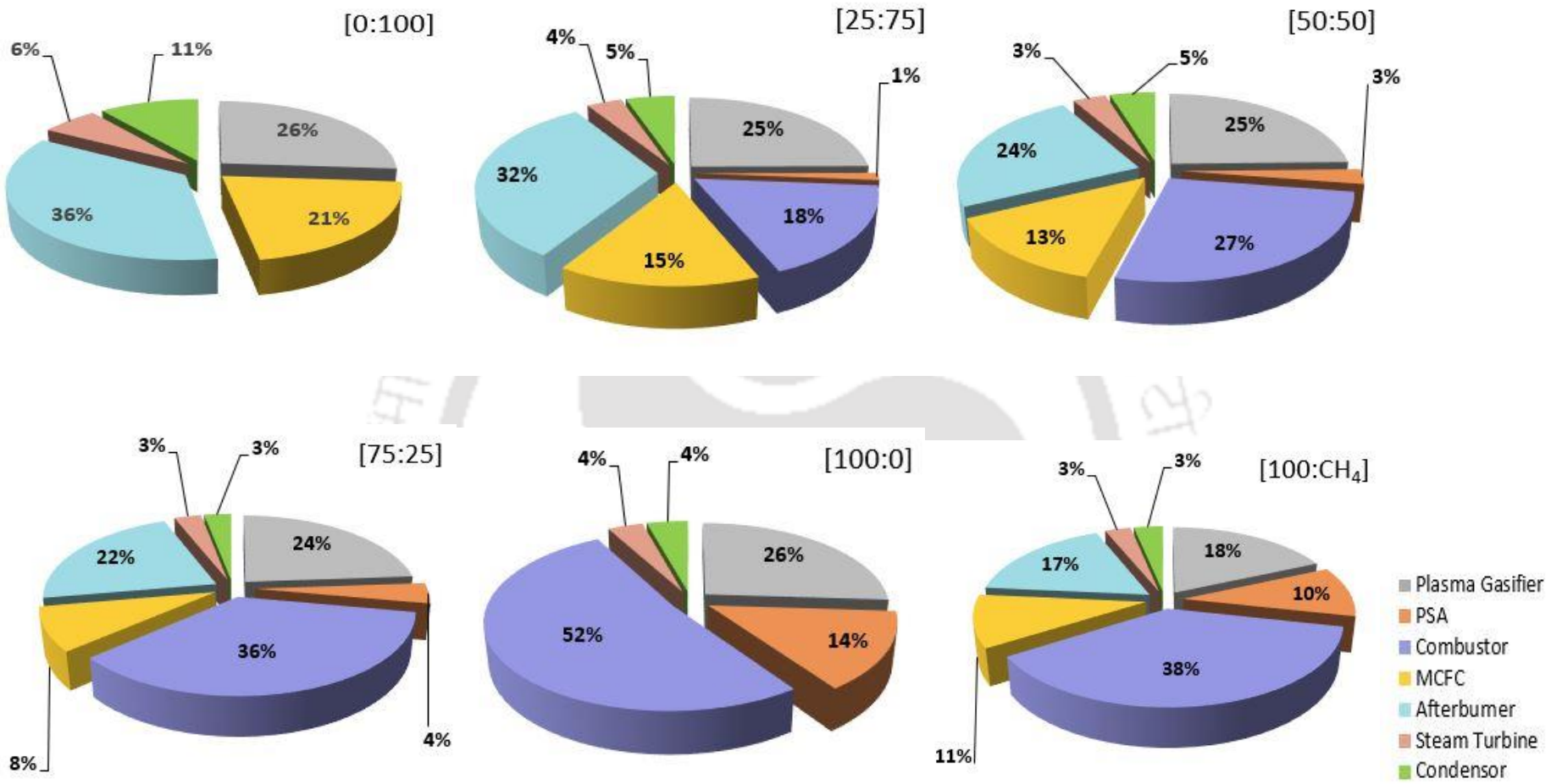

Fig. 7.9. Percentage contribution in exergy destruction for various components based on syngas ratio (PSA: MCFC) and CH_4 as secondary fuel.

integrated MCFC system with 75:25 syngas input to the PSA: MCFC. These are attributed to the irreversibility associated with the chemical reactions taking place inside the reactor, transforming the reactant species into product compounds (Kalinci et al., 2011; Montiel-Bohórquez et al., 2021). In the combustor and afterburner, an exothermic reaction (R10, R11) takes place, releasing immense heat with the flue gas. Moreover, the mixing of the hot product gas with excess air as a moderator destroys a large proportion of exergy in the range of 3-7 MW, i.e., an average of 23% for all cases (Montiel-Bohórquez et al., 2021). As the operating conditions are maintained the same for all the systems, despite higher destruction rates and fraction of fuel supply for Syngas:CH_4 (PSA: MCFC), the overall system efficiency improves due to more power generated by the hybrid process. Similar observations are also noted in the literature (Surywanshi et al., 2019). Results also show that exergy destruction for MCFC is lower comparatively, with a maximum contribution percentage (21%) for 0:100 (PSA: MCFC) ratio due to low irreversibilities caused by the electrochemical reaction (R1, R2).

The net exergy efficiencies are presented in Fig. 7.8 and compared with the corresponding energy efficiencies of the same system configurations. The difference between the energy and exergy efficiencies lies in the range of 2.1-2.56%. This indicates that the system works in the best thermodynamic state and therefore, the exergy destruction is lower (Yazdanfar et al., 2015). Thus, it is useful in analyzing the losses in the system when the energy and exergy analyses are considered together as described. Therefore, the complete MCFC power system provides the highest net energy and exergy efficiencies and lower power consumption. The added advantage of the introduction of secondary fuel, such as CH_4 increases the overall net efficiency of the system.

7.2.3.3. Economic assessment

Economic assessment is conducted based on the net present value (NPV) method and the results are presented in Table 7.3 for the major cases and based on intermediate syngas stream splitting is shown in Fig. 7.10. The levelized cost of syngas (LCOS) of 21.10 $/MWh is identical for all the cases as the modification in the plant comes into effect after the PGU. The specific total plant cost is the lowest for syngas:CH_4 (PSA: MCFC) i.e., when CH_4 is used, the plant cost is about 3877.58 $/kW and this increases with syngas diversion towards MCFC to about 6432.38 $/kW. This higher cost is mainly due to two reasons: (i) the initial investment cost of the plasma gasification, which largely depends on the plasma torch and (ii) the capital costs of MCFC are very high.

The magnitude of COE associated with all the configurations shows a similar trend as mentioned and ranges from 77.48 to 107.93 $/MWh. Despite the higher energy output from the IPGST (0:100) plant, the COE increases due to the higher capital cost of MCFC, as it serves the most significant power production unit for the considered case. Whereas the LCOH (3.94 $/kg) is highest for the 25:75 (PSA: MCFC) case as a consequence of reduced H_2 output. A lower LCOH of 1.01 $/kg can be achieved in the case of 100:0 (PSA: MCFC) as compared to the previously available literature on H_2 production (Khan and Shamim, 2016; Rai et al., 2022; Surywanshi et al., 2021). However, the high values of COE and LCOH can be viewed as a short-term perspective where the plasma torch and MCFC installations are considered in this study at the pre-matured stage as per the current market. In the upcoming years, a trade-off with conventional technologies could lower the specific cost, leading to better economic output in terms of COE. Under the current scenario, the cost of CO_2 avoided (CCA) is found to be following a similar pattern to the COE analysis. It makes up for 2.21 times (81.46 $/ton$CO_2$) for 0:100 (PSA: MCFC) than that of the ratio 100:0, which is 36.83 $/ton CO_2 and double of syngas:CH_4 (37.78 $/ton$CO_2$). The lower CCA value implies that the system is more efficient

than others in terms of cost analysis (Surywanshi et al., 2019). This also minimizes the carbon emission and storage tax by about 20%, which is potentially the major daunting task for any country facing under the Kyoto Protocol.

Table 7.3

Economic performance analysis of IPGST-MCFC.

Process configuration	IPGST-MCFC	IPGST	IPGST-MCFC
Syngas ratio [PSA: MCFC]	[0:100]	[100:0]	[Syngas:CH_4]
Plant cost [M$]			
Total Equipment Cost [TEC]	185.93	143.03	159.61
Total Installation Cost [TIC]	65.68	17.19	38.88
Total Direct Plant Cost [TDPC]	251.60	160.23	198.49
Indirect Cost [IC]	35.22	22.43	27.79
Engineering Procurement Cost [EPC]	286.83	182.66	226.28
Owner and Contingency Cost [OCC]	4302	27.40	33.94
Total Plant Cost [TPC]	329.85	210.06	260.22
Interest During Construction [IDC]	23.09	14.70	18.22
Total Plant Investment [TPI]	352.94	224.76	278.44
Specific total plant cost [$/kW]	6432.38	4340.00	3877.58
COE components [$/MWh]			
Capital cost	80.30	54.18	48.40
Operation & Maintenance cost	17.14	9.90	10.33
Methane cost	-	-	8.63
Fuel cost	5.45	5.45	5.45
CO_2 transport and storage cost	4.51	5.46	4.67
CO_2 emission tax	0.54	2.49	1.66
Total Cost of Electricity (COE)	107.93	77.48	79.15
Levelized Cost of Hydrogen (LCOH)	-	1.01	1.03
Cost of CO_2 avoided [$/ton$_{CO2}$]	81.46	36.83	37.78

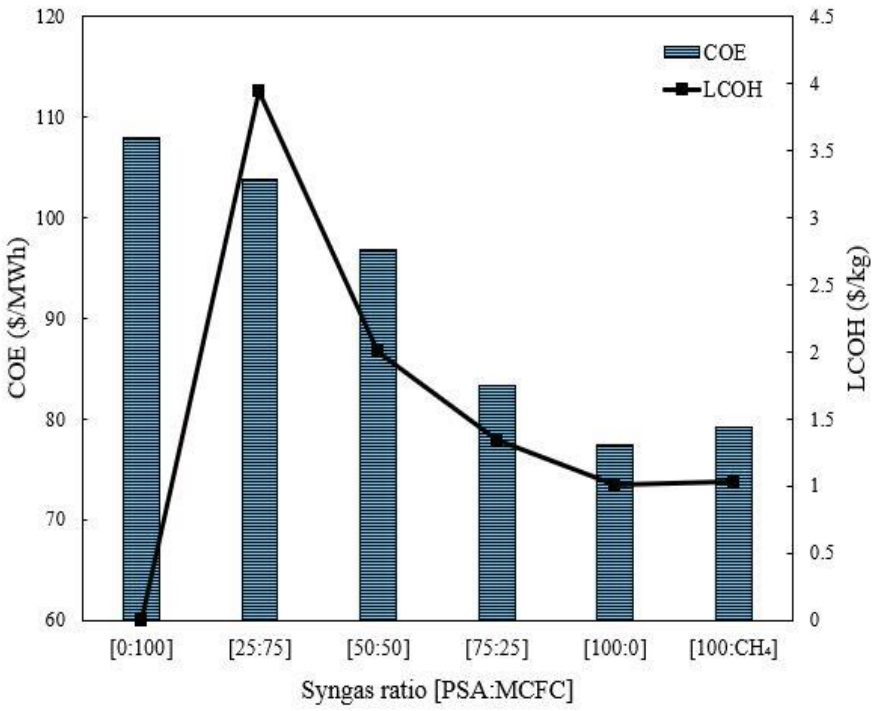

Fig. 7.10. COE and LCOH for different plant scenarios.

The unit exergoeconomic costs reported by Bohorquez et al. (Montiel-Bohórquez et al., 2021) for MSW and COE in this study are on the higher margin due to the low LHV of the feed, which reduces the system's overall output. More meaningful results could be obtained when the MCFC equipment cost gets lower in the range of 500-1000 $/kW, similar to solid oxide fuel cell (SOFC) (Yazdanfar et al., 2015), and the avoidable exergy destruction cost of the plasma torch is minimized. It is clearly understood and evidenced that the CO_2 capture in the intermediate steps is one of the points describing the effectiveness and economic feasibility of the overall plant. Another significant dimension is the processing capacity of the plant, which is quite lower in this study as compared to the established industrial-scale, also termed as the economy of scale.

7.2.3.4. Ecological analysis

Having identified the most imperative measures such as energy, exergy and economic parameters in the previous sections, the environmental assessment becomes necessary to justify its rationality. It is carried out mainly to assess the effect of CO_2 on the system and its surroundings, as reported in Table 7.4. Among all the arrangements, the 100:0 (PSA: MCFC) syngas ratio has the least environmental performance as a large amount of CO_2 comes out of the system that could not be utilized in the MCFC system under its methodology. Similarly, the greenhouse gas emission (GHG) measured by global warming potential (GWP) inclusive of N_2O and CH_4 is also the highest for 100:0 (PSA: MCFC) due to the higher CO_2 concentration in the flue gas. Finally, the relationship between all the cases for CO_2 emissions represented in terms of sustainability index (SI), with exergetic efficiency induces an opposite profile quantitatively i.e., the SI increases if CO_2 impact on the system decreases and vice-versa. The SI increases slight exponentially with net exergetic efficiency ($\eta_{ex,net}$) in their corresponding efficiency frame as described in the literature (Dincer and Rosen, 2021).

Table 7.4

Ecological assessment comparison based on different IPGST-MCFC system.

Process configuration	IPGST-MCFC	IPGST-MCFC	IPGST-MCFC	IPGST-MCFC	IPGST	IPGST-MCFC
Syngas ratio [PSA: MCFC]	[0:100]	[25:75]	[50:50]	[75:25]	[100:0]	[Syngas:CH_4]
Specific CO_2 emission rate [kg/MWh]	19.66	34.51	54.08	76.76	91.65	61.16
Annual CO_2 emission [x 10^6 kg]	7.56	13	20	28.1	33.2	30.8
Annual CO_2 captured [x 10^8 kg]	1.54	1.60	1.66	1.70	1.77	2.10
Average annual CO_2 emission per unit fuel [kg/GJ]	2.80	4.80	7.40	10.40	11.40	9.19
Annual CO_2 avoided per unit fuel [kg/GJ]	57.20	59.10	61.50	63.10	65.40	62.58
Net energy output/CO_2 captured [MW/kg]	8.97	8.47	8.01	7.73	7.39	8.65
Global Warning Potential [$kgCO_{2eq}$/h]	1008.00	1740.12	2686.99	3776.63	4460.63	4144.45
Sustainability Index	1.95	1.91	1.88	1.86	1.85	2.08

7.3. Conclusions

The novel method of MCFC integration with plasma gasification for the co-generation of hydrogen and power is proposed for the four different system configurations. The Aspen simulation is conducted and further, 4-E analyses (energy, exergy, economic and environment) of the overall plants are conducted and compared to draw up the subsequent conclusions:

- Under the application of high temperature in the plasma gasifier (1250-2500 °C) and the sensitivity analysis of gasifying agents such as steam (1.5 kg/s) and O_2 (0.05 kg/s), the RDF feed conversion resulted in 97.71% of combustible fractions (H_2, CO and CH_4) in the syngas and a high H_2/CO ratio of ~1.6 for all the cases.
- The IPGST-MCFC system with additional CH_4 i.e. syngas:CH_4 (PSA: MCFC) ratio has the highest net energy efficiency of 54.12% followed by the IPGST-MCFC [0:100] ratio of 51.28%. Maximum losses occur in the condenser, followed by the combustor for all cases. The energy penalty on CO_2 compression ranges between 1.28-4.50% for all the different plant scenarios except for the 100:0 ratio where the energy penalty also includes the CO_2 removal process, which is higher but in line with the literature.
- The net exergy efficiency is lower by 2.1-2.56% than energy efficiency, which is regarded as the exergy penalty. The highest amount of exergy destruction takes place in the combustor (36%), plasma gasifier (24%) and afterburner (22%) due to the irreversibilities of the chemical reactions.
- The economic analysis indicated a higher specific total plant cost of a maximum of 6432.38 $/kW, and COE above 77 $/MWh for all cases determined but has the potential to reduce with some improvisation. However, the lowest COE and LCOH among all is possessed by 100:0 [PSA: MCFC] ratio, which is 77.48 $/MWh and 1.01 $/kg, respectively and is lower than the reported in the literature. Further, the cost of

CO_2 avoided increases to a maximum of 81.46 $/ton CO_2 despite a higher amount of CO_2 absorption in MCFC.

- The combination of plasma and MCFC can bring down CO_2 emissions by 2.40 x 10^8 kg annually, which can improve the sustainability of the overall process. Also, the specific CO_2 emissions rate of 19.66–91.65 kg/MWh is very much lower than most of the conventional gasification processes. The global warming potential for the [100:0] ratio is the highest in the value of 4460.63 $kgCO_{2eq}/h$.

Therefore, RDF waste is suitable to be processed under plasma conditions for the production of hydrogen and electricity co-generation integrated with fuel cells.

CHAPTER 7B

4-E analyses of plasma gasification integrated chemical looping reforming system for power and hydrogen co-generation using Bakelite and Acrylonitrile Butadiene Styrene based plastic waste feedstocks

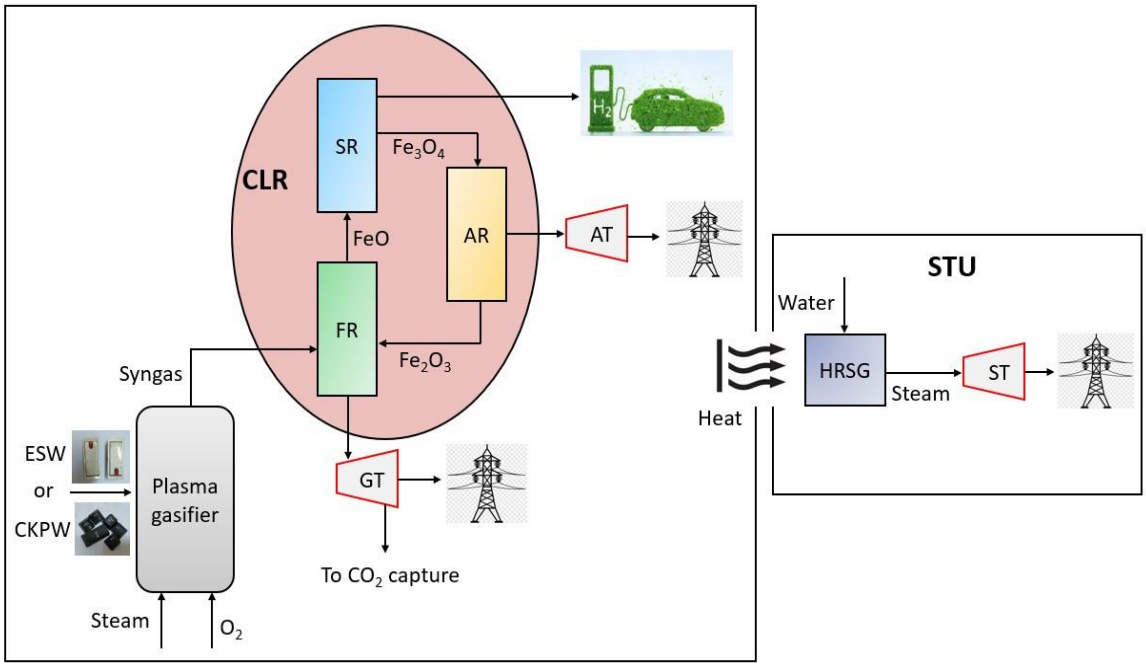

This chapter presents the simulation results based on 4-E analyses of plasma gasification integrated with chemical looping reforming (CLR). The feedstock considered for the study is computer keyboard plastic waste (CKPW), comprising mainly of acrylonitrile butadiene styrene (ABS) and electrical switch waste (ESW) made of bakelite. The wastes are collected from the facilities of the Indian Institute of Technology Guwahati and the compositions are illustrated in Table 3.1.

7.4. System description

7.4.1. Plasma integrated chemical looping reforming (CLR)

The feedstocks to the power plant considered in this study are electrical switch waste (ESW) and computer keyboard plastic waste (CKPW), shown in Fig. 3.1 and their composition are outlined in Table 3.1. A basis of 100 MW (as a reference) of the chemical energy of the fuel is considered in all cases for simulation. The lower heating value (LHV) of ESW and CKPW fuel is 14.05 MJ/kg and 35.31 MJ/kg, respectively, are estimated using a bomb calorimeter. The following cases are simulated (each for both the feed):

Case 1: Plasma integrated CLR system-based steam turbine unit (IPGST-CLR)

Case 2: Plasma integrated CLR system-based combined cycle (IPGCC-CLR)

The overall power plant is divided largely into 4 sections: plasma gasification unit (PGU), chemical looping reforming unit (CLRU), steam turbine unit (STU), and CO_2 and H_2 transport and storage unit, as shown in Fig. 7.11. Generally, the processing of any type of fuel in a power plant requires pre-treatment, such as washing, drying, shredding, etc. (Sahu and V, 2021). This is avoided in a plasma gasification process due to the high temperature (>2000 °C) inside the reactor (Montiel-Bohórquez et al., 2021). Moreover, the fuel (waste) considered for this study is based on source separation from waste feedstock (Lavee and Nardiya, 2013) because of which the cost required for prior handling of the waste is further neglected.

To simplify the analysis of the hybrid system, some basic assumptions are considered (Peng et al., 2021).

(i) Steady-state conditions and thermodynamic equilibrium are considered.

(ii) The pressure drop and heat loss between units are neglected.

(iii) The environmental temperature and pressure are assumed as 25 °C and 101.325 kPa.

(iv) Kinetic and potential energy effects are ignored.

7.4.1.1. Description of the IPGST-CLR power plant

Fig. 7.12 shows the schematic representation of the Aspen flowsheet in Fig. 7.11 based on the IPGST integrated CLR process used in this study. The plasma gasifier utilizes fuel (F) with steam as plasma gas and oxygen as secondary gas under atmospheric pressure, as shown in Fig. 7.11. Steam (S) is generated from a heat recovery steam generator (HRSG) exchanging heat from the various outlet streams of the CLR unit and, oxygen (O_2) is fed into the plasma gasifier from an air separation unit (ASU). The process flow sheet of ASU for oxygen separation is followed from the literature (Aneke and Wang, 2015). The raw syngas leaving the plasma gasifier (G5) gets cooled in a heat exchanger before entering the cleaning section and, the thermal heat of syngas is extracted to generate steam for the steam turbine unit (STU) (Minutillo et al., 2009). The cleaned syngas (G13) from the purification section are sent to a fuel reactor (FR). In the FR, the metal oxy-combustion reactions take place (R3) between the syngas and oxygen carriers (OC). In this study, iron oxide (Fe_2O_3) is considered due to its availability and low cost. The outlet gases (EXH) of the FR containing solid-gas mixture get separated in a cyclone separator (SEP1), whereby the high-temperature gas goes to HRSG and, the reduced OC (FeO) from the FR is sent to a steam reactor (SR). In the SR, the supplied steam (S16) reacts with FeO and forms H_2 with partial oxidation of the OC to Fe_3O_4 (R4). Thereafter, the partially reduced OC (OC-2) is sent to an air reactor (AR) to get fully oxidized into Fe_2O_3 (R5). The sensible heat of the exhaust gas (G16) from the SR is recovered in the HRSG. After the condensation of the unconverted steam, the H_2 is compressed and stored at 60 bar in a 3-stage process-based compression, cooling and storage (CCLS) unit (Khan and Shamim, 2016). The oxidized iron particles in the form of Fe_2O_3 (OC) in the AR (after separation from O_2 depleted air via SEP3) are recycled to the FR while the gas stream from the AR (A3), i.e., O_2-depleted air is sent to the HRSG for heat recovery.

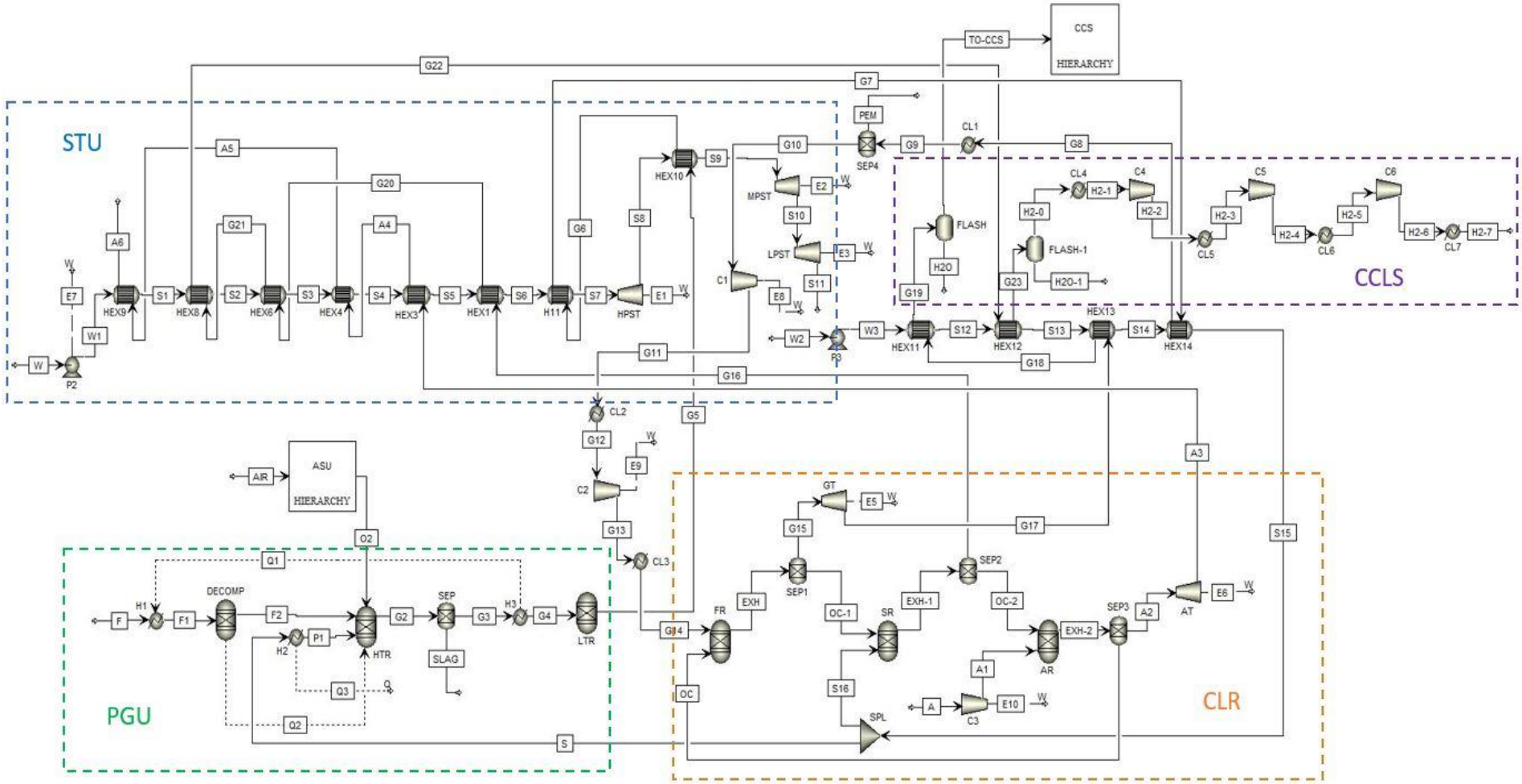

A-Air; **F**-Feed; **P1**-Plasma; **SEP**-Phase separator; **G**-Gas; **C**-Compressor; **W**-Water; **S**-Steam; **E**-Energy/Power produced; **EX**-Exhaust gas; **CL**-Cooler; **SPL**-Split; **PGU**-Plasma gasification unit; **ASU**-Air separation unit; **CLR**-Chemical looping reforming; **STU**-Steam turbine unit; **HPST**-High pressure steam turbine; **MPST**-Medium pressure steam turbine; **LPST**-Low pressure steam turbine; **HEX/H**-Heat exchanger; **OC**-Oxygen carrier; **CCLS**-Compression, cooling and storage

Fig. 7.11. Aspen flow sheet representation of the IPGCC-CLR system.

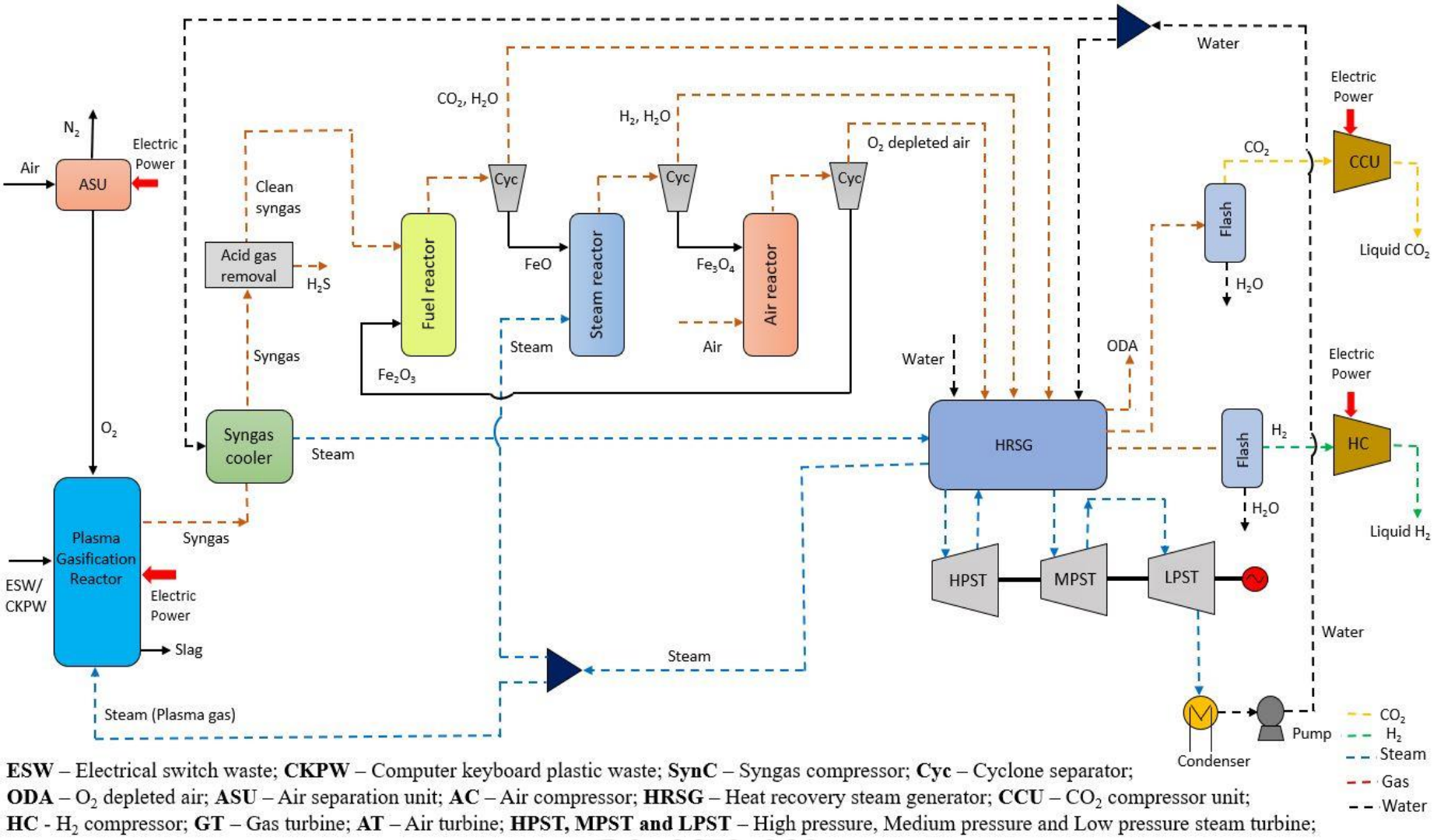

ESW – Electrical switch waste; **CKPW** – Computer keyboard plastic waste; **SynC** – Syngas compressor; **Cyc** – Cyclone separator;
ODA – O_2 depleted air; **ASU** – Air separation unit; **AC** – Air compressor; **HRSG** – Heat recovery steam generator; **CCU** – CO_2 compressor unit;
HC - H_2 compressor; **GT** – Gas turbine; **AT** – Air turbine; **HPST, MPST and LPST** – High pressure, Medium pressure and Low pressure steam turbine;

Fig. 7.12. Schematic diagram of the plasma gasification combined with CLR system at 1bar (IPGST-CLR).

The flue gas stream from the FR (G15) contains primarily CO_2 and H_2O, but in the case of ESW, high N_2 content (11.18 vol.%) inherently present in the fuel dilutes the CO_2 stream, and thereby its separation is highly necessary before CO_2 can be captured and stored. CO_2 with ~90 % purity is recovered from the flue gas stream using a monoethanolamine (MEA) absorption-stripping unit. Then, the captured CO_2 is compressed at 110 bar using 5 inter-cooling stages-based multi-unit compressors (Vairakannu and Kumari, 2016). In the case of the CKPW fuel, due to the absence of sulfur with a low quantity of N_2 (1.65 wt.%), the addition of a clean-up and carbon capture and storage unit (CCS) is avoided and the total CO_2 gas stream is captured by condensing the low-quality steam under room conditions.

7.4.1.2. Description of the IPGCC-CLR power plant

In this system, the raw syngas from the plasma unit is cleaned in the purification section. The cleaned syngas is compressed at 15 bar using 2-stage compression unit with intercooling between the compressors (Surywanshi et al., 2021). As the FR and AR operate under high pressure, the outlet gas stream of FR (G15) and AR (A2) undergoes expansion in a gas turbine (GT) and air turbine (AT), respectively, to produce electricity, as shown in Fig. 7.11 and Fig. 7.13. The process adopted for PGU, STU and CCLS is similar to as reported in Section 7.4.1.1.

7.4.2. Model validation

The flowsheeting employed in this study, including the plasma gasification and CLR system is separately validated with the literature. The model assumptions are taken as per the literature (Surywanshi et al., 2021). As stated earlier, Table 7.1 provides the validation results of the plasma gasification unit, while Table 7.5 and Table 7.6 shows the validation results of the CLR system using the simulation studies by Yang et al., 2021 and the experimental studies by Chen et al., 2011, respectively. The deviation error is found below 2% compared with the simulation results of the literature, the developed model in the study is used further for sensitivity analysis.

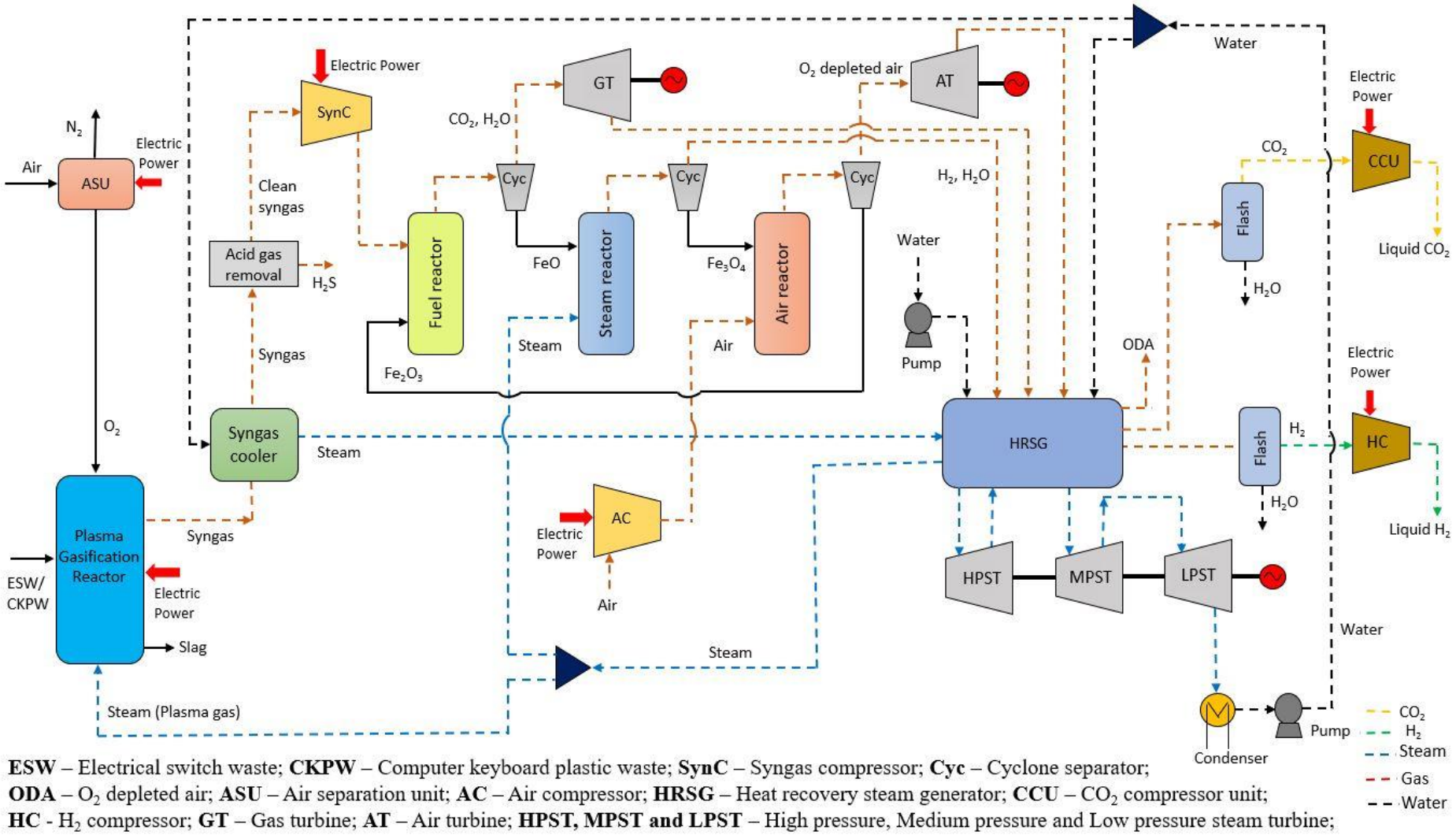

Fig. 7.13. Schematic diagram of the plasma gasification combined with CLR system at 15 bar (IPGCC-CLR).

Table 7.5

Model validation of CLR system based on literature operating at 1 atm (Yang et al., 2021).

Stream	Fuel reactor outlet (900 °C)			Steam reactor outlet (500 °C)			Air reactor outlet (500 °C)		
	Ref (Yang et al., 2021)	This work	Error (%)	Ref (Yang et al., 2021)	This work	Error (%)	Ref (Yang et al., 2021)	This work	Error (%)
Molar flow rate (kmol/h)									
H_2	0.12	0.117	2.5	2.67	2.63	1.5	0	0	-
CO	0.08	0.0785	1.88	0	0	-	0	0	-
CH_4	0	0	-	0	0	-	0	0	-
H_2O	1.88	1.885	0.27	6.33	6.22	1.74	0	0	-
CO_2	0.92	0.928	0.87	0	0	-	0	0	-
O_2	0	0	-	0	0	-	0.22	0.218	0.91
N_2	0	0	-	0	0	-	3.12	3.12	0
Fe_2O_3	0.19	0.187	1.58	0	0	-	4	4	0
FeO	7.43	7.442	0.16	0	0	-	0	0	-
Fe_3O_4	0	0	-	2.67	2.66	0.37	0	0	-

Table 7.6

Model validation of CLR process with an experimental study operating at 1 atm (Chen et al., 2011).

Stream	Fuel reactor outlet (900 °C)			Steam reactor outlet (500 °C)			Air reactor outlet (500 °C)		
	Ref (Chen et al., 2011)	This work	Error (%)	Ref (Chen et al., 2011)[a]	This work	Error (%)	Ref (Chen et al., 2011)	This work	Error (%)
Concentration (vol.%)									
H_2	0	0	-	~ 12.1	3.4	71.9	0	0	-
CO	~ 28	31.46	12.35	~ 0.08	0	-	~ 0.25	0	-
CH_4	0	0	-	0	0	-	0	0	-
H_2O	0	0	-	0	10.8	-	0	0	-
CO_2	~ 6.5	6.04	7.07	~ 0.01	0	-	0	0	-
O_2	0	0	-	0	0	-	~ 19.5	14.46	25.84
N_2	0	0	-	0	85.8	-	0	85.53	-

[a] dry-based.

7.5. Results and discussion

In this section, comprehensive analyses of the overall power plant are carried out and presented for the optimum H_2 co-generation. Firstly, the plasma gasification process is optimized through sensitivity analysis to maximize the production of high calorific value of syngas. Secondly, the effect of the flow rate of syngas, steam and air to the FR, SR and AR, respectively, for the reactivity of oxygen carrier and their impact on the composition of the outlet gas and solid stream of the CLR system are studied. Further, the effect of operating temperature on the net efficiency of the CLR system is evaluated. Lastly, the 4-E (energy, exergy, economic and environmental) analyses are performed with an energy input of 100 MW based on LHV of the feedstock (ESW and CKPW).

7.5.1. Syngas from plasma gasifier

The sensitivity analysis showed that the mass flow rate of fuel, plasma and secondary gas are 7.12 kg/s, 0.5 kg/s and 0.05 kg/s, respectively, for ESW feed and 2.83 kg/s, 1.15 kg/s and 0.21 kg/s, respectively for CKPW feed. The higher values of plasma and secondary gas for CKPW feed are due to the presence of higher carbon content for reactions R6 and R7. Therefore, the energy required to produce steam as plasma gas is found higher i.e. 8.13 MW as compared to 5.3 MW for ESW. This is measured with the enthalpy load of Q3 heat line of the heat exchanger (H2), as shown in Fig. 7.11. However, the higher LHV of the generated syngas can balance this energy penalty to a greater extent by the high temperature attained in the plasma gasifier that converts higher hydrocarbons and toxic by-products to low molecular combustible fractions of the syngas (Kim et al., 2003).

The syngas composition (vol. %) obtained by the ESW-plasma gasification after the LTR (G5) block is 44.52% H_2, 42.49% CO, 0.88% CO_2 and 11.14% N_2 with a negligible fraction of CH_4. The higher value of N_2 is attributed to the high amount of nitrogen content in the ESW

fuel. This decreased the LHV of both the feed and syngas, affecting the process followed. Whereas the CKPW-based plasma gasification produced 56.73% H_2, 42.53% CO and 0.5% CO_2. The higher concentration of H_2 and H_2/CO ratio is mainly due to two reasons: (i) using steam as the gasifying agent favors the water-gas shift reaction (R12) and (ii) higher amount of energy accessible for conversion due to the application of plasma.

7.5.2. Sensitivity analysis

This section details the key functional parameters of the CLR system such as temperature, flow rate of syngas, OC, steam and air. The effect of these parameters on the composition of the outlet streams of each reactor is evaluated. It is performed by changing the specific parameter and keeping others fixed (Surywanshi et al., 2021; Yang et al., 2021). In the case of FR, the syngas flow rate is fixed on the basis of 100 MW of feed chemical energy and hence, the impact of the flow rate of OC (Fe_2O_3) is evaluated. Whereas in the SR and AR, by keeping the optimum flow rates of the reduced OC estimated in the FR as fixed, the steam and air flow rates are optimized. At the adiabatic conditions, the optimum temperature of the reactors is maintained at thermodynamic equilibrium with the excess supply of their inlet gases. As per stoichiometry, the excess percentage of OC, steam and air sent to the FR, SR and AR is estimated as 7%, 33% and 15%, respectively.

7.5.2.1. Effect of inlet syngas/Fe_2O_3 ratio in FR

In the FR, as the syngas reacts with the lattice oxygen provided by the OC (Fe_2O_3), the equilibrium of the reaction (R3) can be largely affected by the change in Fe_2O_3 mass flow rate. Fig. 7.14(a) and Fig. 7.14(b) present the gas and solid flow at the outlet of FR as a function of syngas to Fe_2O_3 ratio. The optimum mass ratio of the syngas/Fe_2O_3 is 0.063 (stoichiometric ratio is 0.069) with a Fe_2O_3 inlet flow rate of 65.87 kg/s and a syngas flow rate (4.16 kg/s). It is attributed to the total oxidation of syngas into CO_2 and H_2O, and the reduction of Fe_2O_3 to

FeO as per reaction R3. With a further increase in the Fe_2O_3 (OC) flow rate and a decrease in the ratios (syngas/Fe_2O_3), the FeO production decreases gradually and Fe_3O_4 emerges in the reactor. Therefore, the production of Fe_3O_4 may not be detrimental to the performance of FR but indirectly affects the SR, which is detailed in the next section. Additionally, the increased OC flow rate increased the conversion of syngas into CO_2 and H_2O in the product gas (Adanez et al., 2012). On the other hand, the operating temperature of the FR as shown in Fig. 7.14(b), shows a uniform rising trend with an increase in the OC flow rate till it reaches the optimal ratio (0.063). The temperature further increases beyond the optimal ratio due to the higher conversion of Fe_2O_3 into Fe_3O_4 than FeO, as given by the exothermic reaction R18 against R3.

$$H_2 + CO + 6Fe_2O_3 \rightarrow H_2O + CO_2 + 4Fe_3O_4 \qquad \Delta H^0_{298K} = -52.82 \text{ kJ/mol} \qquad \text{(R18)}$$

7.5.2.2. Effect of inlet steam/FeO in SR

As shown in Fig. 7.15, the mass ratio of steam to FeO is varied from 0.03 to 0.83. It is seen that H_2 (0.43-0.56 kg/s) gets continuously produced with an increase in the input steam flow rate and H_2O/FeO ratio. The H_2 reached the maximum (~17 vol.%) at the steam/FeO ratio of 0.5 (stoichiometric ratio is 0.37) for a constant FeO (59.27 kg/s) mass flow rate, with 29.85 kg/s of steam. In the meanwhile, FeO gets partially oxidized to Fe_3O_4 (63.67 kg/s) at the optimum ratios of steam/FeO and beyond these values, both the H_2 and solid flow at the outlet remain unchanged. Beyond the optimal point, the addition of excess H_2O decreases its conversion and increases the energy demand for producing the steam (Cormos et al., 2020). It is imperative to note that only FeO reacts with steam to produce H_2. The excess Fe_3O_4 from the FR hinders the steam-FeO reaction, which reduces H_2 production in the SR (Khan and Shamim, 2016). As the outlet stream consists of only H_2 and H_2O, the highly purified H_2 (100%) can be obtained by condensing H_2O. Also, the temperature of the SR decreases with

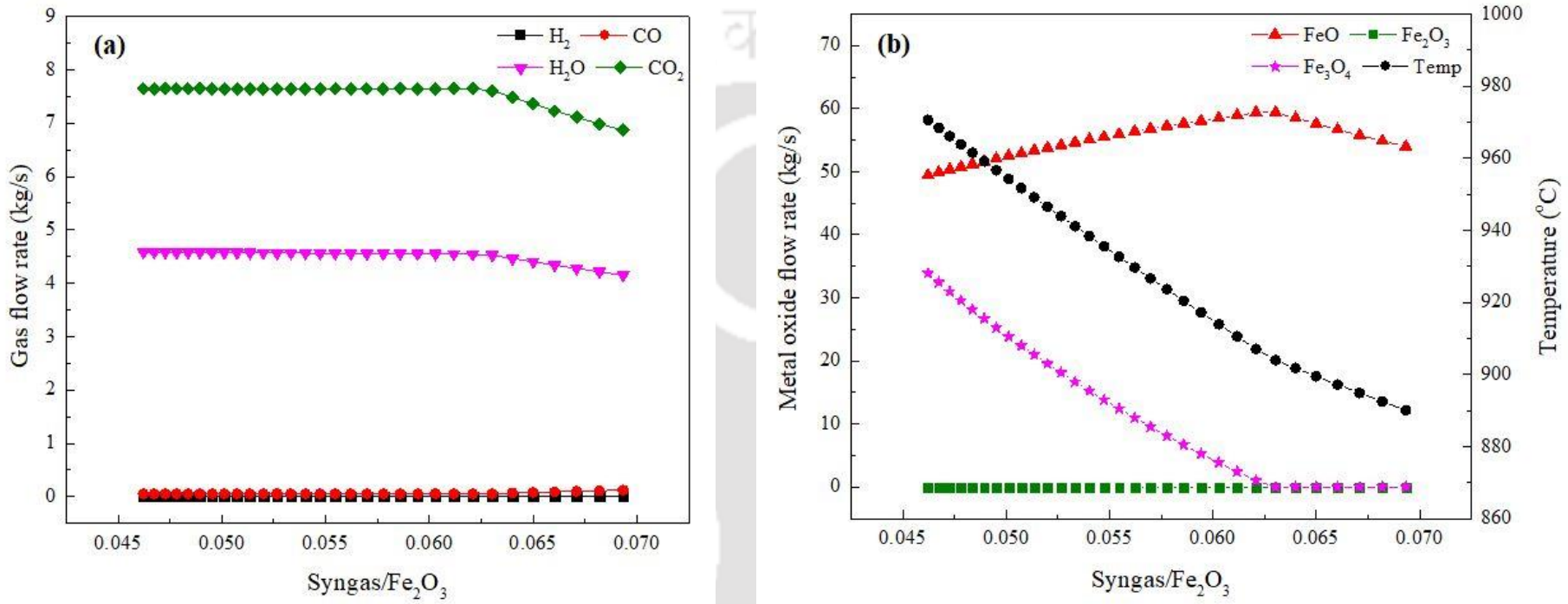

Fig. 7.14. Effect of syngas/Fe_2O_3 ratio on (a) gas flow rate and (b) solid flow rate and temperature in FR.

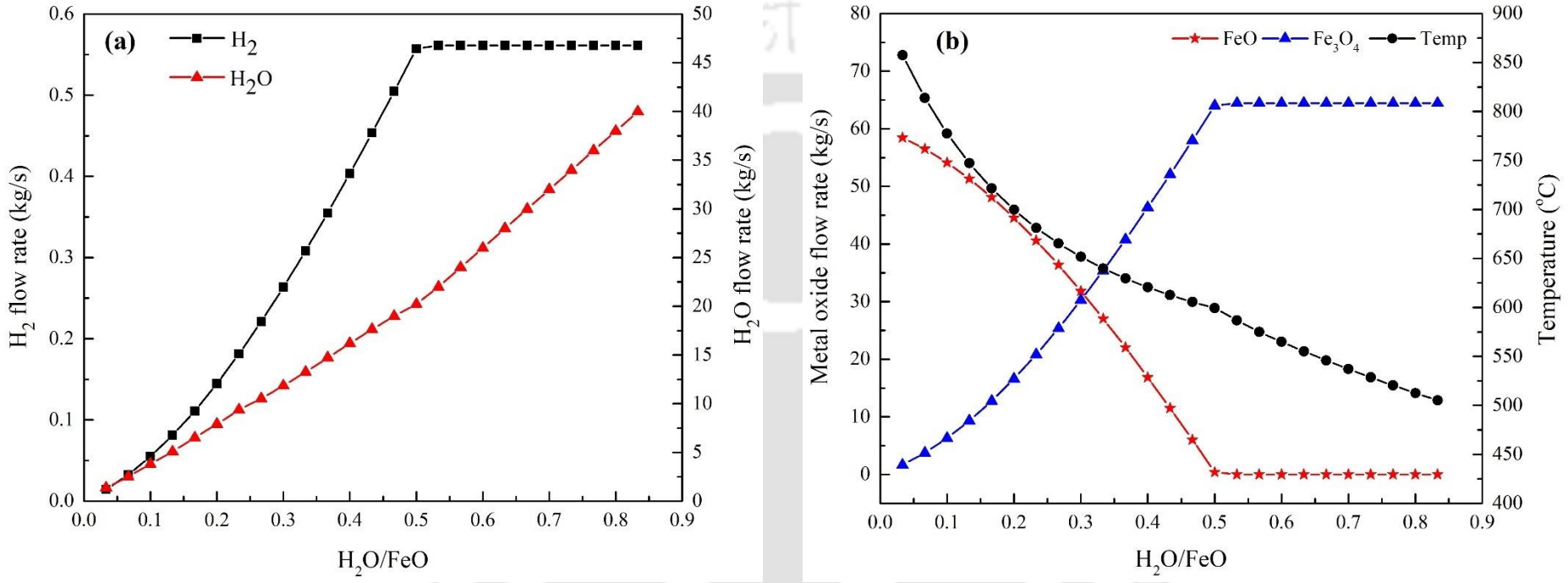

Fig. 7.15. Effect of H_2O/FeO ratio on (a) gas and (b) solid flow rate and temperature in SR.

an increase in the inlet steam/FeO ratio, as shown in Fig. 7.15(b), due to the large amount of thermal energy carried by the outlet H_2O.

7.5.2.3. Effect of inlet air/Fe_3O_4 in AR

This section illustrates the effect of the flow rate of inlet air on the composition of the outlet stream. The partially oxidized OC (Fe_3O_4) from SR undergoes complete oxidization in the AR and the Fe_2O_3 particles are recycled to the FR (Yang et al., 2021). From Fig. 7.16, it can be interpreted that up to air/Fe_3O_4 mass ratio of 0.188 (stoichiometric ratio is 0.169), the conversion of OC (Fe_3O_4 to Fe_2O_3) occurs due to the oxidation of Fe_3O_4 with O_2 in air. Beyond the optimal point of 0.188, the OC does not change and the O_2-depleted air leaves the stream. The temperature shows an increasing trend in Fig. 7.16 due to the exothermic nature of the reaction (R5) followed by the decreasing profile, which is attributed to the dilution of the outlet gas with excess O_2 i.e., all Fe_3O_4 converted into Fe_2O_3 (Khan and Shamim, 2016).

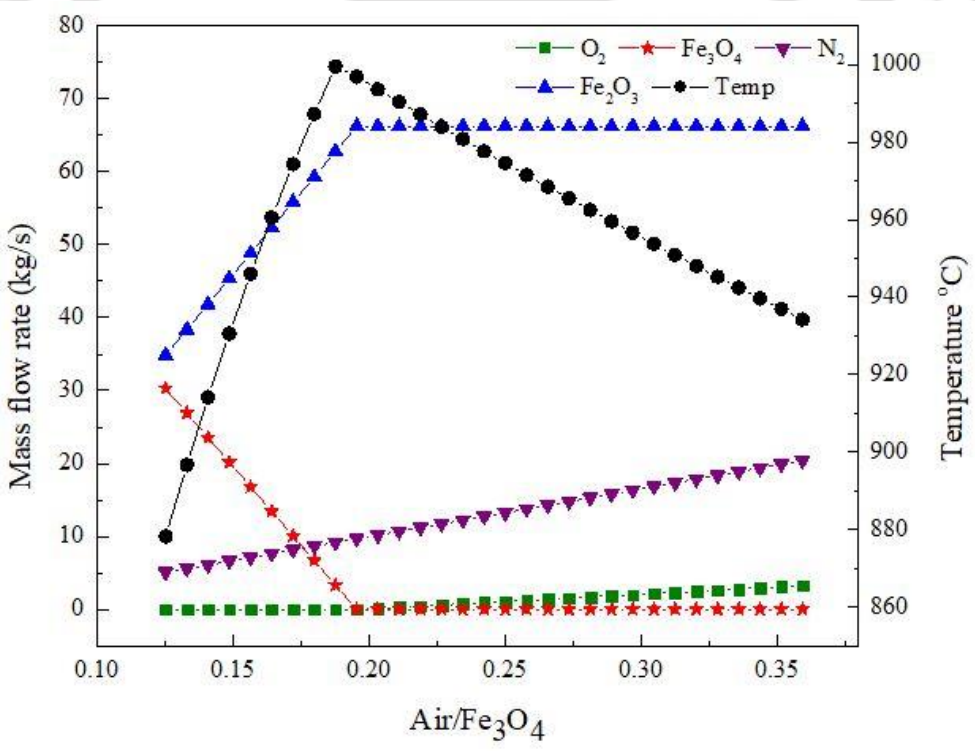

Fig. 7.16. Effect of air/Fe_3O_4 ratio on gas and solid flow rate, and temperature in AR.

7.5.3. 4-E analyses

A macro assessment of the IPGST-CLR and IPGCC-CLR system for the production of electricity and H_2 is carried out in this section. 4-E analyses of plant configurations operating at 1 bar (only steam turbine unit) and 15 bar (both gas and steam turbine unit) are conducted to assess the effects of excess OC, steam and air mass flow rate on the performance of the system.

7.5.3.1. Energy analysis

The thermodynamic performance of the IPGCC-CLR (15 bar) power plant for both feed is shown in Table 7.7. The gross power output is estimated to be 25.28 MW and 28.4 MW for ESW and CKPW, respectively. Among these, around 50% of electric power comes from the steam turbine (ST) and 30% from the gas turbine (GT) units. In the case of ESW, the power consumption for plasma generation, syngas and air compression ranges from 18-21% of gross power output, whereas for CKPW, it varies between 18 and 29%. The energy penalty due to CO_2 capture and compression (23.5% of gross power) is higher for ESW than CKPW (6.67%, only compression) due to the addition of the MEA absorption unit for separating the N_2 content (present inherently in the feed) from the flue gas. And the H_2 compression consumes nearly 4% of the gross power produced. Hydrogen exiting the steam reactor (0.52 kg/s for ESW and 0.554 kg/s for CKPW) has an LHV of 120 MJ/kg (Khan and Shamim, 2016), thus contributing 62.4 MW and 66.48 MW of energy output, respectively.

When the power plant operates at atmospheric pressure (IPGST-CLR), only the ST remains the standalone power generation unit. The results, as shown in Fig. 7.17 and 7.18, indicate a decrease in both the individual and overall efficiencies compared to the combined cycle system (base case i.e. 0% excess OC or air). Though the only ST in this cycle produces higher electric power than the ST of the combined cycle, the net electric power is slightly lower by 2.02 MW for ESW and 2.8 MW for CKPW due to the influence of gas turbine (GT) and air turbine (AT).

The small reduction in H_2 output is because of the lesser amount of oxidant required from OC (Fe_2O_3) in the FR at 1 bar to burn the syngas and therefore, less FeO available for reaction with steam as described in Section 7.5.2.

Table 7.7

Thermodynamic performance of the IPGCC-CLR plant.

Feed		ESW	CKPW
Parameter	Units		
Fuel flow rate	kg/s	7.12	2.83
Fe_2O_3 flow rate	kg/s	57.2	65.87
Plasma power consumption	MW	5.3	8.13
Syngas compression	MW	5.25	5.35
Air compression	MW	4.67	5.24
CO_2 compression	MW	5.95	1.9
H_2 compression	MW	1.09	1.26
Auxiliaries consumption	MW	0.5	0.65
Gas turbine power output	MW	7.56	7.71
Air turbine power output	MW	4.96	5.74
Steam turbine power output	MW	12.76	14.95
Gross power output	MW	25.28	28.4
Hydrogen output	MW	62.4	66.48
Net system electrical output	MW	2.52	5.87
Hydrogen efficiency	%	62.4	66.48
Net electrical efficiency	%	2.52	5.87
Overall energy efficiency	%	64.92	72.35

In Fig. 7.17 and Fig. 7.18, a comparison of the net energy and exergy efficiencies of IPGCC-CLR for both feeds based on excess OC and air is shown. The percentage of excess OC is changed from 0-30%. As per stoichiometry, 7% excess OC is required for the complete conversion of syngas. The increase in the flow rate of OC increases the electrical power output

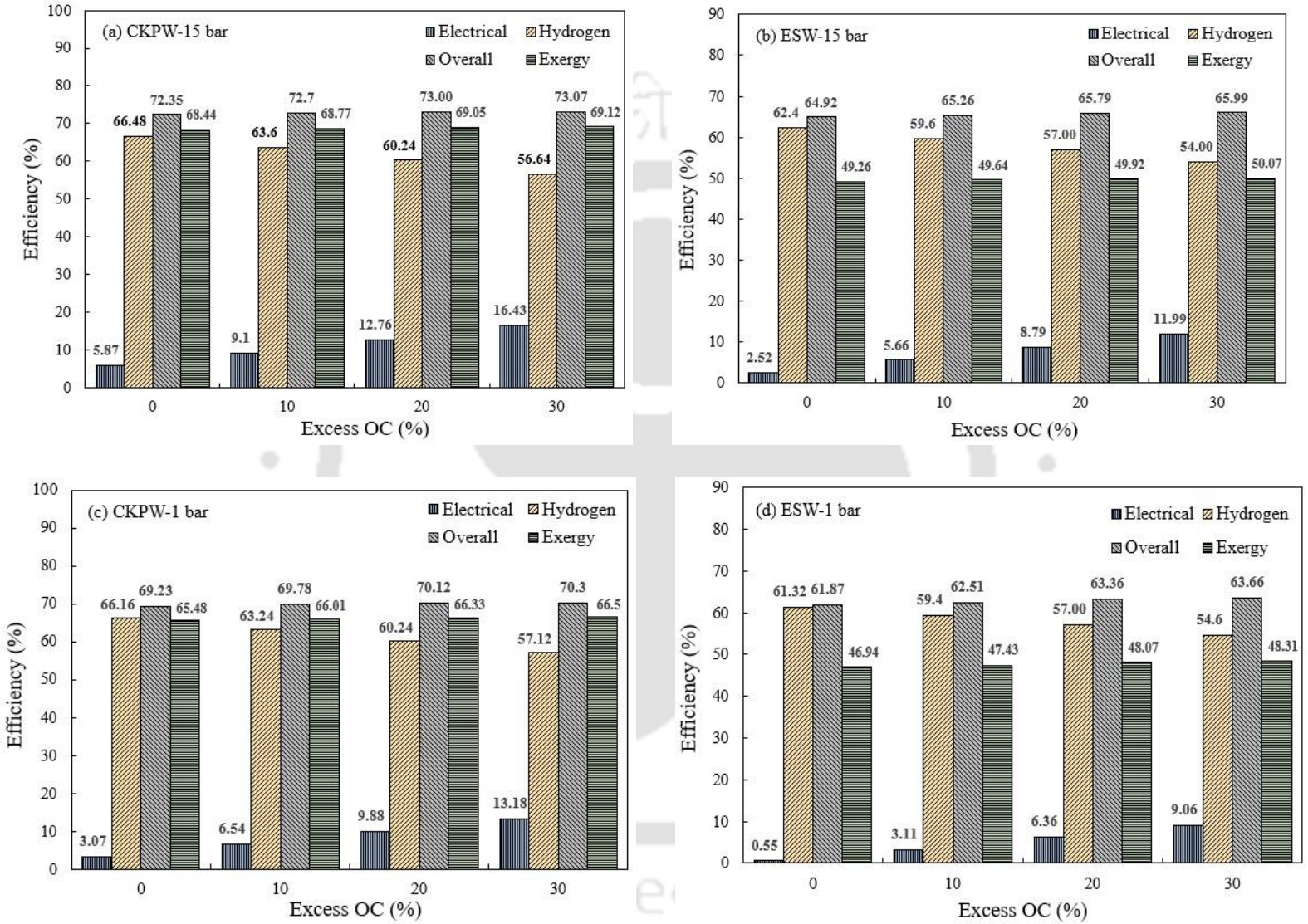

Fig. 7.17. Net energy and exergy efficiencies of IPGCC and IPGST-CLR plant as a function of excess OC for (a), (c) CKPW and (b), (d) ESW.

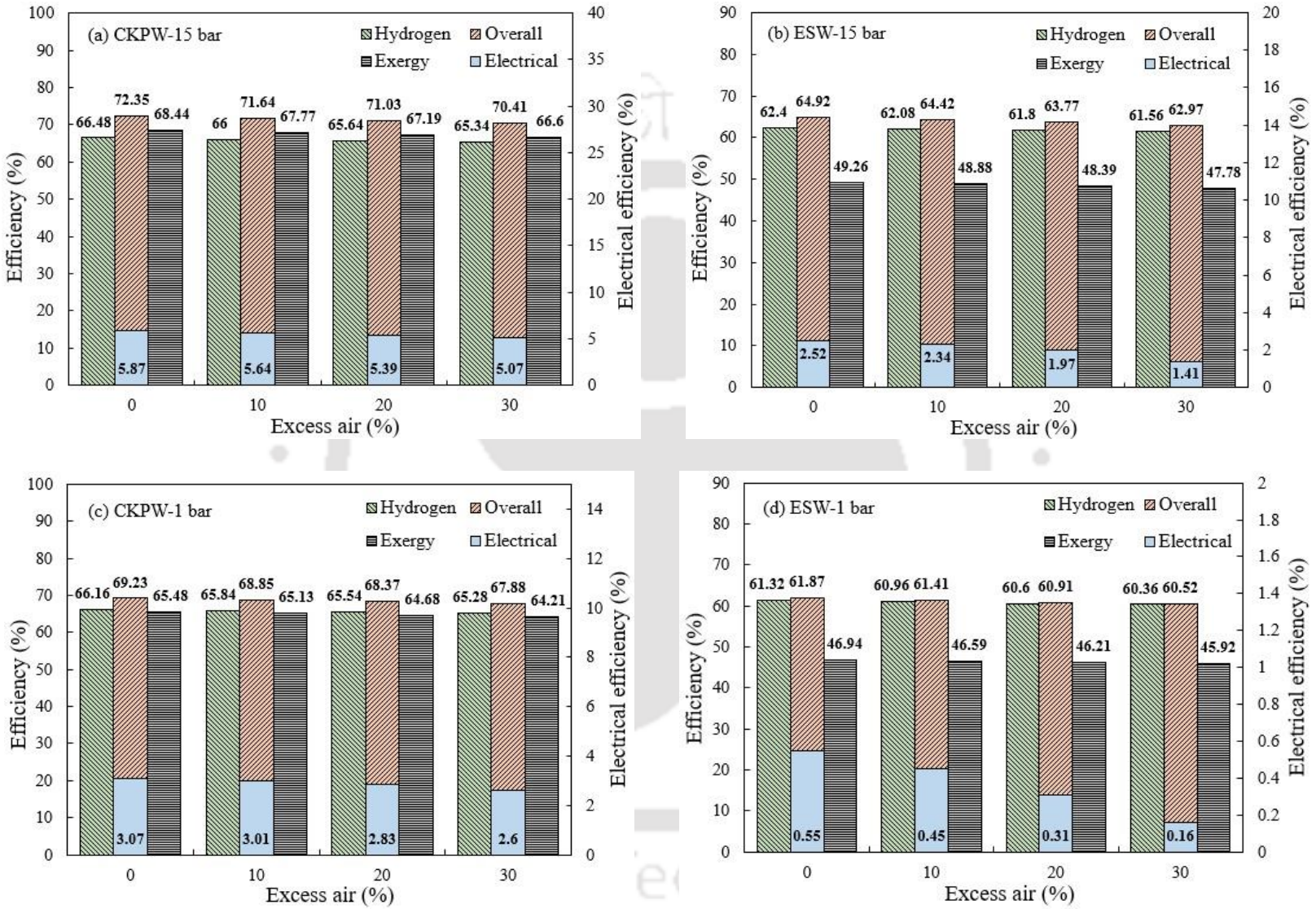

Fig. 7.18. Net energy and exergy efficiencies of IPGCC and IPGST-CLR plant as a function of excess air for (a), (c) CKPW and (b), (d) ESW.

from the gas turbine in the case of IPGCC-CLR. Further, a higher OC flow rate increases the reactor temperature and hence, a large amount of steam is produced for power production in the case of IPGST-CLR. On the other hand, the hydrogen output decreases due to the higher production of Fe_3O_4 than FeO, which does not participate in the reaction to produce H_2. This effect can be understood from Fig. 7.14(b) and reaction R4. Nonetheless, the overall efficiency increases with the excess OC due to the production of higher electrical power than the decrease in the production rate of H_2. It is found that 15% excess OC to that of the stoichiometric amount is required for the complete oxidation of Fe_3O_4 to Fe_2O_3.

A large amount of the inlet air dilutes the concentration of outlet gases in the AR and eventually reduces the temperature as seen in Fig. 7.16. This results in a reduction in the electrical power output from both the air and steam turbines. Moreover, the effect of high temperature in the AR accelerates the production rate of FeO in the FR and subsequently, a higher H_2 production in the SR is estimated. High temperature is essential in FR due to the endothermic nature of the FeO formation. The excess air inlet in the AR causes a low outlet stream temperature, which affects the equilibrium state of FR. This results in the incomplete conversion of the syngas in the FR with an overall lower energy output. Thus, the overall efficiency decreases with the increase in the air flow rate due to the reduction in both electrical power and H_2 output, as shown in Fig. 7.18. It can be interpreted that the temperature in AR plays a vital role in maintaining the energy balance of the entire. The exergy efficiencies follow a similar increasing and decreasing trend, respectively, when related to the overall energy efficiencies with an increase in the OC and air mass flow rates. This is attributed to the strong dependence of the exergy efficiency on the net overall output, as stated in Table 3.4.

An analysis of the power plant co-generating 50% and 10% H_2 (i.e. 31.2 MW and 6.24 MW for ESW) with the rest of the energy available for the production of power is conducted as shown in Table 7.8. This variation is done to address the flexible performance of co-generation.

It is found that despite the decrease in net electrical efficiency with an increase in hydrogen output, the overall efficiency increases. Therefore, it is more advantageous to utilize the chemical energy content in H_2 as a clean fuel than using the thermal energy for power production with minimal loss (Cormos et al., 2020).

7.5.3.2. Exergy analysis

In this section, the exergy destruction rate is estimated for individual major components of the plant configurations. There are insignificant changes in the overall exergy efficiencies under the influence of OC, steam and air mass flow rate from the base case (100% H_2) for both the feedstocks, as shown in Fig. 7.17 and Fig. 7.18. The calculations based on the flexible co-generation of H_2 (50% and 10%) are carried out. Fig. 7.19 displays the percentage contribution of exergy destruction rate for all the individual units of the IPGCC-CLR and IPGST-CLR plant system.

Exergy destruction rate is estimated individually for all the reactors involved in the power system. Irrespective of the process, the plasma gasifier (21.33 MW for ESW and 8.61 MW for CKPW) contributes the largest proportion to the overall exergy destruction, followed by the fuel reactor (14.58 MW for ESW and 9.58 MW for CKPW) and air reactor (6.88 MW for ESW and 4.19 MW for CKPW). This is in alignment with the results of Surywanshi et al., 2021, where the highest destruction rate is achieved in the boiler unit (a combination of air, steam and fuel reactors along with HRSG). It can be attributed to the irreversibilities caused by the reactions and heat transfer processes (Surywanshi et al., 2019). For ESW, an additional increase in exergy destruction rate is due to the presence of N_2 in the fuel, which does not participate in the reaction and dilutes the overall process (Dincer and Rosen, 2021). The net exergy efficiencies deviate negatively by 8-16%, compared to the energy efficiencies for ESW and 2-4% for CKPW. Thus, the exergy destruction rate can be minimized by changing some

Table 7.8

Comparison of 4-E analysis based on hydrogen output for IPGCC-CLR.

Feed		ESW			CKPW		
Parameter	Units	10% H_2	50% H_2	100% H_2	10% H_2	50% H_2	100% H_2
Energy analysis							
Net electrical efficiency	%	29.54	22.25	2.52	41.37	30.10	5.87
Hydrogen efficiency	%	6.24	31.20	62.40	6.65	33.24	66.48
Overall energy efficiency	%	35.78	53.45	64.92	48.02	63.34	72.35
Exergy analysis							
Overall exergy efficiency	%	27.15	40.55	49.26	45.42	59.92	68.44
Economic analysis							
COE	$/MWh	192	133.73	108	110.47	87.57	73.19
LCOH	$/kg	24.97	4.87	2.25	15.57	3.01	1.30
CO_2 avoided cost	$/$ton_{CO2}$	78.45	63.97	51.75	22.76	21.17	20.16
CO_2 removal cost	$/$ton_{CO2}$	65.78	56.55	46.63	23.90	22.43	21.45
Environmental analysis							
Annual CO_2 avoided per unit fuel	kg_{CO2}/GJ	69.44	69.44	69.44	75.94	75.94	75.94
Sustainability Index	--	1.37	1.68	1.97	1.83	2.50	3.17

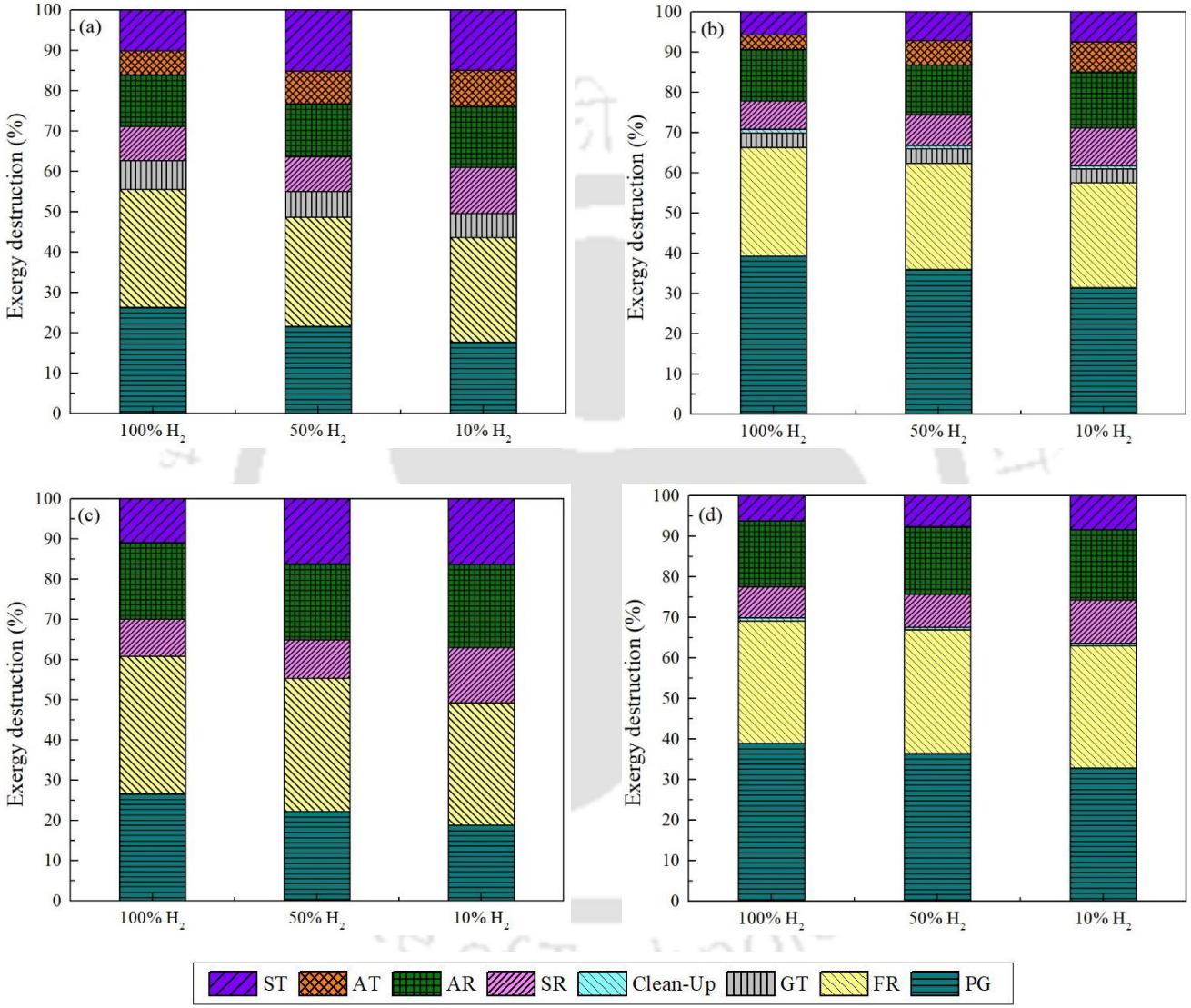

Fig. 7.19. Exergy destruction of various components for IPGCC-CLR (a) CPKW, (b) ESW and IPGST-CLR (c) CKPW, (d) ESW.

parameters such as operating conditions, higher LHV fuels, etc. However, the lowest destruction rate is for 100% H_2 case, when compared to 50% and 10% production of H_2 as shown in Fig. 7.19. This is due to the higher chemical energy flow of hydrogen stream from the SR. It can be seen in the net overall energy and exergy efficiencies in Fig. 7.17. Hence, it is beneficial to integrate with the maximum co-generation of hydrogen.

7.5.3.3. Economic assessment

The results of total equipment cost (TEC), specific total plant cost, COE, LCOH, etc. with H_2 and power generation and the effects of the OC and air flow rates are detailed in this section. Table 7.8 gives a complete analysis of the variation in COE and LCOH under the influence of co-generation. As discussed in Section 7.5.3.1, the same observation is noticed in economic assessment i.e. COE and LCOH values increase with a decrease in H_2 production. The value of LCOH increases around 10 times for the feed scenarios, changing the H_2 production from 100% to 10%, whereas for COE, it increases by 150-180%. The lowest COE (108 $/MWh for ESW and 73.19 $/MWh for CKPW) and LCOH (2.25 $/kg for ESW and 1.3 $/kg for CKPW) value is found for the case of feedstock utilized for 100% production of H_2. In both the cases of COE and LCOH, the benefit of H_2 generation is prominent as compared to electricity generation in terms of the overall energy production. Additionally, the right choice of fuel can avoid the CO_2 removal unit, which can also reduce the total cost significantly (Khan and Shamim, 2016). The COE (95.22 $/MWh for ESW and 59.77 $/MWh for CKPW) and LCOH (1.79 $/kg for ESW and 0.86 $/kg for CKPW) values under atmospheric pressure i.e.,1 bar for 100% H_2 are even more substantial when compared to literature COE value of 67.06 $/MWh (Cormos et al., 2020) and LCOH of 1.66 $/kg (Khan and Shamim, 2019).

The economic performance of all the cases considering the influence of excess OC and air is compared in terms of COE and LCOH. Fig. 7.20(a) and 7.20(b) present the COE and LCOH

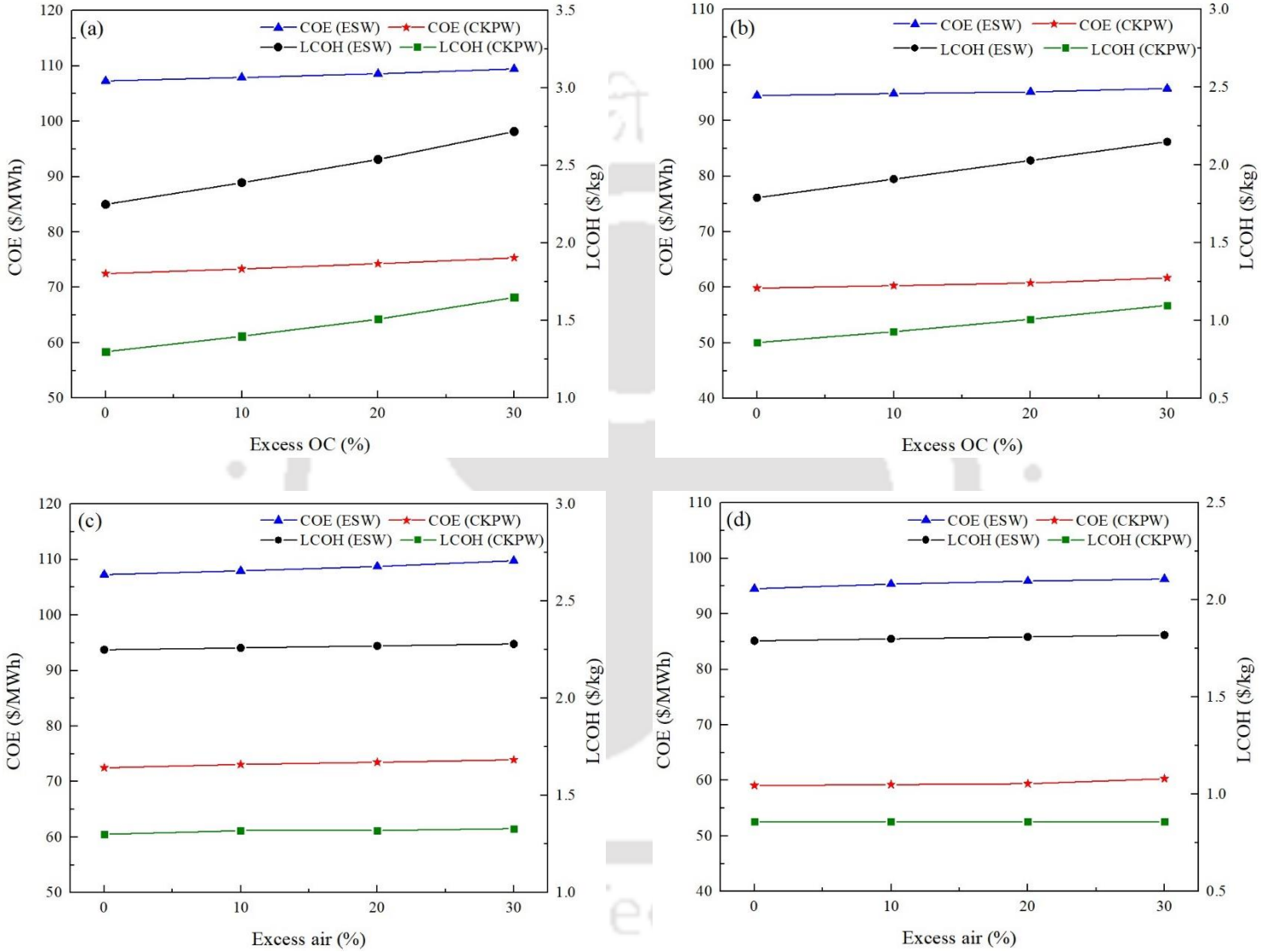

Fig. 7.20. COE and LCOH as a function of excess OC and air for (a), (c) IPGCC-CLR and (b), (d) IPGST-CLR.

values based on the supply of excess OC at 15 bar and 1 bar, respectively. The COE increases in both the scenario of increase in pressure despite the increase in the electric power output, which might be insufficient. However, the increase in LCOH values is more pronounced due to the reduction in H_2 flow from the SR. Whereas, in the case of excess air, the changes in both COE and LCOH show a slightly increasing trend as shown in Fig. 7.20(c) and 7.20(d) because of the decrease in overall energy output.

7.5.3.4. Environmental analysis

The reason for integrating plasma gasification and CLR technology lies in the fact that both processes reduce the negative impact on the environment by minimizing emissions. It can be justified with the values in Table 7.9, where the specific CO_2 emission rate remains between 38 and 69 $/MWh with all the cases for ESW. These values are less than many of the reported values in the literature based on other technologies (Duan et al., 2015; Singh et al., 2017). The higher emission value is found for the 10% H_2 production case, where the net energy output is lower. Whereas for CKPW, these values are zero as all the CO_2 is captured and stored. The annual CO_2 emission and captured are around 1.85×10^7 kg and 1.87×10^8 kg, respectively for ESW, and the annual CO_2 captured for CKPW is 2.05×10^8 kg. The global warming potential (GWP) is around 2450 $kgCO_{2eq}/h$ for ESW and zero for CKPW. The sustainability index (SI) is estimated in the range of 1.3-2 for ESW and 1.8-3.23 for CKPW for all the cases analyzed in the above-mentioned sections. It is clear that using the CKPW feed is more ecological than ESW because of its higher values reflecting a clean and green process.

7.5.3.5. Overall analyses

The results obtained from the analysis of key working parameters (optimum gasifying agent flow rate for maximum fuel conversion in plasma gasifier, feed ratios and temperature of individual CLR reactors) are considered for 4-E analyses to improve system performance. In

Table 7.9

Ecological assessment comparison based of (a) ESW and (b) CKPW feed for IPGCC-CLR system.

Feed	ESW			CKPW		
Parameter	10% H_2	50% H_2	100% H_2	10% H_2	50% H_2	100% H_2
Specific CO_2 emission rate [kg/MWh]	68.14	46.14	38.1	-	-	-
Annual CO_2 emission [x 10^7 kg]	1.83	1.84	1.85	-	-	-
Annual CO_2 captured [x 10^8 kg]	1.85	1.86	1.87	2.03	2.04	2.05
Average annual CO_2 emission per unit fuel [kg/GJ]	6.77	6.83	6.87	-	-	-
Annual CO_2 avoided per unit fuel [kg/GJ]	68.48	69.03	69.44	75.03	75.51	75.94
Net energy output/CO_2 captured [MW/kg]	5.23	7.74	9.35	6.40	8.39	9.53
Global Warning Potential [$kgCO_{2eq}$/h]	2438.10	2458.80	2473.20	-	-	-
Sustainability Index	1.37	1.68	1.97	1.83	2.50	3.17

addition, the comparison studies for flexible hydrogen and electric power (100%, 50% and 10% H_2) co-generation based on 4-E are performed. Maximum H_2 production is favorable for superior overall thermodynamic efficiency, reduced cost and environmental benefits. The most preferred inlet mass feed ratio in the FR, SR and AR for the case of 100% H_2 are found as 0.063, 0.5 and 0.188, respectively, while the operating temperatures are maintained at 900 °C, 600 °C and 1000 °C, respectively for CKPW feedstock. Under these conditions, highly purified H_2 can be produced with the maximum overall energy (72.35%) and exergy (68.44%) efficiency, lower COE (73.19 $/MWh) and LCOH (1.3 $/kg) and highest sustainability index of 3.17. In the case of ESW feedstock, the optimum mass feed ratio is 0.13, 0.54 and 0.18 in the FR, SR and AR, respectively. The operating temperature of SR (598 °C) and AR (997 °C) drops slightly compared to the case of CKPW. Moreover, the thermodynamic efficiency decreases by around ~3 % for the IPGST-CLR plant than that of operating under high pressure (IPGCC-CLR), but the COE is the lowest for IPGST-CLR (CKPW feed) in the entire plant. Irrespective of the feedstock, increasing the excess OC (0-30%) increases the overall efficiency by ~ 1% but on the other hand, the COE also increases by 1.36%. In the case of increasing excess air, the decrease in the overall efficiency resulted in a higher COE by 1.65%.

7.6. Conclusions

The present study critically evaluated the integration of plasma gasification with the CLR system considering two types of contrasting fuel (ESW and CKPW) based on LHV, operating under high (15 bar) and atmospheric (1 bar) pressure levels. The variation in outlet gas and solid flow and temperature with key parameters such as the ratio of OC with syngas, steam and air mass flow rates from the three reactor systems is investigated. A 4-E (energy, exergy, economic and environmental) analyses is conducted to assess the overall performance of all the cases, such as flexible power and H_2 co-generation, effects of excess OC and air mass flow rate. Here are the following observations:

- Under the application of high-temperature plasma gasification, a higher amount of H_2 and CO (85 vol.% for ESW and 94.25 vol.% for CKPW) with an H_2/CO ratio of 1.04 for ESW and 1.34 for CKPW can be obtained.
- The optimum operating temperature from the sensitivity analysis based on the changes in the ratio of syngas, steam and air mass flow rate, and OC is found to be around 900 °C, 598 °C and 1000 °C for FR, SR and AR, respectively. At these ratios, highly purified H_2 (100%) is produced with maximum metal oxide conversion observed in the outlet gas and solid outlet flow stream.
- The highest net overall energy efficiency is obtained in the case of IPGCC-CLR (72.35%) than IPGST-CLR (69.22%) system with CKPW feed for 100 % H_2. However, the increase in the excess OC in the FR to 130% can increase the efficiency further to 73.07% for IPGCC-CLR and 70.3% for IPGST-CLR. Plasma power remains to be on the higher side of energy penalty for all the different power plant scenarios and the CO_2 removal section accounts for an additional penalty for ESW feed.
- The net overall exergy efficiency is lower by ~ 16% for ESW and ~ 4% for CKPW than their corresponding overall energy efficiency for all the plant scenarios. The plasma gasifier has the largest exergy destruction percentage of 31-40% for ESW and fuel reactor (25-29%) in the case of CKPW. These are due to the irreversible nature of the chemical reactions taking place with a higher amount of N_2 in the fuel.
- Although the net overall energy efficiency is lower for the IPGST-CLR than the IPGCC-CLR system, the reverse trend is observed in the economic analysis. The lowest COE (59.77 $/MWh) and LCOH (0.86 $/kg) are obtained in the case of the IPGST-CLR system using CKPW feed. Further, the cost of CO_2 avoided and removal has reached a maximum value of 57.87 $/ton$_{CO2}$ and 53.10 $/ton$_{CO2}$, respectively, for ESW feed in the IPGCC-CLR system.

- All the power plant cases are environmentally viable based on the estimated data. The specific CO_2 emission rate and annual CO_2 emission are lower than that of the conventional gasification process, whereas the higher sustainability index for both feed suggests a good environmental fitness of the overall process.

Therefore, based on the 4-E analyses, the utilization of waste as feed in novel plasma gasification integrated with CLR technology has the potential for commercialization provided the selection of higher LHV fuel, better syngas quality and maximum H_2 production. The energy consumption burden of plasma gasification can be reduced by handling fuel with low moisture content and high LHV. Integrating with a CLR system for the co-generation of H_2 and electric power enhances overall efficiency with low product cost and better environmental outcomes. On the other hand, the high temperature inside the plasma gasifier prohibits the use of the direct-CLR process i.e., the generation and combustion of syngas with OC in the plasma gasifier due to the melting of OC at such temperatures. This creates an additional cost for a separate reactor along with the energy-intensive plasma gasifier.

Chapter 8

Conclusions & Future scope

CHAPTER 8

CONCLUSIONS AND FUTURE SCOPE

This chapter draws the overall conclusions of the present study on the plasma gasification process, including the experimental and simulation work. In addition to that, some recommendations regarding the future scope of research are also illustrated.

8.1 Overall Conclusions

From the overall analyses on plasma gasification of the complex waste feedstocks such as refused derived fuel (RDF), computer keyboard plastic waste (CKPW) and electrical switch waste (ESW), the major conclusions are as follows:

- The plasma gasification of CKPW using CO_2 as a plasma gas has the maximum gas yield of 96.55% at 40 g/10 min, 0.7 lpm of CO_2 flow rate and 1.12 kW among all the experimental results. While the oil yield and the residue yield (including ash of 14 wt.%) of 10.19% and 27.27% are obtained for CKPW at 60 g/10 min (keeping the other two parameters constant) and RDF at 0.5 kW, respectively. If the ash content is ignored, ESW has the lowest feed conversion (~71%).
- The syngas with the highest percentage of H_2 (42.6 vol.%) and CO (51.98 vol.%) can be attained for RDF and CKPW feed, respectively. Correspondingly, at the highest torch power of 2 kW utilizing CKPW feedstock, the LHV of 16.46 MJ/m^3 is obtained. Due to the high hardness and superior thermo-oxidative property of the ESW feed, a maximum value of H_2 (24.36 vol.%), CO (43.61 vol.%) and product gas yield (84.58%) is reached. A medium LHV of 6.16-10.20 MJ/m^3 is found for all ESW feed cases.
- The highest cold gas efficiency (CGE) of 49.90% and exergy efficiency of 48.30% (Case 2) can be achieved in the RDF-plasma process and the lowest CGE (42.33%) and

exergy efficiency (38.99%) is for ESW feed. However, the system's overall efficiency may rise up to 90% with proper recovery of the losses in terms of sensible heat, the energy contained in cooling water, etc., are considered. Further, the lowest levelized cost of syngas (LCOS) value of 23.40-35.24 INR/kWh is estimated for CKPW feed and the highest (40.91-62.44 INR/kWh) for ESW. This indicates the strong influence of torch power on the energy output using complex plastics such that thermodynamic efficiencies are maximized and LCOS is reduced.

- The characterization of the oil product obtained from the CKPW feed showed physicochemical properties similar to diesel, with higher carbon, hydrogen and LHV (39.13 MJ/kg) values and lower oxygen (0.46 wt.%) content. Added reduction in viscosity (3.93 cP) and density (910 kg/m^3), a slight improvement in pH (6.94) and LHV of the CKPW-based oil are beneficial to avoid engine damage. From the residue of all feeds, large amounts of Ti, Ba, Ca, Si, Al and Fe (excluding O) can be recovered for application in healthcare, paints, dye-casting and the cement industry.
- The established quantitative correlation between the dependent and independent variables presented a concurrence among the actual and measured values. The minimum and maximum error of 0.85% and 21% is estimated for CGE using CKPW and RDF, respectively. This exercise provides a basic idea of estimating the output variables from a plasma gasification process.
- Based on the simulation study, the condition of high temperature inside the plasma gasifier (1250-2500 °C) laterally with the correct proportion of gasifying agent (steam and O_2), the conversion degree of the process maximized to produce ~1.8:1 ratio of H_2/CO irrespective of the feed.

- The sensitivity analysis showed that the IPGCC-CLR system using CKPW feed requires an optimal mass ratio of syngas/Fe_2O_3 of 0.063, steam/FeO of 0.5 and air/Fe_3O_4 of 0.188 for the production of highly purified H_2 (100%) of 0.554 kg/s.
- The IPGST-MCFC system with additional CH_4 i.e. Syngas:CH_4 (PSA: MCFC) ratio has the highest net energy efficiency of 54.12%, followed by the IPGST-MCFC [0:100] ratio of 51.28%. However, for an IPGCC-CLR plant, the efficiency can increase up to 72.35% and IPGST-CLR to 69.22% with CKPW feed. The major reason for achieving such high efficiency is the production of a high amount of H_2 (100%) with less energy penalty for the CLR system. Plasma power remains to be on the higher side of the energy penalty (6-22%) for all the different plant scenarios and the CO_2 removal section adds an extra penalty for ESW feed.
- Plasma gasifier, followed by the combustor in MCFC and the fuel reactor in the CLR unit, has the largest exergy destruction rate due to the irreversible nature of the reaction. This reduces the net exergy efficiency of the overall plant to 2.1-2.56% for RDF, ~ 4% for CKPW and ~ 16% for ESW.
- The economic analysis indicated a higher specific total plant cost of a maximum of 6432.38 $/kW and a lower COE of 77.48 $/MWh for the IPGST-MCFC plant using RDF, while the LCOH value is 1.01 $/kg. The lowest COE (59.77 $/MWh) and LCOH (0.86 $/kg) are obtained in the case of the IPGST-CLR system using CKPW feed. Further, the cost of CO_2 avoided increases to a maximum of 81.46 $/ton CO_2 despite a higher amount of CO_2 absorption in MCFC.
- All the co-generation plant cases are environmentally viable based on the estimated data. Also, the specific CO_2 emissions rate of 19.66 – 91.65 kg/MWh for the IPGST-MCFC plant is much lower than most of the conventional gasification processes.

Similarly, the higher sustainability index for all the feed suggests a good environmental finding of the overall process.

Based on the results obtained from the experimental studies and the performance analysis of the MCFC and CLR system based on the key working parameters (for maximum fuel conversion in plasma gasifier), plasma gasification of CKPW is the most preferred route for clean energy generation. Although the LHV of CKPW based syngas is 2 MJ/m^3 (average) greater than that obtained from the RDF, the energy efficiency (CGE) is found 3% lower for CKPW based plasma system. Considering the ESW feed, the input plasma energy is comparable to the RDF process, but the thermosetting behavior of the ESW plastics resulted in lower LHV of syngas and CGE.

Exploring the waste generation scenario, the world generates around 1.68 billion tonnes of RDF (80% of MSW) every year and this is more than 30 times as compared to e-waste generation (60 million tonnes). Only 19% of RDF is recycled while that of CKPW (mainly consist of ABS) is 25%. When related to CO_2 generation, higher elemental carbon in the CKPW feed produces 10 times more CO_2 than the RDF. Therefore, based on the availability of feedstock and kg of CO_2 emissions annually (considering same co-generation systems), RDF is a highly suitable feed for clean and efficient energy production via plasma gasification.

8.2. Future Scope

The future scope of research offers to improve the performance of the plasma gasification process such that waste-to-energy conversion becomes a feasible route. Hence, the following studies can be carried out further:

- Higher capital costs and small-scale operations lower the rate on investment in any process. A comprehensive analysis of incorporating the energy losses into different streams to estimate overall efficiencies and LCOS can be considered.

- The kinetic behavior of the plasma gasification process can be studied to determine the activation energy and rate constants for individual reactions. This intends to predict the stages of feed conversion using different reaction models.
- The impact of in-situ catalytic activity of high ash feedstocks or ex-situ application of catalyst at low plasma power on the syngas composition can be undertaken.
- Residue with a high carbon content that includes hard thermoset feed can be examined further using different physical and chemical methods (pH, electrical conductivity, etc.) and characterization techniques (BET, Hg Porosimetry, etc.) for potential applications as adsorbents, composite additive in the steel industry, etc.
- The feasibility of plasma gasification of the above feedstocks using CO_2 can be studied for chemical production.
- Life cycle assessment (LCA) of the plasma gasification process is essential to state the environmental aspects of the method in terms of global warming, toxicity, eutrophication and acidification potential.

Adams, T.A., Hoseinzade, L., Madabhushi, P.B., Okeke, I.J., 2017. Comparison of CO_2 capture approaches for fossil-based power generation: Review and meta-study. Processes 5. https://doi.org/10.3390/pr5030044

Adanez, J., Abad, A., Garcia-Labiano, F., Gayan, P., De Diego, L.F., 2012. Progress in chemical-looping combustion and reforming technologies. Prog Energy Combust Sci. https://doi.org/10.1016/j.pecs.2011.09.001

Agon, N., Hrabovský, M., Chumak, O., Hlína, M., Kopecký, V., Mašláni, A., Bosmans, A., Helsen, L., Skoblja, S., Van Oost, G., Vierendeels, J., 2016. Plasma gasification of refuse derived fuel in a single-stage system using different gasifying agents. Waste Management 47, 246–255. https://doi.org/10.1016/j.wasman.2015.07.014

Ahmad, Nauman, Ahmad, Nabeel, Maafa, I.M., Ahmed, U., Akhter, P., Shehzad, N., Amjad, U. e. salma, Hussain, M., 2020. Thermal conversion of polystyrene plastic waste to liquid fuel via ethanolysis. Fuel 279. https://doi.org/10.1016/j.fuel.2020.118498

Akhtar, A., Krepl, V., Ivanova, T., 2018. A Combined Overview of Combustion, Pyrolysis, and Gasification of Biomass. Energy and Fuels. https://doi.org/10.1021/acs.energyfuels.8b01678

Alipour Moghadam, R., Yusup, S., Azlina, W., Nehzati, S., Tavasoli, A., 2014. Investigation on syngas production via biomass conversion through the integration of pyrolysis and air–steam gasification processes. Energy Convers Manag 87, 670–675. https://doi.org/10.1016/j.enconman.2014.07.065

Anca-Couce, A., 2016. Reaction mechanisms and multi-scale modelling of lignocellulosic biomass pyrolysis. Prog Energy Combust Sci. https://doi.org/10.1016/j.pecs.2015.10.002

Aneke, M., Wang, M., 2015. Potential for improving the energy efficiency of cryogenic air separation unit (ASU) using binary heat recovery cycles. Appl Therm Eng 81, 223–231. https://doi.org/10.1016/j.applthermaleng.2015.02.034

Areeprasert, C., Khaobang, C., 2018. Pyrolysis and catalytic reforming of ABS/PC and PCB using biochar and e-waste char as alternative green catalysts for oil and metal recovery. Fuel Processing Technology 182, 26–36. https://doi.org/10.1016/j.fuproc.2018.10.006

Arena, U., 2012. Process and technological aspects of municipal solid waste gasification. A review. Waste Management 32, 625–639. https://doi.org/10.1016/j.wasman.2011.09.025

Arif, M., Li, Y., El-Dalatony, M.M., Zhang, C., Li, X., Salama, E.S., 2021. A complete characterization of microalgal biomass through FTIR/TGA/CHNS analysis: An approach for biofuel generation and nutrients removal. Renew Energy 163, 1973–1982. https://doi.org/10.1016/j.renene.2020.10.066

Assad Munawar, M., Hussain Khoja, A., Hassan, M., Liaquat, R., Raza Naqvi, S., Taqi Mehran, M., Abdullah, A., Saleem, F., 2021. Biomass ash characterization, fusion analysis and its application in catalytic decomposition of methane. Fuel 285, 119107. https://doi.org/10.1016/j.fuel.2020.119107

Ayol, A., Tezer Yurdakos, O., Gurgen, A., 2019. Investigation of municipal sludge gasification potential: Gasification characteristics of dried sludge in a pilot-scale downdraft fixed bed gasifier. Int J Hydrogen Energy 44. https://doi.org/10.1016/j.ijhydene.2019.01.014

Aznar, M.P., Caballero, M.A., Sancho, J.A., Francés, E., 2006. Plastic waste elimination by co-gasification with coal and biomass in fluidized bed with air in pilot plant. Fuel Processing Technology 87, 409–420. https://doi.org/10.1016/j.fuproc.2005.09.006

Babinszki, B., Jakab, E., Terjék, V., Sebestyén, Z., Várhegyi, G., May, Z., Mahakhant, A., Attanatho, L., Suemanotham, A., Thanmongkhon, Y., Czégény, Z., 2021. Thermal decomposition of biomass wastes derived from palm oil production. J Anal Appl Pyrolysis 155. https://doi.org/10.1016/j.jaap.2021.105069

Bai, B., Jin, H., Zhu, S., Wu, P., Fan, C., Sun, J., 2019. Experimental investigation on in-situ hydrogenation induced gasification characteristics of acrylonitrile butadiene styrene (ABS)microplastics in supercritical water. Fuel Processing Technology 192, 170–178. https://doi.org/10.1016/j.fuproc.2019.04.020

Barontini, F., Frigo, S., Gabbrielli, R., Sica, P., 2021. Co-gasification of woody biomass with organic and waste matrices in a down-draft gasifier: An experimental and modeling approach. Energy Convers Manag 245, 114566. https://doi.org/10.1016/j.enconman.2021.114566

Belgiorno, V., De Feo, G., Rocca, D., Napoli, R.M.A., 2003. Energy from gasification of solid wastes. Waste management 23, 1–15. https://doi.org/https://doi.org/10.1016/S0956-053X(02)00149-6.

Bhatt, M., Wagh, S., Chakinala, A.G., Pant, K.K., Sharma, T., Joshi, J.B., Shah, K., Sharma, A., 2021. Conversion of refuse derived fuel from municipal solid waste into valuable chemicals using advanced thermo-chemical process. J Clean Prod 329. https://doi.org/10.1016/j.jclepro.2021.129653

Bhoi, P.R., Huhnke, R.L., Kumar, A., Indrawan, N., Thapa, S., 2018. Co-gasification of municipal solid waste and biomass in a commercial scale downdraft gasifier. Energy 163, 513–518. https://doi.org/10.1016/j.energy.2018.08.151

Bhui, B., Das, B., Prabu, V., 2021. Experimental investigations on novel electronic waste based oxygen carriers for direct coal fuelled chemical looping combustion process. Fuel 305, 121535. https://doi.org/10.1016/j.fuel.2021.121535

Bhui, B., V, P., 2021. Chemical looping based co-combustion of high ash Indian coal and rice straw operating under CO_2 in-situ gasification mode. Journal of the Energy Institute 94, 176–190. https://doi.org/10.1016/j.joei.2020.07.004

Birkmann, J., Liwenga, E., Pandey, R., Boyd, E., Djalante, R., Gemenne, F., Filho, W.L., Pinho, P.F., Stringer, L., Wrathall, D., Pörtner, H.-O., Roberts, D.C., Tignor, M., Poloczanska, E.S., Mintenbeck, K., Alegría, A., Craig, M., Langsdorf, S., Löschke, S., Möller, V., Okem, A., Rama, B., 2022. Poverty, Livelihoods and Sustainable Development: Sixth Assessment Report of the Intergovernmental Panel on Climate Change. Cambridge University Press. https://doi.org/10.1017/9781009325844.010

Bogaerts, A., Neyts, E., Gijbels, R., Van Der Mullen, J., 2002. Gas discharge plasmas and their applications, Spectrochimica Acta Part B 57; 609-658. https://doi.org/10.1016/S0584-8547(01)00406-2

Bogner, J., 2007. Waste Management: The Intergovernmental Panel on Climate Change (IPCC). https://www.ipcc.ch/site/assets/uploads/2018/02/ar4-wg3-chapter10-1.pdf

Bouajila, J., Raffin, G., Alamercery, S., Waton, H., Sanglar, C., Grenier-Loustalot, M.F., 2003. Phenolic Resins (IV). Thermal Degradation of Crosslinked Resins in Controlled Atmospheres, Polymers & Polymer Composites 11(5), 345-357. https://doi.org/10.1177/096739110301100501

Cabello, A., Mendiara, T., Abad, A., Izquierdo, M.T., García-Labiano, F., 2022. Production of hydrogen by chemical looping reforming of methane and biogas using a reactive and durable Cu-based oxygen carrier. Fuel 322. https://doi.org/10.1016/j.fuel.2022.124250

Cai, X., Du, C., 2021. Thermal Plasma Treatment of Medical Waste. Plasma Chemistry and Plasma Processing 41. https://doi.org/10.1007/s11090-020-10119-6

Campanari, S., Chiesa, P., Manzolini, G., 2010. CO_2 capture from combined cycles integrated with Molten Carbonate Fuel Cells. International Journal of Greenhouse Gas Control 4, 441–451. https://doi.org/10.1016/j.ijggc.2009.11.007

Campanari, S., Chiesa, P., Manzolini, G., Bedogni, S., 2014. Economic analysis of CO_2 capture from natural gas combined cycles using Molten Carbonate Fuel Cells. Appl Energy 130, 562–573. https://doi.org/10.1016/j.apenergy.2014.04.011

Cao, C., Bian, C., Wang, G., Bai, B., Xie, Y., Jin, H., 2020. Co-gasification of plastic wastes and soda lignin in supercritical water. Chemical Engineering Journal 388. https://doi.org/10.1016/j.cej.2020.124277

Center for Science and Environment, 2021. Waste-Wise Cities: Best practices in municipal solid waste management. https://www.niti.gov.in/sites/default/files/2021-12/Waste-Wise-Cities.pdf

Central Electricity Authority, 2022. National power portal. Ministry of Power. Government of India. https://npp.gov.in/public-reports/cea/monthly/installcap/2022/JUL/capacity1-2022-07.pdf.

Chen, H., Li, J., Li, T., Xu, G., Jin, X., Wang, M., Liu, T., 2022. Performance assessment of a novel medical-waste-to-energy design based on plasma gasification and integrated with a municipal solid waste incineration plant. Energy 245. https://doi.org/10.1016/j.energy.2022.123156

Chen, S., Xiang, W., Xue, Z., Sun, X., 2011. Experimental investigation of chemical looping hydrogen generation using iron oxides in a batch fluidized bed. Proceedings of the Combustion Institute 33, 2691–2699. https://doi.org/10.1016/j.proci.2010.08.010

Chen, W.T., Jin, K., Linda Wang, N.H., 2019. Use of Supercritical Water for the Liquefaction of Polypropylene into Oil. ACS Sustain Chem Eng 7, 3749–3758. https://doi.org/10.1021/acssuschemeng.8b03841

Chin Trento, 2023. Applications of Titanium Dioxide in the Plastic Industry. Stanford Advanced Materials. https://www.samaterials.com/content/application-of-titanium-dioxide-in-the-plastic-industry.html (accessed 4.23.23).

Chu, J.P., Chen, Y.T., Mahalingam, T., Tzeng, C.C., Cheng, T.W., 2006. Plasma vitrification and re-use of non-combustible fiber reinforced plastic, gill net and waste glass. J Hazard Mater 138, 628–632. https://doi.org/10.1016/j.jhazmat.2006.05.107

Chu, J.P., Hwang, I.J., Tzeng, C.C., Kuo, Y.Y., Yu, Y.J., 1998. Characterization of vitrified slag from mixed medical waste surrogates treated by a thermal plasma system, Journal of Hazardous Materials 58, 179-194. https://doi.org/10.1016/S0304-3894(97)00130-1

Chung, W.C., Chang, M.B., 2016. Review of catalysis and plasma performance on dry reforming of CH_4 and possible synergistic effects. Renewable and Sustainable Energy Reviews. https://doi.org/10.1016/j.rser.2016.04.007

Cimerman, R., Račková, D., Hensel, K., 2018. Tars removal by non-thermal plasma and plasma catalysis. J Phys D Appl Phys 51. https://doi.org/10.1088/1361-6463/aac762

Collard, F.X., Blin, J., 2014. A review on pyrolysis of biomass constituents: Mechanisms and composition of the products obtained from the conversion of cellulose, hemicelluloses and lignin. Renewable and Sustainable Energy Reviews. https://doi.org/10.1016/j.rser.2014.06.013

Conesa, J.A., Ortuño, N., Palmer, D., 2020. Estimation of Industrial Emissions during Pyrolysis and Combustion of Different Wastes Using Laboratory Data. Sci Rep 10. https://doi.org/10.1038/s41598-020-63807-w

Cooper, R., Bove, D., Audasso, E., Ferrari, M.C., Bosio, B., 2021. A feasibility assessment of a retrofit Molten Carbonate Fuel Cell coal-fired plant for flue gas CO_2 segregation. Int J Hydrogen Energy 46, 15024–15031. https://doi.org/10.1016/j.ijhydene.2020.09.189

Cormos, A.M., Dumbrava, I., Cormos, C.C., 2020. Evaluation of techno-economic performance for decarbonized hydrogen and power generation based on glycerol thermo-chemical looping cycles. Appl Therm Eng 179. https://doi.org/10.1016/j.applthermaleng.2020.115728

Czernik, S., Bridgwater, A. V., 2004. Overview of applications of biomass fast pyrolysis oil. Energy and Fuels 18, 590–598. https://doi.org/10.1021/ef034067u

Das, P., Tiwari, P., 2018. Valorization of packaging plastic waste by slow pyrolysis. Resour Conserv Recycl 128, 69–77. https://doi.org/10.1016/j.resconrec.2017.09.025

Data Intelo, 2022. Global Thermosetting and Thermoplastics Market by Type. https://dataintelo.com/report/global-thermosetting-and-thermoplastics-market/ (accessed 11.22.22).

Delagrange, S., Pinard, L., Tatibouët, J.M., 2006. Combination of a non-thermal plasma and a catalyst for toluene removal from air: Manganese based oxide catalysts. Appl Catal B 68, 92–98. https://doi.org/10.1016/j.apcatb.2006.07.002

Department of Economic and Social Affairs, 2023. Global Sustainable Development Report. United Nations. https://sdgs.un.org/gsdr/gsdr2023 (accessed 4.14.23).

Dhunna, R., Khanna, R., Mansuri, I., Sahajwalla, V., 2014. Recycling waste bakelite as an alternative carbon resource for ironmaking applications. ISIJ International 54, 613–619. https://doi.org/10.2355/isijinternational.54.613

Diaz, G., Sharma, N., Leal-Quiros, E., Munoz-Hernandez, A., 2015. Enhanced hydrogen production using steam plasma processing of biomass: Experimental apparatus and procedure. Int J Hydrogen Energy 40, 2091–2098. https://doi.org/10.1016/j.ijhydene.2014.12.049

Dincer, I., Rosen, M.A., 2021. Exergy, environment, and sustainable development, in: Exergy. Elsevier, pp. 61–89. https://doi.org/10.1016/B978-0-12-824372-5.00004-X

Du, C., Wu, J., Ma, D., Liu, Y., Qiu, P., Qiu, R., Liao, S., Gao, D., 2015. Gasification of corn cob using non-thermal arc plasma. Int J Hydrogen Energy 40, 12634–12649. https://doi.org/10.1016/j.ijhydene.2015.07.111

Du, Y., Luo, Z., Yang, Yang, Yang, Yiming, Yuan, W., Li, H., Hong, Y., Dai, Z., Zhang, P., Zhao, T., 2023. Theoretical and experimental investigations into the pyrolysis mechanisms of silicon-modified phenolic resin under high temperatures. Carbon N Y 201, 504–519. https://doi.org/10.1016/j.carbon.2022.07.061

Duan, L., Sun, S., Yue, L., Qu, W., Yang, Y., 2015. Study on a new IGCC (Integrated Gasification Combined Cycle) system with CO_2 capture by integrating MCFC (Molten Carbonate Fuel Cell). Energy 87, 490–503. https://doi.org/10.1016/j.energy.2015.05.011

Emun, F., Gadalla, M., Majozi, T., Boer, D., 2010. Integrated gasification combined cycle (IGCC) process simulation and optimization. Comput Chem Eng 34, 331–338. https://doi.org/10.1016/j.compchemeng.2009.04.007

Energy Agency, I., 2021. India Energy Outlook, World Energy Outlook Special Report. https://iea.blob.core.windows.net/assets/1de6d91e-e23f-4e02-b1fb-51fdd6283b22/India_Energy_Outlook_2021.pdf.

Energy Agency, I., 2021. World Energy Outlook. https://iea.blob.core.windows.net/assets/4ed140c1-c3f3-4fd9-acae-789a4e14a23c/WorldEnergyOutlook2021.pdf

Environmental Protection Agency, 2023. Energy Recovery from the Combustion of Municipal Solid Waste (MSW). https://www.epa.gov/smm/energy-recovery-combustion-municipal-solid-waste-msw (accessed 4.14.23).

Fabry, F., Rehmet, C., Rohani, V., Fulcheri, L., 2013. Waste gasification by thermal plasma: A review. Waste Biomass Valorization. https://doi.org/10.1007/s12649-013-9201-7

Falcucci, G., Jannelli, E., Minutillo, M., Ubertini, S., Han, J., Yoon, S.P., Nam, S.W., 2012. Integrated numerical and experimental study of a MCFC-plasma gasifier energy system. Appl Energy 97, 734–742. https://doi.org/10.1016/j.apenergy.2012.01.060

Fazil, A., Kumar, S., Mahajani, S.M., 2022. Downdraft co-gasification of high ash biomass and plastics. Energy 243. https://doi.org/10.1016/j.energy.2021.123055

Fitzpatrick Richard, 2014. PLASMA PHYSICS-An Introduction. CRC Press. https://doi.org/https://doi.org/10.1201/b17263

Galeno, G., Minutillo, M., Perna, A., 2011. From waste to electricity through integrated plasma gasification/fuel cell (IPGFC) system. Int J Hydrogen Energy 36, 1692–1701. https://doi.org/10.1016/j.ijhydene.2010.11.008

Galvita, V., Messerle, V.E., Ustimenko, A.B., 2007. Hydrogen production by coal plasma gasification for fuel cell technology. Int J Hydrogen Energy 32, 3899–3906. https://doi.org/10.1016/j.ijhydene.2007.05.039

Ge, M., Friedrich, J., Vigna, L., 2020. 4 Charts Explain Greenhouse Gas Emissions by Countries and Sectors. World Resources Institute. https://www.wri.org/insights/4-charts-explain-greenhouse-gas-emissions-countries-and-sectors (accessed 8.31.22).

Georgiev, I.B., Mihailov, B.I., 1992. Some general conclusions from the results of studies on solid fuel steam plasma gasification. Fuel 71. https://doi.org/10.1016/0016-2361(92)90239-K

Giuliano, A., Poletto, M., Barletta, D., 2018. Pure hydrogen co-production by membrane technology in an IGCC power plant with carbon capture. Int J Hydrogen Energy 43, 19279–19292. https://doi.org/10.1016/j.ijhydene.2018.08.112

Gomez, E., Rani, D.A., Cheeseman, C.R., Deegan, D., Wise, M., Boccaccini, A.R., 2009. Thermal plasma technology for the treatment of wastes: A critical review. J Hazard Mater. https://doi.org/10.1016/j.jhazmat.2008.04.017

Guo, Q., Cheng, Z., Chen, G., Yan, B., Li, J., Hou, L., Ronsse, F., 2020. Assessment of biomass demineralization on gasification: From experimental investigation, mechanism to potential application. Science of the Total Environment 726. https://doi.org/10.1016/j.scitotenv.2020.138634

Gupta, S., De, S., 2022. An experimental investigation of high-ash coal gasification in a pilot-scale bubbling fluidized bed reactor. Energy 244, 122868. https://doi.org/10.1016/j.energy.2021.122868

Hao, J., Wang, H., Chen, S., Cai, B., Ge, L., Xia, W., 2014. Pyrolysis characteristics of the mixture of printed circuit board scraps and coal powder. Waste Management 34, 1763–1769. https://doi.org/10.1016/j.wasman.2013.10.043

He, W., Xu, B., Lang, L., Yang, W., Liu, H., Zhan, H., Xie, J., Yin, X., Wu, C., 2023. Exploring Simultaneous Upgrading and Purification of Biomass−Gasified Gases Using Plasma Catalysis. Catalysts 13, 686. https://doi.org/10.3390/catal13040686

Hirschenhofer, J.H., Stauffer, D.B., Engleman, R.R., Klett, M.G., 1998. Fourth Edition Fuel Cell Handbook, Fourth Edition Contents.

Hlina, M., Hrabovsky, M., Kavka, T., Konrad, M., 2014. Production of high quality syngas from argon/water plasma gasification of biomass and waste. Waste Management 34, 63–66. https://doi.org/10.1016/j.wasman.2013.09.018

Holland, B.J., Hay, J.N., 2000. Thermal degradation of nylon polymers. Polym Int 49, 943–948. https://doi.org/10.1002/1097-0126(200009)49:9<943::AID-PI400>3.0.CO;2-5

Hrabovsky, M., Hlina, M., Kopecky, V., Maslani, A., Zivny, O., Krenek, P., Serov, A., Hurba, O., 2017. Steam Plasma Treatment of Organic Substances for Hydrogen and Syngas Production. Plasma Chemistry and Plasma Processing 37, 739–762. https://doi.org/10.1007/s11090-016-9783-5

Hrabovsky, M., Konrad, M., Kopecky, V., Hlina, M., Kavka, T., Chumak, O.M., Maslani, A., Oost, G., 2010. Plasma Aided Gasification of Biomass and Plastics using CO_2 as Oxidizer.

Hrabovsky, M., Konrad, M., Kopecky, V., Hlina, M., Kavka, T., van Oost, G., Beeckman, E., Defoort, B., 2006. Gasification of biomass in water/gas-stabilized plasma for syngas production. Czechoslovak Journal of Physics 56. https://doi.org/10.1007/s10582-006-0350-9

Huang, Y., Sekyere, D.T., Zhang, J., Tian, Y., 2023. Fast pyrolysis behaviors of biomass with high contents of ash and nitrogen using TG-FTIR and Py-GC/MS. J Anal Appl Pyrolysis 170. https://doi.org/10.1016/j.jaap.2023.105922

Hwang, I.H., Nakajima, D., Matsuto, T., Sugimoto, T., 2008. Improving the quality of waste-derived char by removing ash. Waste Management 28, 424–434. https://doi.org/10.1016/j.wasman.2006.11.015

IBM, 2021. SPSS Statistics v.20. https://www.ibm.com/products/spss-statistics (accessed 4.15.23).

India Energy, 2023. India Climate & Energy Dashboard. NITI Aayog. https://iced.niti.gov.in/energy/electricity/distribution (accessed 10.13.23).

Jagodzińska, K., Mroczek, K., Nowińska, K., Gołombek, K., Kalisz, S., 2019. The impact of additives on the retention of heavy metals in the bottom ash during RDF incineration. Energy 183, 854–868. https://doi.org/10.1016/j.energy.2019.06.162

Jain, A., Bora, B.J., Kumar, R., Sharma, P., Deka, H., 2023. Theoretical potential estimation and multi-objective optimization of Water Hyacinth (Eichhornia Crassipes) biodiesel powered

diesel engine at variable injection timings. Renew Energy 206, 514–530. https://doi.org/10.1016/j.renene.2023.02.033

Jeong, Y.S., Kim, J.W., Ra, H.W., Seo, M.W., Mun, T.Y., Kim, J.S., 2022. Characteristics of Air Gasification of 10 Different Types of Plastic in a Two-Stage Gasification Process. ACS Sustain Chem Eng 10, 4705–4716. https://doi.org/10.1021/acssuschemeng.2c00251

Jeremiáš, M., Pohořelý, M., Svoboda, K., Manovic, V., Anthony, E.J., Skoblia, S., Beňo, Z., Šyc, M., 2017. Gasification of biomass with CO_2 and H_2O mixtures in a catalytic fluidised bed. Fuel 210. https://doi.org/10.1016/j.fuel.2017.09.006

Jiang, P., Mahmud Parvez, A., Meng, Y., Dong, X., Xu, M., Luo, X., Shi, K., Wu, T., 2021. Novel two-stage fluidized bed-plasma gasification integrated with SOFC and chemical looping combustion for the high efficiency power generation from MSW: A thermodynamic investigation. Energy Convers Manag 236. https://doi.org/10.1016/j.enconman.2021.114066

Jimbo, H., 1996. Plasma melting and useful application of molten slag, Waste Management 16, 417-422. https://doi.org/10.1016/S0956-053X(96)00087-6

Jones, P.T., Geysen, D., Tielemans, Y., Van Passel, S., Pontikes, Y., Blanpain, B., Quaghebeur, M., Hoekstra, N., 2013. Enhanced Landfill Mining in view of multiple resource recovery: A critical review. J Clean Prod. https://doi.org/10.1016/j.jclepro.2012.05.021

Jung, M.R., Horgen, F.D., Orski, S. V., Rodriguez C., V., Beers, K.L., Balazs, G.H., Jones, T.T., Work, T.M., Brignac, K.C., Royer, S.-J., Hyrenbach, K.D., Jensen, B.A., Lynch, J.M., 2018. Validation of ATR FT-IR to identify polymers of plastic marine debris, including those ingested by marine organisms. Mar Pollut Bull 127, 704–716. https://doi.org/10.1016/j.marpolbul.2017.12.061

Kale, M.J., Ojha, D.K., Biswas, S., Militti, J.I., McCormick, A. V., Schott, J.H., Dauenhauer, P.J., Cussler, E.L., 2020. Optimizing Ammonia Separation via Reactive Absorption for Sustainable Ammonia Synthesis. ACS Appl Energy Mater 3, 2576–2584. https://doi.org/10.1021/acsaem.9b02278

Kalinci, Y., Hepbasli, A., Dincer, I., 2011. Exergoeconomic analysis of hydrogen production from plasma gasification of sewage sludge using specific exergy cost method. Int J Hydrogen Energy 36, 11408–11417. https://doi.org/10.1016/j.ijhydene.2010.11.124

Kalinenko, R.A., Kuznetsov, A.P., Levitsky, A.A., Messerle, V.E., Mirokhin, Y.A., Polak, L.S., Sakipov, Z.B., Ustimenko, A.B., 1993. Pulverized Coal Plasma Gasification, Plasma Chemistry and Plasma Processing.

Kaza, S., Yao, L.C., Bhada-Tata, P., Van Woerden, F., 2018. What a Waste 2.0: A Global Snapshot of Solid Waste Management to 2050. Washington, DC: World Bank. https://doi.org/10.1596/978-1-4648-1329-0

Khan H, 2018. Global Syngas Overview. https://www.globalsyngas.org/uploads/downloads/2018-presentations/KEYNOTE-MON-GlobalSyngasOverview-by-Habib-Khan.pdf

Khan, M.N., Shamim, T., 2019. Techno-economic assessment of a chemical looping reforming combined cycle plant with iron and tungsten based oxygen carriers. Int J Hydrogen Energy 44, 11525–11534. https://doi.org/10.1016/j.ijhydene.2019.03.109

Khan, M.N., Shamim, T., 2016. Techno-economic assessment of a plant based on a three reactor chemical looping reforming system. Int J Hydrogen Energy 41, 22677–22688. https://doi.org/10.1016/j.ijhydene.2016.09.016

Kim, S.W., Park, H.S., Kim, H.J., 2003. 100 kW steam plasma process for treatment of PCBs (polychlorinated biphenyls) waste. Vacuum 70, 59–66. https://doi.org/10.1016/S0042-207X(02)00761-3

Kogelschatz, U., 2004. Atmospheric-pressure plasma technology, in: Plasma Physics and Controlled Fusion. https://doi.org/10.1088/0741-3335/46/12B/006

Kroker, T., Kolb, T., Schenk, A., Krawczyk, K., Młotek, M., Gericke, K.H., 2012. Catalytic conversion of simulated biogas mixtures to synthesis gas in a fluidized bed reactor supported by a DBD, in: Plasma Chemistry and Plasma Processing. Springer New York LLC, pp. 565–582. https://doi.org/10.1007/s11090-012-9358-z

Kumar, A., Kandasamy, P., Chakraborty, I., Hangshing, L., 2022. Analysis of energy consumption, heat and mass transfer, drying kinetics and effective moisture diffusivity during foam-mat drying of mango in a convective hot-air dryer. Biosyst Eng. 219, 85–102. https://doi.org/10.1016/j.biosystemseng.2022.04.026.

Kwon, S., Im, S. kyun, 2022. Feasibility of non-thermal plasma gasification for a waste-to-energy power plant. Energy Convers Manag 251. https://doi.org/10.1016/j.enconman.2021.114978

Lavee, D., Nardiya, S., 2013. A cost evaluation method for transferring municipalities to solid waste source-separated system. Waste Management 33, 1064–1072. https://doi.org/10.1016/j.wasman.2013.01.026

Lazzari, E., Schena, T., Marcelo, M.C.A., Primaz, C.T., Silva, A.N., Ferrão, M.F., Bjerk, T., Caramão, E.B., 2018. Classification of biomass through their pyrolytic bio-oil composition using FTIR and PCA analysis. Ind Crops Prod 111, 856–864. https://doi.org/10.1016/j.indcrop.2017.11.005

Lee, C.C., Huffman, G.L., 1996. Medical waste management/incineration, Journal of Hazardous Materials 48, 1-30. https://doi.org/10.1016/0304-3894(95)00153-0

Lee, H.G., Park, H.W., Choi, S., Park, H.S., Park, D.W., 2014. Production of synthesis gas from coal by DC non-transferred steam plasma gasification system, in: Journal of Chemical Engineering of Japan. Society of Chemical Engineers, Japan, pp. 334–339. https://doi.org/10.1252/jcej.13we157

Lemmens, B., Elslander, H., Vanderreydt, I., Peys, K., Diels, L., Oosterlinck, M., Joos, M., 2007. Assessment of plasma gasification of high caloric waste streams. Waste Management 27, 1562–1569. https://doi.org/10.1016/j.wasman.2006.07.027

Leto, L., Dispenza, C., Moreno, A., Calabr, A., 2011. Simulation model of a molten carbonate fuel cell-microturbine hybrid system. Appl Therm Eng 31, 1263–1271. https://doi.org/10.1016/j.applthermaleng.2010.12.029

Li, C., Qi, S., Zhang, D., 2010. Thermal degradation of environmentally friendly phenolic resin/Al 2O3 hybrid composite. J Appl Polym Sci 115, 3675–3679. https://doi.org/10.1002/app.31469

Li, D., Wang, L., Koike, M., Nakagawa, Y., Tomishige, K., 2011. Steam reforming of tar from pyrolysis of biomass over Ni/Mg/Al catalysts prepared from hydrotalcite-like precursors. Appl Catal B 102, 528–538. https://doi.org/10.1016/j.apcatb.2010.12.035

Li, H., Li, T., Wei, X., 2020. Main performance analysis of kitchen waste gasification in a small-power horizontal plasma jet reactor. Journal of the Energy Institute 93, 367–376. https://doi.org/10.1016/j.joei.2019.02.004

Linde, 2023. Purge gas recovery. Germany. https://www.linde-engineering.com/en/images/Brochure%20-%20Purge%20gas%20recovery_tcm19-486079.pdf

Liu, L., Wang, Q., Song, J., Ahmad, S., Yang, X., Sun, Y., 2017. Plasma-assisted catalytic reforming of toluene to hydrogen rich syngas. Catal Sci Technol 7, 4216–4231. https://doi.org/10.1039/c7cy00970d

Liu, L., Zhang, Z., Das, S., Kawi, S., 2019. Reforming of tar from biomass gasification in a hybrid catalysis-plasma system: A review. Appl Catal B. https://doi.org/10.1016/j.apcatb.2019.03.039

Liu, Y., Fan, C., Zhang, H., Zou, J., Zhou, F., Jin, H., 2019. The resource utilization of ABS plastic waste with subcritical and supercritical water treatment. Int J Hydrogen Energy 15758–15765. https://doi.org/10.1016/j.ijhydene.2018.08.012

Lopez, G., Artetxe, M., Amutio, M., Alvarez, J., Bilbao, J., Olazar, M., 2018. Recent advances in the gasification of waste plastics. A critical overview. Renewable and Sustainable Energy Reviews. https://doi.org/10.1016/j.rser.2017.09.032

Materazzi, M., Lettieri, P., Taylor, R., Chapman, C., 2016. Performance analysis of RDF gasification in a two stage fluidized bed-plasma process. Waste Management 47, 256–266. https://doi.org/10.1016/j.wasman.2015.06.016

Messerle, V.E., Mosse, A.L., Ustimenko, A.B., 2018. Processing of biomedical waste in plasma gasifier. Waste Management 79, 791–799. https://doi.org/10.1016/j.wasman.2018.08.048

Ministry of Housing and Urban Affairs, 2018. Guidelines on Usage of Refuse Derived Fuel in various industries. https://mohua.gov.in/upload/uploadfiles/files/93.pdf.

Minutillo, M., Perna, A., di Bona, D., 2009. Modelling and performance analysis of an integrated plasma gasification combined cycle (IPGCC) power plant. Energy Convers Manag 50, 2837–2842. https://doi.org/10.1016/j.enconman.2009.07.002

Mishra, N., Bhui, B., Vairakannu, P., 2019. Comparative evaluation of performance of high and low ash coal fuelled chemical looping combustion integrated combined cycle power generating systems. Energy 169, 305–318. https://doi.org/10.1016/j.energy.2018.12.043

Mondial L, C. DE, 2013. World Energy Scenarios. World Energy Council. https://www.worldenergy.org/assets/downloads/World-Energy-Scenarios_Composing-energy-futures-to-2050_Executive-summary.pdf.

Montiel-Bohórquez, N.D., Agudelo, A.F., Pérez, J.F., 2021. Effect of origin and production rate of MSW on the exergoeconomic performance of an integrated plasma gasification combined cycle power plant. Energy Convers Manag 238. https://doi.org/10.1016/j.enconman.2021.114138

Munir, M.T., Mardon, I., Al-Zuhair, S., Shawabkeh, A., Saqib, N.U., 2019. Plasma gasification of municipal solid waste for waste-to-value processing. Renewable and Sustainable Energy Reviews. https://doi.org/10.1016/j.rser.2019.109461

Müsellim, E., Tahir, M.H., Ahmad, M.S., Ceylan, S., 2018. Thermokinetic and TG/DSC-FTIR study of pea waste biomass pyrolysis. Appl Therm Eng 137, 54–61. https://doi.org/10.1016/j.applthermaleng.2018.03.050

Muvhiiwa, R.F., Sempuga, B., Hildebrandt, D., Van Der Walt, J., 2018. Study of the effects of temperature on syngas composition from pyrolysis of wood pellets using a nitrogen plasma torch reactor. J Anal Appl Pyrolysis 130, 249–255. https://doi.org/10.1016/j.jaap.2018.01.014

Nanda, S., Berruti, F., 2021. Municipal solid waste management and landfilling technologies: a review. Environ Chem Lett 19, 1433–1456. https://doi.org/10.1007/s10311-020-01100-y

National Center for Biotechnology Information, 2023. National Library of Medicine. National Institutes of Health. https://pubchem.ncbi.nlm.nih.gov/ (accessed 4.15.23).

OECD, 2023. Municipal waste. https://doi.org/https://doi.org/10.1787/data-00601-en

OECD, 2022. Global Plastics Outlook. OECD. https://doi.org/10.1787/de747aef-en

Orlando, F., 2010. A Leading Provider of Clean Energy Solutions.

Our Technology. CHO Power. https://www.cho-power.com/ (accessed 1.2.22).

Pan, P., Peng, W., Li, J., Chen, H., Xu, G., Liu, T., 2022. Design and evaluation of a conceptual waste-to-energy approach integrating plasma waste gasification with coal-fired power generation. Energy 238. https://doi.org/10.1016/j.energy.2021.121947

Pang, Y., Hammer, T., Müller, D., Karl, J., 2019. Investigation on the influence of non-thermal plasma on reaction degree of wood gasification in a drop tube reactor. Fuel 253, 95–105. https://doi.org/10.1016/j.fuel.2019.04.165

Paulino, R.F.S., Essiptchouk, A.M., Silveira, J.L., 2020. The use of syngas from biomedical waste plasma gasification systems for electricity production in internal combustion: Thermodynamic and economic issues. Energy. https://doi.org/10.1016/j.energy.2020.117419

Pavlostathis, S.G., 2011. Kinetics and Modeling of Anaerobic Treatment and Biotransformation Processes, in: Comprehensive Biotechnology. Elsevier, pp. 385–397. https://doi.org/10.1016/B978-0-08-088504-9.00385-8

Peng, W., Chen, H., Liu, J., Zhao, X., Xu, G., 2021. Techno-economic assessment of a conceptual waste-to-energy CHP system combining plasma gasification, SOFC, gas turbine and supercritical CO_2 cycle. Energy Convers Manag 245. https://doi.org/10.1016/j.enconman.2021.114622

Periodic Table, 2022. Royal Society of Chemistry. https://www.rsc.org/periodic-table/ (accessed 10.25.22).

Perna, A., Minutillo, M., Jannelli, E., 2016. Hydrogen from intermittent renewable energy sources as gasification medium in integrated waste gasification combined cycle power plants: A performance comparison. Energy 94, 457–465. https://doi.org/10.1016/j.energy.2015.10.143

Perna, A., Minutillo, M., Lubrano Lavadera, A., Jannelli, E., 2018. Combining plasma gasification and solid oxide cell technologies in advanced power plants for waste to energy and electric energy storage applications. Waste Management 73, 424–438. https://doi.org/10.1016/j.wasman.2017.09.022

Pham Huu, T., Gil, S., Da Costa, P., Giroir-Fendler, A., Khacef, A., 2015. Plasma-catalytic hybrid reactor: Application to methane removal. Catal Today 257, 86–92. https://doi.org/10.1016/j.cattod.2015.03.001

Plasma arc waste disposal. Chemeurope. https://www.chemeurope.com/en/encyclopedia/Plasma_arc_waste_disposal.html (accessed 1.2.22).

Plasma Gasification (PGVR). SMS Maharashtra Enviro Power Ltd. https://smsmepl.com/plasma-gasification/ (accessed 1.2.22).

Plasma Gasification. National Energy Technology Laboratory. https://netl.doe.gov/research/Coal/energy-systems/gasification/gasifipedia/westinghouse (accessed 1.2.22).

Power through Plasma. PHOENIX Solutions Co. https://www.phoenixsolutionsco.com/ (accessed 1.2.22).

PRRS_Pyrogenesis. https://www.pyrogenesis.com/

Ptasinski, K.J., Prins, M.J., Pierik, A., 2007. Exergetic evaluation of biomass gasification. Energy 32, 568–574. https://doi.org/10.1016/j.energy.2006.06.024

PTDR- Waste to Energy System. PEAT International. http://www.peat.com/ (accessed 1.2.22).

Puglia, D., Manfredi, L.B., Vazquez, A., Kenny, J.M., 2001. Thermal degradation and fire resistance of epoxy–amine–phenolic blends. Polym Degrad Stab 73, 521–527. https://doi.org/10.1016/S0141-3910(01)00157-4

Puig-Gamero, M., Argudo-Santamaria, J., Valverde, J.L., Sánchez, P., Sanchez-Silva, L., 2018. Three integrated process simulation using aspen plus®: Pine gasification, syngas cleaning and methanol synthesis. Energy Convers Manag 177, 416–427. https://doi.org/10.1016/j.enconman.2018.09.088

Rai, C., Bhui, B., V, P., 2022. Techno-economic analysis of e-waste based chemical looping reformer as hydrogen generator with co-generation of metals, electricity and syngas. Int J Hydrogen Energy 47, 11177–11189. https://doi.org/10.1016/j.ijhydene.2022.01.159

Rath, S.S., Nayak, P., Mukherjee, P.S., Roy Chaudhury, G., Mishra, B.K., 2012. Treatment of electronic waste to recover metal values using thermal plasma coupled with acid leaching - A response surface modeling approach. Waste Management 32, 575–583. https://doi.org/10.1016/j.wasman.2011.11.001

Ravenni, G., Sárossy, Z., Sanna, S., Ahrenfeldt, J., Henriksen, U.B., 2020. Residual gasification char applied to tar reforming in a pilot-scale gasifier: Performance and evolution of char properties for perspective cascade uses. Fuel Processing Technology 210. https://doi.org/10.1016/j.fuproc.2020.106546

Rawlings, R.D., Wu, J.P., Boccaccini, A.R., 2006. Glass-ceramics: Their production from wastes-A Review. J Mater Sci. https://doi.org/10.1007/s10853-006-6554-3

Renewable Energy Agency, I., 2020. Green hydrogen: A guide to policy making. https://www.irena.org/-

/media/Files/IRENA/Agency/Publication/2020/Nov/IRENA_Green_hydrogen_policy_2020.pdf.

Resource Recovery Solutions. Tetronics. https://tetronics.com/ (accessed 1.2.22).

Rodríguez-Reinoso, F., 2001. Activated Carbon and Adsorption, in: Encyclopedia of Materials: Science and Technology. Elsevier, 22–34. https://doi.org/10.1016/B0-08-043152-6/00005-X

Rutberg, P.G., Bratsev, A.N., Kuznetsov, V.A., Popov, V.E., Ufimtsev, A.A., Shtengel', S. V., 2011. On efficiency of plasma gasification of wood residues. Biomass Bioenergy 35, 495–504. https://doi.org/10.1016/j.biombioe.2010.09.010

Rutberg, P.G., Kuznetsov, V.A., Serba, E.O., Popov, S.D., Surov, A. V., Nakonechny, G. V., Nikonov, A. V., 2013. Novel three-phase steam-air plasma torch for gasification of high-caloric waste. Appl Energy 108, 505–514. https://doi.org/10.1016/j.apenergy.2013.03.052

Ryzhkov, A., Bogatova, T., Gordeev, S., 2018. Technological solutions for an advanced IGCC plant. Fuel 214, 63–72. https://doi.org/10.1016/j.fuel.2017.10.099

Sahu, P., V, P., 2021. Techno-economic analysis of co-combustion of Indian coals with municipal solid waste in subcritical and supercritical based steam turbine power generating carbon-negative systems. Energy 233. https://doi.org/10.1016/j.energy.2021.121053

Saini, S., Rao, P., Patil, Y., 2012. City Based Analysis of MSW to Energy Generation in India, Calculation of State-Wise Potential and Tariff Comparison with EU. Procedia Soc Behav Sci 37, 407–416. https://doi.org/10.1016/j.sbspro.2012.03.306

Saleem, F., Zhang, K., Harvey, A.P., 2019. Decomposition of benzene as a tar analogue in CO_2 and H_2 carrier gases, using a non-thermal plasma. Chemical Engineering Journal 360, 714–720. https://doi.org/10.1016/j.cej.2018.11.195

Samal, S., 2017. Thermal plasma technology: The prospective future in material processing. J Clean Prod. https://doi.org/10.1016/j.jclepro.2016.10.154

Sanito, R.C., You, S.J., Chang, T.J., Wang, Y.F., 2020. Economic and environmental evaluation of flux agents in the vitrification of resin waste: A SWOT analysis. J Environ Manage 270. https://doi.org/10.1016/j.jenvman.2020.110910

Shaftel, H., Callery, S., Jackson, R., Bailey, D., 2022. What is the greenhouse effect? NASA Jet Propulsion Laboratory. https://climate.nasa.gov/faq/19/what-is-the-greenhouse-effect/ (accessed 5.25.22).

Shen, Y., Li, X., Yao, Z., Cui, X., Wang, C.-H., 2019. CO_2 gasification of woody biomass: Experimental study from a lab-scale reactor to a small-scale autothermal gasifier. Energy 170, 497–506. https://doi.org/10.1016/j.energy.2018.12.176

Shin, D.H., Hong, Y.C., Lee, S.J., Kim, Y.J., Cho, C.H., Ma, S.H., Chun, S.M., Lee, B.J., Uhm, H.S., 2013. A pure steam microwave plasma torch: Gasification of powdered coal in the plasma. Surf Coat Technol 228. https://doi.org/10.1016/j.surfcoat.2012.04.071

Sikarwar, V.S., Hrabovský, M., Van Oost, G., Pohořelý, M., Jeremiáš, M., 2020. Progress in waste utilization via thermal plasma. Prog Energy Combust Sci. https://doi.org/10.1016/j.pecs.2020.100873

Silveira, J.L., Tuna, C.E., 2003. Thermoeconomic analysis method for optimization of combined heat and power systems. Part I. Prog Energy Combust Sci. https://doi.org/10.1016/S0360-1285(03)00041-8

Singh, U., Rao, A.B., Chandel, M.K., 2017. Economic Implications of CO_2 Capture from the Existing as Well as Proposed Coal-fired Power Plants in India under Various Policy Scenarios. Energy Procedia 114, 7638–7650. https://doi.org/10.1016/j.egypro.2017.03.1896

Spiegl, N., Long, X., Berrueco, C., Paterson, N., Millan, M., 2021. Oxy-fuel co-gasification of coal and biomass for negative CO_2 emissions. Fuel 306, 121671. https://doi.org/10.1016/j.fuel.2021.121671

Spinelli, M., di Bona, D., Gatti, M., Martelli, E., Viganò, F., Consonni, S., 2020. Assessing the potential of molten carbonate fuel cell-based schemes for carbon capture in natural gas-fired combined cycle power plants. J Power Sources 448. https://doi.org/10.1016/j.jpowsour.2019.227223

St, N., Braithwaite, J., 2000. Introduction to gas discharges, Plasma Sources Sci. Technol. Vol. 9

Striūgas, N., Valinčius, V., Pedišius, N., Poškas, R., Zakarauskas, K., 2017. Investigation of sewage sludge treatment using air plasma assisted gasification. Waste Management 64, 149–160. https://doi.org/10.1016/j.wasman.2017.03.024

Suman, S., Panwar, D.S., Gautam, S., 2017. Surface morphology properties of biochars obtained from different biomass waste. Energy Sources, Part A: Recovery, Utilization and Environmental Effects 39, 1007–1012. https://doi.org/10.1080/15567036.2017.1283553

Sun, J., Wang, Q., Wang, W., Wang, K., 2018. Plasma catalytic steam reforming of a model tar compound by microwave-metal discharges. Fuel 234, 1278–1284. https://doi.org/10.1016/j.fuel.2018.07.140

Sun, Y., Qin, Z., Tang, Y., Huang, T., Ding, S., Ma, X., 2021. Techno-environmental-economic evaluation on municipal solid waste (MSW) to power/fuel by gasification-based and incineration-based routes. J Environ Chem Eng 9, 106108. https://doi.org/10.1016/j.jece.2021.106108

Surov, A. V., Popov, S.D., Popov, V.E., Subbotin, D.I., Serba, E.O., Spodobin, V.A., Nakonechny, G. V., Pavlov, A. V., 2017. Multi-gas AC plasma torches for gasification of organic substances. Fuel 203, 1007–1014. https://doi.org/10.1016/j.fuel.2017.02.104

Surywanshi, G.D., Patnaikuni, V.S., Vooradi, R., Anne, S.B., 2021. 4-E and life cycle analyses of a supercritical coal direct chemical looping combustion power plant with hydrogen and power co-generation. Energy 217. https://doi.org/10.1016/j.energy.2020.119418

Surywanshi, G.D., Pillai, B.B.K., Patnaikuni, V.S., Vooradi, R., Anne, S.B., 2019. 4-E analyses of chemical looping combustion based subcritical, supercritical and ultra-supercritical coal-fired power plants. Energy Convers Manag 200. https://doi.org/10.1016/j.enconman.2019.112050

Szente, R.N., Munz, ~ R J, Drouet, M.G., 1992. Electrode Erosion in Plasma Torches, Plasma Chemistry and Plasma Processing 12, 327-343. https://doi.org/10.1007/BF01447029

Tamošiūnas, A., Gimžauskaitė, D., Uscila, R., Aikas, M., 2019. Thermal arc plasma gasification of waste glycerol to syngas. Appl Energy 251. https://doi.org/10.1016/j.apenergy.2019.113306

Tan, Y., 2013. Feasibility Study on Solid Waste to Energy Technological Aspects. https://funginstitute.berkeley.edu/wp-content/uploads/2014/01/SolidWasteToEnergy.pdf

Tang, L., Huang, H., 2005. Plasma pyrolysis of biomass for production of syngas and carbon adsorbent. Energy and Fuels 19, 1174–1178. https://doi.org/10.1021/ef049835b

Tang, L., Huang, H., Hao, H., Zhao, K., 2013. Development of plasma pyrolysis/gasification systems for energy efficient and environmentally sound waste disposal. J Electrostat. https://doi.org/10.1016/j.elstat.2013.06.007

The PEM Process. INENTEC. https://www.inentec.com/ (accessed 1.2.22).

The Pros & Cons of Nuclear Energy: Is it safe? 2018. Spring Power & Gas. https://springpowerandgas.us/the-pros-cons-of-nuclear-energy-is-it-safe/ (accessed 8.31.22).

The World Bank, 2022. Solid waste management. https://www.worldbank.org/en/topic/urbandevelopment/brief/solid-waste-management (accessed 11.22.22).

Titanium Dioxide Market Size, Share & Trends Analysis Report, 2023. Grand View Research. https://www.grandviewresearch.com/industry-analysis/titanium-dioxide-industry (accessed 6.13.23).

Tod Hardin, 2021. Plastic: It's not all the same. Plastic Oceans. https://plasticoceans.org/7-types-of-plastic/ (accessed 10.25.22).

Toonssen, R., Sollai, S., Aravind, P. v., Woudstra, N., Verkooijen, A.H.M., 2011. Alternative system designs of biomass gasification SOFC/GT hybrid systems, in: International Journal of Hydrogen Energy. pp. 10414–10425. https://doi.org/10.1016/j.ijhydene.2010.06.069

Tripathi, P., Rao, L., 2022. Single particle and packed bed combustion characteristics of high ash and high plastic content refuse derived fuel. Fuel 308. https://doi.org/10.1016/j.fuel.2021.121983

Tu, W.K., Shie, J.L., Chang, C.Y., Chang, C.F., Lin, C.F., Yang, S.Y., Kuo, J.T., Shaw, D.G., You, Y. Der, Lee, D.J., 2009. Products and bioenergy from the pyrolysis of rice straw via radio frequency plasma and its kinetics. Bioresour Technol 100, 2052–2061. https://doi.org/10.1016/j.biortech.2008.09.052

Tzeng, C.-C., Kuo, Y.-Y., Huang, T.-F., Lin, D.-L., Yu, Y.-J., 1998. Treatment of radioactive wastes by plasma incineration and vitrification for final disposal, Journal of Hazardous Materials.

Umeda, K., Nakamura, S., Lu, D., Yoshikawa, K., 2019. Biomass gasification employing low-temperature carbonization pretreatment for tar reduction. Biomass Bioenergy 126, 142–149. https://doi.org/10.1016/j.biombioe.2019.05.002

UNFCCC, 2021. United Nations Climate Change Annual Report 2020. https://unfccc.int/sites/default/files/resource/UNFCCC_Annual_Report_2020.pdf.

UNEP, 2020. Waste Management during the COVID-19 Pandemic from Response to Recovery. https://wedocs.unep.org/bitstream/handle/20.500.11822/33416/WMC-19.pdf?sequence=1&isAllowed=y.

United Nations Environment Programme, 2021. Food Waste Index Report. https://www.unep.org/resources/report/unep-food-waste-index-report-2021.

Vaidyanathan, A., Mulholland, J., Ryu, J., Smith, M.S., Circeo, L.J., 2007. Characterization of fuel gas products from the treatment of solid waste streams with a plasma arc torch. J Environ Manage 82, 77–82. https://doi.org/10.1016/j.jenvman.2005.12.006

Vairakannu, P., Kumari, G., 2016. CO_2-Oxy underground coal gasification integrated proton exchange membrane fuel cell operating in a chemical looping mode of reforming. Int J Hydrogen Energy 41, 20063–20077. https://doi.org/10.1016/j.ijhydene.2016.09.022

Van Durme, J., Dewulf, J., Leys, C., Van Langenhove, H., 2008. Combining non-thermal plasma with heterogeneous catalysis in waste gas treatment: A review. Appl Catal B. https://doi.org/10.1016/j.apcatb.2007.09.035

Van Oost, G., Hrabovsky, M., Kopecky, V., Konrad, M., Hlina, M., Kavka, T., 2008. Pyrolysis/gasification of biomass for synthetic fuel production using a hybrid gas-water stabilized plasma torch. Vacuum 83, 209–212. https://doi.org/10.1016/j.vacuum.2008.03.084

Wang, M., Mao, M., Zhang, M., Wen, G., Yang, Q., Su, B., Ren, Q., 2019. Highly efficient treatment of textile dyeing sludge by CO_2 thermal plasma gasification. Waste Management 90, 29–36. https://doi.org/10.1016/j.wasman.2019.04.025

Wang, N., Shen, K., Yu, X., Qian, W., Chu, W., 2013. Preparation and characterization of a plasma treated NiMgSBA-15 catalyst for methane reforming with CO_2 to produce syngas. Catal Sci Technol 3, 2278–2287. https://doi.org/10.1039/c3cy00299c

Wang, S., Wang, Y., Bian, C., Zhong, Y., Jing, X., 2015. The thermal stability and pyrolysis mechanism of boron-containing phenolic resins: The effect of phenyl borates on the char formation. Appl Surf Sci 331, 519–529. https://doi.org/10.1016/j.apsusc.2015.01.062

Wee, J.-H., 2014. Carbon dioxide emission reduction using molten carbonate fuel cell systems. Renewable and Sustainable Energy Reviews 32, 178–191. https://doi.org/10.1016/j.rser.2014.01.034

Will Hall, 2020. Make Hydrogen in India - POLICY BRIEF. https://www.teriin.org/sites/default/files/2020-06/Hydrogen-Policy-Brief.pdf.

Wilson, Brandon, Wilson, Bary, Liss, B., 2013. A Comparative Assessment of Commercial Technologies for Conversion of Solid Waste to Energy. EnviroPower Renewable Inc.

Wilson, D.C. David C., United Nations Environment Programme, International Solid Waste Association, 2015. Global waste management outlook. https://www.unep.org/resources/report/global-waste-management-outlook.

World Meteorological Organization, 2021. Greenhouse gas bulletin: Another year another record. World Meteorological Organization. https://public.wmo.int/en/media/press-release/greenhouse-gas-bulletin-another-year-another-record (accessed 5.25.22).

Yang, Q., Yan, M., Zhang, L., Xia, X., Zhu, Y., Zhang, C., Zhao, B., Ma, X., Wang, X., 2021. Thermodynamic analysis of chemical looping coupling process for coproducing syngas and hydrogen with in situ CO_2 utilization. Energy Convers Manag 231. https://doi.org/10.1016/j.enconman.2021.113845

Yang, Y., Liew, R.K., Tamothran, A.M., Foong, S.Y., Yek, P.N.Y., Chia, P.W., Van Tran, T., Peng, W., Lam, S.S., 2021. Gasification of refuse-derived fuel from municipal solid waste for energy production: a review. Environ Chem Lett. https://doi.org/10.1007/s10311-020-01177-5

Yazdanfar, J., Mehrpooya, M., Yousefi, H., Palizdar, A., 2015. Energy and exergy analysis and optimal design of the hybrid molten carbonate fuel cell power plant and carbon dioxide capturing process. Energy Convers Manag 98, 15–27. https://doi.org/10.1016/j.enconman.2015.03.076

Yu, J., Guo, Q., Gong, Y., Ding, L., Wang, J., Yu, G., 2021. A review of the effects of alkali and alkaline earth metal species on biomass gasification. Fuel Processing Technology. https://doi.org/10.1016/j.fuproc.2021.106723

Zang, G., Jia, J., Tejasvi, S., Ratner, A., Silva Lora, E., 2018. Techno-economic comparative analysis of Biomass Integrated Gasification Combined Cycles with and without CO_2 capture. International Journal of Greenhouse Gas Control 78, 73–84. https://doi.org/10.1016/j.ijggc.2018.07.023

Zhang, K., Harvey, A.P., 2021. CO_2 decomposition to CO in the presence of up to 50% O_2 using a non-thermal plasma at atmospheric temperature and pressure. Chemical Engineering Journal 405. https://doi.org/10.1016/j.cej.2020.126625

Zhang, Q., Dor, L., Fenigshtein, D., Yang, W., Blasiak, W., 2012. Gasification of municipal solid waste in the Plasma Gasification Melting process. Appl Energy 90, 106–112. https://doi.org/10.1016/j.apenergy.2011.01.041

Zhang, Z., Pang, S., 2019. Experimental investigation of tar formation and producer gas composition in biomass steam gasification in a 100 kW dual fluidised bed gasifier. Renew Energy 132, 416–424. https://doi.org/10.1016/j.renene.2018.07.144

Zhao, Z., Huang, H., Wu, C., Li, H., Chen, Y., 2001. Biomass Pyrolysis in an Argon/Hydrogen Plasma Reactor. Eng Life Sci 1, 197–199.

Zhao, Q., Ma, S., Wu, J., Chang, W., Zhang, S., Sun, X., Zhou, B., Lun, Z., Chung, K.H., Shi, Q., 2022. Molecular composition of naphthenic acids in a Chinese heavy crude oil and their impacts on oil viscosity. Pet Sci. https://doi.org/10.1016/j.petsci.2022.09.016

Peer review journals:

- **Roni Mallick** and Prabu Vairakannu, 2022. 4-E analyses of plasma gasification integrated chemical looping reforming system for power and hydrogen co-generation using bakelite and acrylonitrile butadiene styrene based plastic waste feedstocks. *Energy Conversion and Management*, *271*, 116320. https://doi.org/10.1016/j.enconman.2022.116320
- **Roni Mallick** and Prabu Vairakannu, 2023. Energy, exergy, economic and environmental (4-E) analyses of plasma gasification steam cycle integrated molten carbonate fuel cell for hydrogen and power co-generation based on residual waste feedstocks. *International Journal of Hydrogen Energy*, *48(45)*, 16971-16986. https://doi.org/10.1016/j.ijhydene.2023.01.231
- **Roni Mallick** and Prabu Vairakannu, 2023. Experimental investigation of acrylonitrile butadiene styrene plastics plasma gasification. *Journal of Environmental Management, 345*, 118655. https://doi.org/10.1016/j.jenvman.2023.118655
- **Roni Mallick** and Prabu Vairakannu, 2023. CO_2 plasma gasification of bakelite-based electrical switch waste feedstock. *Journal of Cleaner Production, 423,* 138813. https://doi.org/10.1016/j.jclepro.2023.138813
- **Roni Mallick** and Prabu Vairakannu, 2023. Experimental studies on syngas production from plasma gasification of refused derived fuel. *Energy, 288,* 129766. https://doi.org/10.1016/j.energy.2023.129766

Book chapter:

- Pradeep Sahu, **Roni Mallick** and Prabu Vairakannu, 2023. Thermochemical treatment of waste for power generation. Valorization of wastes for sustainable development, *Elsevier*. https://doi.org/10.1016/B978-0-323-95417-4.00009-3
- **Roni Mallick** and Prabu Vairakannu, 2024. Plasma gasification of solid waste for energy generation. Energy from plasma. *Elsevier*.

Conferences:

- **Roni Mallick** and Prabu Vairakannu, "Thermo-economic analysis of plasma gasification integrated steam and combined cycle based on RDF feedstock", *North-East Research Conclave*, 20-22 May, 2022, Indian Institute of Technology Guwahati and Science, Technology and Climate Change Department-Government of Assam, India.

- **Roni Mallick** and Prabu Vairakannu, "Thermo-economic analysis of plasma gasification integrated combined cycle based on bakelite and acrylonitrile butadiene styrene feedstock", *International Conference on Chemical Engineering Innovation & Sustainability (ICEIS 2023)*, 26-27 February, 2023, Jadavpur University, Kolkata.
- **Roni Mallick** and Prabu Vairakannu, "3-E analysis of plasma gasification combined cycle integrated molten carbonate fuel cell for power production based on refused derived fuel feedstock", 20th *International Conference on Sustainable Energy Technologies (SET 2023)*, 15-17 August, 2023, University of Nottingham, United Kingdom.

Workshop:

- "Plasma processing of materials" held at Department of Metallurgical Engineering & Material Science, IIT Bombay and organized by Science and Engineering Research Board (SERB). June 03-22, 2019.